Investigating the Influence of Stereochemistry upon the Properties of Thermoplastic Polymers

by

Connor Stubbs



A thesis submitted to the University of Birmingham for the degree of Doctor of Philosophy

School of Chemistry

College of Engineering and Physical Sciences

University of Birmingham

July 2021

UNIVERSITY OF
BIRMINGHAM

University of Birmingham Research Archive

e-theses repository

This unpublished thesis/dissertation is copyright of the author and/or third parties. The intellectual property rights of the author or third parties in respect of this work are as defined by The Copyright Designs and Patents Act 1988 or as modified by any successor legislation.

Any use made of information contained in this thesis/dissertation must be in accordance with that legislation and must be properly acknowledged. Further distribution or reproduction in any format is prohibited without the permission of the copyright holder.

Abstract

The diverse mechanical and thermal property requirements of modern society have largely been satisfied by polymer materials in the last century. Most materials are almost exclusively synthesized from crude oil derivatives and lack end of life degradation in reasonable time frames, leading to environmental pollution fears. The development of polymers to replace polyolefins will rely on sustainably derived feedstocks from nature. However, extensive study is still required to design degradable polymers from these bio-sourced derivatives that can mechanically compete with petrol-plastics.

Our historical focus on polyolefins revealed that control of the simplest stereo-centres offers extensive manipulation of bulk properties. Derivatives from nature are typically rich in stereochemistry and have unique 3D structures that can be exploited in polymer materials. The goal of this thesis was to understand how stereochemistry within the backbone of linear polymers can be leveraged to manipulate thermal and mechanical properties of synthetic thermoplastics.

Initially a platform to incorporate the desired stereo-center was developed based upon the thiol-ene “Click” reaction. Multiple types of stereoisomerism were incorporated into polyesters and polyurethanes at varying ratios that enabled the tuning of thermal and mechanical properties. Importantly, the presence of crystallinity within one stereoisomer *vs* the other led to the largest property change, but if both were amorphous or crystalline the manipulations were modest. These findings lay down the framework for predicting and designing better thermoplastics. However, a future focus into stereochemistry will be crucial to unlocking the full potential of bio-sourced derivatives.

Acknowledgments

Firstly, I want to thank all Dove and O'Reilly group members past and present that helped, trained, supported, or simply put up with me. It has certainly been one of the more turbulent periods to study in with a lot of highs and lows. But it has been an excellent experience that I would gladly repeat if I could.

I must thank Professor Andrew Dove firstly for accepting me on a PhD, and secondly for welcoming me back for a postdoc. You encouraged and supported some of my stranger ideas and helped me develop into a better, more organized, scientist (One that hopefully won't have to return to school for quite some time). I am grateful for all the opportunities you offered me and helped me improve not only scientific skills, but professional and leadership skills as well. I also want to thank collaborators and their group members for the work and discussions that significantly improved our work: Professor Andrey Dobrynin and Professor Rob Mathers. I'd also like to thank Professor Matt Becker and his group for welcoming me to their lab for a few months and showing me the fun to be had in Akron, Ohio (and that isn't sarcasm).

An unexpectedly tough part of working in research is having to watch your friends leave and realizing all the people you are going to miss. I must thank Kayla, Chiara, Siobhan, Andrew Weems, Sètuhn and Zac who certainly brought the fun and extraordinarily ~~un~~forgettable Christmas gatherings. I have missed the corridor discussion that ranged just about everything and never failed to make me laugh. You all were some of the most knowledgeable and hardworking scientists I know, I am sure we will all see each other at future conferences.

I'd like to thank all past and present members of lab 706 whom made it one of the best labs I have ever worked in. It is the only lab with the magic self-filling wash bottles in neighboring fumehoods (sorry guys). But in all seriousness, the members made the lab. Maher and Vivi, the dynamic duo, whom both brought a great sense of humor and an

answer to every material question I had. Hannah for her meticulous nature that (partially) rubbed off on me and made me question what I was doing more often. Gordon for his *creative* fixes to any lab or equipment issue; I also acknowledge his music tastes, but I certainly don't thank him for it. Equally, I'd like to thank Shannon for a mix of skepticism and humor that is definitely needed in any research project.

It would be impossible to mention lab 706 without thanking Bossman himself. From sharing a Schlenk line with me on my first weeks at Warwick to reading the intro of this very thesis: Josh was there advising, helping, and teaching me every step of the way. Our almost daily discussions gave me a greater insight into my project and the general area than I thought I could ever have, and for that I thank him.

Being part of the O'doveilly team certainly exposes you to a lot of different scientific areas and people from vastly different backgrounds. I'd like to thank: Natalia for reading and improving this thesis last minute, Wei for the numerous project discussions we have had over the past 4 years, and Carl Reynolds for his advice and unforgettable talk on the rheology of cats. But I'd also like to thank the lab 706 neighbours: Lucy and Jenny for the endless corridor discussions and research perspective.

From outside the lab, I must really thank my parents and grandad for the support and inspiration to pursue a PhD in the first place. Thanks for being there all times of the day, ready to talk, even if what I talk about draws a blank expression. I must also thank my friends Ben and Pahim for keeping me sane during lockdown and writing, I look forward to whatever trip you have planned next.

Lastly, I want to thank Anissa. My life got a whole lot better the day she sat at the desk next to me and continued to make it better through my entire PhD. Your support and advice kept me going through the toughest parts and longest days. I particularly admire your unwavering patience, listening to me rant and talk chemistry or project work almost

every waking moment is no easy task. On a professional level, you are an excellent scientist whose questions and critiques improved my projects, science and writing to something I am genuinely proud of. I could not have achieved half of what I did without you.

Table of Contents

List of Figures III
List of Tables and Equations V
List of Symbols, Abbreviations and Acronyms VI
List of publications XI
Author declaration XII
Chapter 1 – Introduction 1
1.1. Structure-property relationships in polymer materials 2
1.1.1. Overview of structure-property relationships 2
1.1.2 Molecular weight in polymers 4
1.1.3 Techniques creating linear polymers 6
1.1.4 Polymer crystallinity 7
1.1.5 Mechanical properties 10
1.1.6 Dynamic Mechanical analysis 12
1.2 Stereochemistry of polymers 13
1.2.1 Stereochemistry in natural polymers 13
1.2.2 Tacticity 15
1.2.3 Backbone stereochemistry 17
1.3 The thiol-ene “Click” reaction 21
1.3.1 Thiol-ene introduction 21
1.3.2 Radical-mediated thiol-ene 22
1.3.3 Nucleophilic thiol-ene – Mechanism 23
1.3.4 Nucleophilic thiol-ene – Trends in reactivity 27
1.4 Thia-Michael addition in polymer materials 30
1.4.1 Linear polymers 30
1.4.2 Networks 34
1.5 Conclusion 36
1.6 References 37
Chapter 2 – Unsaturated Poly(ester-urethanes) with Stereochemically Dependent Thermomechanical Properties 46
2.1 Manuscript details and overview 47
2.2 Supporting Information 50
Chapter 3 – Understanding structure–property relationships of main chain cyclopropane in linear polyesters 51
3.2 Supporting Information 54

Chapter 4 – Stereochemistry Dependent Mechanical Properties in Sugar-Based Degradable Polymers 55
4.1 Manuscript details and overview 56
4.2 Supporting Information 59
Chapter 5 – Chemical Recycling of photocurable resins containing reversible thiol-Michael bonds 60
5.1 Manuscript details and overview 61
5.2 Supporting Information 63
Chapter 6 – Conclusion and outlook 64

List of Figures

Figure 1.1 Illustration of heating a thermoplastic comprised of linear chains (*Left*) and a thermoset structure with crosslinking junctions between the chains (*Right*). 3

Figure 1.2 Summary of structural and composition factors that can be modified in a polymer architecture that influence bulk properties. 4

Figure 1.3 Model plots of molecular weight against conversion for step-growth and chain-growth (controlled and uncontrolled) polymerisation techniques. Including diagrams illustrating the formation of polymers from each technique. 6

Figure 1.4 Typical DSC thermogram of semi-crystalline polymer heating run (solid line) and cooling run (dashed line). Glass transition temperature (T_g), Crystallisation events (T_c and T_{cc}) and melt transition (T_m). 9

Figure 1.5 Diagram illustrating common reported values and features of a tensile curve 11

Figure 1.6 Model DMA thermograms with storage modulus and tan δ plotted against temperature for a linear thermoplastic and a crosslinked polymer. 13

Figure 1.7 Structures of common natural polymers *cis*/*trans*-1,4-polyisoprene and amylose/cellulose to illustrate the stereochemical influence on polymer architecture. 14

Figure 1.8 The different tacticities of polypropylene. 15

Figure 1.9 Tacticity of PLA and its influence on crystallinity and melting temperature. 16

Figure 1.10 a) Scheme of the polycondensation of maleic acid and 1,4-butanediol with a $Ti(OBu)_4$ catalyst and 4-methoxyphenol at varying temperatures. b) Plot of molecular weight (M_w) in kDa and percentage isomerisation (I_{homo}) against reaction temperature (°C). c) Stress *vs* strain curves of poly(butylene-*co*-maleate/fumarate) of varying *cis/trans* content *inset* stress *vs* strain data between 0–100% strain. Adapted from ref. 45 with permission from the Royal Society of Chemistry. 18

Figure 1.11 a) Scheme of the polycondensation of 1,4-cyclohexanedicarboxylic acid and 1,4-butanediol with a $Ti(OBu)_4$ catalyst to yield PBCX where X denotes the percentage *cis* content in the polymer. b) DSC thermograms showing heating scans of PBC12, 36, 44 and 71. c) Stress *vs* strain curves of PBC12, 36, 44 and 71. Adapted from ref. 48 with permission from the Royal Society of Chemistry. 19

Figure 1.12 Mechanism of the radical-mediated thiol-ene reaction. 22

Figure 1.13 Piperidine catalysed thia-Michael addition of thiophenol to 4-phenylbut-3-en-2-one.[70] 23

Figure 1.14 Reaction of hexyl acrylate with 1-hexanethiol catalysed by primary, secondary and tertiary amines. Conversion determined using real-time FT-IR monitoring the consumption of the thiol peak at 2570 cm^{-1}. Adapted from ref. 72 with permission. Copyright 2010 American Chemical Society. 24

Figure 1.15 The generation of the thiolate anion in a base catalysed thia-Michael addition (*Top*). Propagation of the base catalysed thia-Michael addition (*Bottom*). 26

Figure 1.16 Model reaction for investigating the consumption of catalyst-Michael adducts in the presence of a sodium thiolate nucleophile.[77] 27

Figure 1.17 Reactivity trend of numerous Michael acceptors to isooctyl 3-mercaptopropionate.[82] 28

Figure 1.18 The polyaddition of a *bis*-maleimide with various dithiol linkers to form an alternating linear polymer.[94] 30

Figure 1.19 Thermal properties of isosorbide and hydroxymethylfurfural based linear polymers from the polyaddition of a functional diacrylate monomers with various dithiol linkers.[106, 108] 32

Figure 1.20 a) Synthetic Route to azo monomer of triblock co-polymer PEG-*b*-polyazo-*b*-PEG by One-Pot Step-Growth Polymerisation b) Diagram of azo-containing micelle degrading upon heating c) Decrease in M_n determined by GPC of PEG-*b*-polyazo-*b*-PEG heated in water or dimethylacetamide. Adapted from ref. 74 with permission. Copyright 2016 American Chemical Society. 33

Figure 1.21 Diagram illustrating how the selective reactivity of the acrylate functionality over methacrylate affords segmented linear polymers. Reproduced from ref. 127 with permission from the Royal Society of Chemistry. 34

Figure 1.22 a) Synthetic scheme of the thiol-maleimide crosslinker and subsequent crosslinking. Diagram demonstrating the material healing at elevated pH or temperature. b) Stress *vs* strain curve for the self-healing properties of the thiol-maleimide material in different pH buffer solutions. c) Stress *vs* strain curve for the self-healing properties of the thiol-maleimide material at 90 °C. Adapted from ref. 149 with permission from the Royal society of Chemistry. 36

List of Tables and Equations

Equation 1.1 Number average molecular weight equation (M_n) equation, where molecular mass of all polymer chains divided by the number of polymer chains. 4

Equation 1.2 Weight average molecular weight (M_w) equation, where the average is weighted in favour of larger molecules. 5

Equation 1.3 Equation for Dispersity ($Đ$) from number average and weight average molecular weight with the narrowest distributions approaching a value of 1. 5

Equation 1.4 Equation for the calculation of percentage crystallinity (χc) from experimentally obtained enthalpy of melting (ΔH_m), enthalpy of crystallisation (ΔH_c) and enthalpy of melting for 100% crystalline polymer ($\Delta H_m°$) found in literature. 10

Table 1.1 Conjugate addition of 1-hexanethiol to hexyl acrylate 2 M in benzene catalysed by various phosphine catalysts. K_{app} measured by real-time FT-IR.[72] 1-hexanethiol p*K*a = 10.6..... 25

List of Symbols, Abbreviations and Acronyms

2D	2 dimensional
3D	3 dimensional
BD	1,4-butanediol
BDT	1,4-Benzenedimethanethiol
BHT	Butylated hydroxytoluene
CAN	Covalent adaptable network
$CDCl_3$	Deuterated chloroform
$CHCl_3$	Chloroform
CHDA	1,4-cyclohexanedicarboxylic acid
cm	Centimeter
d	day
Da	Dalton
DBN	1,5- diazabicyclo[4.3.0]non-5-ene
DBTDL	Dibutyltin(IV) dilaurate
DBU	1,8-Diazabicyclo[5.4.0]undec-7-ene
$Đ_M$	Dispersity
DMAP	2-Dimethylaminopyridine
DMC	Dimethylcarbonate
DMF	N,N-Dimethylformamide
DMPP	Dimethylphenylphosphine
DMSO	Dimethylsulfoxide
DMSO-d_6	Deuterated dimethylsulfoxide
DMTA	Dynamic mechanical thermal analysis
DnPA	Di-*n*-propylamine
DSC	Differential scanning calorimetry
DVS	Divinyl sulfone
E	Young's modulus
Et_2O	Diethyl ether

EtOAc	Ethyl acetate
FT-IR	Fourier transform infrared
G'	Storage modulus
G''	Loss modulus
G_e	Entanglement modulus
GPa	Gigapascals
GPC	Gel permeation chromatography
h	Hour
HCl	Hydrochloric acid
HDPE	High density polyethylene
HDT	1,6-hexanedithiol
HMF	Hydroxylmethylfurfural
HexAM	Hexylamine
HPLC	High performance liquid chromatography
HRMS	High resolution mass spectrometry
I_{homo}	Isomerisation percentage
J	Joule
K	Kelvin
k_{app}	Apparent rate constant
kDa	Kilodaltons
kg	Kilograms
kPa	Kilopascals
L	Litre
lbs	Pounds
LDPE	Low density polyethylene
$LiAlH_4$	Lithium aluminum hydride
M_e	Entanglement molecular weight
MeOH	Methanol
min	Minute
MJ	Megajoule
mg	Milligram

$MgSO_4$	Magnesium sulfate
mL	Milliliter
mm	Millimeter
mmol	Millimole
MMP	Methyl 3-mercaptopropionate
M_n	Number average molar mass
mol	Mole
M_p	Molecular weight of highest peak
MPa	Megapascals
MS	Mass spectroscopy
mW	Milliwatts
M_w	Mass average molar mass
N	Newtons
$NaHCO_3$	Sodium bicarbonate
NaOH	Sodium hydroxide
NEt_3	Triethylamine
NH_4BF_4	Ammonium tetrafluoroborate
NH_4Cl	Ammonium chloride
nm	Nanometer
NMR	Nuclear magnetic resonance
P	Pressure
P(*n*-Pr)$_3$	Tri-*n*-propylphosphine
Pa	Pascals
PCL	Polycaprolactone
PE	Polyethylene
PEG	Poly(ethylene glycol)
PET	Poly(ethylene terephthalate)
p*K*a	Acid dissociation constant
PLA	Poly(lactic acid)
PMe_2Ph	Dimethylphenylphosphine
$PMePh_2$	Methyldiphenylphosphine

PMMA	Poly(methylmethacrylate)
PP	Polypropylene
PPh_2	Triphenylphosphine
ppm	Parts per million
PS	Polystyrene
PS	Proton Sponge®
PTFE	Poly(tetrafluoroethylene)
ROP	Ring opening polymerisation
s	seconds
SEC	Size exclusion chromatography
T	Temperature
T_c	Crystallization temperature
$T_{d\ 5\%}$	Temperature at 5% weight loss
TEA	Triethylamine
T_g	Glass transition temperature
TGA	Thermogravimetric analysis
THF	Tetrahydrofuran
TLC	Thin layer chromatography
T_m	Melt transition
TOF	Time of flight
TTS	Time temperature superposition
U_T	Tensile toughness
UTS	Ultimate tensile strength
UV	Ultra violet
WLF	Williams-Landel-Ferry
Å	Angstroms
δ	Chemical shift
ΔH_c	Enthalpy of crystallisation
ΔH_m	Enthalpy of melting
$\Delta H_m°$	Enthalpy of melting for 100% crystalline polymer
ε_b	Strain at break

ε_y	Strain at yield
λ	Wavelength
σ_b	Stress at break
σ_y	Stress at yield
τ_e	Rouse time of one entangled segment
µL	Microliter
χ_c	Percentage crystallinity

List of publications

1. AC Weems, KR Delle Chiaie, JC Worch, **CJ Stubbs**, AP Dove, Terpene-and terpenoid-based polymeric resins for stereolithography 3D printing, *Polymer Chemistry* (2019), 10, 5959-5966.
2. **CJ Stubbs**, JC Worch, H Prydderch, ML Becker, AP Dove, Unsaturated Poly(ester-urethanes) with Stereochemically Dependent Thermomechanical Properties, *Macromolecules* (2020), 53, 174-181.
3. **CJ Stubbs**, AP Dove, Understanding structure–property relationships of main chain cyclopropane in linear polyesters, *Polymer Chemistry* (2020), 11, 6251-6258.
4. JC Worch, **CJ Stubbs**, MJ Price, AP Dove, Click Conjugate Additions of S-, N- and O-centered Nucleophiles to Activated Alkynes: From (Bio)Organic to Polymer Chemistry, *Chemical reviews* (2021), 121, 6744-6776.

Author declaration

This thesis is submitted to the University of Birmingham in support of my application for a Doctor of Philosophy award. This work has not been submitted for any degree or award previously.

Parts of the thesis have been published as open access articles in peer reviewed scientific journals or are displayed in manuscript format suitable for publication as outlined in the University of Birmingham alternative thesis format guidelines. Experiments, materials characterisation, data collection and analysis, writing and figure design was performed by myself, except for co-author contributions which are outlined below and before each chapter.

Chapter 2 – Reprinted with permission from: C. J. Stubbs, J. C. Worch, H. Prydderch, M. L. Becker, A. P. Dove, Unsaturated Poly(ester-urethanes) with Stereochemically Dependent Thermomechanical Properties, *Macromolecules* **2020**, *53*, 174-181. Copyright 2020 American Chemical Society.

Dr Josh Worch (University of Birmingham) and Dr Hannah Prydderch (University of Birmingham) provided technical and synthetic advice. Dr Carl Reynolds advised on rheological experimentation and modelling. Prof. Matthew L. Becker (Duke University) provided guidance and editing of this manuscript. Prof. Andrew P. Dove (University of Birmingham) supervised in addition to providing guidance and editing the manuscript.

Chapter 3 - Reprinted from: C. J. Stubbs, A. P. Dove, Understanding structure–property relationships of main chain cyclopropane in linear polyesters, *Polymer Chemistry*, **2020**, *11*, 6251-6258. Copyright Royal Society of chemistry.

Professor Andrew Dove supervised and provided project guidance, in addition to editing the manuscript.

Chapter 4 – Manuscript Submitted: C. J. Stubbs†, J. C. Worch†, H. Prydderch, Z. Wang, R. T. Mathers, A. V. Dobrynin, M. L. Becker, A. P. Dove, Stereochemistry Dependent Mechanical Properties in Sugar-Based Degradable Polymers, *Submitted*.

† denotes equal contribution

Dr Josh Worch (University of Birmingham) synthesised and characterised the monomers and polymers for the project, in addition to performing the hydrolytic degradation experiment. Dr Hannah Prydderch (University of Birmingham) provided technical and synthetic advice including troubleshooting some of the initial synthetic pathways. Prof. Andrey Dobrynin (University of North Carolina-Chapel Hill) and Zilu Wang (University of North Carolina-Chapel Hill) performed Molecular dynamic calculations and polymer chain simulations. Prof. Robert Mathers (Pennsylvania State University) performed degradation calculations. Prof. Matthew Becker (Duke University) and Prof. Andrew Dove (University of Birmingham) supervised the project, in addition to providing guidance and editing the manuscript.

Chapter 5 – Manuscript Prepared: C. J. Stubbs, A. Khalfa, V. Chiaradia, J. C. Worch, A. P. Dove, Chemical Recycling of photocurable resins containing reversible thiol-Michael bonds, *Manuscript Prepared*

Anissa Khalfa (University of Birmingham) performed and characterised NMR spectra for the model reactions and prepolymers. Dr Viviane Chiaradia (University of Birmingham) performed stress relaxation experiments. Dr Josh Worch (University of Birmingham) performed swell testing and gel fraction experiments. Prof. Andrew Dove (University of

Birmingham) supervised the project, in addition to providing guidance and editing the manuscript.

Chapter 1 – Introduction

1.1. Structure-property relationships in polymer materials

Over the past 150 years, our understanding of polymer materials has evolved and enabled us to predict the bulk behaviour of designed polymers. Similar to how the 3D structure and composition of small organic molecules govern their interactions with the environment, and hence their function; the chemistry of polymer buildings blocks also impacts its interactions with its environment and govern its function. However, in the case of polymer materials, their properties are governed by bulk interactions between the chains themselves. For example, the impact of flexibility or rigidity in a bond or structure within a polymer chain has a significant impact on thermal properties, due to increased or restricted polymer chain mobility at the molecular level. It is therefore palpable that any single change in the polymer structure or composition that influences bulk chain-chain interaction will lead to an impact upon the bulk properties of a polymer. This is colloquially referred to as the structure-property relationship.

1.1.1. Overview of structure-property relationships

Polymeric materials can be broken down into two different material-types: thermoplastics and thermosets (Figure 1.1). This classification is used to describe the ability to reshape and deform a material through heating (thermoplastic) or a thermally fixed shape (thermoset). Thermoplastics are conventionally linear chains that can freely move and flow in the polymer matrix once a sufficient temperature is reached. On the other hand, thermosets can be described as an infinite network composed of linear polymer chains with crosslinks between them; with the energy required to break these crosslinks typically surpassing the thermal stability of the bulk material. Some exceptions exist, where the crosslinks are transient at elevated temperature and the network may be remoulded into a new shape, although this is still a developing area.[1] The use of thermoplastics and thermosets is typically application-driven. Thermoplastics may be more recyclable, however they are typically less resistant to solvent and high temperatures compared to

networks. In terms of mechanical properties, thermoplastics are also more susceptible to fatigue with repetitive force deforming the material as the polymer chains are significantly more mobile than the chains in a network.

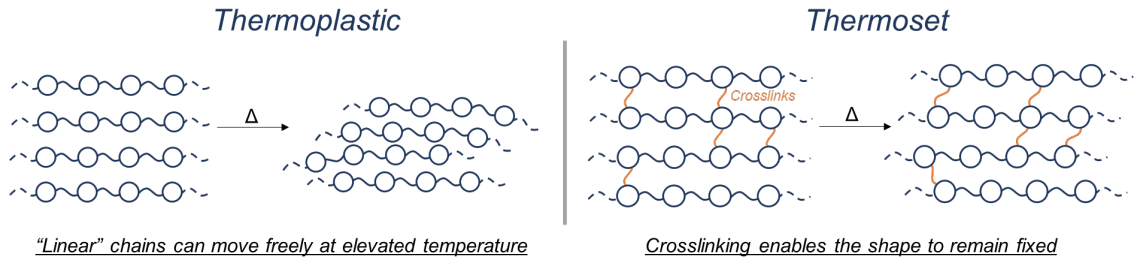


Figure 1.1 Illustration of heating a thermoplastic comprised of linear chains (*Left*) and a thermoset structure with crosslinking junctions between the chains (*Right*).

Despite the inherent differences between thermosets and thermoplastics, the molecular and structural relationships that govern their bulk properties are more or less consistent to one and other (Figure 1.2). The chemical functionality of the polymer (or network) chains influence chain-chain interactions and packing, subsequently impacting the mechanical and thermal properties. This functionality dependence can be exemplified by the amide bond containing nylons *vs* the ester bond containing polyesters. Strong hydrogen bonding character within nylons impart them with comparatively higher strength and stiffness than the weaker dipole bonding character in polyesters.

In addition to chemical functionalities' role in governing bulk properties: topological and structural features also greatly influence material properties. The polymer chain length, their size distribution (dispersity or *Đ*) and structure have a significant effect on the interactions of polymer chains at a molecular level.[2] For example, the impact of branching in low-density polyethylene (LDPE) produces a weaker, more flexible material than its linear counterpart high-density polyethylene (HDPE), despite being functionally analogous.[3-5]

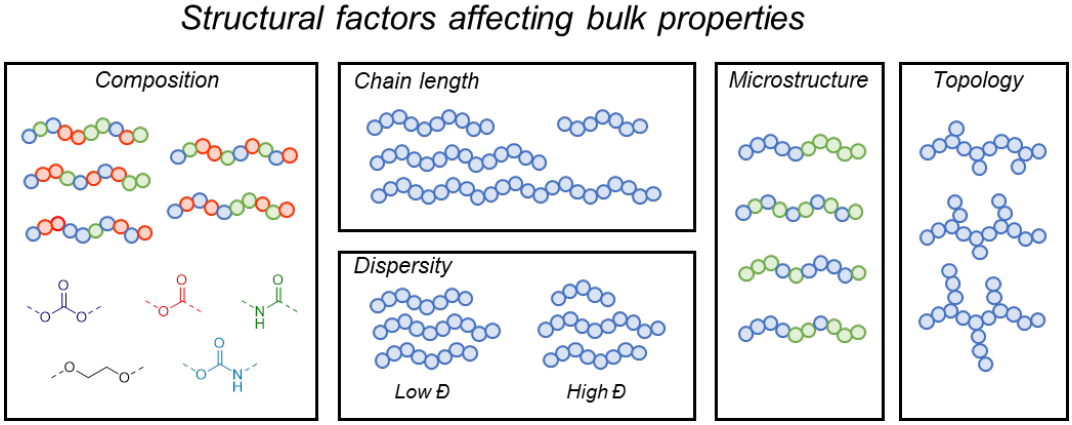


Figure 1.2 Summary of structural and composition factors that can be modified in a polymer architecture that influence bulk properties.

1.1.2 Molecular weight in polymers

Understanding the molecular weight and dispersity of a polymer is important for thermoplastic materials. Low molecular weight polymers will typically produce a brittle deformation whilst higher molecular weights of the same polymer may deform in a more ductile manner. To quantify the molecular weight and dispersity, Size-exclusion chromatography (SEC), or occasionally referred to as Gel Permeation Chromatography (GPC), is employed. Retention times of a polymer sample are evaluated against the retention times of known narrow dispersity standards (such as polystyrene or poly(methylmethacrylate)) which are used to estimate molecular weight. These are some values relevant to polymer properties that can be obtained through SEC, where N_i is the number of polymer chains with molecular mass M_i:

$$M_n = \frac{\sum M_i N_i}{\sum N_i}$$

Equation 1.1 Number average molecular weight equation (M_n) equation, where molecular mass of all polymer chains divided by the number of polymer chains.

$$M_w = \frac{\sum M_i^2 N_i}{\sum M_i N_i}$$

Equation 1.2 Weight average molecular weight (M_w) equation, where the average is weighted in favour of larger molecules.

$$Đ = \frac{M_w}{M_n}$$

Equation 1.3 Equation for Dispersity (*Đ*) from number average and weight average molecular weight with the narrowest distributions approaching a value of 1.

Despite the idealistic model of a linear polymer being elongated polymer chains, thermoplastics are better described as a tangled mesh where entanglements occur at different points in a chain. Another important parameter, particularly in materials characterization, is the chain entanglement molecular weight (M_e), or molecular weight between entanglements. The M_e can be calculated experimentally and is specific to each polymer structure and composition. For example, the pendant phenyl groups of linear polystyrene (PS) give it a comparatively higher backbone rigidity than a flexible alkyl chain in HDPE. Hence, PS (M_e = ~18000 g·mol^{-1}) requires a larger molecular weight than HDPE (M_e = ~1000 g·mol^{-1} to form chain entanglements.[6]

The presence of entanglements in polymers are an important factor in governing the mechanical and thermal properties of a material. As stress is applied to a polymer material, the chains are extended until a chain entanglement is reached. At this point the energy or force required to overcome or unravel the entanglement is greater than elongating a disordered chain, therefore further elongation requires significantly more force or energy. Hence, a linear polymer should possess a significant quantity of chain entanglements (*i.e.* have a molecular weight greater than the M_e) to produce a mechanically robust polymer material.

1.1.3 Techniques creating linear polymers

Different architectures and compositions can be achieved not only through changing the structure of the monomers but also through changing the polymerisation technique. Synthesis of most thermoplastics polymers can be separated into two different classes: chain-growth and step-growth. Chain-growth is a technique where an initiating species begins the growth of a polymer and continues to grow through a propagation mechanism until a termination event occurs. This typically results in rapid polymer formation but produces polydisperse materials with minimal control over the polymer architecture. A subclass of chain-growth offers far more control by eliminating termination events and increasing the initiation rate to produce a more uniform growth of the polymer chain. This leads to a narrower dispersity, controlled M_w and in some cases, better control of the backbone architecture. On the other hand, step-growth polymerisation lacks the initiation step with all monomers able to react with each other to grow the polymer chain. As a result, step-growth also affords a polydisperse polymer with less molecular weight control (Figure 1.3).

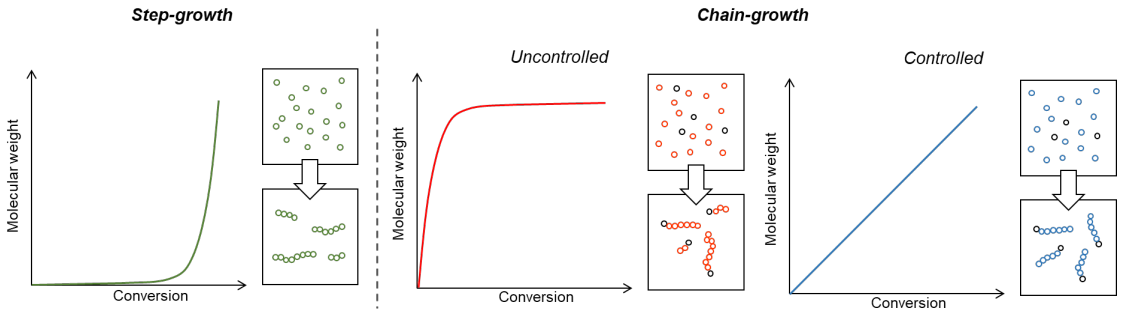


Figure 1.3 Model plots of molecular weight against conversion for step-growth and chain-growth (controlled and uncontrolled) polymerisation techniques. Including diagrams illustrating the formation of polymers from each technique.

Controlled chain-growth can offer the ability to grow different monomers off the polymer chain-end to create a block co-polymer. This has been a particularly prominent technique

in the materials field to combine multiple functionalities into the same chain. A notable example is in the field of thermoplastic elastomers where a hard, rigid polymer block (A) is combined with a softer, flexible block (B) to form polymer chains in various blocky microstructures (AB, ABA, BAB *etc*.). While the softer block enables a plastic-like deformation, the harder block acts as a weak crosslink that can aid the recovery of a material after deformation.

Although controlled chain-growth would appear the superior technique, there are several advantages for step-growth polymerisation. There is a comparatively greater monomer scope for step-growth polymerisation, since a wider range of established organic coupling reactions (*e.g.* condensation, addition, cross-coupling, radical *etc*.) can be exploited in comparison to chain-growth. In turn, this also increases the scope of functionalities that can be incorporated into a polymer backbone or side chain, offering alternative methods to manipulate bulk properties. Nevertheless, both are extensively used to create materials on a commercial scale, such as the step-growth for polyethylene terephthalate (PET) or the chain-growth polymerisation of ethylene to produce PE.

1.1.4 Polymer crystallinity

Depending on composition, functionality and several structural factors, thermoplastics and networks may be either semi-crystalline or amorphous. Unlike conventional small molecules, semi-crystalline polymers have regions of high ordering that are crystalline but also amorphous regions that lack ordering. This is a result of how polymers crystallise; polymer chains are rarely extended and are typically folded or tangled. As such, short-chain segments typically crystallise with the folding of the same chain making up a growing crystalline lamellar. Whilst these lamellar are 2D, they grow in such a way from the nucleation point that they typically form a 3D web of growing lamellar called spherulites, which are commonly observed in polymer materials. However, the lamellar and spherulites always contain some defects where chains do not fold into the same

lamellar and dangle outside the ordering, which contributes to the amorphous regions in the matrix.

The simplest technique to quantify the crystallinity of a polymer material is through Differential Scanning Calorimetry (DSC). Crystallinity is qualitatively observed by the presence of a first order transition in the endothermic direction (T_m) or lack of one for an amorphous material. First order transitions are marked by a change in both the enthalpy and the heat capacity of a sample during the phase transition. Another commonly observed first order transition is a crystallisation transition (T_c and T_{cc}) which can occur in either the heating or cooling run in the exothermic direction. However, this is not diagnostic for crystallinity as some polymers crystallise at different speeds and may not crystallise during the time of the DSC heating and cooling cycles.

A further feature of a DSC thermogram is the observance of the glass transition temperature (T_g) as a pseudo second order transition in the endothermic direction upon either heating or cooling. A second order transition is marked by a change in the heat capacity only with no measurable enthalpy change. The T_g is a particularly important characteristic of polymer materials as it denotes the shift from a glassy brittle state to a rubbery state. Whilst the precise molecular processes that underpin the T_g remain unknown, leading theories generally describe it as the temperature at where a significant motion of the polymer chains can occur. Figure 1.4 shows a typical heating and cooling thermogram for a semi-crystalline polymer obtained from a DSC.

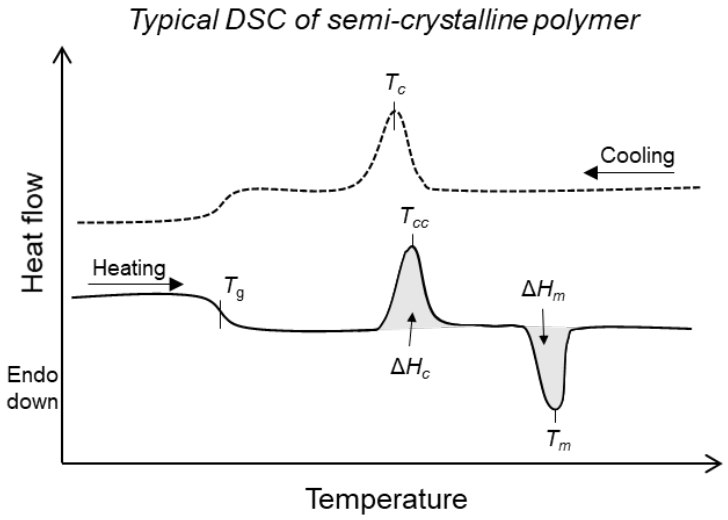


Figure 1.4 Typical DSC thermogram of semi-crystalline polymer heating run (solid line) and cooling run (dashed line). Glass transition temperature (T_g), Crystallisation events (T_c and T_{cc}) and melt transition (T_m).

The temperature at which the T_m occurs can qualitatively infer the crystallinity of the sample, but the enthalpy of the melt transitions (ΔH_m) is often used to calculate the extent of the crystallinity. For common commercial polymers, the ΔH_m can be used to estimate percentage crystallinity (χ_c) using literature values of enthalpy for 100% crystalline analogues (Equation 1.4).[7, 8] This is particularly useful for quality control and categorising different products in industry, such as Polyethylene (PE). Linear high-density PE (HDPE, χ_c = 90%+) and branched low-density PE (LDPE, χ_c = 50–60%) have different accepted ranges of percentage crystallinity due to the linear *vs* branching structure: either promoting, or precluding chain order.[9] The significant differences in their crystallinity drives their divergent mechanical properties, and hence, the applications for which they are used.

$$\chi_c = \frac{\Delta H_m - \Delta H_c}{\Delta H_m^\circ}$$

Equation 1.4 Equation for the calculation of percentage crystallinity (χ_c) from experimentally obtained enthalpy of melting (ΔH_m), enthalpy of crystallisation (ΔH_c) and enthalpy of melting for 100% crystalline polymer (ΔH_m°) found in literature.

There are many factors relating to the structure and composition of the polymer that influences the percentage crystallinity of a thermoplastic. However, the processing conditions of a polymer can significantly influence the nature and extent of polymer chain ordering. Rapid cooling from polymer melt reduces the time at which polymer chains are mobile, and therefore can inhibit ordering of the chains resulting in a reduced overall crystallinity. Once the temperature is below the T_g, the chains are essentially immobile and lack the required motion to crystallise. The inverse is also true, if a polymer is held isothermally above the T_g but below the melt temperature (typically referred to as annealing), the polymer chains remain mobile and can yield a greater level of crystallinity.[10, 11] As an example, polyethylene terephthalate (PET) can be processed to be amorphous or highly crystalline with minimal changes with the cooling rate (1–10 $K \cdot s^{-1}$), which has a considerable impact on other bulk properties such as oxygen permeability.[12, 13] Given the intimate connection between crystallinity and bulk properties, quantifying polymer crystallisation is of particular importance to industry and designing future polymer materials.[14]

1.1.5 Mechanical properties

Polymer materials are broadly applicable in a vast range of settings and require different properties for their desired use. They can also be subject to a number of different mechanical stresses such as shear, compressive, tensile, bending, abrasion, ripping, among others. Conventionally, the tensile properties of the materials are reported as they are appropriate for most applications, and specific properties such as strength, stiffness,

toughness and elasticity can be clearly determined from a stress *vs* strain curve. Figure 1.5 shows a simple diagram of the features typically observed on a stress *vs* strain curve for a thermoplastic, and some curve shapes of commodity thermoplastic and elastic materials.

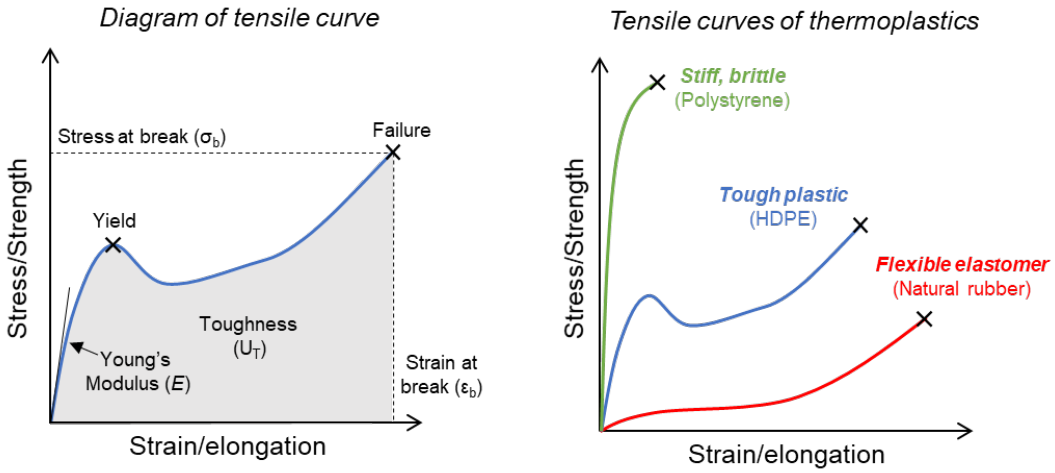


Figure 1.5 Diagram illustrating common reported values and features of a tensile curve

To summarise the key values and features of a stress *vs* strain in figure 1.5:

Engineering stress (σ) – quantifies the force per the initial cross-sectional area of the sample and is typically reported as Pa or $N \cdot m^{-2}$.

Strain (ε) – elongation of sample divided by the initial length of sample, typically reported as a percentage or in decimal form. (*i.e.* 200% strain refers to a sample elongated twice the initial length)

Young's modulus (E) – quantifies the initial stiffness of the sample and calculated from the initial gradient (σ/ε) and is typically reported in Pascals (Pa).

Yield point – the point where stress levels or drops from a maxima and is typically reported as yield stress (σ_y) in Pa and strain at yield (ε_y) as a percentage or as a decimal.

Failure – the point where the material breaks and is reported as stress at break (σ_b), or ultimate tensile strength (UTS) in Pa, and strain at break (ε_b) as a percentage or as a decimal.

Tensile toughness (U_T) – the area under the stress *vs* strain curve relating to the total amount of energy required to take a material to failure and is typically reported as $J \cdot m^{-3}$.

As exemplified in figure 1.5, polymer materials can adopt an impressive range of mechanical properties to satisfy diverse property requirements. However, manipulation between the different material classes (plastic *vs* elastic *vs* glass) is typically achieved by altering polymer architectures and/or backbone chemistries. For example, linear HDPE and branched LDPE are compositionally similar but their topological differences alter their crystallinity. As such, both display a stress-strain curve characteristic of a tough plastic, but their strength and stiffness differ in magnitude. LDPE is significantly weaker and more flexible (E = 0.14–0.3 GPa, UTS = 7–17 MPa) in contrast to HDPE (E = 0.7–1.4 GPa, UTS = 20–40 MPa).[6] This highlights how a polymer of the same composition with a different structure influences mechanical properties, but ultimately produces an analogous stress *vs* strain profile.

1.1.6 Dynamic Mechanical analysis

A common way of simultaneously characterising thermal transitions and mechanical properties of polymer materials is through Dynamic Mechanical Analysis (DMA). A typical experiment features a fabricated polymer sample being subjected to an oscillating force across a desired temperature range. The viscoelastic response, characteristic to most thermoplastics, is separated into the elastic component (storage modulus, G') and viscous component (loss modulus, G"). A ratio of these components, called tan δ, can also be used to identify transitions in mechanical properties such as the T_g and polymer flow temperature. Figure 1.6 displays a model DMA thermogram with storage modulus and tan δ plotted against temperature for a linear and crosslinked polymer. Near the T_g a

pronounced decrease in the storage modulus (elastic component) is observed along with an increase of the loss modulus (viscous component). At a certain temperature, that is dependent upon the specific thermal properties of the polymer, thermoplastics will begin to flow. In contrast, a conventional crosslinked polymer does not flow and maintains a rubbery plateau until thermal degradation.

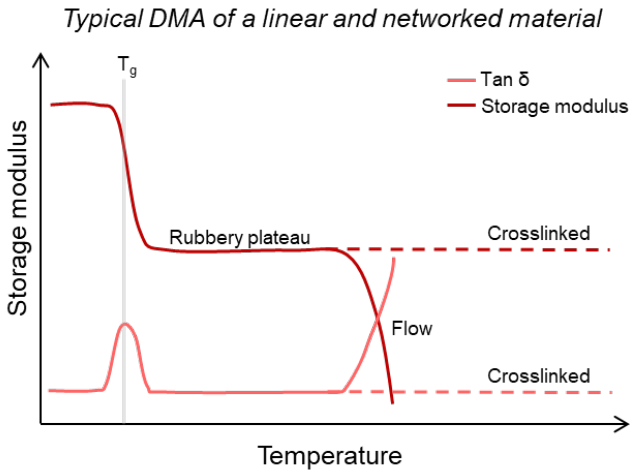


Figure 1.6 Model DMA thermograms with storage modulus and tan δ plotted against temperature for a linear thermoplastic and a crosslinked polymer.

1.2 Stereochemistry of polymers

1.2.1 Stereochemistry in natural polymers

Polymers found in nature have an unprecedented way of fulfilling complex roles and the demands required to sustain life. This can only be attributed to the precise 3D arrangement of molecules and atoms that impart bio-polymers with unique structure and function. Nature achieved this through its ability to use and control stereochemistry in polymer backbones so a desired function can be achieved from the structure. The importance of stereochemistry in nature can be illustrated by two abundant polysaccharides, amylose and cellulose, which differ by a single stereocenter within the repeat unit. Cellulose, the β-anomeric form, is a polymer that promotes structural integrity

in plant cells whilst amylose, the α-anomeric form, lacks a robust bulk structure and can be easily digested unlike cellulose (Figure 1.7).[15] These properties can be explained through polymer chain packing, where the amylose structure precludes packing and hence crystallisation, whilst the cellulose structure promotes it.[16]

Nature has also produced materials that display differing mechanical and thermal properties based on their stereochemistry. Natural rubber (*cis*-1,4-polyisoprene) has long been used to create strong flexible materials such as tyres, whilst its lesser-known analogue Gutta-Percha (*trans*-1,4-polyisoprene) is a comparatively harder and stiffer material that found application in golf balls and dentistry fillings.[17-19] These mechanical properties are a result of their stereochemistry: the *trans* isomer promotes chain ordering in Gutta-Percha evidenced by a T_m between 40–60 °C with a ΔH_m of 53 J·g^{-1}. Whilst the *cis* isomer impedes the necessary packing with the only T_m observed at 0 °C with a ΔH_m of 14 J·g^{-1}.[20-22]

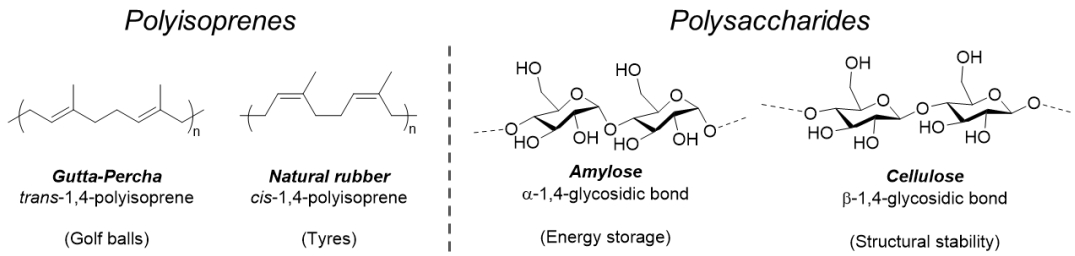


Figure 1.7 Structures of common natural polymers *cis*/*trans*-1,4-polyisoprene and amylose/cellulose to illustrate the stereochemical influence on polymer architecture.

These early examples indicated how stereochemistry can be exploited to manipulate bulk properties of polymers with a similar architecture, to a somewhat greater degree than the constitutional isomers of LDPE and HDPE mentioned earlier. The observations of these property differences not only led to the study of stereochemistry in synthetic polymers, but the invention of techniques that can control stereochemistry within the backbone of synthetic polymers.[23]

1.2.2 Tacticity

Hermann Staudinger, accredited for proving the existence of macromolecules, was the first to suggest stereochemistry's impact on polymer structures.[24] However, impetus into the area was greatly driven by Natta's report in 1954 on the synthesis of semi-crystalline polypropylene (PP).[25] Previously, the synthesis of PP had generally yielded amorphous materials which lacked the molecular ordering required to crystallise in the same manner as other polyolefins at the time, limiting its commercial usage.[26] Natta's PP was crystalline due to the stereoregular relationship of neighbouring pendant methyl groups which became known as isotactic-PP (Figure 1.8). The relationship of neighbouring chiral atoms in a polymer backbone became known as tacticity. Since its initial coining, more expanded classifications have been identified such as syndiotacticity and heterotacticity. Polymers in this class typically feature an intermediate crystallinity between atactic and isotactic analogues.[27]

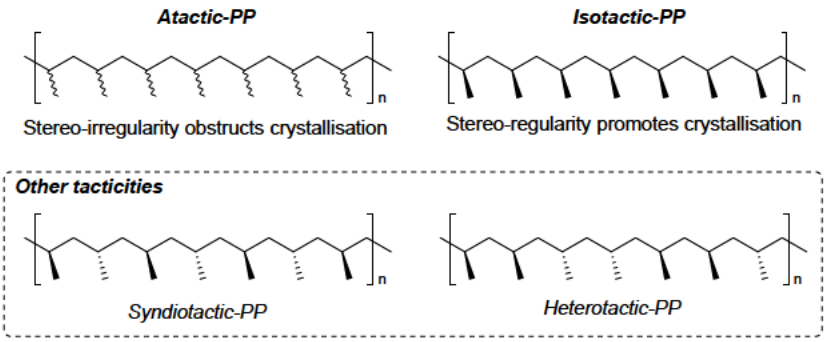


Figure 1.8 The different tacticities of polypropylene.

The success, both commercially and synthetically, of isotactic-PP led to an intense focus on refining the synthesis of polyolefins with varying stereo-control.[28-30] Both polystyrene (PS) and polymethylmethacrylate (PMMA) have been synthesised with isotactic and syndiotactic control, however these property improvements against atactic analogues are marginal due to the high T_g, which renders the materials glassy at ambient temperature.[31, 32]

The emphasis on polyolefins has begun to dwindle in recent years, primarily due to their lack of environmental degradation which is causing growing pollution concerns. Consequently, research focus has shifted to synthesizing environmentally degradable plastics from natural derivatives, that offer a competitive mechanical performance to crude oil predecessors. The fermentation of naturally abundant carbohydrates has yielded a number of unique monomers, such as lactic acid, used in the production of polylactic acid (PLA).[33] Although initially discovered by the step-growth polymerisation of lactic acid by Carothers, PLA only gained wide notoriety when it was made from the ring opening polymerisation (ROP) of the lactic acid dimer, lactide, to achieve high molecular weight polyesters.[34] An additional feature was the presence of a pendant methyl group which could be leveraged in a similar manner to PP to enhance thermal and mechanical properties (Figure 1.9). Over the past few decades, several catalysts and synthetic techniques have been developed to achieve the same stereo-control as polyolefins.[35-37] It was found that atactic and heterotactic PLA both lack a T_m making them amorphous polymers with poorer mechanical properties. However, syndiotactic and isotactic PLA possess enough order to crystallise and exhibit T_ms, with isotactic having a highest T_m suggesting more efficient crystallisation.[38]

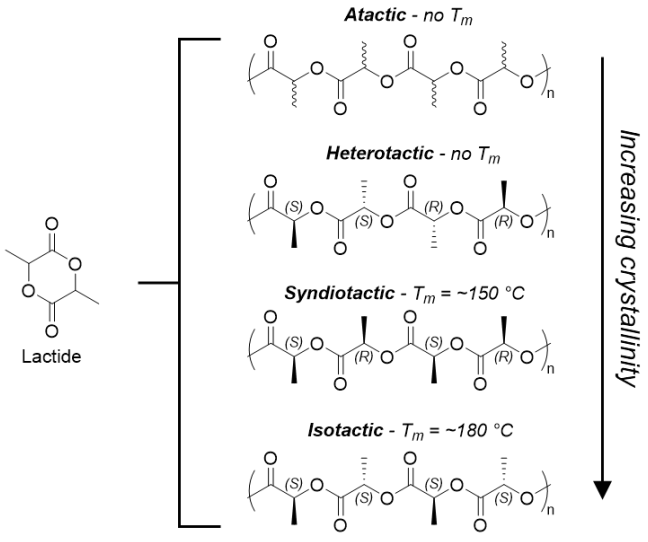


Figure 1.9 Tacticity of PLA and its influence on crystallinity and melting temperature.

Both isotactic and atactic PLA have a similar T_g (50–60 °C), however the crystallinity of isotactic PLA produces a significantly higher tensile strength (UTS = 50 MPa) than the atactic analogue (UTS = 29 MPa).[39] Interestingly, the property relationship to stereochemistry translates to its hydrolytic degradability where isotactic PLA degrades far slower than the atactic analogue, however this may simply be the influence of crystallinity alone which has long been known to inhibit hydrolytic degradation rates.[40, 41]

1.2.3 Backbone stereochemistry

The relationship of stereochemistry to thermomechanical properties is typically explained through packing and crystallinity. Polyisoprene produces the strongest material when the chain adopts the *trans* isomer, however other polymers containing alkene stereochemistry display the opposite trend. One of the first unsaturated polymers synthesised was the fully conjugated polyacetylene.[42, 43] Whilst most studies had focussed upon its excellent conductive properties, one study investigated the mechanical properties of polyacetylene with varying ratios of *cis/trans* stereochemistry. Increasing the *cis* content in polyacetylene led to a more extensible sample (*i.e.* higher strain at break than the *trans* analogues), but this also correlated with an increased strength. Polyacetylene with a 98% *cis* content had a higher UTS (~37 MPa) than the 96% *trans* content (~24 MPa).[44] The opposing strength trend between polyacetylene (*cis* isomer stronger) and polyisoprene (*trans* isomer stronger) suggested the functionality of the polymers also played a significant role in how stereoisomerism influences mechanical properties.

The shift from the olefinic-based monomers to bio-sourced derivatives opened new synthetic avenues to incorporate stereochemistry. A recent study described the synthesis of unsaturated polyesters from the polycondensation of maleic acid with 1,4-butanediol, two bio-sourced derivatives (Figure 1.10a).[45] Unfortunately, the high temperatures required to achieve a moderate M_w value (~30 kDa) triggered significant isomerisation (~25%). Whilst a fully *cis*-containing polymer was unachievable from this technique, the

stereochemistry of the polyester could be effectively tuned at a reasonable M_w. The 100% *trans* polymer displayed a tensile curve characteristic of a strong, brittle glass, however with increasing *cis* content, the extensibility of the polymer increased significantly, imparting the materials with characteristic plastic behaviour (Figure 1.10c).

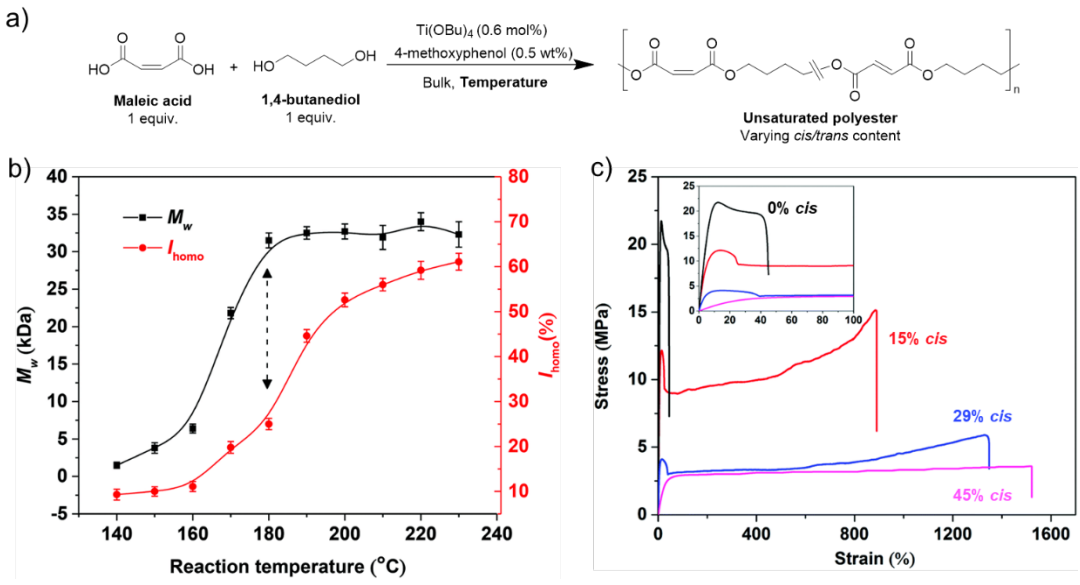


Figure 1.10 a) Scheme of the polycondensation of maleic acid and 1,4-butanediol with a $Ti(OBu)_4$ catalyst and 4-methoxyphenol at varying temperatures. b) Plot of molecular weight (M_w) in kDa and percentage isomerisation (I_{homo}) against reaction temperature (°C). c) Stress *vs* strain curves of poly(butylene-*co*-maleate/fumarate) of varying *cis/trans* content *inset* stress *vs* strain data between 0–100% strain. Adapted from ref. 45 with permission from the Royal Society of Chemistry.

Isomerisation, oxidation, and other radical side-reactions impede the synthesis of stereo-controlled unsaturated polymers at a reasonable molecular weight. However, conformationally locked ring structures offer similar geometric configurations as the alkene moiety but are less susceptible to side reactions. Difunctional cyclohexylene compounds are particularly common in the synthesis of linear polymer, although stereochemistry on the ring is often ignored or only the *trans* isomer is investigated because it is more

thermodynamically stable.[46, 47] One study investigated the influence of stereochemistry of the cyclohexylene ring on thermal and mechanical properties.[48] A range of polyesters from 1,4-cyclohexanedicarboxylic acid (CHDA) and 1,4-butanediol with varying *cis/trans* content were synthesised by varying the initial feed of the respective isomer in the polycondensation (Figure 1.11a). Unfortunately, the isomerisation of both the *cis* and *trans* analogues during synthesis precluded the fabrication of a stereochemically pure polymer, yet a range of *cis/trans* contents (12–71% *cis*) could be accessed on a reasonable scale.

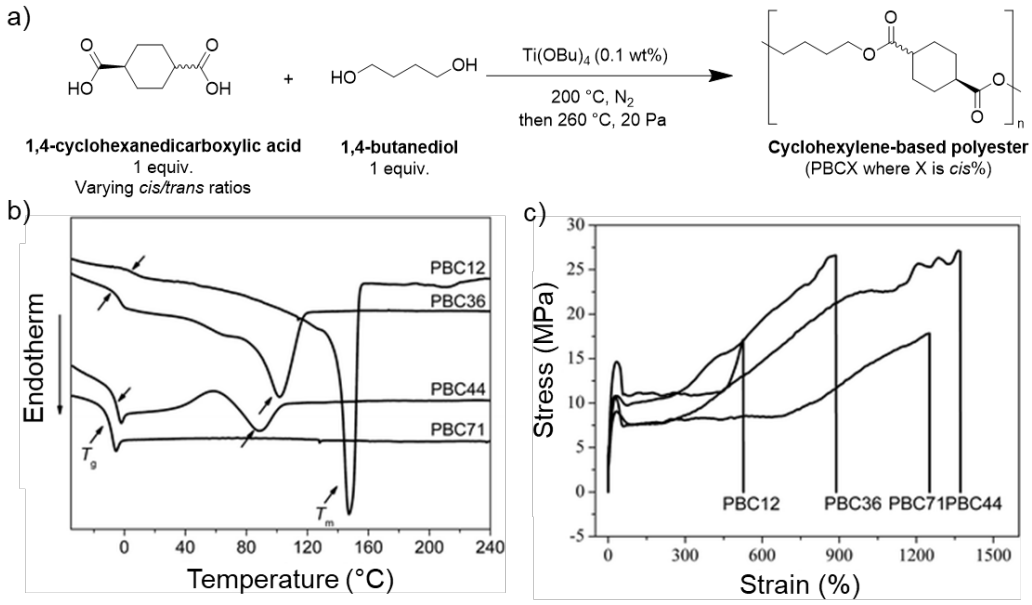


Figure 1.11 a) Scheme of the polycondensation of 1,4-cyclohexanedicarboxylic acid and 1,4-butanediol with a $Ti(OBu)_4$ catalyst to yield PBCX where X denotes the percentage *cis* content in the polymer. b) DSC thermograms showing heating scans of PBC12, 36, 44 and 71. c) Stress *vs* strain curves of PBC12, 36, 44 and 71. Adapted from ref. 48 with permission from the Royal Society of Chemistry.

The general trends of cyclohexylene stereochemistry within the linear polymer displayed a similar dependence as polyisoprene, with the high *cis*-content (PBC71) showing no crystallinity but increasing the *trans* content shows a higher crystallinity from the appearance of a T_m (Figure 1.11b). The higher crystallinity and ordering of the *trans*

containing polymers also impede chain movement, leading to an increasing T_g as the T_m increases. However, this trend was limited to the thermal properties, with no clear trend between the tensile properties and the *cis/trans* content. The highest *trans* content polymer (PBC12) was the stiffest material (E = 157 ± 7 MPa) but, rather nonintuitively, had the lowest stress at break (σ_b = 17 ± 1 MPa). A mixture of *cis*/*trans* contents (PBC44) displayed both the highest tensile strength (σ_b = 28 ± 1 MPa) and the highest elongation at break (ε_b = 1360 ± 28 %). The authors hypothesised that the *trans*-isomer created regions of high-order and were significantly "harder" than regions of the *cis*-isomer which are "softer". The "harder" *trans*-rich segments are crystalline and require more force to deform. On the other hand, the "softer" amorphous regions can be deformed easier and can undergo strain hardening, or strain-induced crystallisation, as the chains are stretched. This is evidenced by the increasing strength at higher strain (Figure 1.11c). The tensile data suggests a balance of these regions formed from the mixed *cis/trans* content imparts the material with superior strength and elongation compared to either single stereoisomer.

Previous work has demonstrated the importance of backbone stereochemistry on bulk polymer properties. However, there is currently a lack of understanding or a universal model to predict how stereochemistry can influence bulk properties. This is partially a result of traditional polycondensation conditions isomerising stereocenters during polymerisation, besides a historic focus upon polyolefins limiting the scope of polymers that were investigated. Further complications arise from the same stereoisomers displaying opposite trends in different polymer, making predictions for stereochemistry challenging. This research area will become increasingly important as society transitions from plastics derived from crude oil to bio-sourced structures, which typically contain multiple stereocenters.[38, 49, 50]

1.3 The thiol-ene “Click” reaction

Understanding the fundamental relationship between composition and structure of polymers to their bulk properties has required the constant application of novel organic reactions. Utilising the library of organic chemistry has enabled the synthesis of polymers with new functionalities and heteroatoms that can be exploited to achieve unique properties. Continual study and usage of novel organic chemistry in materials science maintains the discovery of more advanced materials and will lead to a better understanding of structure-property relationships.

1.3.1 Thiol-ene introduction

Alkene hydrothiolyation, or thiol-ene, has been an important reaction type since its discovery over a century ago. The addition of a thiol containing compound to an alkene is useful not only as a coupling reaction, but also as a simple way to incorporate a sulfur heteroatom into a structure. Both the alkene and thiol functionality are relatively abundant either naturally or can be obtained from the simple synthetic conversion of a range of functionalities. Usage of this reaction surged since 2007 when thiol-ene gained wide recognition as a “Click” reaction.[51-53] The term “Click” was coined to describe a modular, stereoselective reaction boasting very high yields from mild conditions, with few sensitivities (environmental and functional group *etc.*) from readily available and stable functionalities. Due to these features, “Click” reactions are exceedingly prevalent in polymer and materials chemistry.[54, 55]

Thiol-ene is an umbrella term that encompasses two different reactions with different mechanisms: radical-mediated thiol-ene and thia-Michael addition. The former can occur between any thiol moiety and unhindered alkene in the presence of radicals, whilst the latter requires an electron deficient alkene and typically a base catalyst to occur. Both reaction types fulfil the majority of “Click” criteria and have been recognised as such.[52]

1.3.2 Radical-mediated thiol-ene

The modularity, high conversion, and regioselectivity for the anti-Markovnikov adduct are some of the key features that exemplified the radical-mediated thiol-ene addition as a "Click" reaction. The mechanism itself begins with the generation of a thiyl radical in the initiation step, followed by the addition to an alkene in the propagation step (Figure 1.12). A hydrogen is then abstracted from another thiol to form the product and regenerate another thiyl radical in the chain transfer step. Initiation of this simple reaction is typically achieved through the use of a radical initiator but can also be achieved from thermally or photochemically produced radicals.[56, 57]

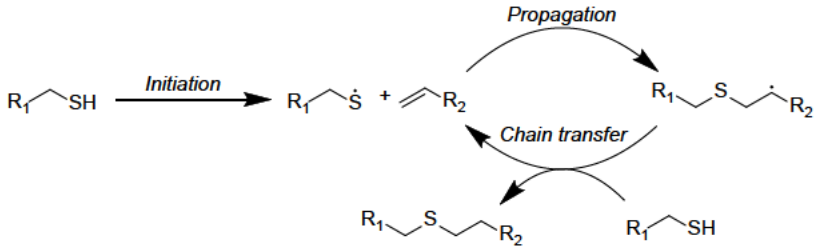


Figure 1.12 Mechanism of the radical-mediated thiol-ene reaction.

The modularity of the -ene structure is one of the most attractive features of this reaction, however this also has a large impact on the reactivity. Typically, a higher electron density on the alkene increases the overall reactivity (Vinyl ether > allyl ether > acrylate), however there remain some exceptions, such as norbornene's unusually high reactivity and, the significantly lower reactivity of methacrylic functionality *vs* the acrylic.[58] The release of bond strain upon thiol addition to the norbornene structure drives its exceptionally high reactivity making it one of the most reactive functionalities to radical thiol-ene. On the other hand, the α-methyl of the methacrylate stabilises the radical intermediate and slows the chain-transfer, or hydrogen abstraction step.

Radical-mediated thiol-ene is not without drawbacks, as previously mentioned, the electronics of the alkene can impact its overall reactivity, even falling below the standards

of the "Click" criteria. Nevertheless, the prevalence of side reactions is the most detrimental aspect to the radical thiol-ene addition. The chaotic character of radicals arises the issue of termination reactions, this can lead to unwanted disulfide formation, homopolymerisation of the alkenes, and even double additions.[59] The prevalence of these termination reactions ultimately disrupts the efficiency of the chain transfer step, consequently impacting the reaction outcome.[56]

Nevertheless, radical thiol-ene is a particular well-used reaction in polymers and other macromolecular technologies. There are some examples of the radical thiol-ene reaction being used to create linear polymers,[60, 61] but generally, the reaction is used for surface functionalisation[62] and networked polymers,[63] including hydrogels[64, 65] and coatings.[66-69]

1.3.3 Nucleophilic thiol-ene – Mechanism

One of the earliest examples of thia-Michael addition was in 1905 by Ruhemann, where 4-phenylbut-3-en-2-one was reacted with thiophenol using a catalytic amount of piperidine (Figure 1.13).[70] This reaction was performed neat, in an open atmosphere and gave a noticeable exotherm upon addition of the catalyst; early indicators of its "Click" properties.

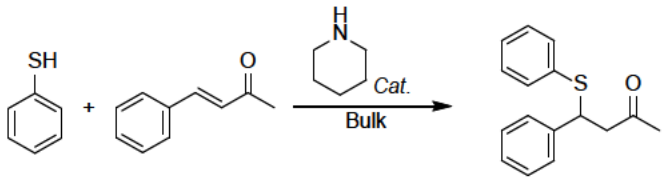


Figure 1.13 Piperidine catalysed thia-Michael addition of thiophenol to 4-phenylbut-3-en-2-one.[70]

The archetypal thia-Michael reaction is a base-catalysed conjugate addition of a thiol to a suitably electron deficient alkene called a Michael acceptor, named after Arthur Michael and his discovery of the conjugate addition.[71] A generated thiolate anion attacks the Michael acceptor at the β-carbon position to form a thia-Michael enolate. This intermediate is then protonated to form the stable thia-Michael adduct. Whilst the

mechanism is a seemingly simple, the initial generation of the thiolate anion and propagation of the reaction itself is considerably more nuanced.

Historically, the use of base catalysis suggested a simple deprotonation formed the thiolate anion. An extensive mechanistic study into the catalysis of thia-Michael addition by Bowman and co-workers in 2010, suggested the deprotonation occurred *via* two different mechanisms.[72] Initially, the influence of primary, secondary and tertiary amines was investigated, due to the extensive use of amine catalysis in thia-Michael addition.[70, 73] Equimolar equivalents of hexyl acrylate and 1-hexanethiol catalysed by hexylamine, di-*n*-propylamine and triethylamine were monitored by real-time FT-IR (Figure 1.14).

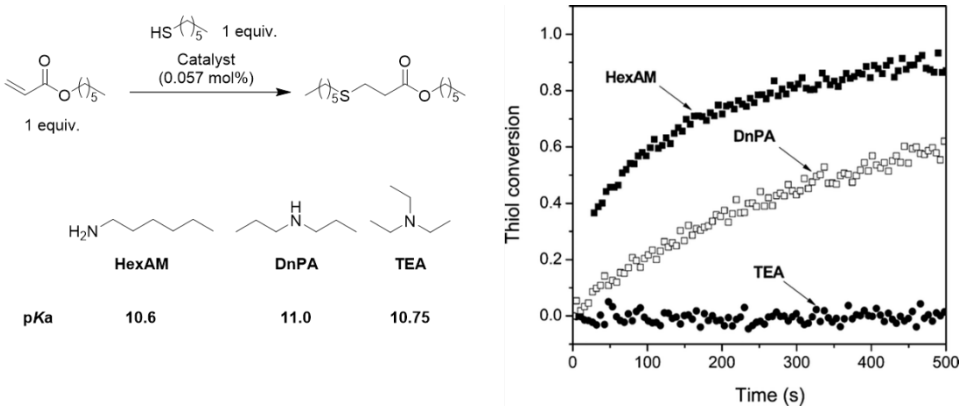
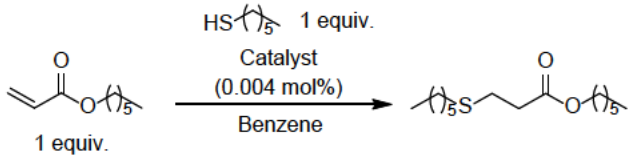


Figure 1.14 Reaction of hexyl acrylate with 1-hexanethiol catalysed by primary, secondary and tertiary amines. Conversion determined using real-time FT-IR monitoring the consumption of the thiol peak at 2570 cm^{-1}. Adapted from ref. 72 with permission. Copyright 2010 American Chemical Society.

The reactivity trend (1° > 2° > 3°) was found to favour the least sterically hindered amine, however, the trend did not correlate with the p*K*a of the catalyst conjugate acid (Figure 1.14). This trend could be explained by steric bulkiness around the amine centre hindering deprotonation but is unlikely to explain the vast difference in reaction rate. It was concluded that the nucleophilicity of the amine catalysts correlated better with the observed reaction rate. The influence of catalyst nucleophilicity was further investigated

using common amine bases: 1,8-diazabicyclo[5.4.0]undec-7-ene (DBU), 1,5-diazabicyclo[4.3.0]non-5-ene (DBN) and N,N,N',N'-tetramethyl 1,8-naphthalenediamine (Proton Sponge®, PS). A similar dependence was found DBN > DBU >> PS, where the more nucleophilic catalysts (DBN and DBU) were multiple magnitudes faster than the non-nucleophilic PS. Given the high reactivity of the nucleophilic amine catalysts, Bowman and co-workers also investigated the use of phosphine catalysts (Table 1.1).[72]



Catalyst	p*K*a	$K_{app}/10^{-4}$ (mol L^{-1} s^{-1})
P(*n*-Pr)$_3$	8.64	1810
PMe_2Ph	6.49	430
$PMePh_2$	4.59	0.987
PPh_3	2.73	0.0125

Table 1.1 Conjugate addition of 1-hexanethiol to hexyl acrylate 2 M in benzene catalysed by various phosphine catalysts. K_{app} measured by real-time FT-IR.[72] 1-hexanethiol p*K*a = 10.6.

Despite the significantly lower basicity of phosphine catalysts, they were profoundly more active than the amine catalysts, requiring lower catalyst loading and dilution in benzene to give measurable rate. The reactivity trend observed (P(*n*-Pr)$_3$ > PMe_2Ph >> $PMePh_2$ > PPh_3) correlated well with the relative nucleophilicity of aryl and alkyl substituted phosphines.[74] It became clear the thia-Michael reaction was likely being catalysed *via* two mechanisms: the first is a typical base deprotonation of the thiol functionality to produce the thiolate nucleophile. The second occurs from the nucleophilic attack of the catalyst to the Michael acceptor generating an enolate intermediate, which then deprotonates a thiol

to form the thiolate anion (Figure 1.15). Once the thiolate is generated, addition to a Michael acceptor regenerates an enolate intermediate that can deprotonate another thiol propagating the reaction.

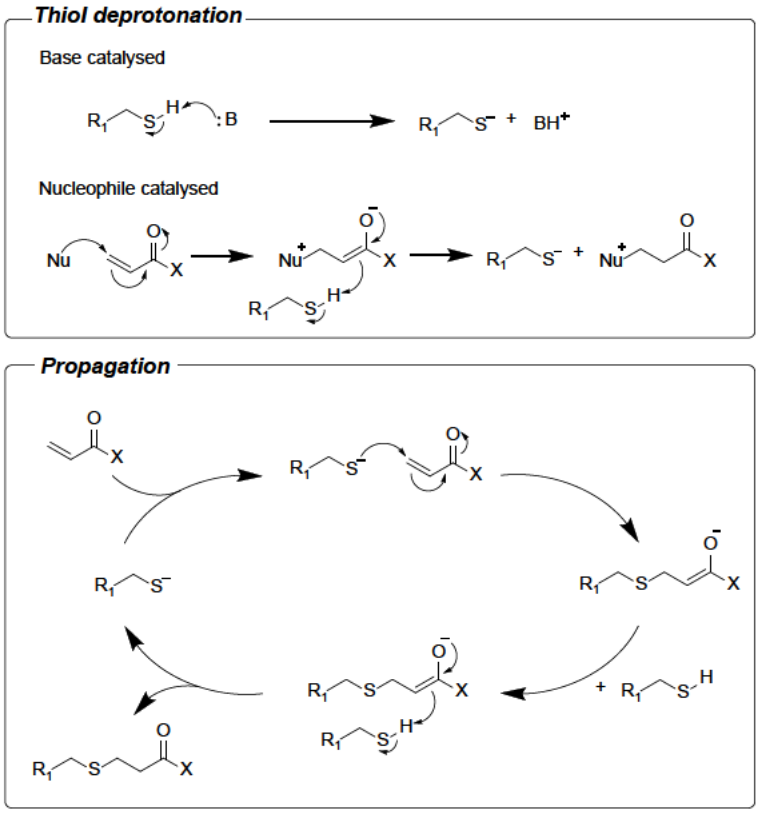


Figure 1.15 The generation of the thiolate anion in a base-catalysed thia-Michael addition (*Top*). Propagation of the base catalysed thia-Michael addition (*Bottom*).

Whilst both of these mechanisms are widely accepted,[75] there were early concerns that the catalyst-Michael conjugate was stable and persisted in the reaction limiting the final yield.[76] However, this has been disproven, with a study demonstrating the near-quantitative liberation of common base catalysts from their catalyst-Michael conjugates (DMAP and DBU) in the presence of thiolate anions (Figure 1.16).[77] This suggested the catalyst-Michael adducts were only transient in nature and the thia-Michael adduct was considerably more stable.

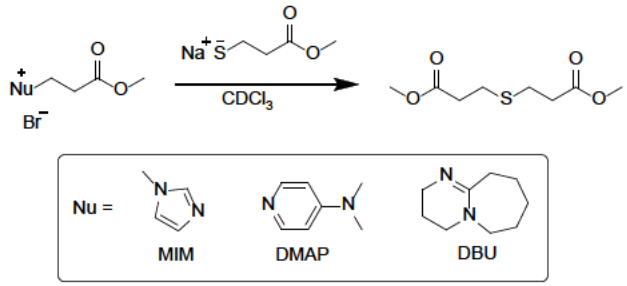


Figure 1.16 Model reaction for investigating the consumption of catalyst-Michael adducts in the presence of a sodium thiolate nucleophile.[77]

Despite their increased nucleophilicity, fears for the unwanted stable aza-Michael addition continues to prevent the use of primary and secondary amines. An investigation into the formation of the by-products only found trace quantities of the undesired aza-Michael addition in a hexylamine catalysed reaction.[78] Measurable quantities of the aza-Michael product (4%) could only be achieved when equimolar or a tenfold excess of the primary amine was used with the thiol and Michael acceptor, yet the thia-Michael adduct still dominated (96%) in both cases.

It is worth noting, that whilst the conversion, reactivity, modularity, and minimal by-product formation of the thia-Michael addition is conducive to the "Click" requirements, thiols and some commonly used phosphine catalysts are both subject to slow oxidation at atmospheric conditions. These side reactions themselves are not competitive with the thia-Michael addition, hence the reaction does not require oxygen-free conditions, but the storage of these reagents typically requires some special handling under an inert atmosphere.

1.3.4 Nucleophilic thiol-ene – Trends in reactivity

The presence of an activated, or electron deficient, alkene is one of the key prerequisites for a thia-Michael addition. There are numerous examples of alkene functionalities that are sufficiently activated to be attacked in a thia-Michael addition. Most common among these are the carbonyl-based species (acrylate, methacrylate, enone, acrylamide,

maleimide, *etc.*) but other uncommon electron-withdrawing functionalities have also been used (sulfonyl-, cyano-, oxazoline). Whilst most of these functionalities are relatively uncommon in nature, they can be grafted to abundant functionalities using simple synthetic modifications (*e.g.* esterification of an alcohol to provide an acrylate). This modularity of the Michael acceptors is a crucial feature that has led to its recognition as a "Click" reaction.

The vast scope of suitable Michael acceptors also influences their reactivity and has been well investigated with several computational and experimental studies.[79-81] One notable study by Du Prez and co-workers investigated the reaction of isooctyl 3-mercaptopropionate to multiple Michael acceptors catalysed by both phosphine and amine compounds.[82] As expected, the vast difference in electrophilicity in the Michael acceptors had a influence on reactivity and a trend was established (Figure 1.17).

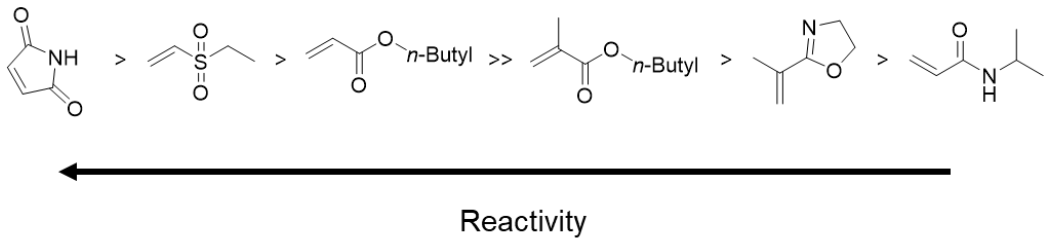


Figure 1.17 Reactivity trend of numerous Michael acceptors to isooctyl 3-mercaptopropionate.[82]

Maleimides are, by far, the most active Michael-acceptor, achieving quantitative yields in less than a minute in uncatalysed reactions. The rest of the Michael acceptors required either amine or phosphine catalysis to achieve the same conversion, but generally proceeded slower than addition to the maleimide. Vinyl sulfone and acrylate functionality also reacted to quantitative yields catalysed with TEA and DMPP (1 mol% loading). However, methacrylate was found to be considerably less active than the acrylate when catalysed by TEA (10% yield after 14 h) but can achieve higher yields using DBU (97%

yield after 24 mins); this has been attributed to the stabilising effect of the α-methyl in the enolate intermediate inhibiting the propagation step.[72] *N*-isopropylacrylamide and isopropenyl oxazoline are the poorest Michael acceptors, both achieving less than 50% yield even on long reaction times (> 10 h). These poor reactivities have been attributed to the delocalisation of the activating group, which leads to a lower electron withdrawing ability upon the alkene group.

Thiols, or mercaptans, are excellent nucleophiles on account of their low p*K*a's that enable easy deprotonation to form thiolate anions. This is a result of the size of the sulfur atom that enables excellent stabilisation of a negative charge. Despite their excellent nucleophilicity, the rate of Michael addition is impacted by the thiol substitution (1°, 2° and 3°). A recent study by Bowman and co-workers investigated the reaction rate of hexylacrylate to *n*-, *sec*-, *tert*-butylthiol and found a significant reduction in reaction rate and final conversion when using more substituted thiols.[83] The increasing steric bulk of substituted thiols hinders deprotonation of the thiol in the deprotonation and propagation steps.

It is worth noting that the thia-Michael addition displays reversibility, with an early study noting the prevalence of bond dissociation of thia-Michael adducts upon heating.[84] Soon after, a general trend for increasing bond reversibility was established against the Michael acceptor (ketone > nitrile > amide), and correlated well with the acidity of the α-hydrogen to the electron withdrawing functionality.[85] Much later, the reversibility was found to be highly dependent on pH, where a Michael adduct in a pH 8 solution could equilibrate in less than 30 mins but became irreversible at low pH.[86] Most of the mechanistic study into the reversibility of Michael-adducts has been specific to biological applications due to its activity at physiological conditions.[87] As such, there is limited understanding in substrate effects on the reversibility of thia-Michael bonds, but highlights a future area of study.

1.4 Thia-Michael addition in polymer materials

The “Click” thia-Michael addition is an extraordinarily versatile reaction and is extensively adopted in numerous applications. As such, the area is too extensive to provide an exhaustive account, but many reviews cover a significant portion of the area.[88-90]

1.4.1 Linear polymers

One of the earliest uses of thia-Michael addition was to create linear polymers *via* step-growth polyaddition. The high conversion of the “Click” reaction is particularly advantageous for step-growth polymerisation, but the key feature of the thia-Michael addition is the breadth of suitable Michael acceptors. One early example reacted difunctional acrylamides with alkyl dithiols in the presence of a base to form an alternating linear polyamide.[91] This was further adapted to poly-imides and -esters using difunctional maleate and maleimide containing monomers.[92] Generally, these thermoplastics were found to be semi-crystalline with increasing melting temperatures (T_m = 100–192 °C) as the length of the dithiol linker decreased (Figure 1.18).[93, 94] Unfortunately, these maleate/maleic end-group functionalities have a tendency to homopolymerise and crosslink in the presence of a base,[95] which was later utilised for *in situ* crosslinking to form rubbery network materials.[96]

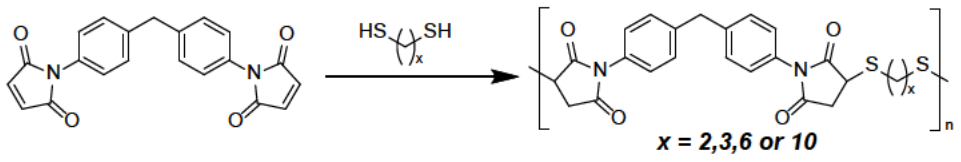


Figure 1.18 The polyaddition of a *bis*-maleimide with various dithiol linkers to form an alternating linear polymer.[94]

The vinyl sulfone Michael acceptor is a relatively under-utilised functionality in nucleophilic thiol-ene addition. However, it has found application in the area of optics as a consequence of the incorporation of sulfur atoms, which is particularly relevant to optical

applications due to their high atomic refraction.[97] Ueda and co-workers have reported a series of high sulfur content polymers synthesised from the polyaddition of dithiols to divinyl sulfone (DVS).[98-100] The linear alternating polymers demonstrate good refractive indexes. However, the research in this area is somewhat limited, highlighting a potential opportunity to utilise the vinyl sulfone moiety for further optics applications.

The most commonly used Michael acceptor for thia-Michael addition in linear polymers is the acrylate.[101] The combination of simple synthetic methods to afford the acrylic functionality and the high reactivity to the thiol-ene reaction has made it increasingly popular. Additionally, polymers made from the thia-Michael addition of acrylates are in-built with a hydrolysable ester, providing functionality that can degrade in environmental conditions.[102] One key application of thia-Michael addition is the incorporation of bio-sourced derivatives, which occasionally lack the same reactivity and functionality to be used in commercial polymerisation routes.[103] For example, isosorbide is a commonly touted natural derivative that can be employed in polymer materials, however, the hydroxy functionalities have asymmetric and poor reactivity, limiting its use in a commercial setting.[104, 105] Nevertheless, by using thiol-ene polyaddition to incorporate the structure, this issue can be avoided. Long and co-workers found that isosorbide di-acrylate can polymerise with various dithiols to afford high molecular weight materials (> 40 kg·mol^{-1}).[106] All synthesised isosorbide polymers were amorphous, but the T_g could be carefully tuned (ΔT_g = 25 °C) by altering the dithiol linker (Figure 1.19). Another popular natural derivative that has also been polymerised using the nucleophilic thiol-ene addition is hydroxylmethylfurfural (HMF).[107] The T_g of the HMF-containing polymers could also be manipulated by altering the length of the dithiol (Figure 1.19).[108]

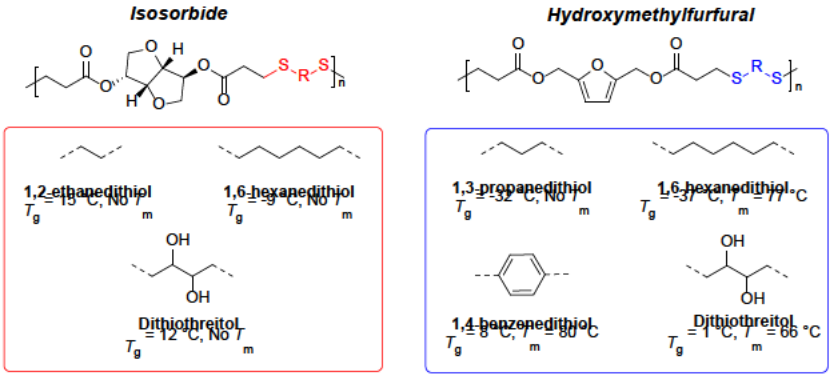


Figure 1.19 Thermal properties of isosorbide and hydroxymethylfurfural based linear polymers from the polyaddition of a functional diacrylate monomers with various dithiol linkers.[106, 108]

Whilst this technique can be used to create high molecular weight polymers containing HMF, it can also be used to create segmented, or block, co-polymers. Using a similar procedure, oligomeric HMF with thiol end-groups could be synthesised using a slight excess of the dithiol monomer. This thiol-ending polymer could be reacted with acrylate ending PLA polymers to yield an ABA-type polymer.[109] The polymer displayed thermal properties characteristic of ABA architectures, namely two T_gs representative of each polymer block can be observed. One above ambient temperature (T_g = 44 °C) for PLA and one below (T_g = -27 °C) for the oligomeric HMF unit. ABA architectures are useful materials as they can combine the stiffness of the "glassy" section with the extensibility of the "soft" section, which is absent in fully "glassy" materials.

It has become increasingly prevalent to use nucleophilic thiol-ene polyaddition to create oligomers bearing a reactive functionality at the end groups for block co-polymers, nano particles and radically curable resins.[110-118] A particularly memorable application of the nucleophilic thiol-ene addition created an oligomeric polymer containing an azo-backbone, which could be fabricated into an ABA polymer by coupling PEG-acrylates to the thiol end-groups (Figure 1.20).[119] These ABA architectures can be assembled into micelles and nanoparticles with the azo-linkage at the core. The azo linkage is susceptible to homolytic

dissociation upon heating and UV activation, hence the particles and micelles could be broken on-demand through the azo-bond fission upon heating.[120] The mild conditions of the thia-Michael addition enabled the synthesis of these ABA polymers and subsequent assembly into micelles without degrading the bond, highlighting the potential to fabricate other sensitive groups into the polymer for further applications.

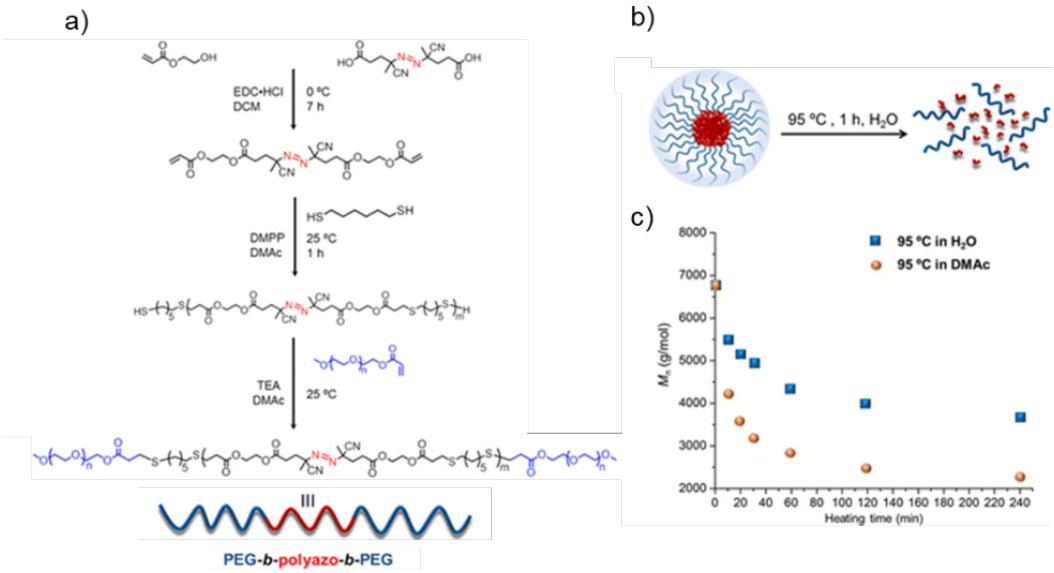


Figure 1.20 a) Synthetic Route to azo monomer of triblock co-polymer PEG-*b*-polyazo-*b*-PEG by One-Pot Step-Growth Polymerisation b) Diagram of azo-containing micelle degrading upon heating c) Decrease in M_n determined by GPC of PEG-*b*-polyazo-*b*-PEG heated in water or dimethylacetamide. Adapted from ref. 74 with permission. Copyright 2016 American Chemical Society.

Functional group tolerance and chemoselectivity are fundamental requirements for a "Click" reaction that the thia-Michael addition satisfies. Its selectivity for activated alkenes has been exploited in several applications, where a polymer/monomer containing an activated alkene can be reacted selectively whilst a present un-activated alkene remains untouched.[121, 122] This can be a convenient method to achieve sequential reactions in one-pot to yield polymers with compositional control.[123] This selectivity is not only restricted to Michael acceptors *vs* un-activated alkenes and alkynes, but an emerging area is

exploiting the reactivity differences between distinct Michael acceptors. As mentioned in the previous section and exemplified in a number of studies, the reaction rate is heavily dependent on the Michael acceptor.[124] For example, a mixture of methyl methacrylate and methyl acrylate reacted with a single equivalent of thiol yields the thia-acrylate product at a quantity 200 times greater than the thia-methacrylate product.[125, 126] This reactivity discrepancy was exploited by Long and co-workers to create segmented polymers with the acrylate terminating units reacting, almost selectively, before the methacrylate units (Figure 1.21).[127] Whilst these polymers were segmented, the material lacked phase separation typical of hard/soft segmented thermoplastics. Nevertheless, the use of different Michael acceptors for selective thiol addition highlights another feature that can be exploited in future applications.

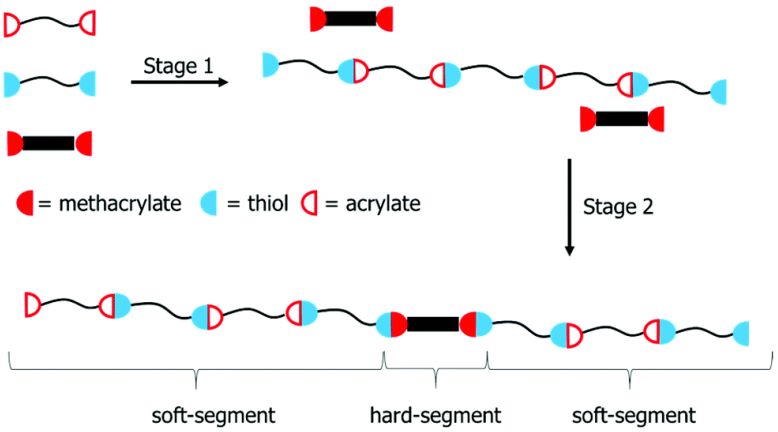


Figure 1.21 Diagram illustrating how the selective reactivity of the acrylate functionality over methacrylate affords segmented linear polymers. Reproduced from ref. 127 with permission from the Royal Society of Chemistry.

1.4.2 Networks

Thia-Michael addition is used extensively in networked polymers and has found applications in hydrogels[128-131], photocurable resins[132], coatings[133], nanoparticle assembly[134-136], actuators[137] and thermosets.[138, 139]

However, key emerging areas are utilising the reversibility of thia-Michael addition, one area, in particular, is Covalently adaptable networks (CANs).[140] Networked materials are typically fixed materials and lack an ability to reshape or repair after the material is damaged. Dynamic bond containing networks, or CANs, impart the network with reversible bonds that can be broken and reformed upon exposure to a stimulus such as heat, light[141] or mechanical force.[142] This can be used to re-heal material properties[143], reverse material aging[144] and even remould the material into a distinctly new shape.[145] Konkolewicz and co-workers demonstrated a thermoset laden with thiol-acrylate Michael bonds could be thermally healed to achieve comparable mechanical properties to the virgin material at 90 °C.[146] Later, the platform was adapted to contain a thiol-maleimide adduct, which is known to dissociate under heating and aqueous conditions such as high pH.[147, 148] The soft network was fabricated by radical mediated homo-polymerisation of acrylate and diacrylate monomers containing the thiol-maleimide bond (Figure 1.22).[149] A cut sample could be healed upon exposure to high pH values for shorter periods of time, whilst exposure to heat (90 °C) required significantly longer to achieve the same healing efficiency. The authors also created a control network that lacked the dynamic bond. Whilst the healing efficiency was considerably poorer than the dynamic network, the material achieved some healing, likely driven by hydrogen bonding interactions from the 2-hydroxyethyl acrylate. Nevertheless, the dynamic thia-Michael bond has proven significant reversibility under thermal and base stimulus which has translated well to network materials. Further study in the area will provide a better understanding and push the boundaries of what the dynamic bond can achieve.

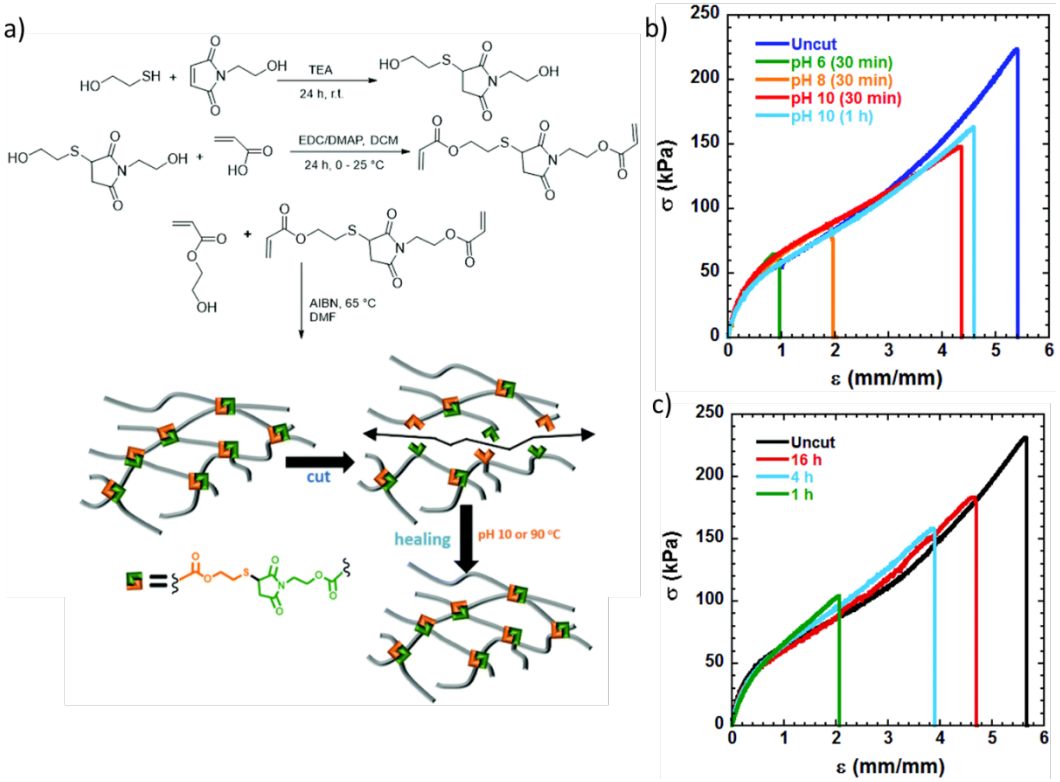


Figure 1.22 a) Synthetic scheme of the thiol-maleimide crosslinker and subsequent crosslinking. Diagram demonstrating the material healing at elevated pH or temperature. b) Stress *vs* strain curve for the self-healing properties of the thiol-maleimide material in different pH buffer solutions. c) Stress *vs* strain curve for the self-healing properties of the thiol-maleimide material at 90 °C. Adapted from ref. 149 with permission from the Royal society of Chemistry.

1.5 Conclusion

Since the initial discovery of polymers as materials, momentous advances in our understanding of polymers and how structure and composition influence their bulk behaviour. In parallel, synthetic procedures and characterisation techniques have provided insight into designing better, stronger materials that satisfied our ever-increasing mechanical demands. Regrettably, our efforts predominately focussed upon techniques relating to polyolefins and other non-degradable materials derived from crude oil.

In the past few decades, there has been a growing focus on bio-sourced derivatives and how they can be used to create competitive polymers to today's petrol-based plastics. Derivatives from nature are rich in stereochemistry and typically have a complex 3D structure that can be exploited to create polymers with unique properties. Our historical focus on polyolefins revealed that control of the simplest stereo-centres offers extensive manipulation of bulk properties. Therefore, it is reasonable to assume that a similar level of control applied would offer a greater manipulation of properties. Currently, our understanding of bio-sourced structures and their influence on properties is limited owing to our focus on olefin systems and synthetic difficulties in creating polymers that bear these naturally-sourced building blocks.

The development of "Click" chemistry has the potential to bridge these divides by offering control, high reactivity, and functional group tolerance. Thia-Michael addition has proven a formidable tool in creating polymer materials using mild conditions. It is even used to create polymers from bio-sourced, stereochemistry-containing derivatives where traditional synthetic routes have proven challenging. The latest advancements in thia-Michael addition have also shown exceptional chemoselectivity that can be exploited to fabricate sequence-controlled polymers. Adapting "Click" reactions to impart, and more importantly, control, polymers with stereochemistry is a clear path to further our insight into structure-property relationships. Through a better understanding, chemists and materials scientists can develop better, more versatile plastics than the current petrol-derived polyolefins.

1.6 References

1. W. Denissen, J. M. Winne and F. E. Du Prez, Vitrimers: permanent organic networks with glass-like fluidity, *Chem. Sci.*, **2016**, *7*, 30-38.
2. D. T. Gentekos, R. J. Sifri and B. P. Fors, Controlling polymer properties through the shape of the molecular-weight distribution, *Nat. Rev. Mater.*, **2019**, *4*, 761-774.
3. G. Sarkhel, A. Banerjee and P. Bhattacharya, Rheological and Mechanical Properties of LDPE/HDPE Blends, *Polym-Plast. Technol.*, **2006**, *45*, 713-718.

4. Q. Fu, Y. Men and G. Strobl, Understanding of the tensile deformation in HDPE/LDPE blends based on their crystal structure and phase morphology, *Polymer*, **2003**, *44*, 1927-1933.
5. A. Peacock, *Handbook of polyethylene: structures: properties, and applications*, CRC press, **2000**.
6. J. E. Mark, *Physical properties of polymers handbook*, Springer, **2007**.
7. Y. Kong and J. N. Hay, The measurement of the crystallinity of polymers by DSC, *Polymer*, **2002**, *43*, 3873-3878.
8. Y. Kong and J. N. Hay, The enthalpy of fusion and degree of crystallinity of polymers as measured by DSC, *Eur. Polym. J.*, **2003**, *39*, 1721-1727.
9. M. Munaro and L. Akcelrud, Correlations between composition and crystallinity of LDPE/HDPE blends, *J. Polym. Res.*, **2008**, *15*, 83-88.
10. E. Zhuravlev, J. W. P. Schmelzer, B. Wunderlich and C. Schick, Kinetics of nucleation and crystallization in poly(ε-caprolactone) (PCL), *Polymer*, **2011**, *52*, 1983-1997.
11. C. E. Koning, L. Teuwen, A. De Plaen and J. P. Mercier, Enhancement of the crystallinity of a thermoplastic polyimide, *Polymer*, **1996**, *37*, 5619-5625.
12. A. A. Natu, E. A. Lofgren and S. A. Jabarin, Effect of morphology on barrier properties of poly(ethylene terephthalate), *Polym. Eng. & Sci.*, **2005**, *45*, 400-409.
13. J. P. Jog, Crystallization of Polyethyleneterephthalate, *J. Macromol. Sci.,* **1995**, *35*, 531-553.
14. D. Mileva, D. Tranchida and M. Gahleitner, Designing polymer crystallinity: An industrial perspective, *Polym. Crystallization*, **2018**, *1*, e10009.
15. A. M. Striegel, Influence of Anomeric Configuration on Mechanochemical Degradation of Polysaccharides: Cellulose versus Amylose, *Biomacromolecules*, **2007**, *8*, 3944-3949.
16. H. Miyamoto, M. Ago, C. Yamane, M. Seguchi, K. Ueda and K. Okajima, Supermolecular structure of cellulose/amylose blends prepared from aqueous NaOH solutions and effects of amylose on structural formation of cellulose from its solution, *Carbohydr. Res.*, **2011**, *346*, 807-814.
17. E. Kent and F. Swinney, Properties and applications of trans-1, 4-polyisoprene, *Ind. Eng. Chem. Prod. RD*, **1966**, *5*, 134-138.
18. H. Schilder, A. Goodman and W. Aldrich, The thermomechanical properties of gutta-percha: I. The compressibility of gutta-percha, *Or. Surg. Or. Med. Or. Pa.*, **1974**, *37*, 946-953.
19. A. Goodman, H. Schilder and W. Aldrich, The thermomechanical properties of gutta-percha: II. The history and molecular chemistry of gutta-percha, *Or. Surg. Or. Med. Or. Pa.*, **1974**, *37*, 954-961.
20. P. Boochathum and S. Chiewnawin, Vulcanization of cis- and trans-polyisoprene and their blends: crystallization characteristics and properties, *Eur. Polym. J.*, **2001**, *37*, 429-434.
21. C. W. Bunn and W. L. Bragg, Molecular structure and rubber-like elasticity - III. Molecular movements in rubber-like polymers, *P. Roy. Soc. Lond. A. Mat.*, **1942**, *180*, 82-99.
22. W. Cooper and G. Vaughan, Crystallization of gutta percha and synthetic trans-1,4-Polyisoprenes, *Polymer*, **1963**, *4*, 329-340.
23. G. W. Coates and R. M. Waymouth, Oscillating Stereocontrol: A Strategy for the Synthesis of Thermoplastic Elastomeric Polypropylene, *Science*, **1995**, *267*, 217.
24. H. Staudinger, A. A. Ashdown, M. Brunner, H. A. Bruson and S. Wehrli, Über hochpolymere Verbindungen. 22. Mitteilung. Über die Konstitution des Poly-indens, *Helv. Chim. Acta*, **1929**, *12*, 934-957.
25. G. Natta, P. Pino, P. Corradini, F. Danusso, E. Mantica, G. Mazzanti and G. Moraglio, Crystalline high polymers of α-olefins, *J. Am. Chem. Soc.*, **1955**, *77*, 1708-1710.

26. J. Karger-Kocsis, *Polypropylene: An A-Z reference*, ed. J. Karger-Kocsis, Springer Netherlands, Dordrecht, **1999**.
27. G. W. Coates, Precise Control of Polyolefin Stereochemistry Using Single-Site Metal Catalysts, *Chem. Rev.*, **2000**, *100*, 1223-1252.
28. G. Natta, Properties of isotactic, atactic, and stereoblock homopolymers, random and block copolymers of α-olefins, *J. Polym. Sci.*, **1959**, *34*, 531-549.
29. G. W. Coates, P. D. Hustad and S. Reinartz, Catalysts for the Living Insertion Polymerization of Alkenes: Access to New Polyolefin Architectures Using Ziegler–Natta Chemistry, *Angew. Chem. Int. Ed.*, **2002**, *41*, 2236-2257.
30. G. J. Domski, J. M. Rose, G. W. Coates, A. D. Bolig and M. Brookhart, Living alkene polymerization: New methods for the precision synthesis of polyolefins, *Prog. Polym. Sci.*, **2007**, *32*, 30-92.
31. F. Karasz, H. Bair and J. O'reilly, Thermal properties of atactic and isotactic polystyrene, *J. Phys. Chem.*, **1965**, *69*, 2657-2667.
32. G. Natta, P. Corradini and I. Bassi, Crystal structure of isotactic polystyrene, *Il Nuovo Cimento (1955-1965)*, **1960**, *15*, 68-82.
33. P. Van Wouwe, M. Dusselier, E. Vanleeuw and B. Sels, Lactide Synthesis and Chirality Control for Polylactic acid Production, *ChemSusChem*, **2016**, *9*, 907-921.
34. R. Mehta, V. Kumar, H. Bhunia and S. N. Upadhyay, Synthesis of Poly(Lactic Acid): A Review, *J. Macromol. Sci. Polymer Rev.*, **2005**, *45*, 325-349.
35. T. M. Ovitt and G. W. Coates, Stereochemistry of Lactide Polymerization with Chiral Catalysts: New Opportunities for Stereocontrol Using Polymer Exchange Mechanisms, *J. Am. Chem. Soc.*, **2002**, *124*, 1316-1326.
36. P. Hormnirun, E. L. Marshall, V. C. Gibson, A. J. P. White and D. J. Williams, Remarkable Stereocontrol in the Polymerization of Racemic Lactide Using Aluminum Initiators Supported by Tetradentate Aminophenoxide Ligands, *J. Am. Chem. Soc.*, **2004**, *126*, 2688-2689.
37. B. M. Chamberlain, M. Cheng, D. R. Moore, T. M. Ovitt, E. B. Lobkovsky and G. W. Coates, Polymerization of Lactide with Zinc and Magnesium β-Diiminate Complexes: Stereocontrol and Mechanism, *J. Am. Chem. Soc.*, **2001**, *123*, 3229-3238.
38. J. C. Worch, H. Prydderch, S. Jimaja, P. Bexis, M. L. Becker and A. P. Dove, Stereochemical enhancement of polymer properties, *Nat. Rev. Chem.*, **2019**, *3*, 514-535.
39. I. Engelberg and J. Kohn, Physico-mechanical properties of degradable polymers used in medical applications: A comparative study, *Biomaterials*, **1991**, *12*, 292-304.
40. L. Fambri, A. Pegoretti, R. Fenner, S. D. Incardona and C. Migliaresi, Biodegradable fibres of poly(l-lactic acid) produced by melt spinning, *Polymer*, **1997**, *38*, 79-85.
41. C. C. Chu, Hydrolytic degradation of polyglycolic acid: Tensile strength and crystallinity study, *J. Appl. Polym. Sci.*, **1981**, *26*, 1727-1734.
42. A. M. Saxman, R. Liepins and M. Aldissi, Polyacetylene: Its synthesis, doping and structure, *Prog. Polym. Sci.*, **1985**, *11*, 57-89.
43. C. I. Simionescu and V. Percec, Progress in polyacetylene chemistry, *Prog. Polym. Sci.*, **1982**, *8*, 133-214.
44. H. Shirakawa and S. Ikeda, Preparation and morphology of as-prepared and highly stretch-aligned polyacetylene, *Synth. Met.*, **1980**, *1*, 175-184.
45. Y. Yu, Z. Wei, X. Leng and Y. Li, Facile preparation of stereochemistry-controllable biobased poly(butylene maleate-co-butylene fumarate) unsaturated copolyesters: a chemoselective polymer platform for versatile functionalization via aza-Michael addition, *Polym. Chem.*, **2018**, *9*, 5426-5441.

46. T. E. Sandhya, C. Ramesh and S. Sivaram, Copolyesters Based on Poly(butylene terephthalate)s Containing Cyclohexyl and Cyclopentyl Ring: Effect of Molecular Structure on Thermal and Crystallization Behavior, *Macromolecules*, **2007**, *40*, 6906-6915.
47. D. J. Brunelle and T. Jang, Optimization of poly(1,4-cyclohexylidene cyclohexane-1,4-dicarboxylate) (PCCD) preparation for increased crystallinity, *Polymer*, **2006**, *47*, 4094-4104.
48. F. Liu, J. Zhang, J. Wang, X. Liu, R. Zhang, G. Hu, H. Na and J. Zhu, Soft segment free thermoplastic polyester elastomers with high performance, *J. Mater. Chem. A*, **2015**, *3*, 13637-13641.
49. F. Della Monica and A. W. Kleij, From terpenes to sustainable and functional polymers, *Polym. Chem.*, **2020**, *11*, 5109-5127.
50. S. Pandey, B. S. Rajput and S. H. Chikkali, Refining plant oils and sugars to platform chemicals, monomers, and polymers, *Green Chem.*, **2021**, *23*, 4255-4295.
51. H. C. Kolb, M. G. Finn and K. B. Sharpless, Click Chemistry: Diverse Chemical Function from a Few Good Reactions, *Angew. Chem. Int. Ed.*, **2001**, *40*, 2004-2021.
52. A. Gress, A. Völkel and H. Schlaad, Thio-Click Modification of Poly[2-(3-butenyl)-2-oxazoline], *Macromolecules*, **2007**, *40*, 7928-7933.
53. A. Dondoni, The Emergence of Thiol–Ene Coupling as a Click Process for Materials and Bioorganic Chemistry, *Angew. Chem. Int. Ed.*, **2008**, *47*, 8995-8997.
54. A. B. Lowe, Thiol–ene "click" reactions and recent applications in polymer and materials synthesis: a first update, *Polym. Chem.*, **2014**, *5*, 4820-4870.
55. T. O. Machado, C. Sayer and P. H. H. Araujo, Thiol-ene polymerisation: A promising technique to obtain novel biomaterials, *Eur. Polym. J.*, **2017**, *86*, 200-215.
56. S. P. S. Koo, M. M. Stamenović, R. A. Prasath, A. J. Inglis, F. E. Du Prez, C. Barner-Kowollik, W. Van Camp and T. Junker, Limitations of radical thiol-ene reactions for polymer–polymer conjugation, *J. Polym. Sci. A Polym. Chem.*, **2010**, *48*, 1699-1713.
57. N. B. Cramer, J. P. Scott and C. N. Bowman, Photopolymerizations of Thiol−Ene Polymers without Photoinitiators, *Macromolecules*, **2002**, *35*, 5361-5365.
58. C. E. Hoyle, T. Y. Lee and T. Roper, Thiol–enes: Chemistry of the past with promise for the future, *J. Polym. Sci. A Polym. Chem.*, **2004**, *42*, 5301-5338.
59. L.-T. T. Nguyen, J. Devroede, K. Plasschaert, L. Jonckheere, N. Haucourt and F. E. Du Prez, Providing polyurethane foams with functionality: a kinetic comparison of different "click" and coupling reaction pathways, *Polym. Chem.*, **2013**, *4*, 1546-1556.
60. C. R. Morgan, F. Magnotta and A. D. Ketley, Thiol/ene photocurable polymers, *J. Polym. Sci. Polym. Chem. Ed.*, **1977**, *15*, 627-645.
61. E. Kobayashi., T. Obata, S. Aoshima, J. Furukawa, Polyaddition of Dithiol Compounds to Diethynyl Compounds: Kinetics of the Model Addition Reaction of Thiophenol to Ethynylbenzene, *Polym. J.,* **1990**, *22*, 1035-1042.
62. D. Sticker, R. Geczy, U. O. Häfeli and J. P. Kutter, Thiol–Ene Based Polymers as Versatile Materials for Microfluidic Devices for Life Sciences Applications, *ACS Appl. Mater. Interfaces*, **2020**, *12*, 10080-10095.
63. E. A. Hoff, G. X. De Hoe, C. M. Mulvaney, M. A. Hillmyer and C. A. Alabi, Thiol–Ene Networks from Sequence-Defined Polyurethane Macromers, *J. Am. Chem. Soc.*, **2020**, *142*, 6729-6736.
64. P. M. Kharkar, M. S. Rehmann, K. M. Skeens, E. Maverakis and A. M. Kloxin, Thiol–ene Click Hydrogels for Therapeutic Delivery, *ACS Biomater. Sci. Eng.*, **2016**, *2*, 165-179.
65. H. Shih and C.-C. Lin, Cross-Linking and Degradation of Step-Growth Hydrogels Formed by Thiol–Ene Photoclick Chemistry, *Biomacromolecules*, **2012**, *13*, 2003-2012.

66. B. Wei, L. Ouyang, J. Liu and D. C. Martin, Post-polymerization functionalization of poly(3,4-propylenedioxythiophene) (PProDOT) via thiol–ene “click” chemistry, *J. Mater. Chem. B*, **2015**, *3*, 5028-5034.
67. A. Pogantsch, S. Rentenberger, G. Langer, J. Keplinger, W. Kern and E. Zojer, Tuning the Electroluminescence Color in Polymer Light-Emitting Devices Using the Thiol-Ene Photoreaction, *Adv. Funct. Mater.*, **2005**, *15*, 403-409.
68. O. D. McNair, B. J. Sparks, A. P. Janisse, D. P. Brent, D. L. Patton and D. A. Savin, Highly Tunable Thiol–Ene Networks via Dual Thiol Addition, *Macromolecules*, **2013**, *46*, 5614-5621.
69. C. Resetco, B. Hendriks, N. Badi and F. Du Prez, Thiol–ene chemistry for polymer coatings and surface modification – building in sustainability and performance, *Mater. Horizons*, **2017**, *4*, 1041-1053.
70. S. Ruhemann, V.—The combination of mercaptans with olefinic ketonic compounds, *J. Chem. Soc., Trans.*, **1905**, *87*, 17-25.
71. A. Michael, Ueber die Addition von Natriumacetessig- und Natriummalonsäureäthern zu den Aethern ungesättigter Säuren, *J. Prakt. Chem.*, **1887**, *35*, 349-356.
72. J. W. Chan, C. E. Hoyle, A. B. Lowe and M. Bowman, Nucleophile-Initiated Thiol-Michael Reactions: Effect of Organocatalyst, Thiol, and Ene, *Macromolecules*, **2010**, *43*, 6381-6388.
73. K. Sanui and N. Ogata, The Catalytic Effect of Alcohol and Mercaptan on the Michael Reaction of Acrylates, *Bull. Chem. Soc. Jpn.*, **1967**, *40*, 1727-1727.
74. W. A. Henderson Jr and S. A. Buckler, The nucleophilicity of phosphines, *J. Am. Chem. Soc.*, **1960**, *82*, 5794-5800.
75. G. B. Desmet, M. K. Sabbe, D. R. D'Hooge, P. Espeel, S. Celasun, G. B. Marin, F. E. Du Prez and M.-F. Reyniers, Thiol-Michael addition in polar aprotic solvents: nucleophilic initiation or base catalysis?, *Polym. Chem.*, **2017**, *8*, 1341-1352.
76. G.-Z. Li, R. K. Randev, A. H. Soeriyadi, G. Rees, C. Boyer, Z. Tong, T. P. Davis, C. R. Becer and D. M. Haddleton, Investigation into thiol-(meth)acrylate Michael addition reactions using amine and phosphine catalysts, *Polym. Chem.*, **2010**, *1*, 1196-1204.
77. V. Drogkaris and B. H. Northrop, Byproducts formed During Thiol-Acrylate Reactions Promoted by Nucleophilic Aprotic Amines: Persistent or Reactive?, *ChemPlusChem*, **2020**, *85*, 2466-2474.
78. S. H. Frayne and B. H. Northrop, Evaluating Nucleophile Byproduct Formation during Phosphine- and Amine-Promoted Thiol–Methyl Acrylate Reactions, *J. Org. Chem.*, **2018**, *83*, 10370-10382.
79. A. Böhme, A. Laqua and G. Schüürmann, Chemoavailability of Organic Electrophiles: Impact of Hydrophobicity and Reactivity on Their Aquatic Excess Toxicity, *Chem. Res. Toxicol.*, **2016**, *29*, 952-962.
80. D. S. Allgäuer, H. Jangra, H. Asahara, Z. Li, Q. Chen, H. Zipse, A. R. Ofial and H. Mayr, Quantification and Theoretical Analysis of the Electrophilicities of Michael Acceptors, *J. Am. Chem. Soc.*, **2017**, *139*, 13318-13329.
81. S. Huang, K. Kim, G. M. Musgrave, M. Sharp, J. Sinha, J. W. Stansbury, C. B. Musgrave and C. N. Bowman, Determining Michael acceptor reactivity from kinetic, mechanistic, and computational analysis for the base-catalyzed thiol-Michael reaction, *Polym. Chem.*, **2021**, *12*, 3619-3628.
82. L.-T. T. Nguyen, M. T. Gokmen and F. E. Du Prez, Kinetic comparison of 13 homogeneous thiol–X reactions, *Polym. Chem.*, **2013**, *4*, 5527-5536.
83. K. F. Long, H. Wang, T. T. Dimos and C. N. Bowman, Effects of Thiol Substitution on the Kinetics and Efficiency of Thiol-Michael Reactions and Polymerizations, *Macromolecules*, **2021**, *54*, 3093-3100.

84. C. F. H. Allen and G. P. Happ, THE THERMAL REVERSIBILITY OF THE MICHAEL REACTION: I. NITRILES, *Can. J. Chem.*, **1964**, *42*, 641-649.
85. C. F. H. Allen and W. J. Humphlett, THE THERMAL REVERSIBILITY OF THE MICHAEL REACTION: V. THE EFFECT OF THE STRUCTURE OF CERTAIN THIOL ADDUCTS ON CLEAVAGE, *Can. J. Chem.*, **1966**, *44*, 2315-2321.
86. T. J. Schmidt, G. Lyß, H. L. Pahl and I. Merfort, Helenanolide type sesquiterpene lactones. Part 5: The role of glutathione addition under physiological conditions, *Biorg. Med. Chem.*, **1999**, *7*, 2849-2855.
87. B. Shi and M. F. Greaney, Reversible Michael addition of thiols as a new tool for dynamic combinatorial chemistry, *Chem. Commun.*, **2005**, 886-888.
88. B. D. Mather, K. Viswanathan, K. M. Miller and T. E. Long, Michael addition reactions in macromolecular design for emerging technologies, *Prog. Polym. Sci.*, **2006**, *31*, 487-531.
89. D. P. Nair, M. Podgórski, S. Chatani, T. Gong, W. Xi, C. R. Fenoli and C. N. Bowman, The Thiol-Michael Addition Click Reaction: A Powerful and Widely Used Tool in Materials Chemistry, *Chem. Mater.*, **2014**, *26*, 724-744.
90. C. E. Hoyle and C. N. Bowman, Thiol–Ene Click Chemistry, *Angew. Chem. Int. Ed.*, **2010**, *49*, 1540-1573.
91. D. L. Murfin, K. Hayashi and L. E. Miller, N,N'-(disubstitutedmethylene)bisacrylamides: Preparation and polymerization, *J. Polym. Sci. A1*, **1970**, *8*, 1967-1980.
92. N. D. Ghatge and R. A. N. Murthy, Polyimidothioether polymers, *Polymer*, **1981**, *22*, 1250-1256.
93. J. E. White and M. D. Scaia, Polymerization of N,N'-bismaleimido-4,4'-diphenylmethane with arenedithiols. Synthesis of some new polyimidosulphides, *Polymer*, **1984**, *25*, 850-854.
94. J. V. Crivello, Polyimidothioethers, *J. Polym. Sci., Polym. Chem. Ed.*, **1976**, *14*, 159-182.
95. Y. Nakayama and G. Smets, Radical and anionic homopolymerization of maleimide and N-n-butylmaleimide, *J. Polym. Sci. A Polym. Chem.*, **1967**, *5*, 1619-1633.
96. L. R. Dix, J. R. Ebdon and P. Hodge, Chain extension and crosslinking of telechelic oligomers—II. Michael additions of bisthiols to bismaleimides, bismaleates and bis(acetylene ketone)s to give linear and crosslinked polymers, *Eur. Polym. J.*, **1995**, *31*, 653-658.
97. D. A. Boyd, Sulfur and Its Role In Modern Materials Science, *Angew. Chem. Int. Ed.*, **2016**, *55*, 15486-15502.
98. R. Okutsu, Y. Suzuki, S. Ando and M. Ueda, Poly(thioether sulfone) with High Refractive Index and High Abbe's Number, *Macromolecules*, **2008**, *41*, 6165-6168.
99. Y. Suzuki, T. Higashihara, S. Ando and M. Ueda, Synthesis and Characterization of High Refractive Index and High Abbe's Number Poly(thioether sulfone)s based on Tricyclo[5.2.1.02,6]decane Moiety, *Macromolecules*, **2012**, *45*, 3402-3408.
100. Y. Suzuki, T. Higashihara, S. Ando and M. Ueda, Synthesis of High Refractive Index Poly(thioether sulfone)s With High Abbe's Number Derived from 2,5-is(sulfanylmethyl)-l,4-dithiane, *Polym. J.*, **2009**, *41*, 860-865.
101. S. Tomasi, R. Bizzarri, R. Solaro and E. Chiellini, Poly(Ester-Sulfide)S from Oligo(Oxyethylene)Dithiols and Bis(Acrylates), *J. Bioact. Compat. Polym.*, **2002**, *17*, 3-21.
102. J. Vandenbergh, K. Ranieri and T. Junkers, Synthesis of (Bio)-Degradable Poly(β-thioester)s via Amine Catalyzed Thiol−Ene Click Polymerization, *Macromol. Chem. Phys.*, **2012**, *213*, 2611-2617.
103. A. C. Pauly and F. di Lena, Incorporating amino acid sequences into the backbone chain of polymers through thiol-ene chemistry, *Polymer*, **2015**, *72*, 378-381.
104. D. J. Saxon, A. M. Luke, H. Sajjad, W. B. Tolman and T. M. Reineke, Next-generation polymers: Isosorbide as a renewable alternative, *Prog. Polym. Sci.*, **2020**, *101*, 101196.

105. F. Fenouillot, A. Rousseau, G. Colomines, R. Saint-Loup and J. P. Pascault, Polymers from renewable 1,4:3,6-dianhydrohexitols (isosorbide, isomannide and isoidide): A review, *Prog. Polym. Sci.*, **2010**, *35*, 578-622.
106. N. G. Moon, F. Mazzini, A. M. Pekkanen, E. M. Wilts and T. E. Long, Sugar-Derived Poly(β-thioester)s as a Biomedical Scaffold, *Macromol. Chem. Phys.*, **2018**, *219*, 1800177.
107. D. Zhang, M.-J. Dumont and A. Cherestes, An efficient strategy for the synthesis of 5-hydroxymethylfurfural derivative based poly(β-thioether ester) via thiol-Michael addition polymerization, *RSC Adv.*, **2016**, *6*, 83466-83470.
108. D. Zhang and M.-J. Dumont, Synthesis, characterization and potential applications of 5-hydroxymethylfurfural derivative based poly(β-thioether esters) synthesized via thiol-Michael addition polymerization, *Polym. Chem.*, **2018**, *9*, 743-756.
109. D. Zhang and M.-J. Dumont, 5-Hydroxymethylfurfural Derivative Based Thermoplastic Elastomers Synthesized via Thiol-Michael Addition Reaction Utilizing Poly(lactic acid) as Hard End Blocks, *Macromol. Chem. Phys.*, **2018**, *219*, 1800039.
110. J. Shin, H. Matsushima, J. W. Chan and C. E. Hoyle, Segmented Polythiourethane Elastomers through Sequential Thiol−Ene and Thiol−Isocyanate Reactions, *Macromolecules*, **2009**, *42*, 3294-3301.
111. J. Vandenbergh, G. Ramakers, L. van Lokeren, G. van Assche and T. Junkers, Synthesis of degradable multi-segmented polymers via Michael-addition thiol–ene step-growth polymerization, *RSC Adv.*, **2015**, *5*, 81920-81932.
112. K. Dan and S. Ghosh, One-Pot Synthesis of an Acid-Labile Amphiphilic Triblock Copolymer and its pH-Responsive Vesicular Assembly, *Angew. Chem. Int. Ed.*, **2013**, *52*, 7300-7305.
113. N. Wang, A. Dong, M. Radosz and Y. Shen, Thermoresponsive degradable poly(ethylene glycol) analogues, *J. Biomed. Mater. Res. A*, **2008**, *84A*, 148-157.
114. S. Orman, C. Hofstetter, A. Aksu, F. Reinauer, R. Liska and S. Baudis, Toughness enhancers for bone scaffold materials based on biocompatible photopolymers, *J. Polym. Sci. A Polym. Chem.*, **2019**, *57*, 110-119.
115. K. Dan and S. Ghosh, Stimuli responsive triblock copolymers by chain-growth polymerization from telechelic macroinitiators prepared via a step-growth polymerization, *Polym. Chem.*, **2014**, *5*, 3901-3909.
116. C. Xiao, J. Ding, L. Ma, C. Yang, X. Zhuang and X. Chen, Synthesis of thermal and oxidation dual responsive polymers for reactive oxygen species (ROS)-triggered drug release, *Polym. Chem.*, **2015**, *6*, 738-747.
117. H. Li, S. Thanneeru, L. Jin, C. J. Guild and J. He, Multiblock thermoplastic elastomers via one-pot thiol–ene reaction, *Polym. Chem.*, **2016**, *7*, 4824-4832.
118. K. Jin, E. K. Leitsch, X. Chen, W. H. Heath and J. M. Torkelson, Segmented Thermoplastic Polymers Synthesized by Thiol–Ene Click Chemistry: Examples of Thiol–Norbornene and Thiol–Maleimide Click Reactions, *Macromolecules*, **2018**, *51*, 3620-3631.
119. H. Sun, D. J. Dobbins, Y. Dai, C. P. Kabb, S. Wu, J. A. Alfurhood, C. Rinaldi and B. S. Sumerlin, Radical Departure: Thermally-Triggered Degradation of Azo-Containing Poly(β-thioester)s, *ACS Macro Lett.*, **2016**, *5*, 688-693.
120. E. Kot and A. Bismarck, Polyacrylamide Containing Weak Temperature Labile Azo Links in the Polymer Backbone, *Macromolecules*, **2010**, *43*, 6469-6475.
121. H. Durmaz, M. Butun, G. Hizal and U. Tunca, Postfunctionalization of polyoxanorbornene via sequential Michael addition and radical thiol-ene click reactions, *J. Polym. Sci. A Polym. Chem.*, **2012**, *50*, 3116-3125.
122. L. Yu, Z. Zhang, Y.-Z. You and C.-Y. Hong, Synthesis of sequence-controlled polymers via sequential thiol-ene and amino-yne click reactions in one pot, *Eur. Polym. J.*, **2018**, *103*, 80-87.

123. Z. Zhang, Z.-B. Tan, C.-Y. Hong, D.-C. Wu and Y.-Z. You, One-pot sequential multicomponent reaction and a multicomponent polymerization method for the synthesis of topologically different polymers, *Polym. Chem.*, **2016**, *7*, 1468-1474.
124. N. Zaquen, B. Wenn, K. Ranieri, J. Vandenbergh and T. Junkers, Facile design of degradable poly(β-thioester)s with tunable structure and functionality, *J. Polym. Sci. A Polym. Chem.*, **2014**, *52*, 178-187.
125. S. Chatani, M. Podgórski, C. Wang and C. N. Bowman, Facile and Efficient Synthesis of Dendrimers and One-Pot Preparation of Dendritic–Linear Polymer Conjugates via a Single Chemistry: Utilization of Kinetically Selective Thiol–Michael Addition Reactions, *Macromolecules*, **2014**, *47*, 4894-4900.
126. S. H. Frayne, R. R. Murthy and B. H. Northrop, Investigation and Demonstration of Catalyst/Initiator-Driven Selectivity in Thiol-Michael Reactions, *J. Org. Chem*, **2017**, *82*, 7946-7956.
127. N. G. Moon, R. J. Mondschein and T. E. Long, Poly(β-thioesters) containing monodisperse oxamide hard segments using a chemoselective thiol-Michael addition reaction, *Polym. Chem.*, **2017**, *8*, 2598-2608.
128. T. Wang, Y. Han, Y. Bai, Q. Zhu, D. Quan and X. Liu, Poly(ether-carbonate) based hydrogel with tunable mechanical strength and enhanced bioactivity prepared by Michael addition, *Polymer*, **2020**, *188*, 122115.
129. O. Yom-Tov, D. Seliktar and H. Bianco-Peled, PEG-Thiol based hydrogels with controllable properties, *Eur. Polym. J.*, **2016**, *74*, 1-12.
130. P. M. Kharkar, K. L. Kiick and A. M. Kloxin, Design of thiol- and light-sensitive degradable hydrogels using Michael-type addition reactions, *Polym. Chem.*, **2015**, *6*, 5565-5574.
131. O. Guaresti, S. Basasoro, K. González, A. Eceiza and N. Gabilondo, In situ cross–linked chitosan hydrogels via Michael addition reaction based on water–soluble thiol–maleimide precursors, *Eur. Polym. J.*, **2019**, *119*, 376-384.
132. A. O. Konuray, X. Fernández-Francos and X. Ramis, Curing kinetics and characterization of dual-curable thiol-acrylate-epoxy thermosets with latent reactivity, *React. Funct. Polym.*, **2018**, *122*, 60-67.
133. J. Wu, C. Wang, C. Mu and W. Lin, A waterborne polyurethane coating functionalized by isobornyl with enhanced antibacterial adhesion and hydrophobic property, *Eur. Polym. J.*, **2018**, *108*, 498-506.
134. C. Wang, M. Podgórski and C. N. Bowman, Monodisperse functional microspheres from step-growth “click” polymerizations: preparation, functionalization and implementation, *Mater. Horizons*, **2014**, *1*, 535-539.
135. C. Wang, X. Zhang, M. Podgórski, W. Xi, P. Shah, J. Stansbury and C. N. Bowman, Monodispersity/Narrow Polydispersity Cross-Linked Microparticles Prepared by Step-Growth Thiol–Michael Addition Dispersion Polymerizations, *Macromolecules*, **2015**, *48*, 8461-8470.
136. O. Z. Durham and D. A. Shipp, Polymer Colloids from Step-Growth Thiol-X Polymerizations, *Polym. Rev.*, **2021**, *61*, 54-79.
137. A. H. Gelebart, M. Mc Bride, A. P. H. J. Schenning, C. N. Bowman and D. J. Broer, Photoresponsive Fiber Array: Toward Mimicking the Collective Motion of Cilia for Transport Applications, *Adv. Funct. Mater.*, **2016**, *26*, 5322-5327.
138. S. Parker, R. Reit, H. Abitz, G. Ellson, K. Yang, B. Lund and W. E. Voit, High-Tg Thiol-Click Thermoset Networks via the Thiol-Maleimide Michael Addition, *Macromol. Rapid Commun.*, **2016**, *37*, 1027-1032.
139. M. Podgórski, S. Chatani and C. N. Bowman, Development of Glassy Step-Growth Thiol-Vinyl Sulfone Polymer Networks, *Macromol. Rapid Commun.*, **2014**, *35*, 1497-1502.

140. P. Chakma and D. Konkolewicz, Dynamic Covalent Bonds in Polymeric Materials, *Angew. Chem. Int. Ed.*, **2019**, *58*, 9682-9695.
141. Y. Yang, Z. Pei, X. Zhang, L. Tao, Y. Wei and Y. Ji, Carbon nanotube–vitrimer composite for facile and efficient photo-welding of epoxy, *Chem. Sci.*, **2014**, *5*, 3486-3492.
142. N. De Alwis Watuthanthrige, B. Ahammed, M. T. Dolan, Q. Fang, J. Wu, J. L. Sparks, M. B. Zanjani, D. Konkolewicz and Z. Ye, Accelerating dynamic exchange and self-healing using mechanical forces in crosslinked polymers, *Mater. Horizons*, **2020**, *7*, 1581-1587.
143. J. J. Cash, T. Kubo, A. P. Bapat and B. S. Sumerlin, Room-Temperature Self-Healing Polymers Based on Dynamic-Covalent Boronic Esters, *Macromolecules*, **2015**, *48*, 2098-2106.
144. N. Sowan, H. B. Song, L. M. Cox, J. R. Patton, B. D. Fairbanks, Y. Ding and C. N. Bowman, Light-Activated Stress Relaxation, Toughness Improvement, and Photoinduced Reversal of Physical Aging in Glassy Polymer Networks, *Adv. Mater.*, **2021**, *33*, 2007221.
145. C. J. Kloxin and C. N. Bowman, Covalent adaptable networks: smart, reconfigurable and responsive network systems, *Chem. Soc. Rev.*, **2013**, *42*, 7161-7173.
146. B. Zhang, Z. A. Digby, J. A. Flum, P. Chakma, J. M. Saul, J. L. Sparks and D. Konkolewicz, Dynamic Thiol–Michael Chemistry for Thermoresponsive Rehealable and Malleable Networks, *Macromolecules*, **2016**, *49*, 6871-6878.
147. O. Koniev, G. Leriche, M. Nothisen, J.-S. Remy, J.-M. Strub, C. Schaeffer-Reiss, A. Van Dorsselaer, R. Baati and A. Wagner, Selective Irreversible Chemical Tagging of Cysteine with 3-Arylpropiolonitriles, *Bioconjug. Chem.*, **2014**, *25*, 202-206.
148. A. D. Baldwin and K. L. Kiick, Reversible maleimide–thiol adducts yield glutathione-sensitive poly(ethylene glycol)–heparin hydrogels, *Polym. Chem.*, **2013**, *4*, 133-143.
149. P. Chakma, L. H. Rodrigues Possarle, Z. A. Digby, B. Zhang, J. L. Sparks and D. Konkolewicz, Dual stimuli responsive self-healing and malleable materials based on dynamic thiol-Michael chemistry, *Polym. Chem.*, **2017**, *8*, 6534-6543.

Chapter 2 – Unsaturated Poly(ester-urethanes) with Stereochemically Dependent Thermomechanical Properties

2.1 Manuscript details and overview

Title: Unsaturated Poly(ester-urethanes) with Stereochemically Dependent Thermomechanical Properties

Authors: Connor J. Stubbs[1], Joshua C. Worch[1], Hannah Prydderch[1], Matthew L. Becker[2], and Andrew P. Dove[1]*

Affiliations: [1] School of Chemistry, University of Birmingham, Edgbaston, Birmingham B15 2TT, United Kingdom.

[2] Department of Chemistry, Department of Mechanical Engineering & Materials Science, Department of Orthopaedic Surgery, Duke University, 308 Research Drive, Durham, North Carolina 27708, United States

Journal: Macromolecules

Year: 2020

Volume: 53

Page numbers: 174-181

DOI: 10.1021/acs.macromol.9b01700

Submitted: 13th of August 2019

Published: 23rd of December 2019

Copyright statement: Adapted with permission from: C. J. Stubbs, J. C. Worch, H. Prydderch, M. L. Becker, A. P. Dove, Unsaturated Poly(ester-urethanes) with

Stereochemically Dependent Thermomechanical Properties, *Macromolecules* **2020**, *53*, 174-181. Copyright 2020 American Chemical Society.

Permissions: This article and its supporting information are available, free of charge, at https://pubs.acs.org/doi/full/10.1021/acs.macromol.9b01700.

Co-author contributions: Dr Josh Worch (University of Birmingham) and Hannah Prydderch (University of Birmingham) provided technical and synthetic advice. Dr Carl Reynolds advised on rheological experimentation and modelling. Prof. Matthew L. Becker (Duke University) provided guidance and editing of this manuscript. Prof. Andrew P. Dove (University of Birmingham) supervised in addition to providing guidance and editing the manuscript.

Overview: The objective of this chapter was to design a platform that enabled the creation of unsaturated linear polymers with pre-determined *cis/trans* content at a suitable scale and molecular weight for thermomechanical testing. Whilst previous reports confirmed alkene stereochemistry had a significant impact on the thermal and mechanical properties, they were unable to achieve a predetermined *cis/trans* ratio due to isomerisation reactions or synthetic challenges. Hence it was important to study how the absolute control of the *cis/trans* ratio could be used to manipulate thermal and mechanical properties.

Our designed platform utilised thiol-Michael “click” to create polymers from step-growth polyaddition of difunctional monomers containing both *cis/trans* stereochemistry, in addition to a saturated control. The polymers could be synthesised in high M_w (>100 kDa) and the desired stereochemistry was retained. Differential scanning calorimetry and FT-IR revealed a trend in crystallinity (saturated > *trans* >> *cis*) that could be explained through packing and hydrogen bonding. The *cis* configuration precludes efficient packing, whereas the *trans* configuration promotes more efficient ordering. The saturated polymer is the

most crystalline as chain rotation isn't restricted by an alkene bond. These trends translate to their tensile properties where stiffness positively correlates with crystallinity but the elongation at break negatively correlates.

Next, we wanted to elucidate how varying quantities of the *cis/trans* stereoisomers in a copolymer can impact properties. By varying feed ratios of the *cis/trans* monomer, random unsaturated copolymers of a predetermined *cis/trans* content could be obtained. Generally, the higher *trans* content increased the crystallinity, consequently increasing the strength and stiffness. Our study highlighted how varying the stereochemistry in a polymer can lead to a change in crystallinity and subsequently a change in the mechanical properties they display.

Macromolecules
Cite This: Macromolecules 2020, 53, 174 181
Article
pubs.acs.org/Macromolecules

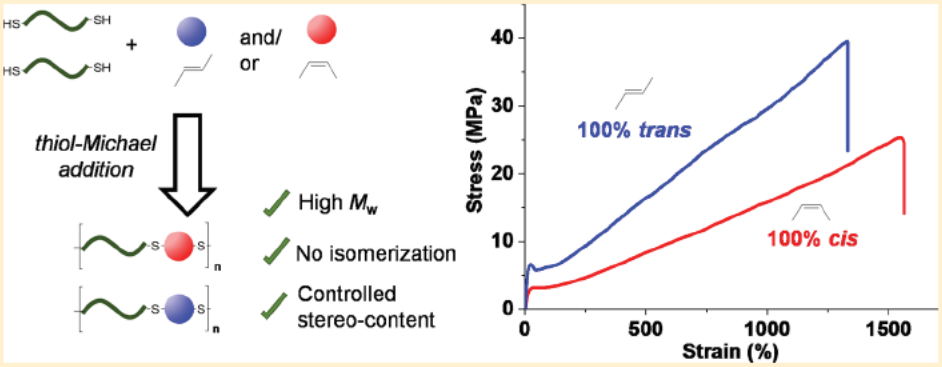
Unsaturated Poly(ester-urethanes) with Stereochemically Dependent Thermomechanical Properties

Connor J. Stubbs,[§] Joshua C. Worch,[§] Hannah Prydderch,[§] Matthew L. Becker,[†] and Andrew P. Dove*[,§]

[§]School of Chemistry, University of Birmingham, Edgbaston, Birmingham, B15 2TT, U.K.

[†]Department of Chemistry, Department of Mechanical Engineering & Materials Science, Department of Orthopaedic Surgery, Duke University, 308 Research Drive, Durham, North Carolina 27708, United States

Supporting Information



ABSTRACT: Polymer crystallinity is known to be dependent upon backbone stereochemistry, and this concept has emerged as an effective means of altering bulk material properties. Herein we describe a simple, step growth polymerization to synthesize unsaturated poly(ester urethane)s using the thiol Michael addition reaction. The absolute control of alkene stereochemistry (0−100% trans content) in the polymer backbone was achieved by varying the cis/trans double bond content of the monomer feedstock. In turn, the crystallinity of the polymer was systematically varied which manifested in control over the resultant tensile properties such as Young's modulus, ultimate tensile strength, and elongation at break. Generally, the crystallinity and tensile strength were positively correlated with increasing trans double bond content within the polymer.

INTRODUCTION

High performance elastomeric materials are widely exploited in a diverse range of applications such as aerospace, tissue engineering, and wearable electronics.[1−3] The ability to systematically control the mechanical and thermal properties of materials through modification of the chemical structure within polymers is hence of high importance. In most synthetic polymeric materials, this control is achieved by changing the chemical nature of the monomers such as increasing chain length, backbone stiffness, or altering functional groups. In contrast, Nature's polymers use fewer building blocks but impart an additional complexity to the structure−property relationship by leveraging stereochemistry.[4−6] Fully harnessing the structural complexity of biopolymers remains elusive, but the manipulation of thermomechanical properties is an achievable target with the use of stereochemistry.[6] While the stereochemical dependence of mechanical properties within synthetic materials such as polylactide and vinyl polymers such as polypropylene are long established,[7−12] much less work has focused on the application of cis/trans stereochemistry within the polymer backbone to control the materials' properties.

The presence of cis/trans stereoisomerism in both ring systems and double bonds has been used to create polymers in which the thermomechanical properties are controlled by the stereochemistry of the monomer unit. Use of conformationally locked rigid rings, such as isohexides or cyclohexylene, has been harnessed to create polyesters and polyurethanes through scalable polycondensation routes.[13−18] While incorporation of these groups results in stereochemically dependent thermo mechanical properties, the molecular weights of the resultant polymers are generally modest (M_w < 100 kDa), thus limiting their mechanical properties.

Double bond stereochemistry within polymer backbones is known to lead to dramatic changes in thermomechanical properties and is exemplified by polyisoprene (natural rubber or gutta percha) and its analogues.[19−21] Synthetically this is primarily achieved through the application of maleic and fumaric acids to polymer systems;[22−24] however, the extreme conditions that are required in polycondensation (reaction

Received: August 13, 2019
Revised: November 21, 2019
Published: December 23, 2019

Downloaded via UNIV OF BIRMINGHAM on July 26, 2021 at 13:57:00 (UTC).
See https://pubs.acs.org/sharingguidelines for options on how to legitimately share published articles.

© 2019 American Chemical Society

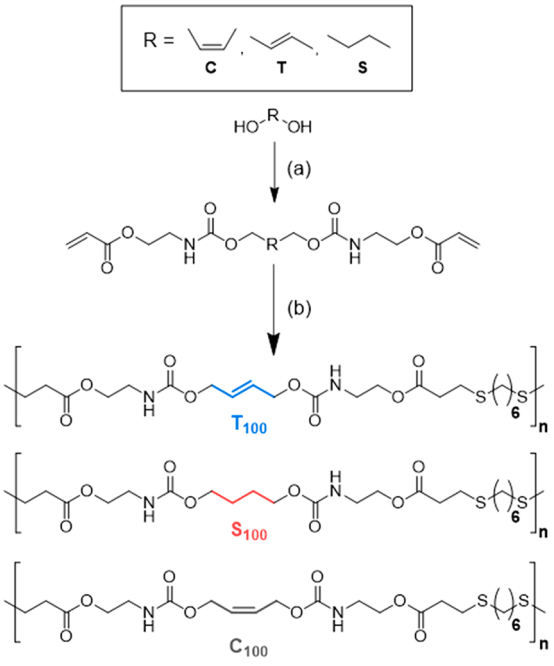
DOI: 10.1021/acs.macromol.9b01700
Macromolecules 2020, 53, 174−181

temperatures >200 °C) typically lead to some isomerization of the monomers and/or polymers.[25] A recent example yielded 1,4 butandiol maleate copolymers at a moderate molecular weight (M_w = 32 kDa) via step growth polymerization.[26] While the thermomechanical dependence on the polymer stereo chemistry was clear, unwanted isomerization at polymerization temperatures (>140 °C) led to loss of stereopurity of the double bond in the polymer backbone.

More recently, some of us have reported that polymers with stereochemically controlled double bonds in their backbone can be accessed through a simple nucleophilic thiol−yne addition to afford high molecular weight (M_w > 100 kDa) polymers.[27] Here the stereochemistry was dictated by the reaction polarity and the basicity of the amine catalyst, enabling control of the cis content between 32% and 80%.[28] Despite the demonstration of stereochemically dependent thermomechanical properties, the ability to access materials with higher levels of stereospecificity remained elusive.

Herein we present a simple protocol to afford unsaturated polymers with absolute control over alkene stereochemistry through the application of monomers with predefined stereochemistry with the absence of isomerization (Scheme 1). Using a room temperature thiol Michael addition to achieve a step growth polyaddition,[29−33] the cis/trans double bond content of the polymers was controlled by simply controlling the feed ratio of monomers. The stereochemical definition of the polymer controlled the crystallinity and, subsequently, the thermomechanical properties of the resultant materials.

Scheme 1. Synthesis of Poly(ester urethane)s from Saturated and Stereodefined Diols[a]



[a](a) 2.1 equiv of 2 isocyanatoethyl acrylate, 0.2 mol % of dibutyl tin(IV) dilaurate, THF, 22 °C. (b) 1 equiv of 1,6 hexanedithiol, 2 mol % dimethylphenylphosphine (DMPP), DMF, 22 °C. Homopolymers denoted as $X_{(\%\ \text{molarity of diacrylate in polymer})}$, where X is C, T, S for cis, trans, saturated (for example, saturated homopolymer = $\mathbf{S}_{100}$).

Homopolymer Synthesis and Characterization. We envisioned a simple protocol to afford alkene containing monomers suitable for step growth polymerization. Four carbon unsaturated diols (cis or trans) and a saturated diol were reacted with a commercially available isocyanate to afford diacrylate monomers, cis (**C**), trans (**T**), and saturated (**S**), that were suitable for step growth polymerization. Initially, the diacrylates were reacted with 1,6 hexanedithiol in the presence of a phosphine catalyst to yield high molecular weight (M_w > 100 kDa) polymers (Scheme 1, Supporting Information). Notably, ^{1}H NMR spectroscopic analysis of the polymers indicated complete stereochemical retention along the back bone (Figure 1).

Polymer films for mechanical testing were prepared by melt processing the polymers under pressure between 90 and 120 °C for 10 min. The polymers remained soluble after processing which indicated that no significant cross linking had occurred, and ^{1}H NMR spectroscopic analysis of the processed samples confirmed no appreciable isomerization of the alkene units, thus highlighting their robust thermal stability. Each film was annealed for 7 d at 23 °C in an incubator to ensure thermal equilibration before the thermomechanical properties and characterization were assessed on annealed films (Figure 1).

To separate molecular chain entanglements from the tensile properties of the system, rheology was performed. Isothermal frequency sweeps were performed on the homopolymers to calculate entanglement molecular weight (M_e) using poly disperse double reptation theory (Supporting Information Figure S25 and Table 1).[34] All homopolymers possessed low M_e values that suggests all samples contain a high level of entanglement. $\mathbf{C}_{100}$ possessed a marginally higher M_e, indicating that the geometry of the double bond affects the entanglements of linear polymer systems.

The mechanical tests show that $\mathbf{T}_{100}$ and $\mathbf{S}_{100}$ are both tough plastics with good ductility. Both possess similar tensile properties. In contrast, $\mathbf{C}_{100}$ has a comparatively lower Young's modulus with a higher elongation at break, but it features a lower ultimate tensile strength (UTS). These results show that the stereochemistry of the double bond successfully controls the mechanical properties of the polymeric materials. Similar to the relationship between the stereochemistry of its double bond and mechanical properties of polyisoprene, the planarity of the backbone is disrupted by the cis configuration which precludes efficient chain packing to yield a more disordered system that is softer and more flexible. This disruption in the chains can be further understood by infrared (IR) analysis of hydrogen bonding in the homopolymers.

Analysis of the IR spectra reveal two distinct signals for the N−H moieties in urethanes, hydrogen bonded and "free" N−H bonds at a slightly higher wavenumber.[35] The observed IR frequency of the homopolymers reveals a sharp signal (3310 cm^{-1}) that is indicative of hydrogen bonding and a broad shoulder (~3590 cm^{-1}) that is indicative of "free" N−H bonds. Increased broadness and a reduction in the intensity of the hydrogen bonding signal (3310 cm^{-1}) in the $\mathbf{C}_{100}$ spectrum indicates that a lower amount of hydrogen bonding is present in the system in comparison to $\mathbf{T}_{100}$ and $\mathbf{S}_{100}$ (Figure 2).

Inevitably, with varying levels of hydrogen bonding and chain packing, investigating the crystallinity of this system will help to further elucidate stereochemistry's influence on the polymer properties. Thus, we investigated the thermal properties of the polymers to assess the degree of crystallinity in each system.

DOI: 10.1021/acs.macromol.9b01700
Macromolecules 2020, 53, 174−181

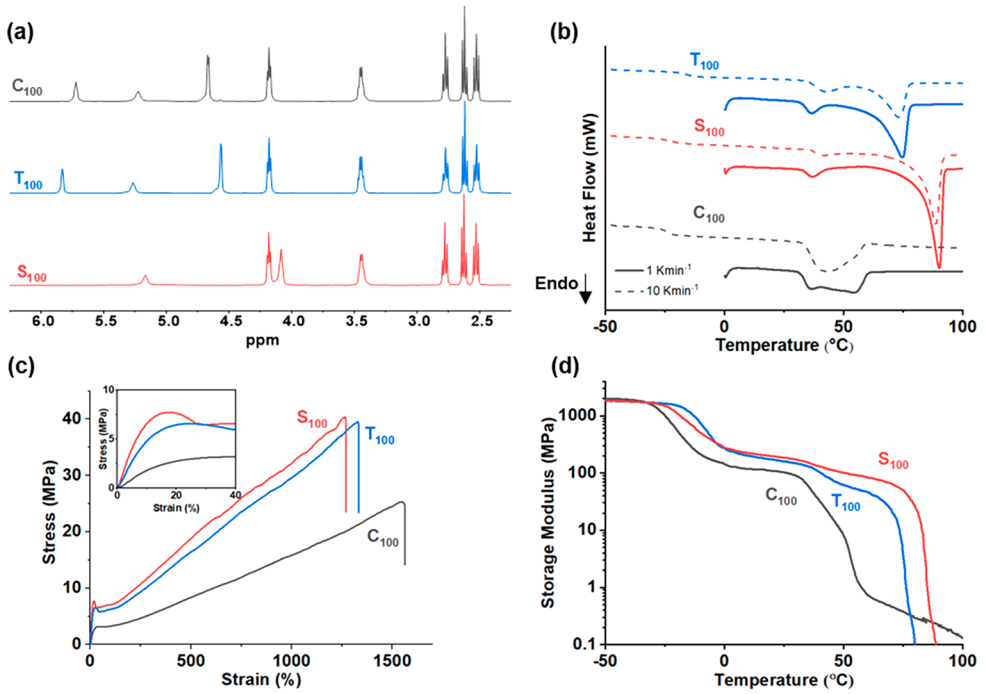


Figure 1. (a) ^{1}H NMR spectra of homopolymers in $CDCl_3$ (400 MHz, 298 K). (b) Differential scanning calorimetry thermograms of homopolymers for 1st heating cycle (dashed lines = 10 K·min^{-1} and solid lines = 1 K·min^{-1}). (c) Representative stress vs strain plot of 7 day annealed homopolymers (n = 5). Inset data between 0 and 40% strain. (d) Dynamic mechanical thermal analysis thermograms of storage modulus vs temperature performed in tensile configuration (frequency = 1 Hz, 2 K·min^{-1}. Representative curve shown, n = 3).

Table 1. Thermal and Tensile Data of Annealed Homopolymers

	M_n [a] (kDa)	M_w [a] (kDa)	$Đ_M$ [a]	M_e [b] (kDa)	T_g [c] (°C)	T_m [c] (°C)	ΔH_m [c] (J g^{-1})	E [d] (MPa)	σ_b [e] (MPa)	ε_b [f] (%)
$\mathbf{S_{100}}$	30.8	139	4.51	2.12	19	90.2	41.3	81 ± 8	37 ± 2.7	1191 ± 76
$\mathbf{T_{100}}$	28.7	103	3.57	2.01	14	74.6	37.2	66 ± 11	39 ± 8	1232 ± 96
$\mathbf{C_{100}}$ [g]	34.8	250	7.19	3.23	18		27.0	25 ± 4	23 ± 2	1481 ± 53

[a] M_w and $Đ_M$ were determined by size exclusion chromatography (DMF, 0.5% w/w NH_4BF_4) analysis against poly(methyl methacrylate) (PMMA) standards. [b] Calculated from the fitting of polydisperse double reptation theory to TTS master plots (Figure S25). [c] The T_m was taken as the minimum of the final transition, T_g was obtained from 2nd heating cycle, total enthalpy of melting (ΔH_m) was calculated by integration of all endothermic transitions from DSC thermograms. [d] Young's modulus. [e] Stress at break. [f] Strain at break (n = 5). Uncertainty is presented as the standard deviation of samples. [g] Sample C_{100} had multiple melt transitions that were indistinguishable at the heating rate.

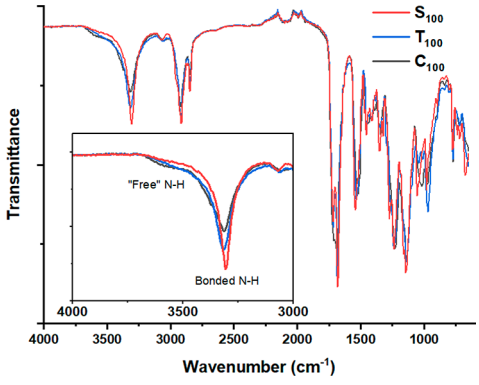
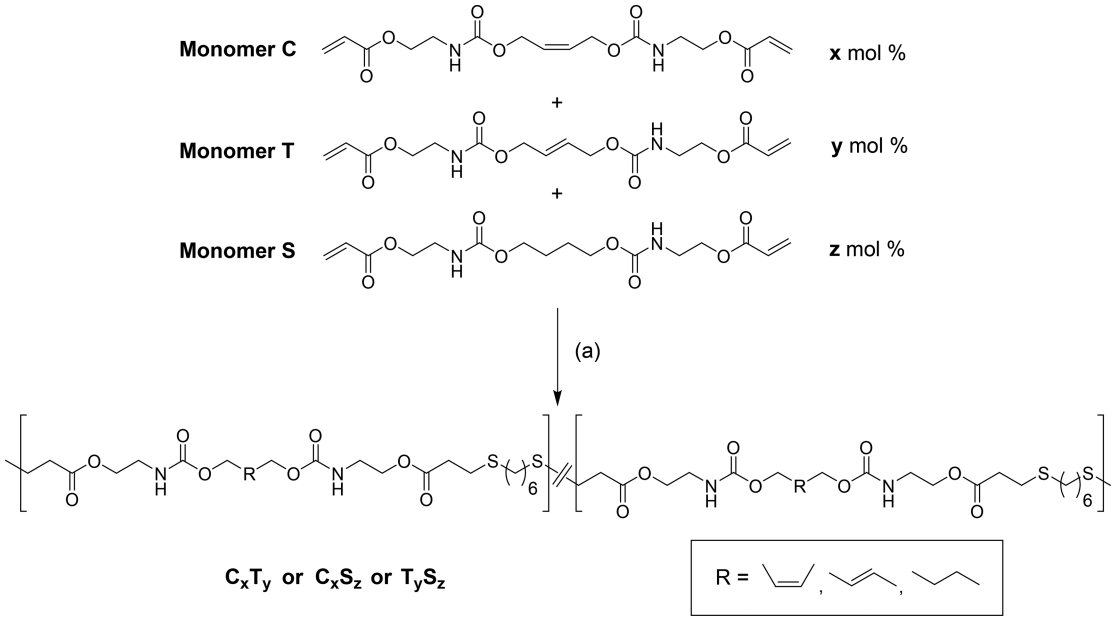


Figure 2. IR spectrum of fabricated homopolymer films. Inset data between 3000 and 4000 cm^{-1} (N–H region).

Homopolymer Thermal Properties. The thermal properties of each homopolymer were assessed by differential scanning calorimetry (DSC) and dynamic mechanical thermal analysis (DMTA). Initial DSC thermograms were obtained at a heating and cooling rate of 10 K·min^{-1}; however, upon observation of melt transitions, samples were tested at 1 K·min^{-1} to increase the resolution of the multiple thermal transitions. Each homopolymer displayed melt transitions (T_m) in the first heating cycle of the DSC thermogram which indicates that each material is semicrystalline in nature.[36] Unsurprisingly, $\mathbf{T_{100}}$ and $\mathbf{S_{100}}$ possess comparable melt temperatures (with two distinct transitions), total melting enthalpy (ΔH_m), and DSC thermogram profiles (Figure 1C). Once again, the $\mathbf{C_{100}}$ sample was drastically different. Specifically, a broad melting profile with multiple transitions was observed and the ΔH_m was significantly smaller (Figure 1C, Table 1). Because ΔH_m can be correlated to bulk crystallinity, the relative crystallinity for the polymers was determined to be $\mathbf{S_{100}} > \mathbf{T_{100}} \gg \mathbf{C_{100}}$. Furthermore, the polymer crystallinity was positively correlated with Young's modulus and negatively correlated with elongation at break (Figure 1B, Table 1). Unusually, all the homopolymers possessed multiple melt transitions; this phenomenon is not commonly observed for alternating copolymers and is more commonly seen in materials that possess a distinct segmental structure (e.g., block or multiblock copolymers).[37,38] In a previous study of semicrystalline materials possessing a similar thermal profile, the lower temperature melt transition was

DOI: 10.1021/acs.macromol.9b01700
Macromolecules 2020, 53, 174–181

Scheme 2. Synthesis of Random Copolymers from Diacrylate Monomers[a]



[a](a) 1 equiv of 1,6 hexanedithiol, 2 mol % of DMPP, DMF at 22 °C.

Table 2. Thermal and Tensile Data of Random Copolymers and Blend

	M_n[a] (kDa)	M_w[a] (kDa)	$Đ_M$[a]	T_g[b] (°C)	T_m[b] (°C)	ΔH_m[b] (J g^{-1})	E[c] (MPa)	σ_b[d] (MPa)	ε_b[e] (%)	U_T[f] (MJ m^{-2})
$C_{50}S_{50}$	34.9	209	5.99	19	77.9	35.9	53 ± 7	33 ± 3	1508 ± 74	255 ± 28
$C_{50}T_{50}$	38.7	208	5.37	16	52.0	25.1	35 ± 4	26 ± 3	1558 ± 75	199 ± 27
blended ($C_{50}T_{50}$)[g]				17		37.0	52 ± 8	25 ± 3	1075 ± 106	156 ± 28

[a]M_w and $Đ_M$ was determined by SEC (DMF, 0.5 wt %/wt NH_4BF_4) analysis against poly(methyl methacrylate) (PMMA) standards. [b]The T_m was taken as the minimum of the final transition, T_g was obtained from 2nd heating cycle, total enthalpy of melting (ΔH_m) was calculated by integration of all endothermic transitions from DSC thermograms (Supporting Information). [c]Young's modulus. [d]Stress at break. [e]Strain at break. [f]Tensile toughness (n = 5 except blended sample where n = 3). Uncertainty presented as the standard deviation of samples. An additional copolymer mixing the trans and saturated moiety ($T_{50}S_{50}$) was synthesized, and data can be found in Supporting Information. [g]Blended sample had multiple melt transitions that were indistinguishable at the heating rate.

correlated to short range crystalline ordering and the higher temperature transitions to overall longer range order in the system.[36,39] Comparing C_{100} and T_{100} (or S_{100}) it is possible that the disorder introduced by the cis moiety prevents the longer range order that may be observed in the latter. The morphology of these nonsegmented poly(ester urethanes) are currently being studied using microscopy.

DMTA was used to further analyze the thermomechanical properties of the homopolymers in which samples of annealed polymer films were subjected to thermal sweeps in the tensile mode. For each polymer, three distinct phases were apparent which correspond to the glassy state at low temperatures (storage modulus >1 GPa), followed by a wide rubbery plateau above the glass transition and polymer flow at the respective melt transition. For the storage modulus, a considerably larger decrease is observed in the C_{100} sample in comparison to the other derivatives which is intuitive for a softer sample at room temperature. The final decrease in storage modulus is characteristic of melting and this corroborates well with the melting transitions observed in the DSC thermograms. Another feature of interest is a slight decrease in storage modulus between the rubbery plateau and melting event that is only observed in T_{100} and S_{100}. The temperature of this DMTA transition occurs roughly at the same temperature as the first melt transition in the DSC thermograms. This softening of material once a melt transition is reached could indicate the possibility of phase separation, whereby a phase losing its crystallinity reduces the influence on the materials' bulk properties.[23]

Copolymer and Blend Preparation. Because the stereo chemistry is fully retained in the final polymer, the monomer feed ratio can be used to precisely target the cis/trans content of the resultant polymers. By varying the monomer feed ratio in a copolymerization of mixed monomers (e.g., monomers **C**/**T** or monomers **C**/**S**), random copolymers with various cis content were synthesized in an effort to manipulate the thermomechanical properties (Scheme 2). ^{1}H NMR spectro scopic analysis of the copolymers indicated that the stereo chemical ratio in the feedstock was undisturbed in the isolated polymer (see Supporting Information). A 1:1 blended sample of C_{100} and T_{100} homopolymers was fabricated into a thin film to assess any differences to the analogous copolymer sample.

Copolymer and Blend Tensile Testing. The copolymers and blend were processed using the same conditions as the homopolymers, annealed for 7 d, and subjected to uniaxial tensile testing. The $C_{50}S_{50}$ copolymer sample displayed mechanical properties intermediate between the respective homopolymers (Table 2), but it was found to have increased stiffness and possess higher toughness than C_{100}. Contrastingly, the mechanical properties of the cis/trans copolymer ($C_{50}T_{50}$)

DOI: 10.1021/acs.macromol.9b01700
Macromolecules 2020, 53, 174−181

were almost identical to $\mathbf{C}_{100}$ which indicates that the mechanical properties of the sample were dominated by the packing of the cis double bond. Thus, in comparison to the trans double bond, the saturated linking unit had a stronger influence on final material properties at the same respective ratios. The blended material (50/50 mixture of $\mathbf{C}_{100}$ and $\mathbf{T}_{100}$) appeared to have a larger Young's modulus compared to the $\mathbf{C}_{100}$ sample, but at the sacrifice of elongation at break and tensile toughness. Notably, the blend had a Young's modulus similar to the trans homopolymer ($\mathbf{T}_{100}$); a stark contrast to the cis/trans copolymer ($\mathbf{C}_{50}\mathbf{T}_{50}$). The polymers were further subjected to thermal analysis to better understand the crystallinity of the system and elaborate on the mechanical trend (Figure 3).

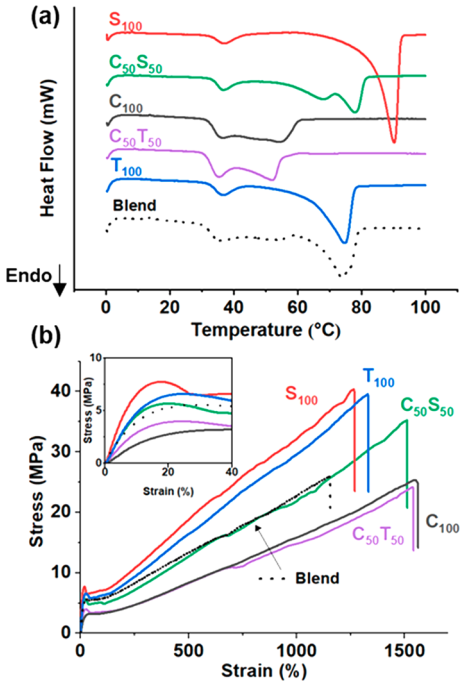


Figure 3. Representative uniaxial extension and thermal properties of 7 day annealed copolymers and a cis/trans blend. (a) First heating cycle DSC thermograms of annealed copolymers at a heating rate of 1 K·min^{-1} (b) Stress vs strain plots of representative samples from the annealed copolymers at a strain rate of 10 mm·min^{-1}. Inset data between 0 and 40% strain.

Copolymer and Blend Thermal Properties. The thermal properties of the copolymers and the blend were assessed by DSC analysis with a heating rate of 1 K·min^{-1}. The melt transitions observed in $\mathbf{C}_{50}\mathbf{S}_{50}$ were shifted to higher temperatures, and the total enthalpy of melting was larger than $\mathbf{C}_{100}$, indicating that the saturated linker resulted in increased crystallinity compared to when double bond containing monomers were used (Figure 3A). Simultaneously, increasing the cis double bond content disrupted the crystallinity enough to allow for a more ductile sample. A balance between the two competing moieties (cis, less ordered; saturated, more ordered) in $\mathbf{C}_{50}\mathbf{S}_{50}$ is apparent in both thermal and tensile properties. Contrary to $\mathbf{C}_{50}\mathbf{S}_{50}$, the $\mathbf{C}_{50}\mathbf{T}_{50}$ sample had a similar DSC profile and total enthalpy of melting as the purely cis containing $\mathbf{C}_{100}$. This can be rationalized by the trans unit producing less order in the system than the saturated configuration, leading to the cis moiety within the backbone disrupting crystallization. Curiously, the blend had a similar DSC profile, total enthalpy of melting, and hence similar crystallinity, as the purely trans sample $\mathbf{T}_{100}$. However, the comparative copolymer $\mathbf{C}_{50}\mathbf{T}_{50}$ was similar to the purely cis containing $\mathbf{C}_{100}$. This demonstrates that incorporation of the cis moiety into a chain of crystalline trans units, as a copolymer, disrupts crystallinity while simple physical blending does not translate this disruption.

The clear manipulation of crystallinity and tensile properties observed in $\mathbf{C}_{50}\mathbf{S}_{50}$ copolymer demonstrated that tensile enhancement was possible in copolymers. However, the copolymers demonstrated that the trans double bond had negligible impacts on copolymer crystallinity at 50% content, and an increased amount of trans double bond content would be required to alter the thermomechanical properties.

Stereocontrolled Copolymers. To fully understand the effects of the trans double bond in a cis/trans copolymer system, more copolymers with various cis/trans ratios were prepared and tested using uniaxial tensile testing. Similarity among tensile properties is very apparent in samples containing 0−50% trans content (Table 3) because the UTS varies between 19 and 26 MPa and elongation at break only fluctuates from 1300 to 1500% (Figure 4). Compared to the 100% cis polymer ($\mathbf{C}_{100}$), the polymer with 75% trans content ($\mathbf{C}_{25}\mathbf{T}_{75}$) is stronger ($\Delta$UTS ~ 9 MPa) and displays an increase of ~300% elongation at break compared with the 100% trans sample ($\mathbf{T}_{100}$). Interestingly, the slight deviation from linearity is reproducibly observed in the tensile curves, most notably for ($\mathbf{C}_{75}\mathbf{T}_{25}$). We attribute this to crystal slippage that is observed in some semicrystalline systems. While this is more prevalent in polyolefin based systems, there are some examples of more polar polymers displaying this behavior.[40,41] However, it is clear that alkene stereochemistry can be rationally leveraged to adjust bulk mechanical properties such as tensile strength, flexibility, and elongation at break by simply adjusting monomer ratios in this simple system to afford

Table 3. SEC Characterization and Tensile Data for Stereocontrolled Copolymers

	M_n[a] (kDa)	M_w[a] (kDa)	$Đ_M$[a]	T_g[b] (°C)	T_m[c] (°C)	ΔH_m[d] (J g^{-1})	E[e] (MPa)	σ_b[f] (MPa)	ε_b[g] (%)	U_T[h] (MJ m^{-2})
$\mathbf{C}_{100}$	29.0	250	7.19	18		27.0	25 ± 4	23 ± 2	1481 ± 53	174 ± 17
$\mathbf{C}_{75}\mathbf{T}_{25}$	36.6	194	5.30	17	51.3	27.6	35 ± 5	19 ± 3	1307 ± 160	137 ± 30
$\mathbf{C}_{50}\mathbf{T}_{50}$	38.7	208	5.37	16	52.0	25.1	35 ± 4	26 ± 3	1558 ± 75	199 ± 27
$\mathbf{C}_{25}\mathbf{T}_{75}$	30.8	129	4.18	15	69.0	32.6	46 ± 6	30 ± 4	1436 ± 164	233 ± 48
$\mathbf{T}_{100}$	26.0	103	3.57	14	74.6	37.2	66 ± 11	39 ± 8	1232 ± 96	261 ± 72

[a]M_w and $Đ_M$ was determined by SEC (DMF, 0.5 wt %/wt NH_4BF_4) analysis against poly(methyl methacrylate) (PMMA) standards. [b]The T_g was obtained from 2nd heating cycle (Supporting Information). [c]The T_m was taken as the minimum of the final transition. [d]Total enthalpy of melting (ΔH_m) was calculated by integration of all endothermic transitions. [e]Young's modulus. [f]Stress at break. [g]Strain at break. [h]Tensile toughness n = 5. Uncertainty presented as the standard deviation of samples.

DOI: 10.1021/acs.macromol.9b01700
Macromolecules 2020, 53, 174−181

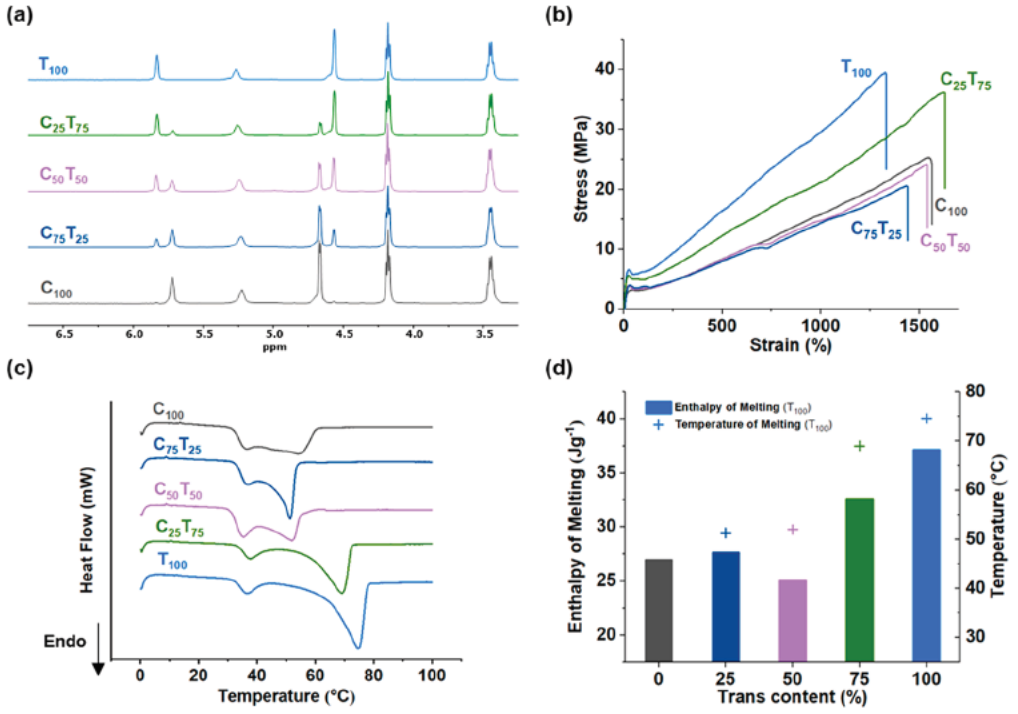


Figure 4. (a) NMR spectra of stereocontrolled copolymers in ($CDCl_3$, 400 MHz, 298 K). (b) Representative stress vs strain curves of 7 day annealed copolymers. (c) DSC thermograms of stereocontrolled copolymers for the 1st heating cycle at 1 K·min^{-1}. (d) Maximum melt transition peak and enthalpy of melting vs trans double bond content in stereocontrolled copolymers.

copolymers with varied cis/trans content. It is interesting that mechanical properties of cis/trans copolymers are significantly different from respective homopolymers only when trans content >50%, however cis/saturated materials display properties in between the respective homopolymers for the 50% system. We hypothesized that crystallinity was driving the observed differences in bulk properties for the cis/trans copolymers so we examined their thermal properties.

Analysis of the polymer samples by DSC revealed a positive correlation between trans double bond content and the melt transition. Specifically, the melting behavior became better resolved with the second melt transition shifting to increasingly higher temperature after 50% trans content was surpassed, while polymers containing ≤50% trans content had similar melting temperatures. The trend for total melt enthalpy was less clear because the value remained relatively consistent for samples with ≤50% trans content before increasing significantly thereafter (Figure 4C). Nonetheless, the crystallinity increased dramatically at 75% trans double bond content which indicates that the trans double bond becomes a dominating influence in controlling the crystallinity of the materials at this threshold. A similar "inflection point" has been observed around 50% cis content in other alkene containing polyesters.[28] However, it should be noted that the stereochemical trends were reversed for this case, i.e., crystallinity and UTS increased with cis content. Further investigation of these polymers and/or the synthesis of alternative alkene containing scaffolds can help to reconcile such disparities and provide a more rational platform for tuning thermomechanical properties.

CONCLUSION

A polymer system containing cis/trans alkene stereochemistry has been designed that can afford high molecular weight polymers without compromising stereochemical purity during polymerization and subsequent material processing. For the unsaturated polymers, the stereochemical content influenced the thermomechanical properties, and this was further correlated to the degree of crystallinity within the sample. Polymer crystallinity is extremely important in the determination of thermomechanical properties, and moreover, precision tuning of crystallinity can be challenging and often involves more demanding synthetic endeavors and/or drastic changes to the resultant polymer microstructure. The manipulation of polymer alkene stereochemistry to modify bulk crystallinity presents a much more accessible path to materials possessing tunable stiffness, tensile strength, and flexibility.

ASSOCIATED CONTENT

Supporting Information

The Supporting Information is available free of charge at https://pubs.acs.org/doi/10.1021/acs.macromol.9b01700.

Experimental details of monomer, polymer, and copolymer synthesis including NMR spectroscopy and SEC characterization. Full tensile, DSC, and DMTA data for all synthesized polymers as well as an additional synthesized polymer: $T_{50}S_{50}$ (PDF)

AUTHOR INFORMATION

Corresponding Author

*E mail:

ORCID

Matthew L. Becker: 0000 0003 4089 6916

Andrew P. Dove: 0000 0001 8208 9309

DOI: 10.1021/acs.macromol.9b01700
Macromolecules 2020, 53, 174−181

Author Contributions

The manuscript was written through contributions of all authors. All authors have given approval to the final version of the manuscript. C.J.S. performed all synthesis and thermo mechanical experimentation with assistance from J.C.W. and H.P. We thank Dr. Carl Reynolds for his advice and assistance with rheological experiments.

Notes

The authors declare no competing financial interest.

■ ACKNOWLEDGMENTS

This project has received funding from the European Research Council (ERC) under the European Union's Horizon 2020 research and innovation program under grant agreement no. 681559 to support C.J.S. J.C.W. acknowledges funding from the European Union's Horizon 2020 research and innovation program under the Marie Sklodowska Curie grant agreement no. 751150.

■ ABBREVIATIONS

M_w, Mass average molar mass; M_e, entanglement molecular weight; M_n, number average molar mass; NMR, nuclear magnetic resonance; SEC, size exclusion chromatography; DSC, differential scanning calorimetry; DMTA, dynamic mechanical thermal analysis; DMF, *N*,*N* dimethylformamide; PMMA, poly(methyl methacrylate); UTS, ultimate tensile strength; T_g, glass transition temperature; $Đ_M$, dispersity; TGA, thermal gravimetric analysis; THF, tetrahydrofuran; TTS, time−temperature superposition; WLF, Williams−Landel−Ferry

■ REFERENCES

(1) Serrano, M. C.; Chung, E. J.; Ameer, G. A. Advances and applications of biodegradable elastomers in regenerative medicine. *Adv. Funct. Mater.* **2010**, *20*, 192−208.
(2) Gerratt, A. P.; Michaud, H. O.; Lacour, S. P. Elastomeric electronic skin for prosthetic tactile sensation. *Adv. Funct. Mater.* **2015**, *25*, 2287−2295.
(3) Kuder, I. K.; Arrieta, A. F.; Raither, W. E.; Ermanni, P. Variable stiffness material and structural concepts for morphing applications. *Prog. Aerosp. Sci.* **2013**, *63*, 33−55.
(4) McLaughlin, C. K.; Hamblin, G. D.; Sleiman, H. F. Supra molecular DNA assembly. *Chem. Soc. Rev.* **2011**, *40*, 5647−5656.
(5) Astbury, W.; Bell, F. O. Molecular structure of the collagen fibres. *Nature* **1940**, *145*, 421.
(6) Worch, J. C.; Prydderch, H.; Jimaja, S.; Bexis, P.; Becker, M. L.; Dove, A. P. Stereochemical enhancement of polymer properties. *Nat. Rev. Chem.* **2019**, *3*, 514−535.
(7) Radano, C. P.; Baker, G. L.; Smith, M. R. Stereoselective polymerization of a racemic monomer with a racemic catalyst: direct preparation of the polylactic acid stereocomplex from racemic lactide. *J. Am. Chem. Soc.* **2000**, *122*, 1552−1553.
(8) Coates, G. W.; Waymouth, R. M. Oscillating Stereocontrol: A Strategy for the Synthesis of Thermoplastic Elastomeric Polypropy lene. *Science* **1995**, *267*, 217.
(9) Natta, G. Properties of isotactic, atactic, and stereoblock homopolymers, random and block copolymers of α olefins. *J. Polym. Sci.* **1959**, *34*, 531−549.
(10) Fox, T. G.; Garrett, B. S.; Goode, W. E.; Gratch, S.; Kincaid, J. F.; Spell, A.; Stroupe, J. D. Crystalline Polymers of Methyl Methacrylate. *J. Am. Chem. Soc.* **1958**, *80*, 1768−1769.
(11) Anderson, K. S.; Schreck, K. M.; Hillmyer, M. A. Toughening polylactide. *Polym. Rev.* **2008**, *48*, 85−108.
(12) Wanamaker, C. L.; Bluemle, M. J.; Pitet, L. M.; O'Leary, L. E.; Tolman, W. B.; Hillmyer, M. A. Consequences of polylactide stereochemistry on the properties of polylactide polymenthide polylactide thermoplastic elastomers. *Biomacromolecules* **2009**, *10*, 2904−2911.
(13) Liu, F.; Zhang, J.; Wang, J.; Liu, X.; Zhang, R.; Hu, G.; Na, H.; Zhu, J. Soft segment free thermoplastic polyester elastomers with high performance. *J. Mater. Chem. A* **2015**, *3*, 13637−13641.
(14) Xing, D. D.; Jia, Y. W.; Li, D. F.; Wang, X. L.; Wang, Y. Z. Novel Multiblock Poly(ε caprolactone) Copolyesters Containing D Glucose Derivatives with Different Bicyclic Structures. *ACS Sustainable Chem. Eng.* **2017**, *5*, 7040−7051.
(15) Kieber, R. J.; Silver, S. A.; Kennemur, J. G. Stereochemical effects on the mechanical and viscoelastic properties of renewable polyurethanes derived from isohexides and hydroxymethylfurfural. *Polym. Chem.* **2017**, *8*, 4822−4829.
(16) Paszkiewicz, S.; Szymczyk, A.; Pawlikowska, D.; Irska, I.; Taraghi, I.; Pilawka, R.; Gu, J.; Li, X.; Tu, Y.; Piesowicz, E. Synthesis and characterization of poly (ethylene terephthalate co 1, 4 cyclo hexanedimethylene terephtlatate) block poly (tetramethylene oxide) copolymers. *RSC Adv.* **2017**, *7*, 41745−41754.
(17) Qiu, J.; Liu, F.; Zhang, J.; Na, H.; Zhu, J. Non planar ring contained polyester modifying polylactide to pursue high toughness. *Compos. Sci. Technol.* **2016**, *128*, 41−48.
(18) Yoon, W. J.; Hwang, S. Y.; Koo, J. M.; Lee, Y. J.; Lee, S. U.; Im, S. S. Synthesis and characteristics of a biobased high T g terpolyester of isosorbide, ethylene glycol, and 1,4 cyclohexane dimethanol: effect of ethylene glycol as a chain linker on polymerization. *Macromolecules* **2013**, *46*, 7219−7231.
(19) Bhowmick, A.; Kuo, C.; Manzur, A.; Arthur, A. M.; Intyre, D. M. Properties of cis and trans polyisoprene blends. *J. Macromol. Sci., Part B: Phys.* **1986**, *25*, 283−306.
(20) Kent, E.; Swinney, F. Properties and applications of trans 1, 4 polyisoprene. *Ind. Eng. Chem. Prod. Res. Dev.* **1966**, *5*, 134−138.
(21) Baboo, M.; Dixit, M.; Sharma, K.; Saxena, N. S. Mechanical and thermal characterization of cis polyisoprene and trans polyisoprene blends. *Polym. Bull.* **2011**, *66*, 661−672.
(22) DiCiccio, A. M.; Coates, G. W. Ring opening copolymerization of maleic anhydride with epoxides: a chain growth approach to unsaturated polyesters. *J. Am. Chem. Soc.* **2011**, *133*, 10724−10727.
(23) Tang, T.; Moyori, T.; Takasu, A. Isomerization free polycondensations of cyclic anhydrides with diols and preparation of polyester gels containing cis or trans carbon double bonds via photo cross linking and isomerization in the gels. *Macromolecules* **2013**, *46*, 5464−5472.
(24) Wilson, J. A.; Luong, D.; Kleinfehn, A. P.; Sallam, S.; Wesdemiotis, C.; Becker, M. L. Magnesium catalyzed polymerization of end functionalized poly(propylene maleate) and poly(propylene fumarate) for 3D printing of bioactive scaffolds. *J. Am. Chem. Soc.* **2018**, *140*, 277−284.
(25) Grobelny, J. Nmr study of maleate (cis)—fumarate (trans) isomerism in unsaturated polyesters and related compounds. *Polymer* **1995**, *36*, 4215−4222.
(26) Yu, Y.; Wei, Z.; Leng, X.; Li, Y. Facile preparation of stereochemistry controllable biobased poly (butylene maleate co butylene fumarate) unsaturated copolyesters: a chemoselective polymer platform for versatile functionalization via aza Michael addition. *Polym. Chem.* **2018**, *9*, 5426−5441.
(27) Truong, V. X.; Dove, A. P. Organocatalytic, regioselective nucleophilic "click" addition of thiols to propiolic acid esters for polymer−polymer coupling. *Angew. Chem.* **2013**, *125*, 4226−4230.
(28) Bell, C. A.; Yu, J.; Barker, I. A.; Truong, V. X.; Cao, Z.; Dobrinyin, A. V.; Becker, M. L.; Dove, A. P. Independent control of elastomer properties through stereocontrolled synthesis. *Angew. Chem., Int. Ed.* **2016**, *55*, 13076−13080.
(29) Chan, J. W.; Hoyle, C. E.; Lowe, A. B.; Bowman, M. Nucleophile initiated thiol Michael reactions: effect of organocatalyst, thiol, and ene. *Macromolecules* **2010**, *43*, 6381−6388.
(30) Lowe, A. B.; Hoyle, C. E.; Bowman, C. N. Thiol yne click chemistry: A powerful and versatile methodology for materials synthesis. *J. Mater. Chem.* **2010**, *20*, 4745−4750.

DOI: 10.1021/acs.macromol.9b01700
Macromolecules 2020, 53, 174−181

(31) Lowe, A. B. Thiol−ene "click" reactions and recent applications in polymer and materials synthesis: a first update. *Polym. Chem.* **2014**, *5*, 4820−4870.
(32) Vandenbergh, J.; Ranieri, K.; Junkers, T. Synthesis of (Bio) Degradable Poly(β thioester)s via Amine Catalyzed Thiol−Ene Click Polymerization. *Macromol. Chem. Phys.* **2012**, *213*, 2611−2617.
(33) Shin, J.; Matsushima, H.; Chan, J. W.; Hoyle, C. E. Segmented Polythiourethane Elastomers through Sequential Thiol−Ene and Thiol−Isocyanate Reactions. *Macromolecules* **2009**, *42*, 3294−3301.
(34) Likhtman, A. E.; McLeish, T. C. B. Quantitative Theory for Linear Dynamics of Linear Entangled Polymers. *Macromolecules* **2002**, *35*, 6332−6343.
(35) Coleman, M. M.; Lee, K. H.; Skrovanek, D. J.; Painter, P. C. Hydrogen bonding in polymers. 4. Infrared temperature studies of a simple polyurethane. *Macromolecules* **1986**, *19*, 2149−2157.
(36) Frick, A.; Rochman, A. Characterization of TPU elastomers by thermal analysis (DSC). *Polym. Test.* **2004**, *23*, 413−417.
(37) Galanos, E.; Grune, E.; Wahlen, C.; Müller, A. H.; Appold, M.; Gallei, M.; Frey, H.; Floudas, G., Tapered Multiblock Copolymers Based on Isoprene and 4 Methylstyrene: Influence of the Tapered Interface on the Self Assembly and Thermomechanical Properties. *Macromolecules* **2019**, *52*, 1577.
(38) Basterretxea, A.; Gabirondo, E.; Flores, I.; Etxeberria, A.; Gonzalez, A.; Müller, A. J.; Mecerreyes, D.; Coulembier, O.; Sardon, H., Isomorphic Polyoxyalkylene Copolyethers Obtained by Copoly merization of Aliphatic Diols. *Macromolecules* **2019**, *52*, 3506.
(39) Briber, R. M.; Thomas, E. L. The structure of MDI/BDO based polyurethanes: Diffraction studies on model compounds and oriented thin films. *J. Polym. Sci., Polym. Phys. Ed.* **1985**, *23*, 1915−1932.
(40) Lucas, J. C.; Failla, M. D.; Smith, F. L.; Mandelkern, L.; Peacock, A. J. The double yield in the tensile deformation of the polyethylenes. *Polym. Eng. Sci.* **1995**, *35*, 1117−1123.
(41) Zhou, C.; Guo, H.; Li, J.; Huang, S.; Li, H.; Meng, Y.; Yu, D.; de Claville Christiansen, J.; Jiang, S. Temperature dependence of poly(lactic acid) mechanical properties. *RSC Adv.* **2016**, *6*, 113762−113772.

DOI: 10.1021/acs.macromol.9b01700
Macromolecules 2020, 53, 174−181

2.2 Supporting Information

Unsaturated poly(ester-urethanes) with stereochemically-dependent thermomechanical properties

Connor J. Stubbs[§], Joshua C. Worch[§], Hannah Prydderch[§], Matthew L. Becker[†], Andrew P. Dove[§*]*

[§]School of Chemistry, University of Birmingham, Edgbaston, Birmingham, B15 2TT, UK

[†] Department of Chemistry, Department of Mechanical Engineering & Materials Science, Department of Orthopaedic Surgery, Duke University, 308 Research Drive, Durham, NC 27708

Contents of PDF

Materials **2**
Methods **2-5**
Synthetic procedures **5-11**
NMR Spectroscopy of Monomers **12-14**
NMR Spectroscopy of Polymers **15-22**
Polymer Size Exclusion Chromatography table **23**
Size Exclusion Chromatograms **24-25**
Rheological Frequency Sweeps and Time-Temperature Supposition (TTS) **26**
***M*$_e$ Calculation table** **27**
IR of Homopolymers **28**
Thermomechanical Table Overview **29**
Differential scanning calorimetry thermograms **30-32**
Thermogravimetric analysis plot **33**
Tensile Stress *vs* Strain curves **34-35**
Dynamic Mechanical Thermal Analysis **36-37**
References **38**

Materials

The following chemicals were used as they were received: 1,4-Butanediol (Sigma-Aldrich, 99%), *cis*-2-butene-1,4-diol (Acros, 97%), 2-butyne-1,4-diol (Sigma-Aldrich, 99%), d_1–Chloroform (Apollo scientific, >99.8%), Dibutyltin(IV) dilaurate (DBTDL, Sigma Aldrich, 95%), Diethyl ether (Et_2O, Sigma-Aldrich, ≥99.7%), N,N'-dimethylformamide (DMF, Fisher scientific, 99.5%), Dimethylphenylphosphine (Me_2PPh, Sigma-Aldrich, 99%), Ethyl acetate (EtOAc: VWR, ≥99.5%), n-hexane (VWR, ≥95%), Lithium aluminium hydride ($LiAlH_4$: Sigma-Aldrich, 95%), Tetrahydrofuran (THF: Sigma-Aldrich, ≥99.9%).

1,6-hexanedithiol (Sigma-Aldrich, 97%) was distilled under vacuum before use and stored under N_2 in a Schlenk-flask. *Trans*-2-butene-1,4-diol was synthesized according to literature procedure.[1]

Methods

NMR characterization

All NMR experiments were performed at 298 K on a Bruker DPX-400 NMR instrument equipped operating at 400 MHz for ^1H (100.57 MHz for ^{13}C). ^1H NMR spectra are referenced to residual protio solvent (7.26 for $CDCl_3$) and ^{13}C NMR spectra are referenced to the solvent signal (δ 77.2 for $CDCl_3$). The resonance multiplicities are described as s (singlet), d (doublet), t (triplet), q (quartet) or m (multiplet).

High Resolution Mass Spectrometry (HRMS)

High Resolution Electrospray Ionization Mass Spectrometry was performed in the School of Chemistry at University of Birmingham on a Waters Xevo G2-XS QTof Quadrupole Time-of-Flight mass spectrometer

Fourier-transform Infared spectroscopy (FTIR)

FTIR spectroscopy was carried out using an Agilent Technologies Cary 630 FTIR spectrometer. 16 Scans from 600 to 4000 cm^{-1} were taken at a resolution of 4 cm^{-1}, and the spectra were corrected for background absorbance.

Size Exclusion Chromatography (SEC)

SEC measurements were performed on an Agilent 1260 Infinity II Multi-Detector GPC/SEC System fitted with RI and ultraviolet (UV) detectors (λ = 309 nm) and PLGel 3 µm (50 × 7.5 mm) guard column and two PLGel 5 µm (300 × 7.5 mm) mixed-C columns with DMF with 5 mM NH_4BF_4 as the eluent (flow rate 1 mL/min, 50 °C). A 12-point calibration based on poly(methyl methacrylate) standards (PMMA, Easivial PM, Agilent) was applied for determination of molecular weights.

Dynamic mechanical thermal analysis (DMTA)

Thin polymer films were fabricated using a Specac Atlas™ Manual Hydraulic Press 15T fitted with Specac heated plates. Films with a thickness of 0.5 ± 0.1 mm were prepared by melt compressing the polymers under *ca*. 5 kN of force in a hot press followed by cooling to ambient temperature in the press whilst under compression. Polymer samples were in an aluminum rectangular spacer (40 × 50 × 0.5 mm) between PTFE sheets and placed between heated plates at 100 °C unless stated otherwise* and then cooled to ambient temperature maintaining 5 kN of force. Film samples were visually inspected for deformation and bubbles before annealing for 7 days at 25 °C. Samples were cut into rectangular bars (6 × 11 × 0.5 mm). Samples were measured in tension on Mettler-Toledo DMA 1 with a thermal sweep (2 $K \cdot min^{-1}$) from -50 °C to 120 °C with a frequency of 1 Hz and preload force of 0.1 N.

*Sample S_{100} was pressed at 120 °C due to higher melt transition.

Differential scanning calorimetry (DSC)

Determination of the thermal characteristic of the polymer were carried out using a STARe system DSC3 with auto-sampler (Mettler Toledo, Switzerland). Disc shapes measuring 5 mm in diameter and 0.4 - 0.6 mm in thickness weighing between 9-14 mg were cut from 7 day annealed polymer films (preparation listed in DMTA procedure). Sample discs were positioned in 40 μL aluminum pans. Thermograms obtained with a heating rate of 10 $K \cdot min^{-1}$ were recorded from -50 – 200 °C with a 10 $K \cdot min^{-1}$ heating and cooling rate over two cycles. The glass transition temperature (T_g) was determined by the minimum of the first derivative in the second heating cycle of DSC. Thermograms obtained with a heating rate of 1 $K \cdot min^{-1}$ were recorded from 0 – 100 °C on a single cycle. Total enthalpy of melting (ΔH_m) was calculated from integration and normalization of all endothermic peaks present.

Thermal gravimetric analysis (TGA)

TGA data was obtained using a Q50 - Thermogravimetric Analyzer (TA instruments)**.** Thermograms were recorded under an N_2 atmosphere at a heating rate of 10 $K \cdot min^{-1}$, from 25 − 500 °C, with an average sample weight of *ca*. 10 mg. Decomposition temperatures were reported as the 5% weight loss temperature ($T_{d\,5\%}$).

Tensile testing

Tensile tests were performed using 7 day-annealed polymer films fabricated using a vacuum compression machine (TMP Technical Machine Products Corp.) Polymer samples were placed between a rectangular mould (50 × 50 × 0.5 mm) and placed in the compression machine with the vacuum on. The machine was heated to 100 °C unless otherwise stated, once temperature was reached sample was degassed 3 times and 5 lbs × 1000 of pressure was applied and held for 5 minutes. The machine was then cooled to ambient temperature and samples were visually

inspected for deformation and bubbles. Polymer films were annealed at 25 °C for 7 days before dumbbell shaped samples were cut using custom ASTM Die D-638 Type 5 (Neck dimensions 7.11 × 1.70 × 0.5 mm). Tensile tests were carried out using Instron (Instron 5543 Universal Testing Machine) at room temperature (25 ± 1 °C). A pre-stress of 0.01 MPa was applied and elongated at 10 mm·min^{-1} until failure. The reported results are average values from 5 samples (unless otherwise specified) with the standard deviation presented as the uncertainty.

*Sample S_{100} was pressed at 120 °C due to higher melt transition.

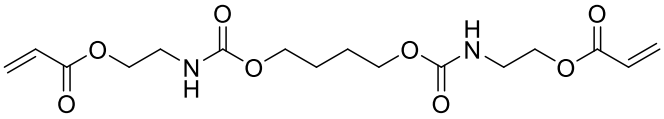
Rheology and M_e calculation

Rheology was performed on an Anton Paar MCR 302 using a PP8 geometry on discs (8 × 1 mm) cut out of homopolymers films fabricated using a Specac Atlas™ Manual Hydraulic Press 15T fitted with Specac heated plates(as detailed in DMTA method). Temperature was controlled with a P-PTD 200/AIR Peltier and a P-PTD 200 hood. Frequency sweeps were performed at 1% strain from 1 to 400 rad s^{-1} at 5°C intervals between the temperatures of 80°C to 110°C. G' and G'' were overlayed to a single spectrum at a reference temperature of 85 °C by applying a Williams-Landel-Ferry (WLF) time-temperature superposition. Molecular entanglement was extracted by fitting polydisperse double reptation theory in the REPTATE software package.[2] Molecular weights obtained from SEC, were discretized to 10 values per decade and used as theory input. The adjustable parameters in the fitting were G_e (Entanglement modulus) M_e (entanglement molecular weight) τ_e (Rouse time of one entangled segment) and the value of M_0 was kept to a value of 0.001 kg·mol^{-1}as recommended.

Synthetic procedures

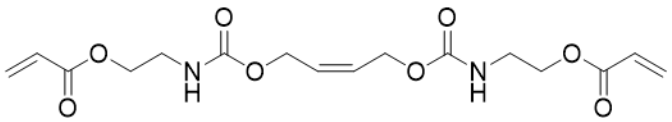
Required inert conditions were implemented using conventional Schlenk-techniques under dry N_2 with dimethylphenylphosphine (DMPP) and 1,6-hexanedithiol stored in Schlenk flasks.

Synthesis of 4,11-dioxo-5,10-dioxa-3,12-diazatetradecane-1,14-diyl diacrylate (Monomer S)



A single necked 100 mL round bottom flask was charged with 1,4-butanediol (4.5 g, 50 mmol, 1.00 equiv) dissolved in THF (26 mL) and cooled to 0 °C with an ice bath. The solution was stirred and 2-isocyanatoethyl acrylate (14.8 g, 105 mmol, 2.10 equiv) was charged *via* syringe. DBTL (60 µL, 0.2 mol%) was added to the solution and left to stir for overnight *ca.* 16 h. During this time a white precipitate was formed, the remaining solvent was then removed under vacuum. The resulting white powder was purified by recrystallization from EtOAc/Hexanes to afford title compound as a white crystalline solid (15.4 g, 83%). ^{1}H NMR (400 MHz; 298 K; $CDCl_3$) 6.46-6.40 (dd, J = 24, 1.6 Hz, 2H, **H**HC=CH) 6.17-6.08 (dd, J = 36.2, 14 Hz, 2H, H_2C=C**H**) 5.88-5.84 (dd, J = 12, 2 Hz, 2H, H**H***C*=CH) 5.00 (s broad due to rotamers, 2H, O=C-N**H**) 4.23 (t, J = 7.2 Hz, 4H, O-C**H**$_2$-CH_2-CH_2) 4.09 (s poor resolution, 4H, O-C**H**$_2$-CH_2-NH) 3.51-3.46 (q, J = 7.2 Hz, 4H, H_2C-C**H**$_2$-NH) 1.68 (m, 4H, C**H**$_2$-CH_2-CH_2) ^{13}C NMR (100.57 MHz; 298 K; $CDCl_3$) 166.24, 156.69, 131.63, 128.14, 64.78, 63.76, 40.27, 25.77. FTIR 3349 (N-H) 1710 (C=O ester) 1683 (C=O urethane) 1631 cm^{-1} (C=C). HRMS (ESI-TOF) (*m*/*z*): $[M + H]^+$ calculated for $C_{16}H_{24}N_2O_8Na$, 395.1430; found, 395.1432.

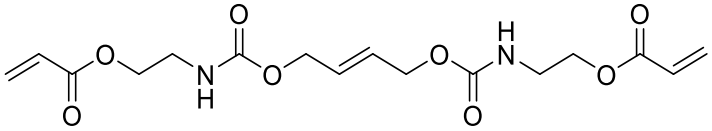
Synthesis of (Z)-4,11-dioxo-5,10-dioxa-3,12-diazatetradec-7-ene-1,14-diyl diacrylate (Monomer C)



A single necked 100 mL round bottom flask was charged with *cis*-2-butene-1,4-diol (5.45 g, 62 mmol, 1.00 equiv) dissolved in THF (28 mL) and cooled to 0 °C with an ice bath. The solution was stirred and 2-isocyanatoethyl acrylate (18.30 g, 132 mmol, 2.12 equiv) was charged *via*

syringe. DBTL (71 µL, 0.2 mol%) was added to the solution and left to stir for 6 h. The solvent was removed under vacuum *Note: Heating should be avoided to prevent undesirable crosslinking reactions during solvent removal*. The resulting white powder was purified by recrystallization from EtOAc/Hexanes to afford title compound as a white powder (18.5 g, 80.7%). ^{1}H NMR (400 MHz; 298 K; $CDCl_3$) 6.45-6.39 (dd, *J*= 26, 2Hz, 2H, **H**HC=CH) 6.14-6.07 (dd, *J*= 14, 23.2 Hz, 2H, H_2C=C**H**) 5.89-5.86 (dd, *J*= 12, 2 Hz, 2H, H**H***C*=CH) 5.72 (s, 2H, **H**C=CH) 5.08 (s broad due to rotamers, 2H, O=C-N**H**) 4.67 (d, J= 6 Hz, 4H, O-C**H**$_2$-CH) 4.22 (t, *J*= 7.2 Hz, 4H, O-C**H**$_2$-CH_2) 3.49 (q, *J*= 7.6Hz, 4H, H_2C-C**H**$_2$-NH) ^{13}C NMR (100.57 MHz; 298 K; $CDCl_3$) 166.21, 156.29, 131.63, 128.40, 128.10, 64.14, 60.72, 40.32. FTIR 3334 (N-H) 1713 (C=O ester) 1687 (C=O urethane) 1635 cm^{-1} (C=C). HRMS (ESI-TOF) (*m*/*z*): $[M + H]^+$ calculated for $C_{16}H_{22}N_2O_8Na$, 393.1273; found, 395.1274.

Synthesis of (E)-4,11-dioxo-5,10-dioxa-3,12-diazatetradec-7-ene-1,14-diyl diacrylate (Monomer T)



A single necked 100 mL round bottom flask was charged with *trans*-2-butene-1,4-diol (4.16 g, 47 mmol, 1.00 Equiv) and THF (22 mL) before being cooled to 0 °C with an ice bath. The solution was stirred and 2-isocyanatoethyl acrylate (14 g, 101 mmol, 2.05 equiv) was charged *via* syringe. DBTL (55 µL, 0.2 mol%) was added to the solution and left to stir for 2 h. During this time a white precipitate was formed. The remaining solvent was removed under vacuum and the resulting white powder was purified by recrystallization from toluene to afford title compound as a white crystal (15.2 g, 87%). ^{1}H NMR (400 MHz; 298 K; $CDCl_3$) 6.44-6.38 (dd, *J*= 22.8 Hz, 2Hz, 2H, **H**HC=CH) 6.17-6.08 (dd, *J*= 36.8, 14 Hz, 2H, H_2C=C**H**) 5.88-5.83 (m obscured, H**H***C*=CH) 5.83 (m obscured, **H**C=CH) 5.03 (s broad, 2H, O=C-N**H**) 4.58 (s poor resolution, O-C**H**$_2$-CH) 4.24 (t, J=

8 Hz, 4H, O-C**H**$_2$-CH$_2$) 3.52-3.47 (q, *J*= 7.2Hz, 4H, H$_2$C-C**H**$_2$-NH) ^{13}C NMR (100.57 MHz; 298 K; $CDCl_3$) 166.03, 156.03, 131.48, 128.23, 127.91, 64.47, 63.51, 40.15. FTIR 3335 (N-H) 1713 (C=O ester) 1687 (C=O urethane) 1635 cm^{-1} (C=C). HRMS (ESI-TOF) (*m*/*z*): $[M + H]^+$ calculated for $C_{16}H_{22}N_2O_8Na$, 393.1274; found, 393.1276.

Standard step-growth Polymerization procedure (Example given S_{100} polymer)

A scintillation vial was charged with 1,6-hexanedithiol (1.9873 g, 13.2 mmol, 1.00 equiv) and another scintillation vial is charged with monomer S (4.9285 g, 13.3 mmol, 1.00 equiv). The contents of both scintillations vials were dissolved in DMF (52 mL) and quantitatively transferred to a 100 mL single necked round bottom flask and stirred at ambient temperature. Whilst stirring, polymerization was initiated with DMPP (38 μL, 2 %mol) and left to stir. Initially an exotherm was observed with a visible increase in viscosity. After 2 h the polymer solution was precipitated in Et_2O (1000 mL) and left to stir for an hour before decanting the supernatant. The remaining polymer was dried *in vacuo* at 100 °C for 2 h in order to remove residual DMF and Et_2O. SEC analysis (DMF + 5 mM NH_4BF_4) M_w = 139 kDa, M_n = 30.8 kDa, M_p = 117 kDa, $Đ_M$ = 4.51. ^{1}H NMR (400 MHz; 298 K; $CDCl_3$) 5.17 (s broad, 2H, O=C-N**H**), 4.20 – 4.16 (t, *J* = 5.3 Hz, 4H, O-C**H**$_2$-CH$_2$-NH), 4.10 – 4.07 (d, *J* = 5.6 Hz, 4H, O-C**H**$_2$-CH$_2$-CH$_2$), 3.46 – 3.42 (q, *J* = 5.5 Hz, 4H, H$_2$C-C**H**$_2$-NH), 2.80 – 2.76 (t, *J* = 7.2 Hz, 4H, O=C-CH$_2$-C**H**$_2$-S), 2.66 – 2.60 (t, *J* = 7.0 Hz, 4H, S-C**H**$_2$-CH$_2$-CH$_2$), 2.57 – 2.51 (t, *J* = 7.4 Hz, 4H, O=C-C**H**$_2$-CH$_2$-S), 1.78 – 1.64 (m, 4H obscured, CH$_2$-C**H**$_2$-CH$_2$-O), 1.64 – 1.52 (m, 4H, C**H**$_2$-CH$_2$-S), 1.45 – 1.32 (m, 4H, C**H**$_2$-CH$_2$-CH$_2$-S). ^{13}C NMR (100.57 MHz; 298 K; $CDCl_3$) 172.06, 156.74, 64.75, 63.86, 40.17, 34.85, 32.19, 29.51, 28.53, 27.15, 25.79.

Polymer characterization

C_{100} polymer: SEC analysis (DMF + 5mM NH_4BF_4) M_w = 250 kDa, M_n = 34.8 kDa, M_p = 109 kDa, $Đ_M$ = 7.19. ^{1}H NMR (400 MHz; 298 K; $CDCl_3$) 5.73 – 5.71 (t, J = 4.1 Hz, 2H, **H**C=CH), 5.27 – 5.24 (t, J = 6.0 Hz, 2H, O=C-N**H**), 4.70 – 4.63 (d, J = 4.3 Hz, 4H, **H**C-CH=CH), 4.24 – 4.16 (t, J = 5.3 Hz, 4H, O-C**H**$_2$-CH_2-NH), 3.46 – 3.40 (q, J = 5.6 Hz, 4H, H_2C-C**H**$_2$-NH), 2.79 – 2.76 (t, J = 7.3 Hz, 4H, O=C-CH_2-C**H**$_2$-S), 2.64 – 2.60 (t, J = 7.2 Hz, 4H, S-C**H**$_2$-CH_2-CH_2), 2.55 – 2.51 (t, J = 7.4 Hz, 4H, O=C-C**H**$_2$-CH_2-S), 1.62 – 1.55 (m, 4H, C**H**$_2$-CH_2-S), 1.48 – 1.22 (m, 4H, C**H**$_2$-CH_2-CH_2-S). ^{13}C NMR (100.57 MHz; 298 K; $CDCl_3$) 172.05, 156.36, 128.38, 63.79, 60.76, 40.22, 34.83, 32.17, 29.48, 28.51, 27.14.

T_{100} polymer: SEC analysis (DMF + 5mM NH_4BF_4) M_w = 103 kDa, M_n = 28.7 kDa, M_p = 89 kDa, $Đ_M$ = 3.57. ^{1}H NMR (400 MHz; 298 K; $CDCl_3$) 5.83 (s, 2H, **H**C=CH), 5.28 – 5.25 (s broad, 2H, O=C-N**H**), 4.57 – 4.56 (d, J = 3.2 Hz, 4H, **H**C-CH=CH), 4.19 – 4.16 (t, J = 5.3 Hz, 4H, O-C**H**$_2$-CH_2-NH), 3.50 – 3.39 (q, J = 5.5 Hz, 4H, H_2C-C**H**$_2$-NH), 2.79 – 2.75 (t, J = 7.3 Hz, 4H, O=C-CH_2-C**H**$_2$-S), 2.64 – 2.60 (t, J = 7.0 Hz, 4H, S-C**H**$_2$-CH_2-CH_2), 2.54 – 2.51 (t, J = 7.3 Hz, 4H, O=C-C**H**$_2$-CH_2-S), 1.65 – 1.50 (m obscured, 4H, C**H**$_2$-CH_2-S), 1.44 – 1.32 (m, 4H, C**H**$_2$-CH_2-CH_2-S). ^{13}C NMR (100.57 MHz; 298 K; $CDCl_3$) 172.05, 156.32, 128.41, 64.64, 63.81, 40.23, 34.85, 32.19, 29.49, 28.51, 27.15.

$C_{50}S_{50}$ polymer: SEC analysis (DMF + 5mM NH_4BF_4) M_w = 209 kDa, M_n = 34.9 kDa, M_p = 94 kDa, $Đ_M$ = 5.99. ^{1}H NMR (400 MHz; 298 K; $CDCl_3$) 5.72-5.70 (s, 1H, **H**C=CH), 5.22 (s, 1H overlapping, *cis* O=C-N**H**), 5.16 (s, 1H overlapping, *saturated* O=C-N**H**), 4.67-4.66 (d, J = 4.3 Hz, 2H, **H**C-CH=CH), 4.19-4.15 (t, J = 5.3 Hz, 4H, O-C**H**$_2$-CH_2-NH), 4.08 (s, 2H, O-C**H**$_2$-CH_2-CH_2), 3.46-3.43 (d, J = 5.9 Hz, 4H, H_2C-C**H**$_2$-NH), 2.81 – 2.73 (m, 4H, O=C-CH_2-C**H**$_2$-S), 2.63-2.60 (t, J = 8.2 Hz, 4H, S-C**H**$_2$-CH_2-CH_2), 2.55 – 2.49 (t, J = 7.9 Hz 4H, O=C-C**H**$_2$-CH_2-S), 1.67

(s, 2H, CH_2-C**H**$_2$-CH_2-O), 1.61-1.54 (m, 4H, C**H**$_2$-CH_2-S), 1.44 – 1.34 (m, 4H, C**H**$_2$-CH_2-CH_2-S). ^{13}C NMR (100.57 MHz; 298 K; $CDCl_3$) 172.05, 156.75, 156.36, 128.39, 64.75, 63.86, 63.79, 60.77, 40.23, 40.16, 34.84, 32.19, 29.49, 28.52, 27.15, 25.78.

$T_{50}S_{50}$ polymer: SEC analysis (DMF + 5mM NH_4BF_4) M_w = 141 kDa, M_n = 34.4 kDa, M_p = 77 kDa, $Đ_M$ = 4.09. ^{1}H NMR (400 MHz; 298 K; $CDCl_3$) 5.91 – 5.75 (s, 1H, **H**C=CH), 5.26 (s, 1H, *trans* O=C-N**H**), 5.18 (s, 1H, *saturated* O=C-N**H**), 4.56 (d, *J* = 3.3 Hz, 2H, **H**C-CH=CH), 4.23 – 4.12 (t, *J* = 5.6 Hz, 4H, O-C**H**$_2$-CH_2-NH), 4.08-4.06 (s, 2H, O-C**H**$_2$-CH_2-CH_2), 3.44 (m, *J* = 5.3 Hz, 4H, H_2C-C*H*$_2$-NH), 2.77 (t, J = 7.2 Hz, 4H, O=C-CH_2-C**H**$_2$-S), 2.62 (t, *J* = 7.2 Hz, 4H, S-C**H**$_2$-CH_2-CH_2), 2.52 (t, *J* = 7.3 Hz, 4H, O=C-C**H**$_2$-CH_2-S), 1.72 – 1.63 (m, 2H, CH_2-C**H**$_2$-CH_2-O), 1.57 (q, *J* = 7.1 Hz, 5H, C**H**$_2$-CH_2-S), 1.45 – 1.26 (m, 4H, C**H**$_2$-CH_2-CH_2-S). ^{13}C NMR (100.57 MHz; 298 K; $CDCl_3$) 172.04, 156.74, 156.31, 128.41, 64.73, 64.63, 63.85, 63.79, 40.22, 40.16, 34.83, 32.18, 29.48, 28.51, 27.14, 25.77.

$C_{75}T_{25}$ Polymer: SEC analysis (DMF + 5mM NH_4BF_4) M_w = 194 kDa, M_n = 36.6 kDa, M_p = 70 kDa, $Đ_M$ = 5.30. ^{1}H NMR (400 MHz; 298 K; $CDCl_3$) 5.83 (s, 0.5H, *trans* **H**C=CH), 5.73-5.71 (s, 1.5H, *cis* **H**C=CH), 5.29 – 5.19 (m broad, 2H, O=C-N**H**), 4.67 (d, J = 4.3 Hz, 3H, *cis* **H**C-CH=CH), 4.57-4.56 (d, J = 3.1 Hz, 1H, *trans* **H**C-CH=CH), 4.19-4.17 (t, J = 5.3 Hz, 4H, O-C**H**$_2$-CH_2-NH), 3.47-3.42 (q, J = 5.4 Hz, 4H, H_2C-C**H**$_2$-NH), 2.79-2.76 (t, J = 7.2 Hz, 4H, O=C-CH_2-C**H**$_2$-S), 2.63-2.60 (t, J = 7.2 Hz, 4H, S-C**H**$_2$-CH_2-CH_2), 2.54-2.50 (t, J = 7.3 Hz, 4H, O=C-C**H**$_2$-CH_2-S), 1.62-1.55 (m, 4H, C**H**$_2$-CH_2-S), 1.42-1.37 (m, 4H, C**H**$_2$-CH_2-CH_2-S). ^{13}C NMR (100.57 MHz; 298 K; $CDCl_3$) 172.07, 156.38, 128.41, 64.66, 63.81, 60.78, 40.25, 34.85, 32.20, 29.50, 28.53, 27.17.

$C_{50}T_{50}$ Polymer: SEC analysis (DMF + 5mM NH_4BF_4) M_w = 208 kDa, M_n = 38.7 kDa, M_p = 87 kDa, $Đ_M$ = 5.37. ^{1}H NMR (400 MHz; 298 K; $CDCl_3$) 5.83 (s broad, 1H, *trans* **H**C=CH), 5.72 (s,

1H, *cis* **H**C=CH), 5.24 (s, 2H, O=C-N**H**), 4.67 (d, J = 4.3 Hz, 2H, *cis* **H**C-CH=CH), 4.57 (d, J = 3.2 Hz, 2H, *trans* **H**C-CH=CH), 4.18 (t, J = 5.3 Hz, 4H, O-C**H**$_2$-CH$_2$-NH), 3.52 – 3.39 (m, 4H, H$_2$C-C**H**$_2$-NH), 2.81 – 2.74 (m, 4H, O=C-CH$_2$-C**H**$_2$-S), 2.65 – 2.59 (m, 4H, S-C**H**$_2$-CH$_2$-CH$_2$), 2.53 (t, J = 7.9 Hz, 4H, O=C-C**H**$_2$-CH$_2$-S), 1.65 – 1.52 (m, obscured, C**H**$_2$-CH$_2$-S), 1.44 – 1.34 (m, 4H, C**H**$_2$-CH$_2$-CH$_2$-S). ^{13}C NMR (100.57 MHz; 298 K; $CDCl_3$) 172.05, 156.33, 128.41, 64.64, 63.80, 60.76, 40.23, 34.84, 32.19, 29.48, 28.51, 27.15.

C$_{25}$T$_{75}$ Polymer: SEC analysis (DMF + 5mM NH_4BF_4) M_w = 129 kDa, M_n = 30.8 kDa, M_p = 61 kDa, $Đ_M$ = 4.18. ^{1}H NMR (400 MHz; 298 K; $CDCl_3$) 5.83 – 5.82 (s broad, 1.5H, *trans* **H**C=CH), 5.72-5.70 (s, 0.5H, *cis* **H**C=CH), 5.25 (s broad, 2H, O=C-N**H**), 4.66 (d, *J* = 4.3 Hz, 1H, *cis* **H**C-CH=CH), 4.56 (d, *J* = 3.2 Hz, 3H, *trans* **H**C-CH=CH), 4.18 (t, *J* = 5.3 Hz, 4H, O-C**H**$_2$-CH$_2$-NH), 3.45 (q, *J* = 5.5 Hz, 4H, H$_2$C-C**H**$_2$-NH), 2.77 (t, *J* = 7.0 Hz, 4H, O=C-CH$_2$-C**H**$_2$-S), 2.62 (t, *J* = 7.0 Hz, 4H, S-C**H**$_2$-CH$_2$-CH$_2$), 2.56 – 2.47 (m, 4H, O=C-C**H**$_2$-CH$_2$-S), 1.57 (q, *J* = 7.2 Hz, 4H, C**H**$_2$-CH$_2$-S), 1.46 – 1.33 (m, 4H, C**H**$_2$-CH$_2$-CH$_2$-S). ^{13}C NMR (100.57 MHz; 298 K; $CDCl_3$) 172.06, 156.32, 128.43, 64.66, 63.83, 60.77, 40.25, 34.86, 32.21, 29.51, 28.53, 27.17.

NMR spectra of monomers

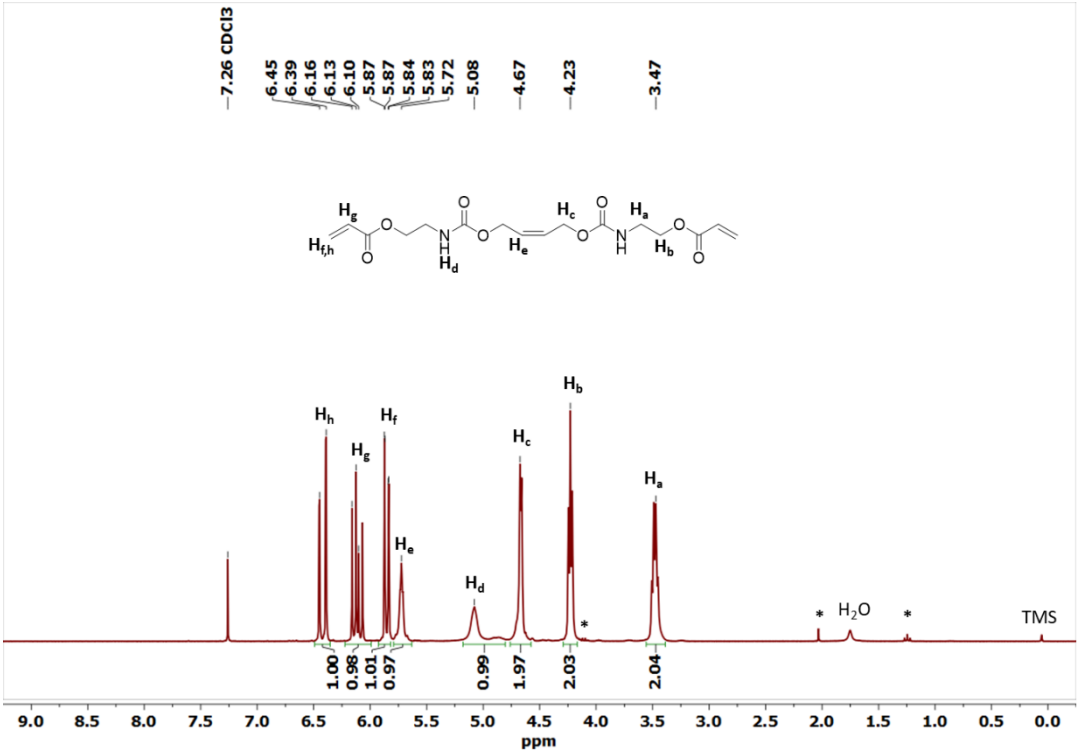


Figure S1. ^{1}H NMR of monomer C (400 MHz; 298 K; $CDCl_3$).

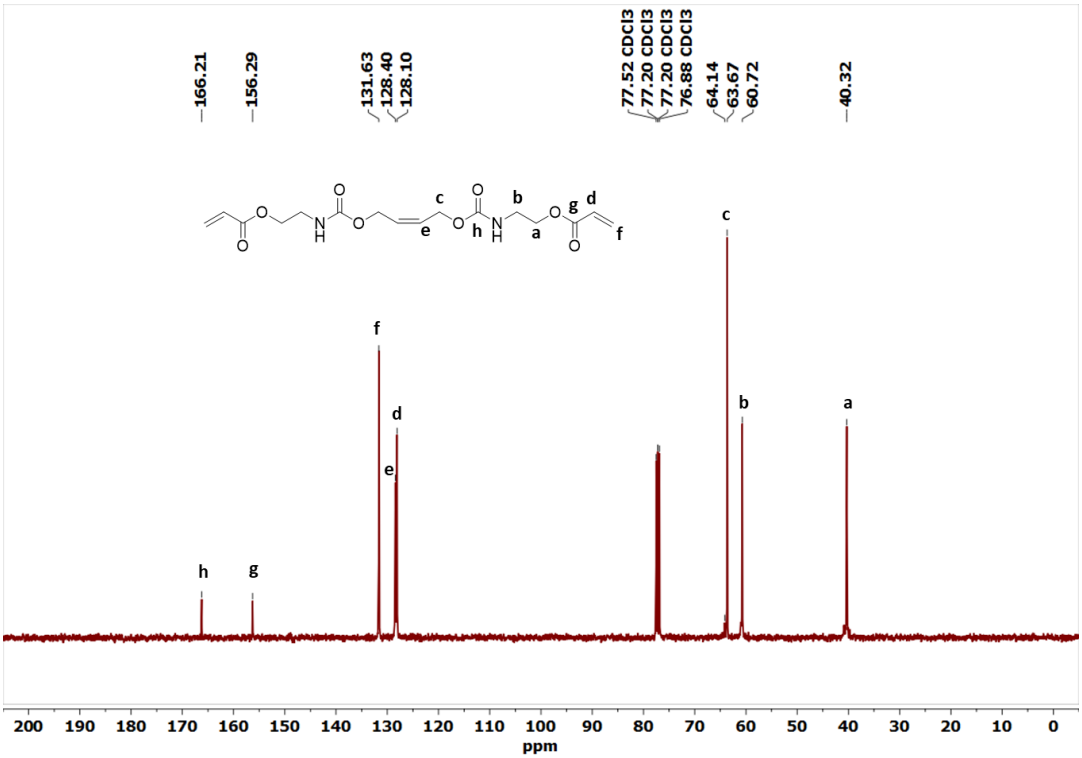


Figure S2. ^{13}C NMR spectrum of monomer C (100.57 MHz; 298 K; $CDCl_3$).

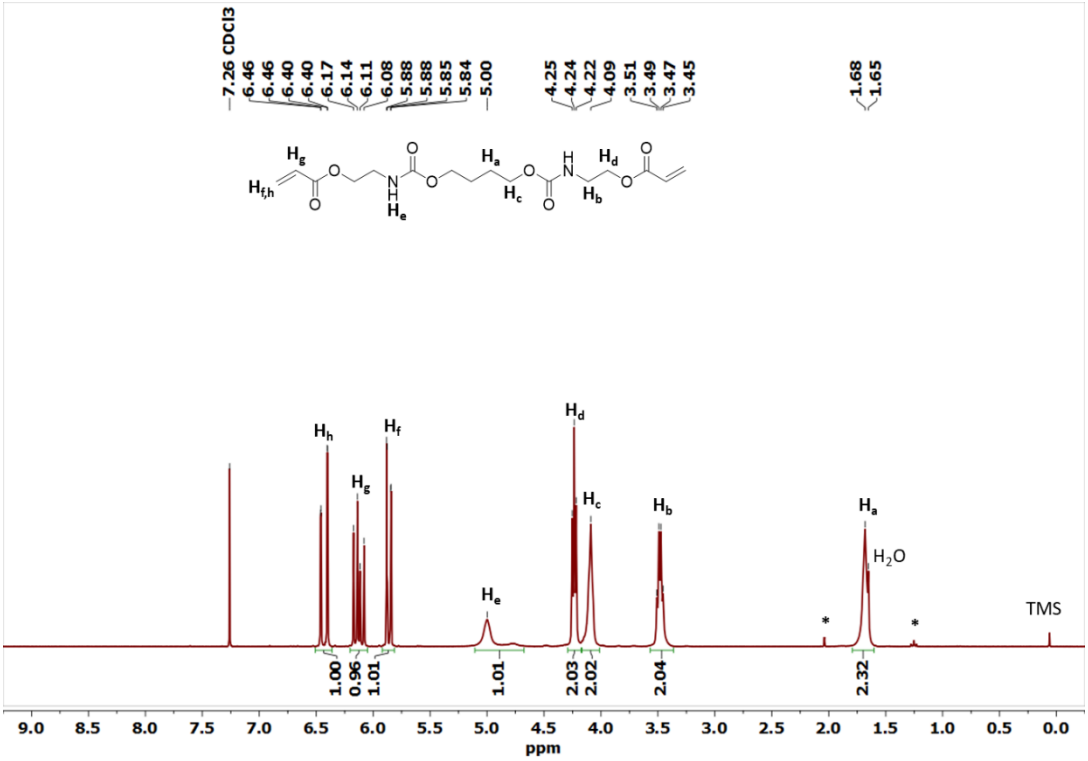


Figure S3. ^{1}H NMR of monomer S (400 MHz; 298 K; $CDCl_3$). * - EtOAc in $CDCl_3$

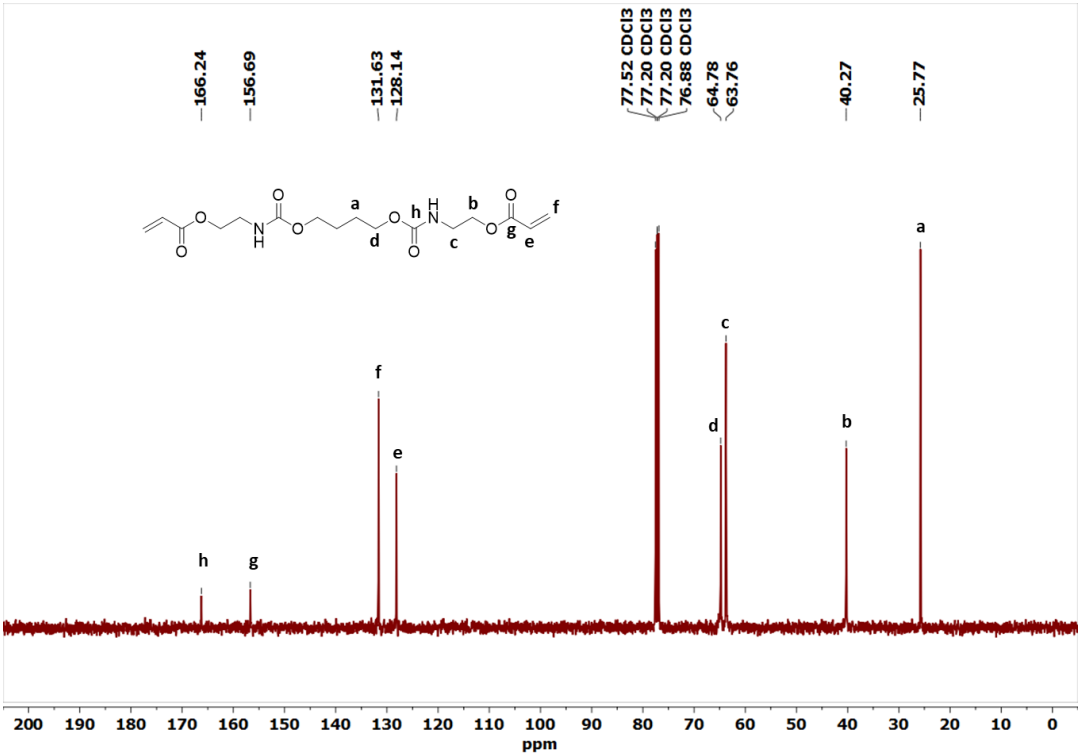


Figure S4. ^{13}C NMR spectrum of monomer S (100.57 MHz; 298 K; $CDCl_3$).

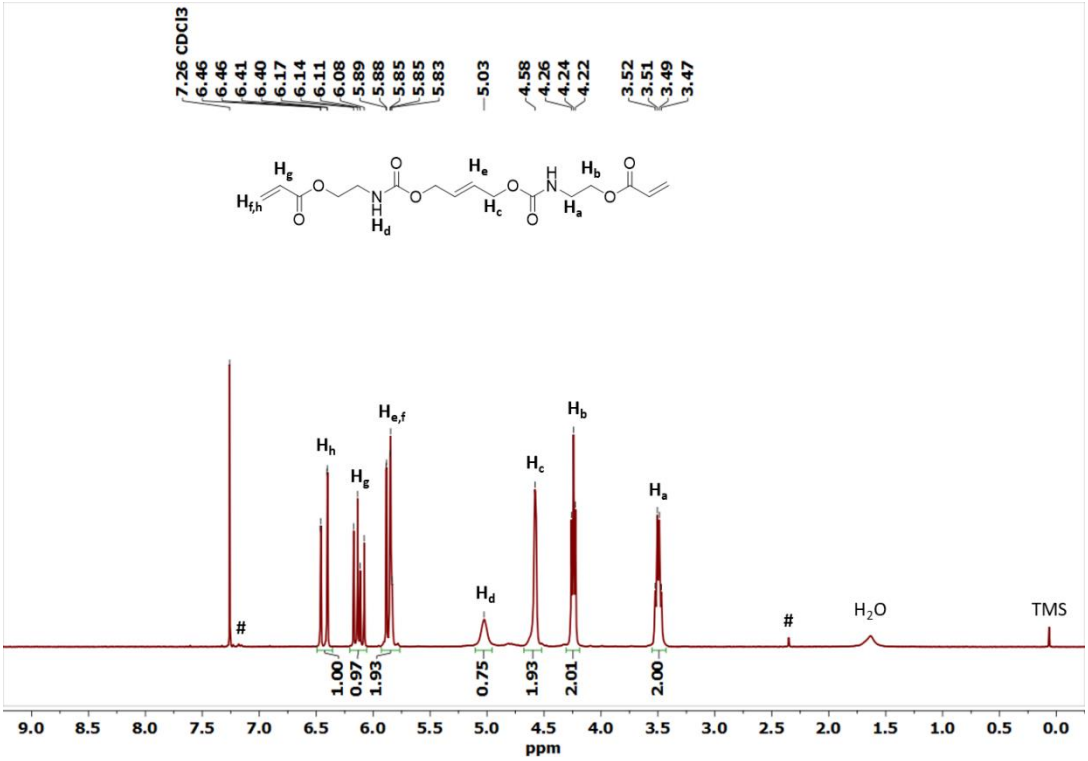


Figure S5. ^{1}H NMR of monomer T (400 MHz; 298 K; $CDCl_3$). # - Toluene in $CDCl_3$

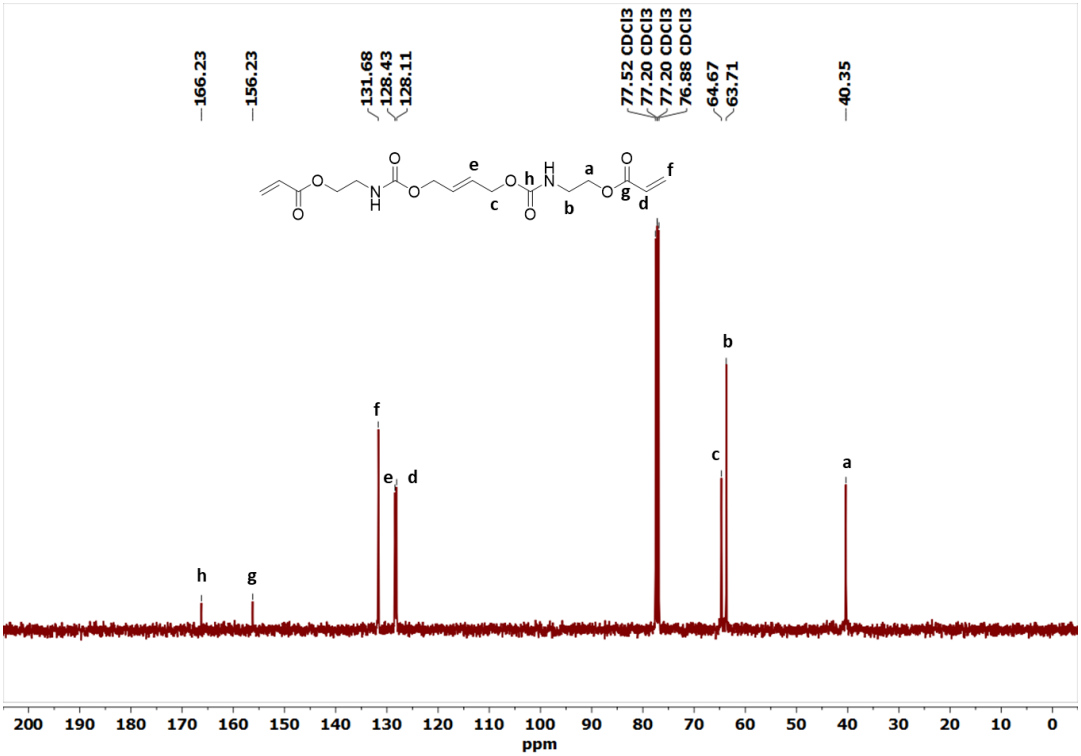


Figure S6. ^{13}C NMR spectrum of monomer T (100.57 MHz; 298 K; $CDCl_3$).

NMR spectra of Homopolymers

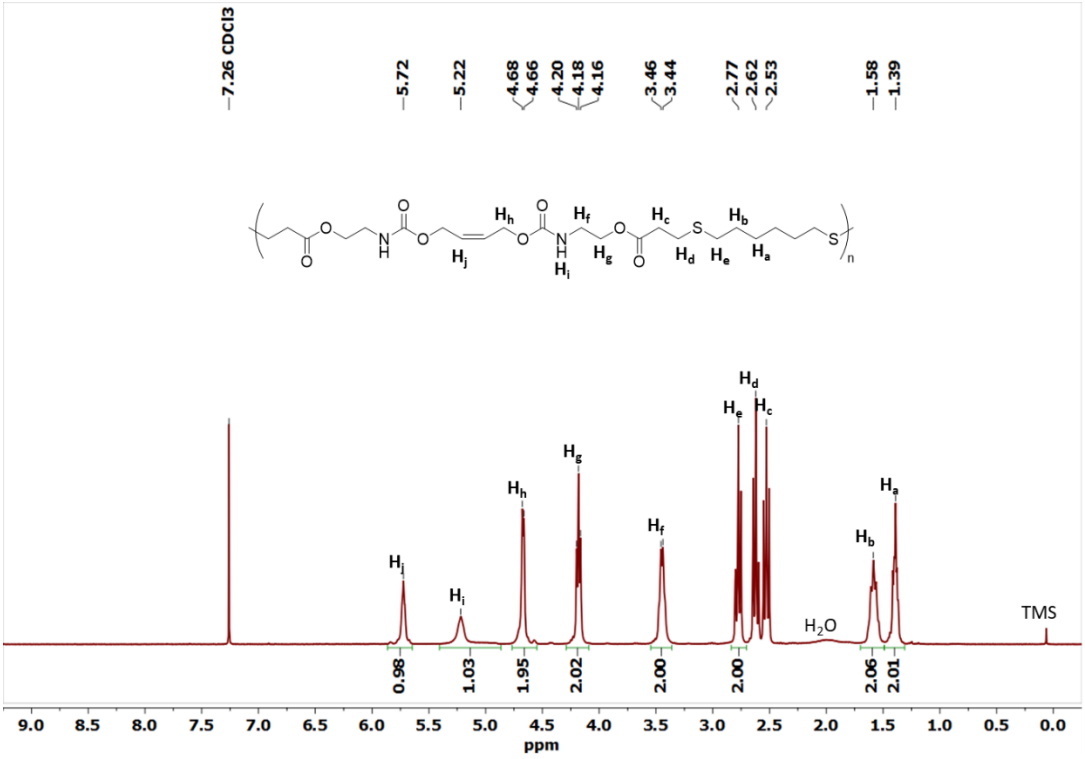


Figure S7. ^{1}H NMR of polymer C_{100} (400 MHz; 298 K; $CDCl_3$).

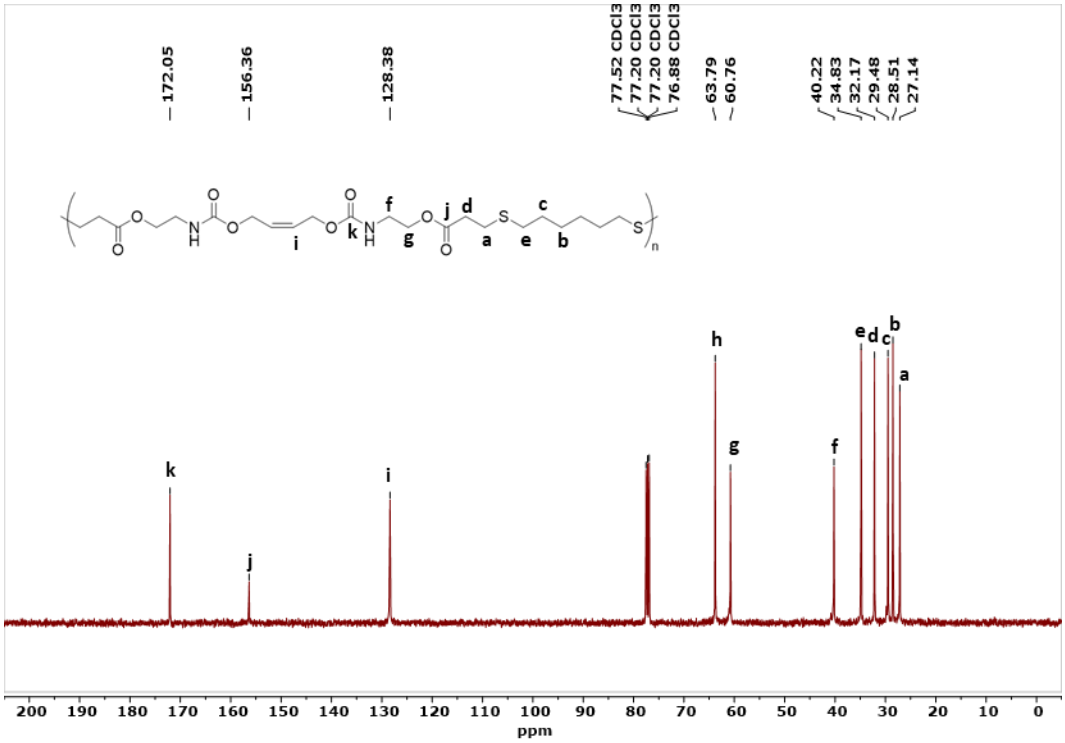


Figure S8. ^{13}C NMR spectrum of polymer C_{100} (100.57 MHz; 298 K; $CDCl_3$).

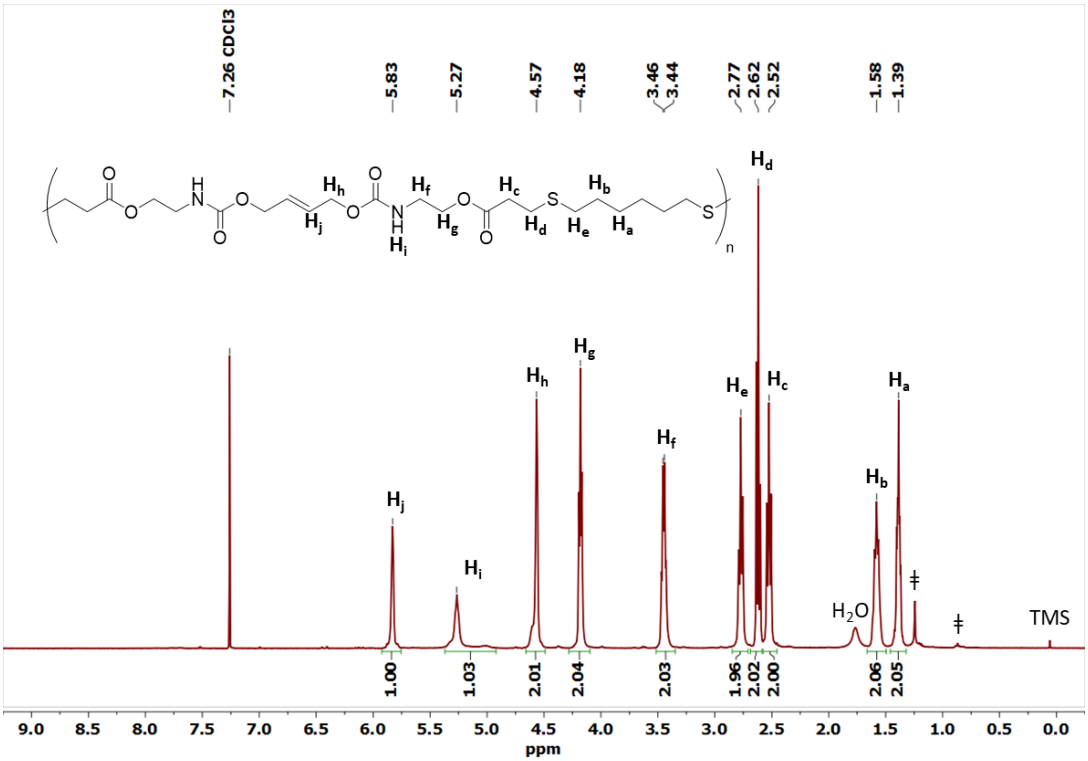


Figure S9. ^{1}H NMR of polymer T_{100} (400 MHz; 298 K; $CDCl_3$). ǂ - Aliphatic grease in $CDCl_3$

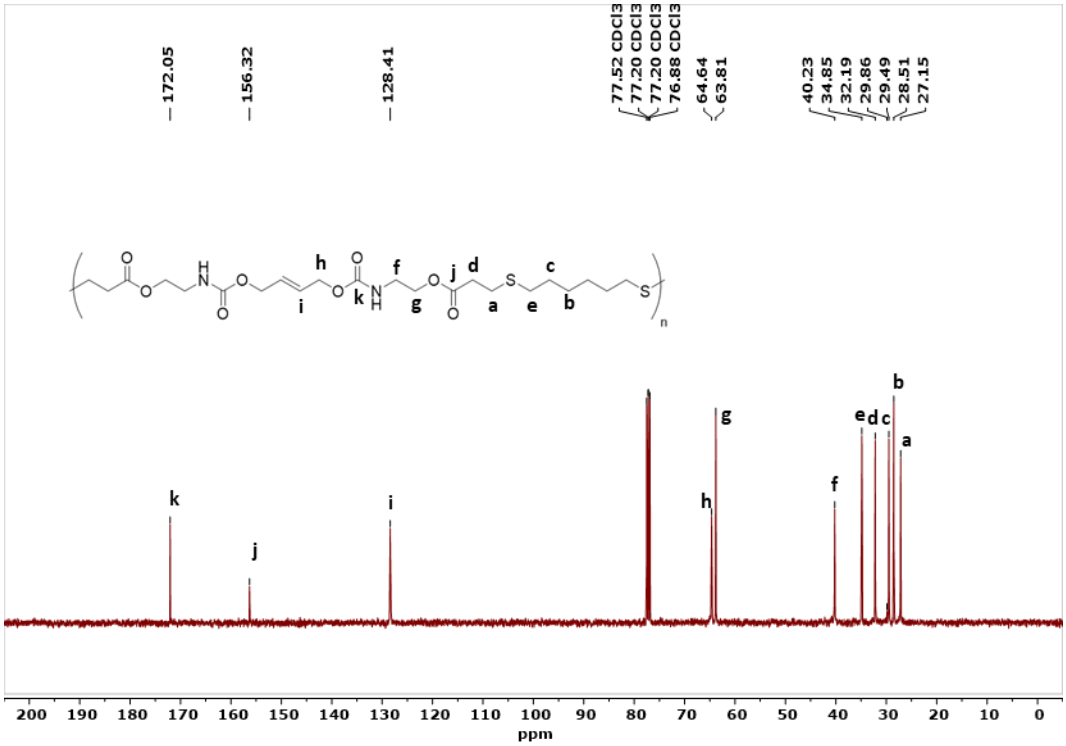


Figure S10. ^{13}C NMR spectrum of polymer T_{100} (100.57 MHz; 298 K; $CDCl_3$).

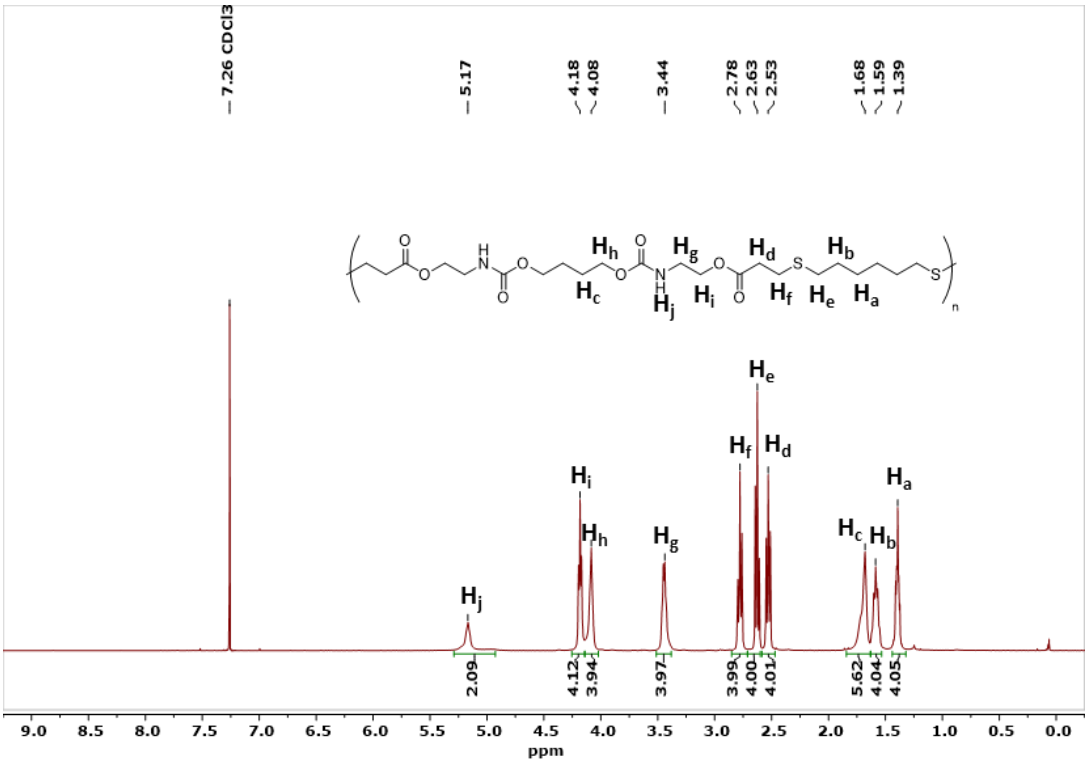


Figure S11. ^{1}H NMR of polymer S_{100} (400 MHz; 298 K; $CDCl_3$).

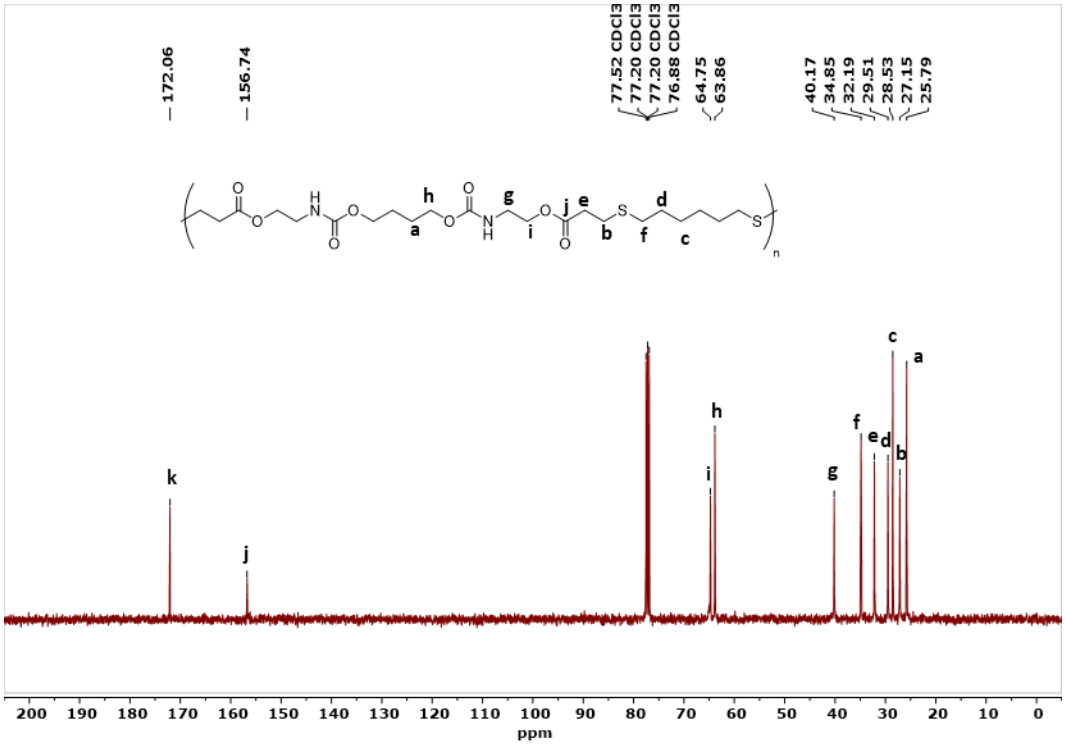


Figure S12. ^{13}C NMR spectrum of polymer S_{100} (100.57 MHz; 298 K; $CDCl_3$)

NMR spectra of Copolymers

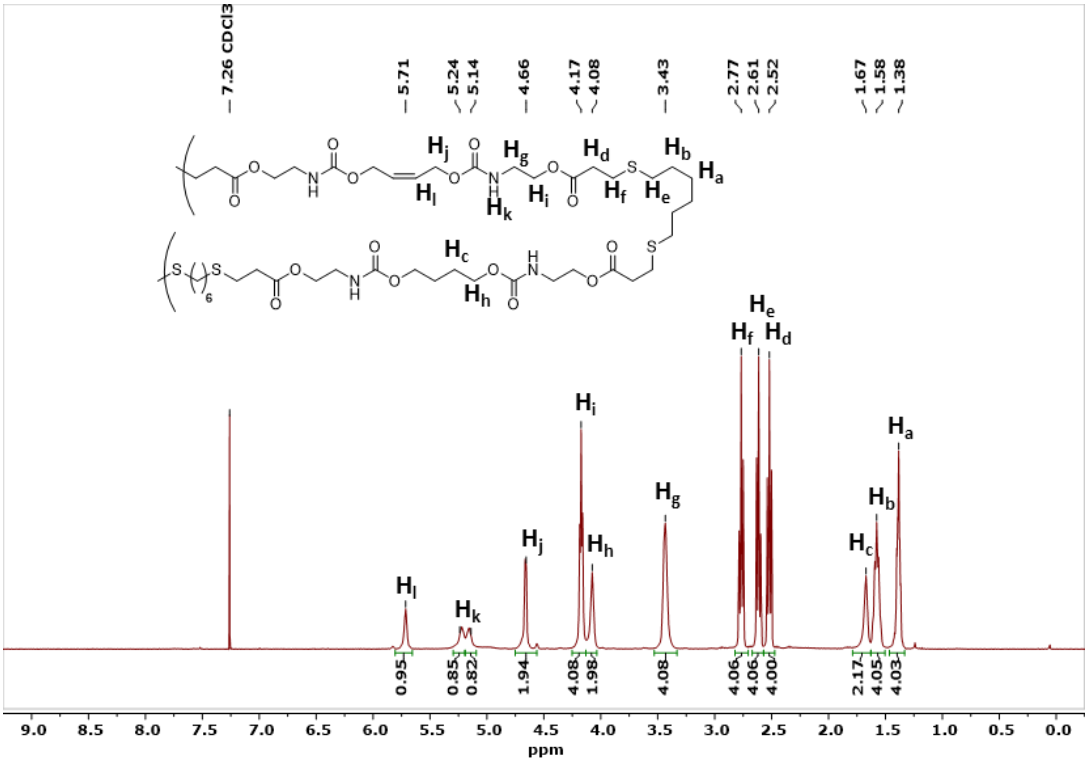


Figure S13. ^{1}H NMR of polymer $C_{50}S_{50}$ (400 MHz; 298 K; $CDCl_3$).

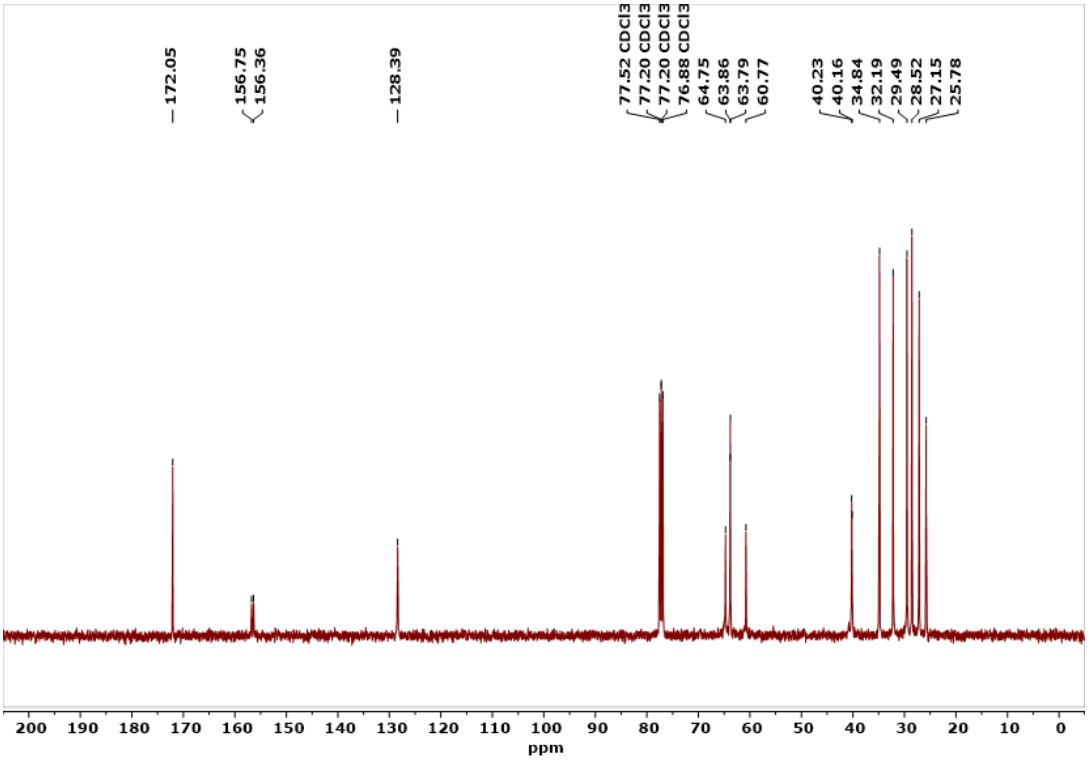


Figure S14. ^{13}C NMR spectrum of polymer $C_{50}S_{50}$ (100.57 MHz; 298 K; $CDCl_3$).

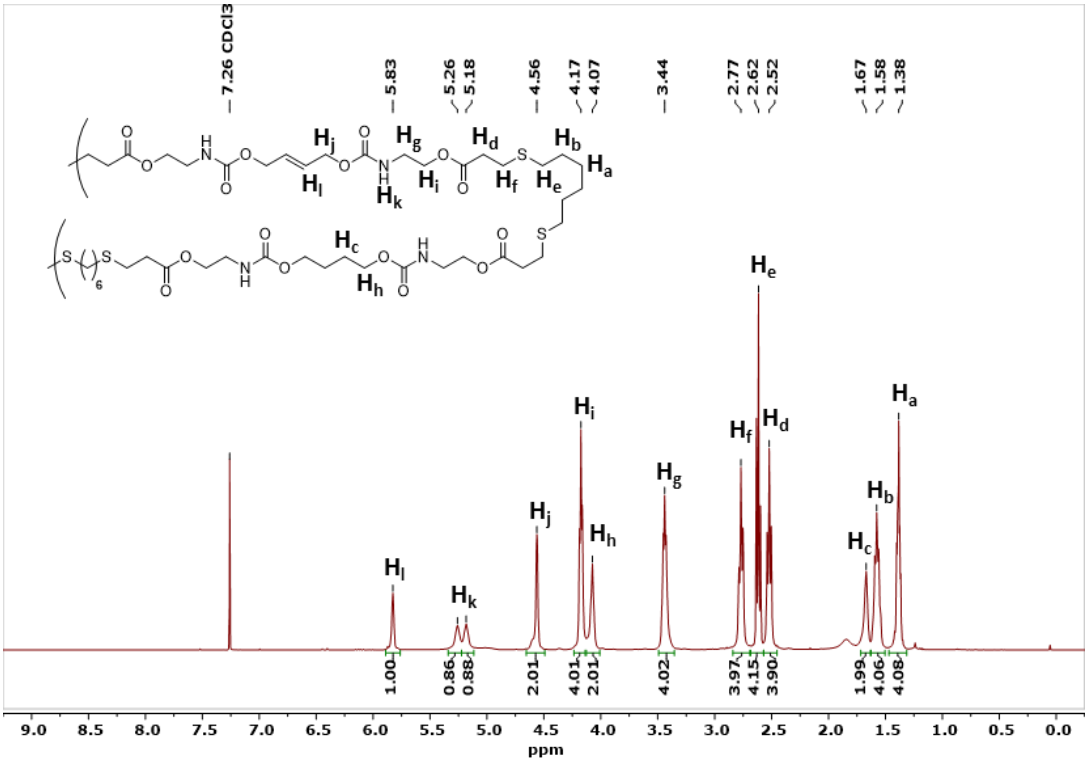


Figure S15. ^{1}H NMR of polymer $T_{50}S_{50}$ (400 MHz; 298 K; $CDCl_3$).

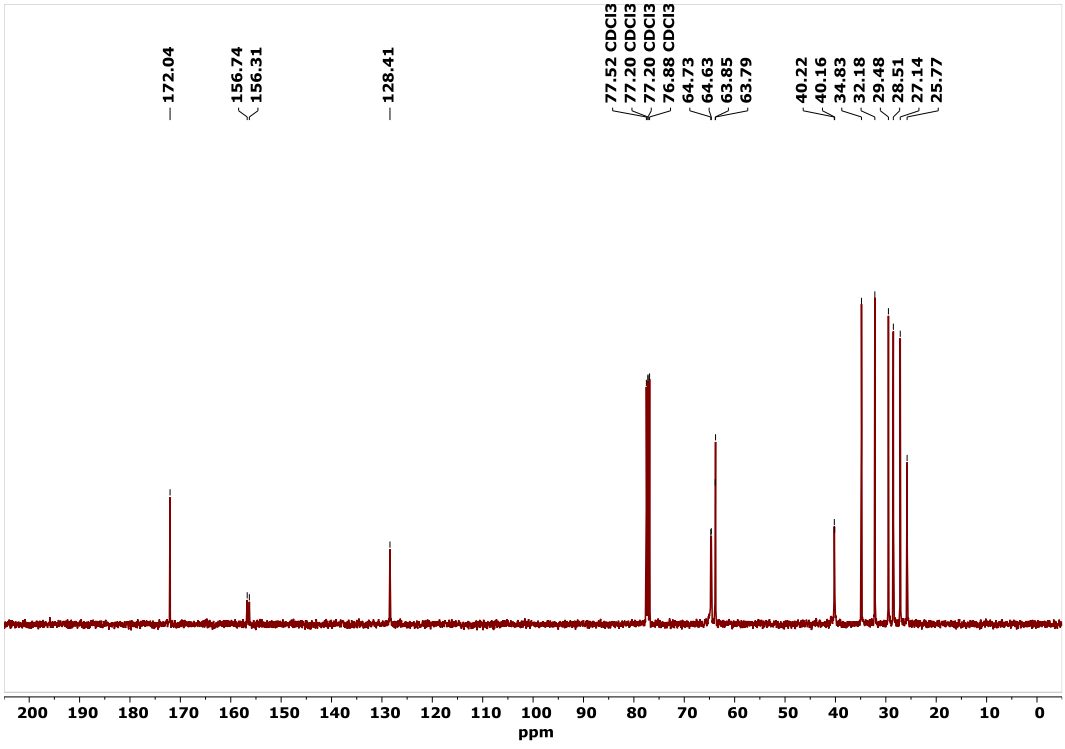


Figure S16. ^{13}C NMR spectrum of polymer $T_{50}S_{50}$ (100.57 MHz; 298 K; $CDCl_3$).

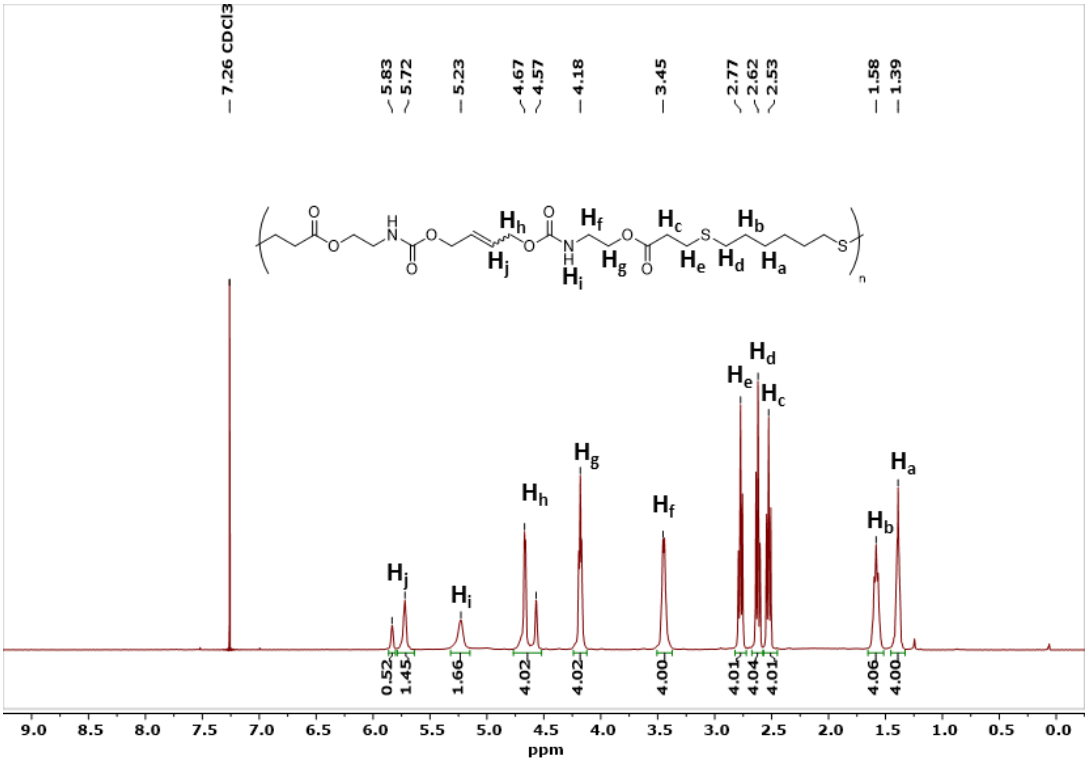


Figure S17. ^{1}H NMR of polymer $C_{75}T_{25}$ (400 MHz; 298 K; $CDCl_3$).

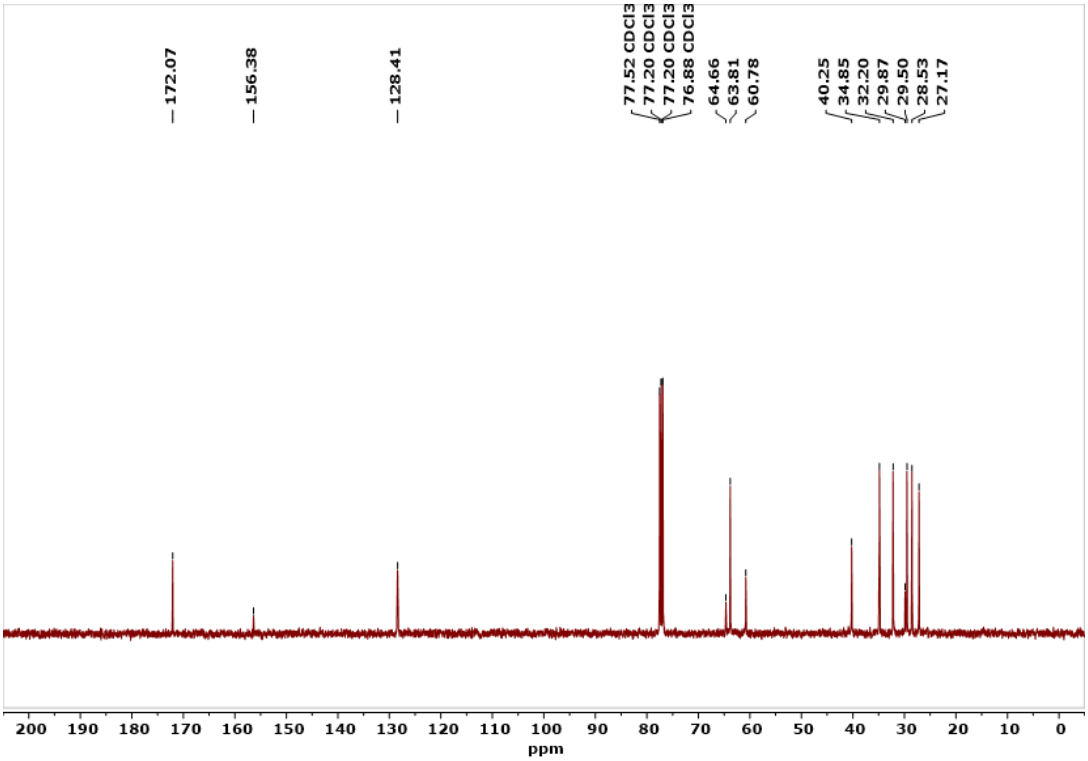


Figure S18. ^{13}C NMR spectrum of polymer $C_{75}T_{25}$ (100.57 MHz; 298 K; $CDCl_3$).

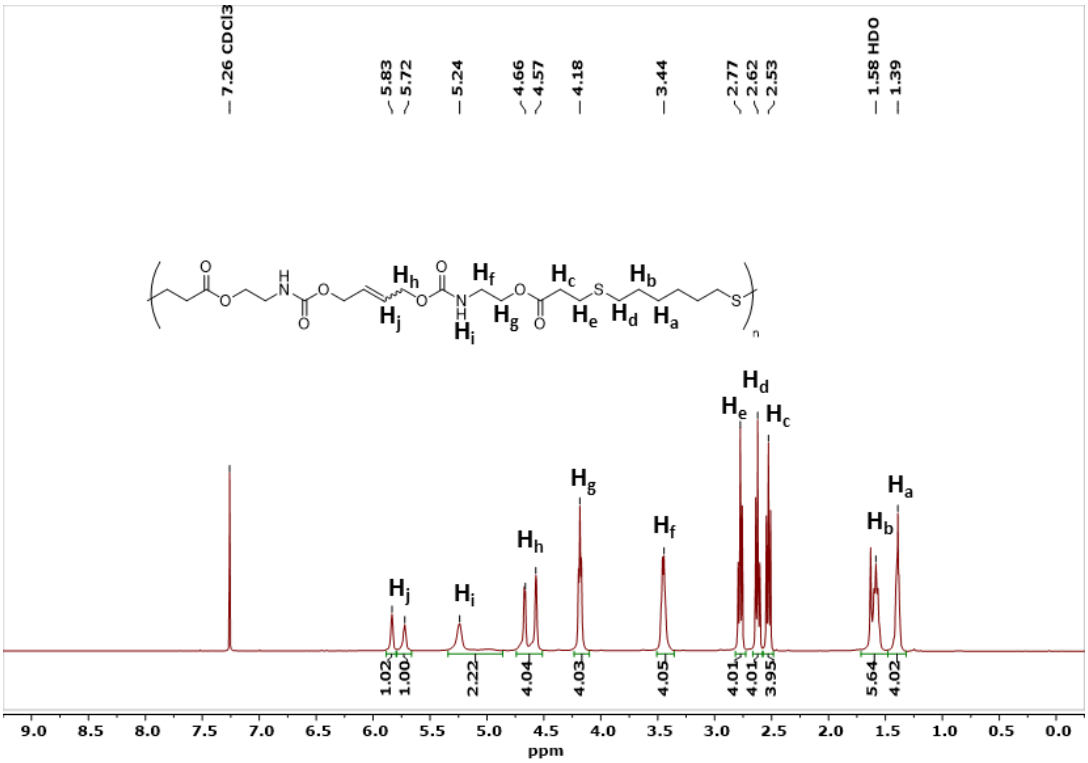


Figure S19. ^{1}H NMR of polymer $C_{50}T_{50}$ (400 MHz; 298 K; $CDCl_3$).

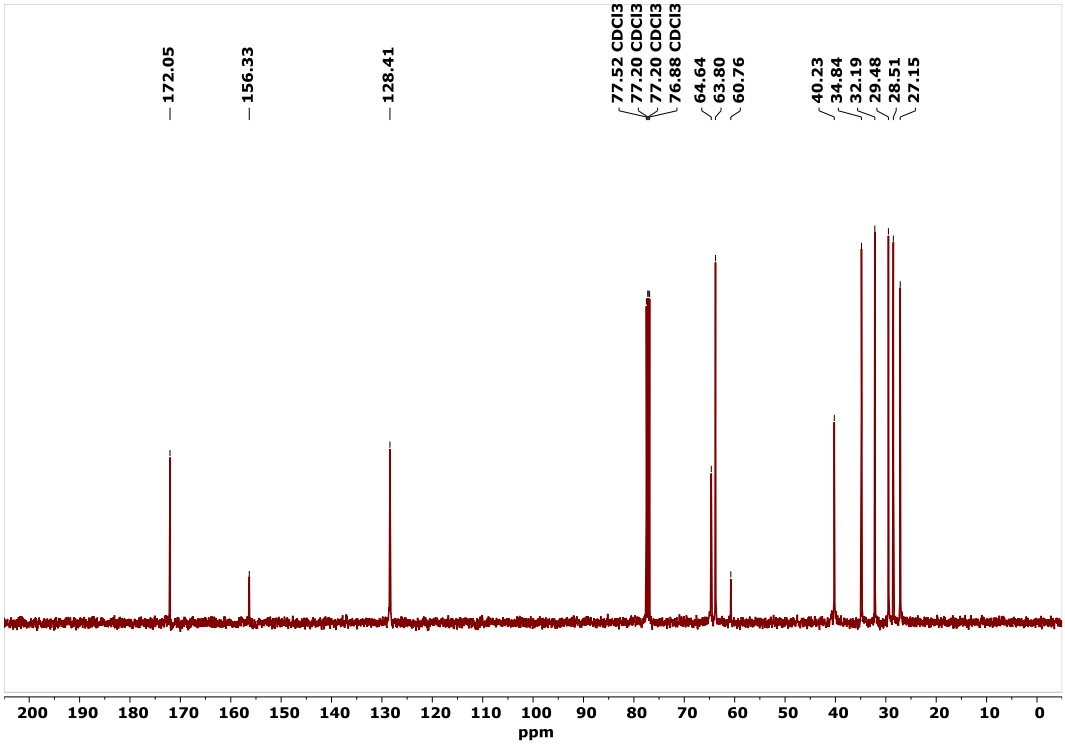


Figure S20. ^{13}C NMR spectrum of polymer $C_{50}T_{50}$ (100.57 MHz; 298 K; $CDCl_3$).

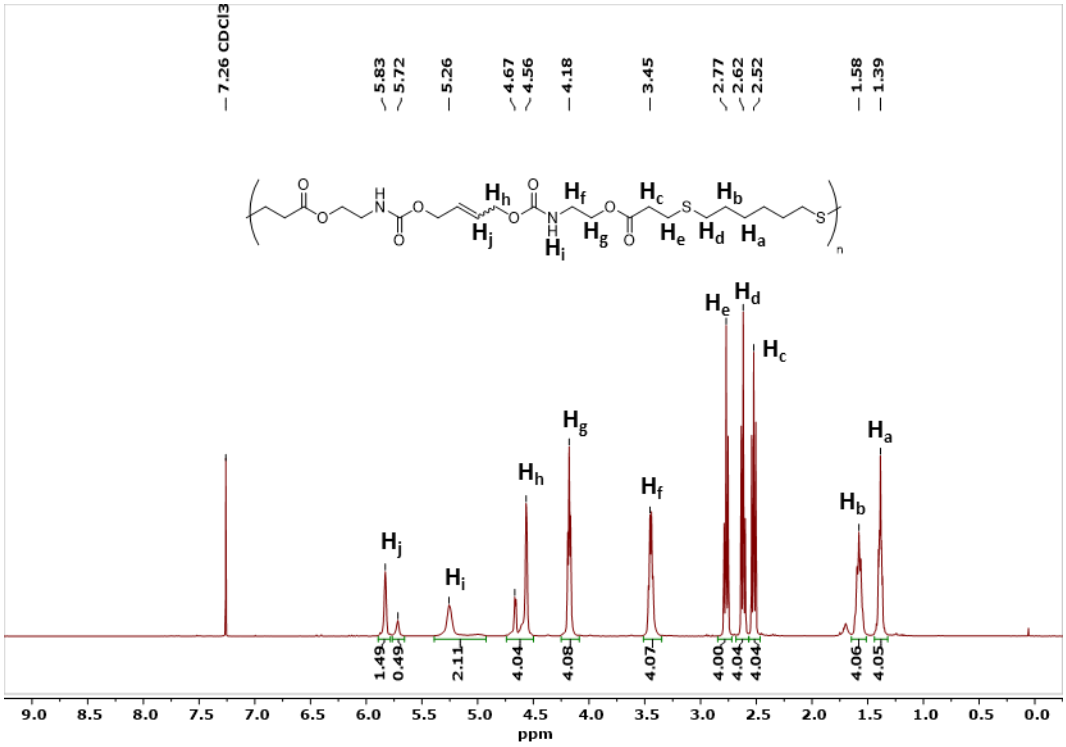


Figure S21. ^{1}H NMR of polymer $C_{25}T_{75}$ (400 MHz; 298 K; $CDCl_3$).

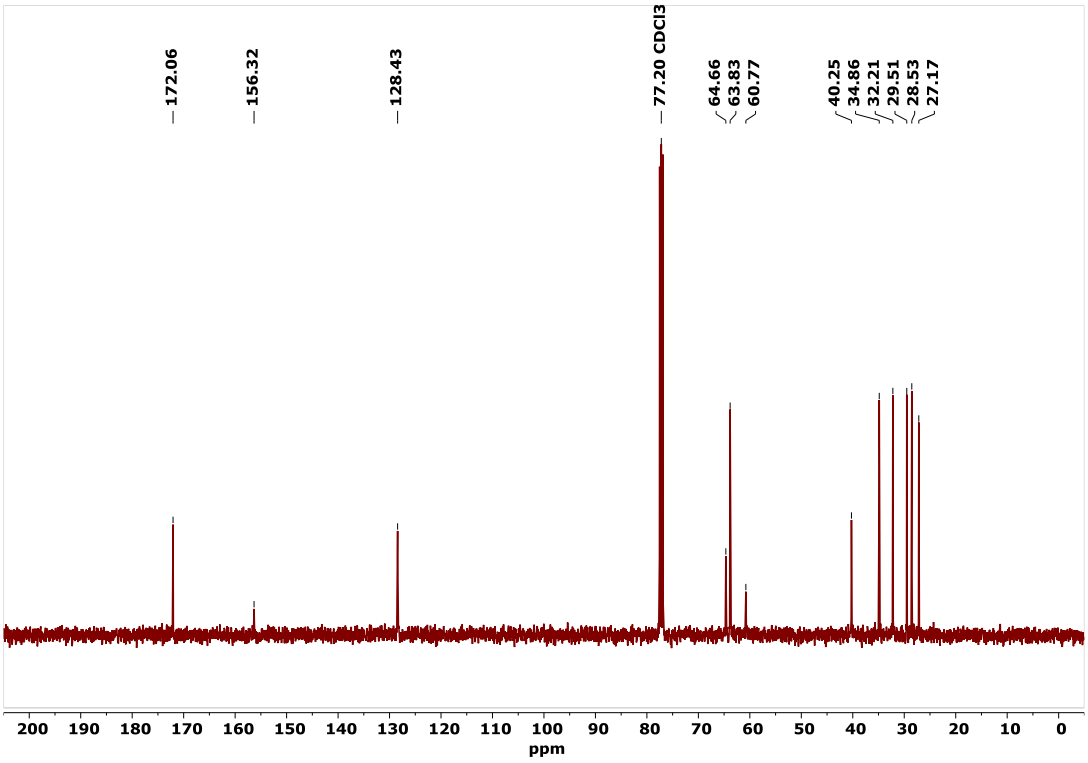


Figure S22. ^{13}C NMR spectrum of polymer $C_{25}T_{75}$ (100.57 MHz; 298 K; $CDCl_3$).

Size exclusion chromatography (SEC) overview

Table S1. Table of polymer characterization using SEC

	Characterization			
	M_w (kDa)	M_n (kDa)	M_p (kDa)	$Đ_M$
C_{100}	250	34.8	109	7.19
T_{100}	103	28.7	89	3.57
S_{100}	139	30.8	117	4.51
C_{75} T_{25}	194	36.6	70	5.30
C_{50} T_{50}	208	38.7	87	5.37
C_{25} T_{75}	129	30.8	61	4.18
$C_{50}S_{50}$	209	34.9	94	5.99
$T_{50}S_{50}$	141	34.4	77	4.09

M_n, M_w, M_p and $Đ_M$ were determined by SEC (DMF, 0.5% wt/wt NH_4BF_4) analysis against poly(methyl methacrylate) (PMMA) standards.

SEC data of Homopolymers

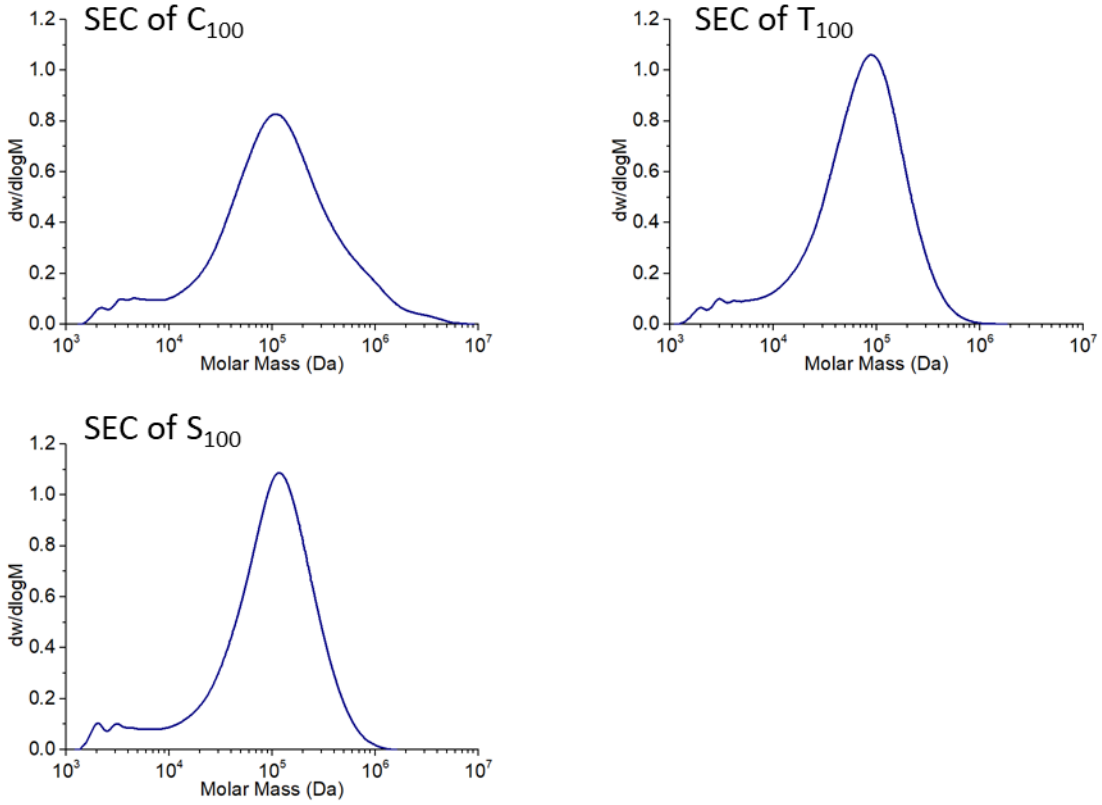


Figure S23. Size exclusion chromatograms of homopolymers (DMF, 0.5% wt/wt NH_4BF_4) analysis against poly(methyl methacrylate) (PMMA) standards.

SEC data of Copolymers

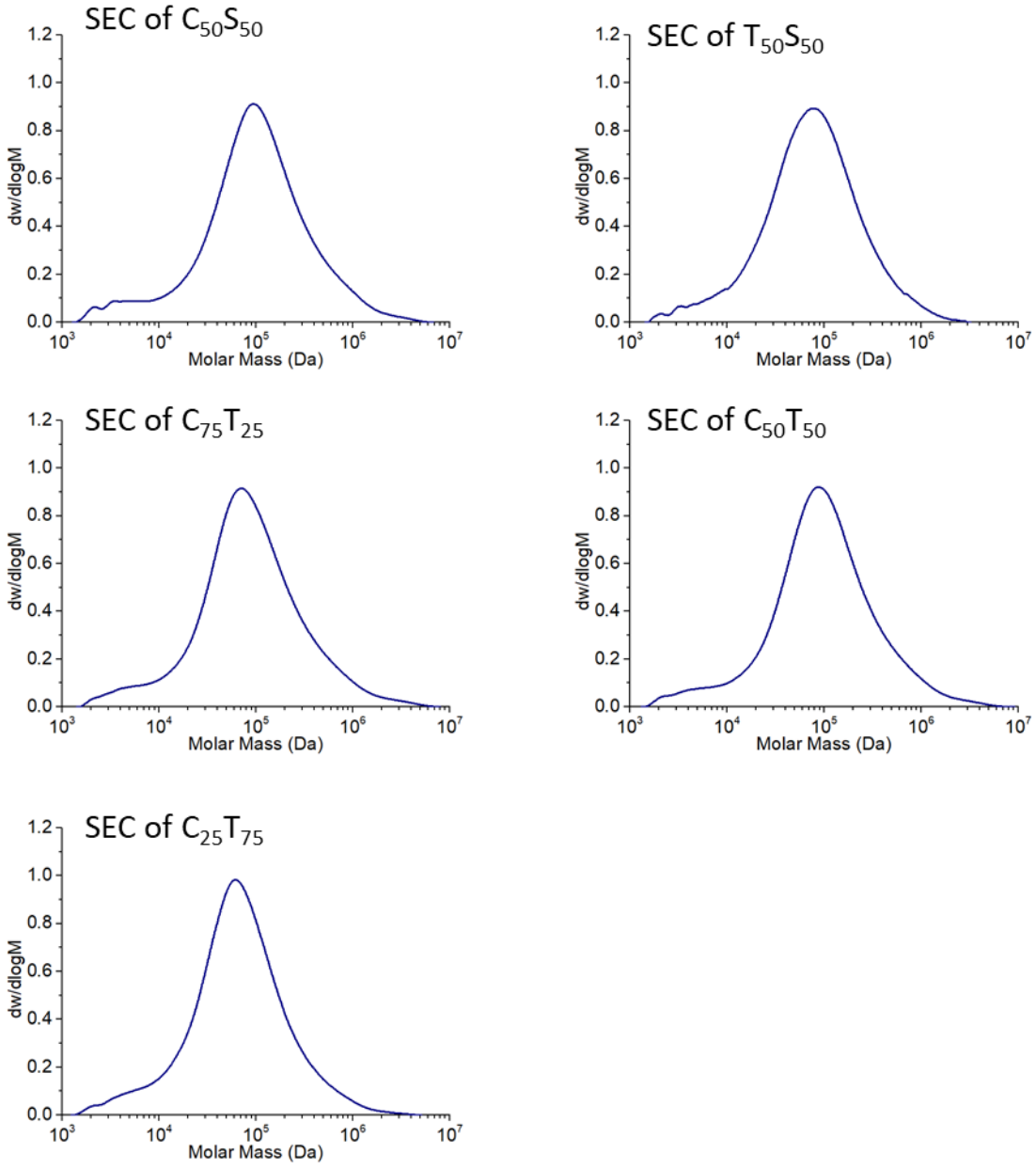


Figure S24. Size exclusion chromatograms of copolymers (DMF, 0.5% wt/wt NH_4BF_4) analysis against poly(methyl methacrylate) (PMMA) standards.

Frequency Sweeps and TTS

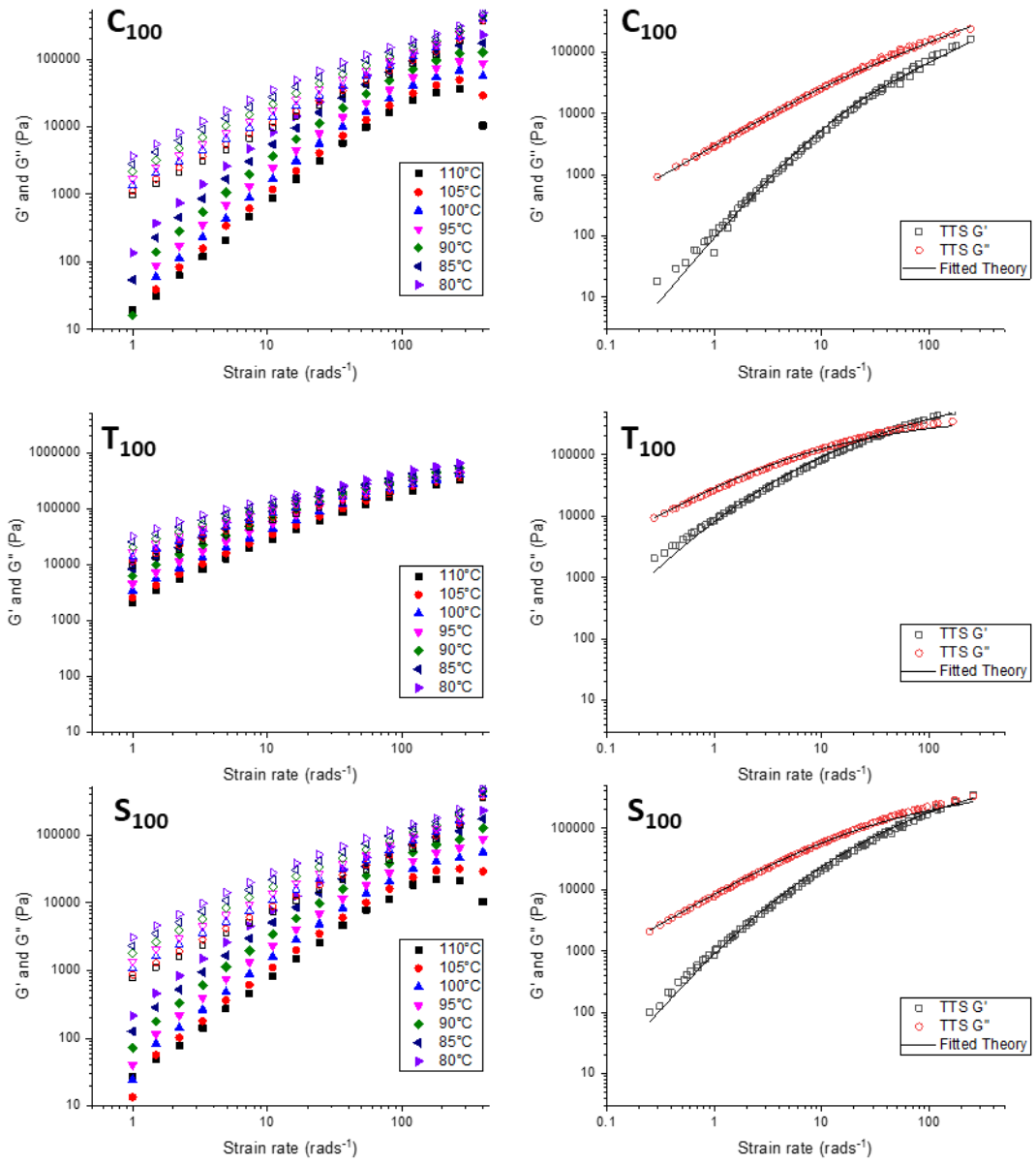


Figure S25. Frequency sweeps of homopolymers between 80 and 110°C (LHS). Time-Temperature superposition (TTS) created from shifting data to 85°C using a WLF superposition (RHS).

Table S2. Values calculated from polydisperse double reptation theory of TTS

	M_e (kDa)	G_e (MPa)	τ_e (μs)
C_{100}	3.23	9.73	4.42
T_{100}	2.01	4.94	2.70
S_{100}	2.12	7.03	2.51

Values calculated using double reptation theory of TTS shown in Figure S25. M_0 was kept at 0.001 kg/mol and **α** was kept at 1.

IR spectra of Homopolymers

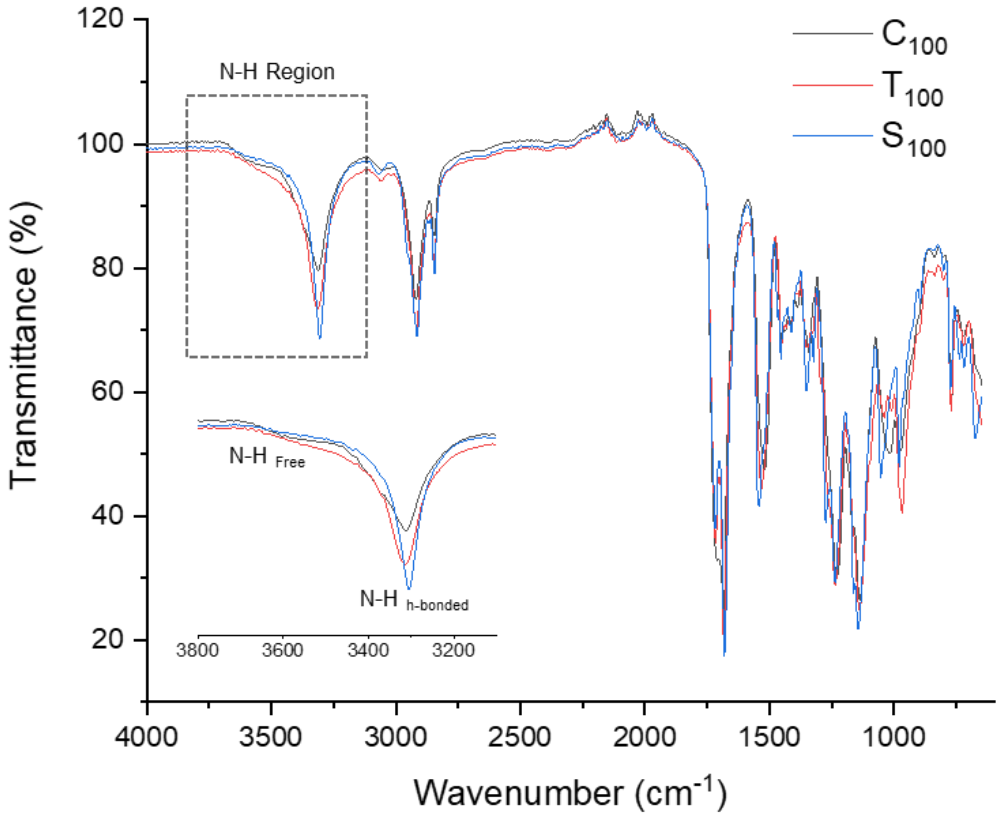


Figure S26. Infared-Spectra of homopolymer films with N-H region (*inset*) highlighted to demonstrate variation in Hydrogen-bonding.

Thermomechanical data overview

Table S3. Thermal and tensile properties of polymer samples

	Thermal					**Tensile**			
	T_g[a] (°C)	$T_{m,1}$[b] (°C)	$T_{m,2}$[c] (°C)	ΔH_m[d] (J·g^{-1})	$T_{d,5\%}$[e] (°C)	E[f] (MPa)	σ_b[g] (MPa)	ε_b[h] (%)	U_T[i] (MJm^{-2})
C_{100}*	-18	-	-	-27.0	302	25±4	23±2	1481±53	174±17
T_{100}	-14	36.2	74.6	-37.2	301	66±11	39±8	1232±96	261±72
S_{100}	-19	37.0	90.2	-41.3	302	81±8	37±3	1191±76	248±28
C_{75} T_{25}	-17	36.7	51.3	-27.6	290	35±5	19±3	1307±156	137±30
C_{50} T_{50}	-16	35.1	52.0	-25.1	296	35±4	26±3	1558±75	199±27
C_{25} T_{75}	-15	37.5	69.0	-32.6	296	46±6	30±4	1436±164	233±48
$C_{50}S_{50}$ ǂ	-19	36.7	77.9	-35.9	292	53±7	33±3	1508±74	255±28
$T_{50}S_{50}$	-16	37.4	77.9	-38.4	293	75±8	40±2	1379±67	294±22
Blend*	-17	-	-	-37	-	52±8	25±3	1075±106	156±28

(a) The T_g was obtained from 2nd heating cycle (b) The $T_{m,1}$ was taken as the minimum of the first transition (c) The $T_{m,2}$ was taken as the minimum of the last transition (d) Total enthalpy of melting (ΔH_m) was calculated by integration of all endothermic transitions. (e) Temperature after 5% weight loss obtained from thermogravimetric analysis (f) Young's modulus (g) Stress at break (h) Strain at break (i) Tensile toughness n=5. Uncertainty presented as the standard deviation of samples. * Multiple peaks visible with little to no resolution. ǂ Three endothermic peaks visible $T_{m,2}$ was taken as the peak at the highest temperature.

DSC data

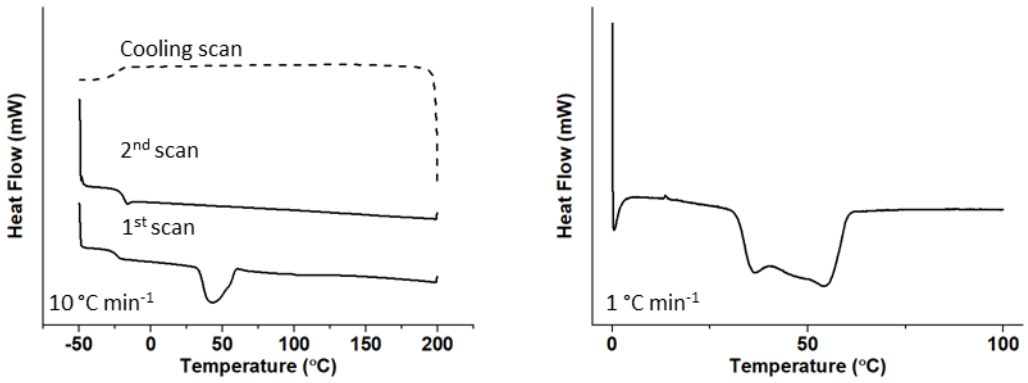


Figure S27. DSC thermograms of C_{100} polymer

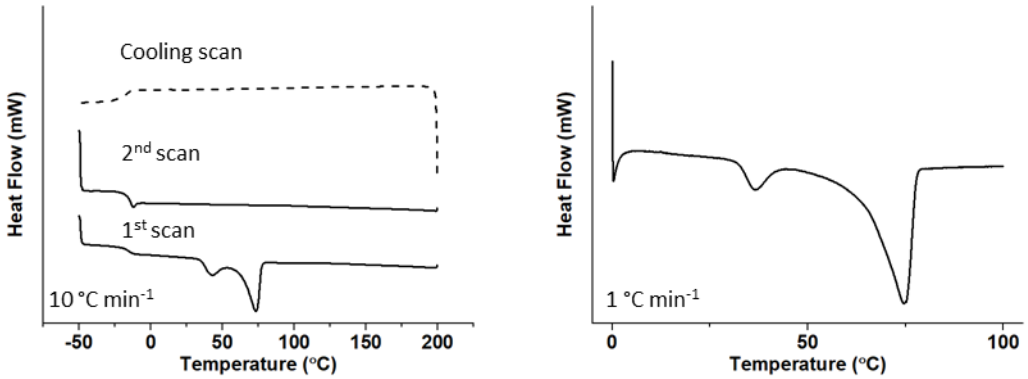


Figure S28. DSC thermograms of T_{100} polymer

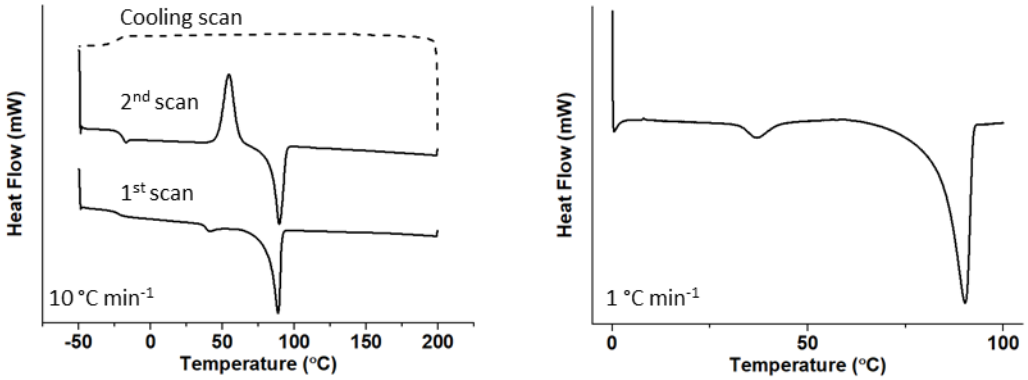


Figure S29. DSC thermograms of S_{100} polymer

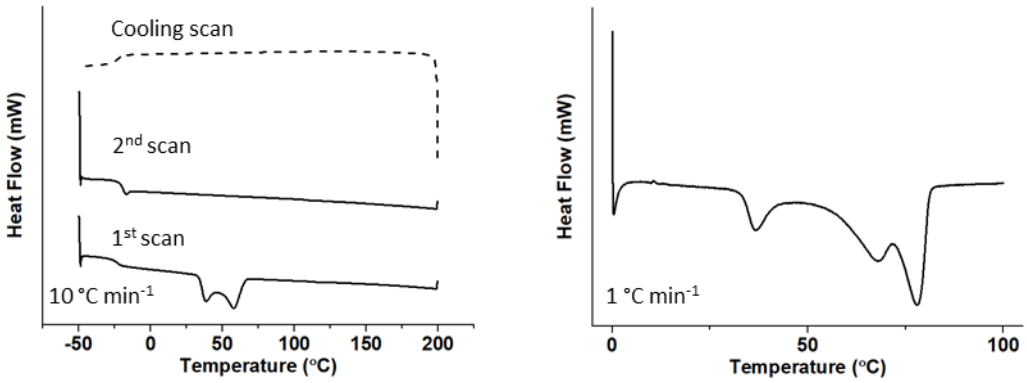


Figure S30. DSC thermograms of $C_{50}S_{50}$ polymer

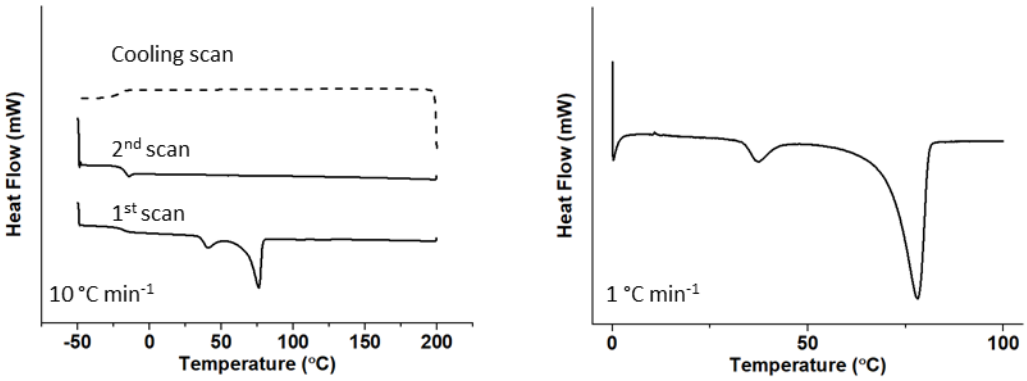


Figure S31. DSC thermograms of $T_{50}S_{50}$ polymer

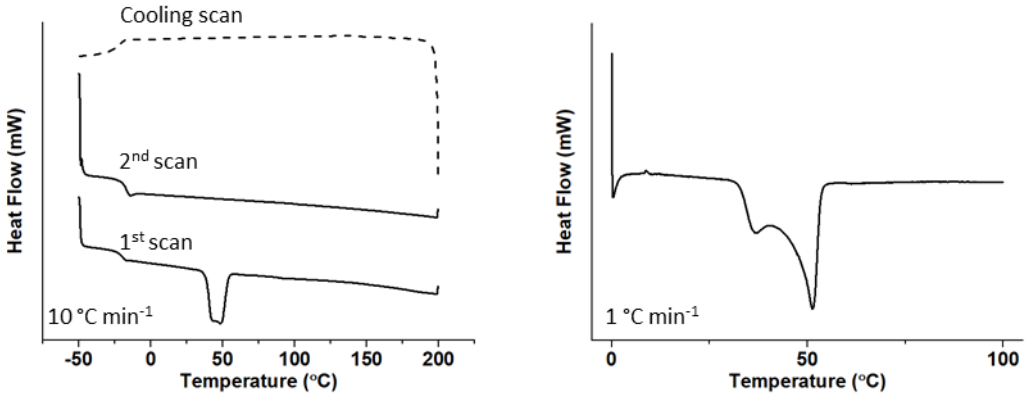


Figure S32. DSC thermograms of $C_{75}T_{25}$ polymer

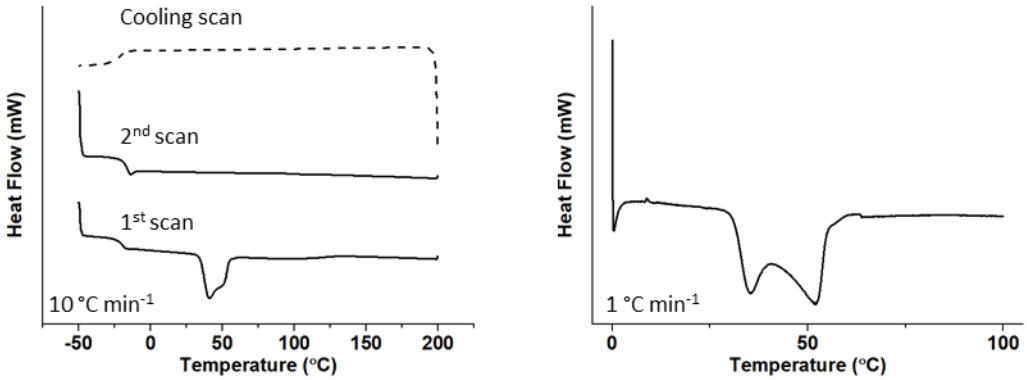


Figure S33. DSC thermograms of $C_{50}T_{50}$ Polymer

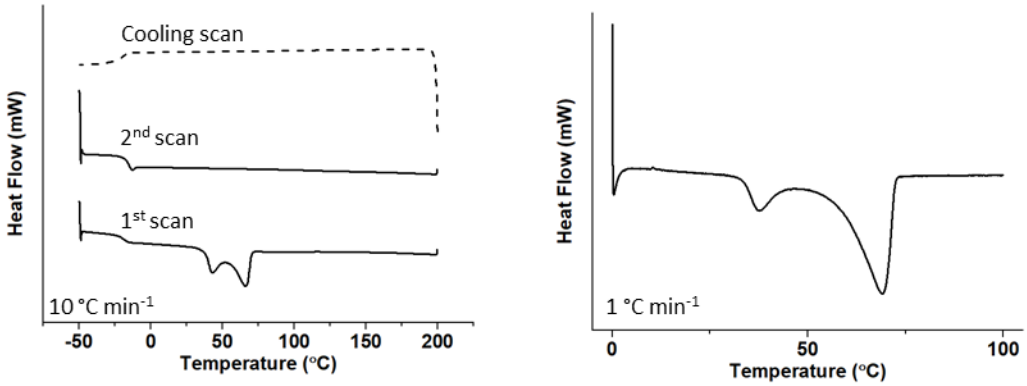


Figure S34. DSC thermograms of $C_{25}T_{75}$ Polymer

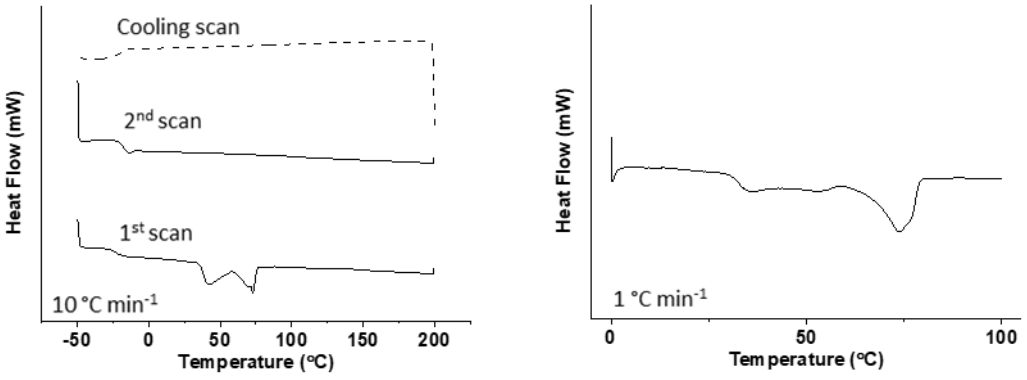


Figure S35. DSC thermograms of Blended polymer sample (1:1 T_{100} and C_{100}**)**

Both DSC thermogram scans at different heating rates were run after 7 days of annealing. Total enthalpy of melting was taken from the 1 °C min^{-1} scan and T_g was taken from 2nd heating run from the 10 °C min^{-1} scan.

TGA Data

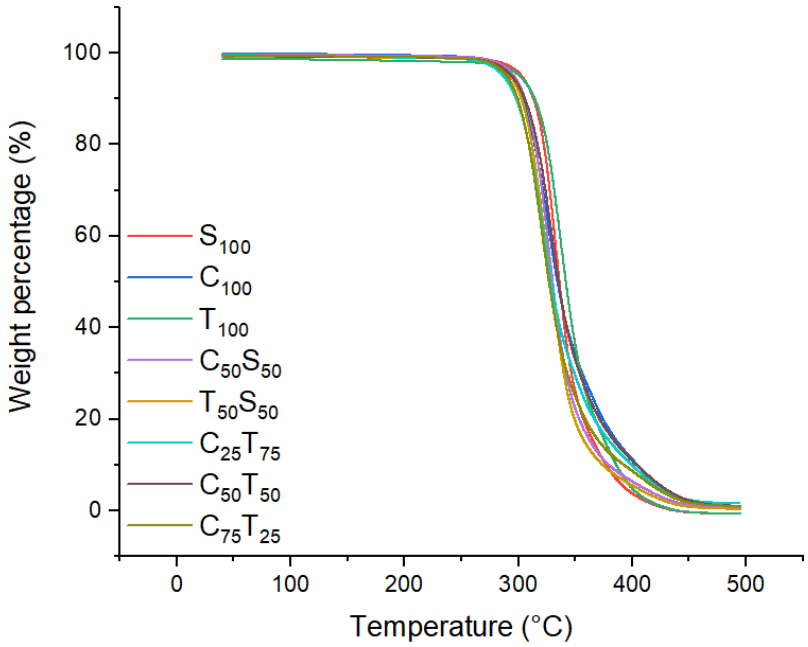


Figure S36. Thermogravimetric analysis was also taken on 7 day annealed polymer films.

Tensile data of homopolymers

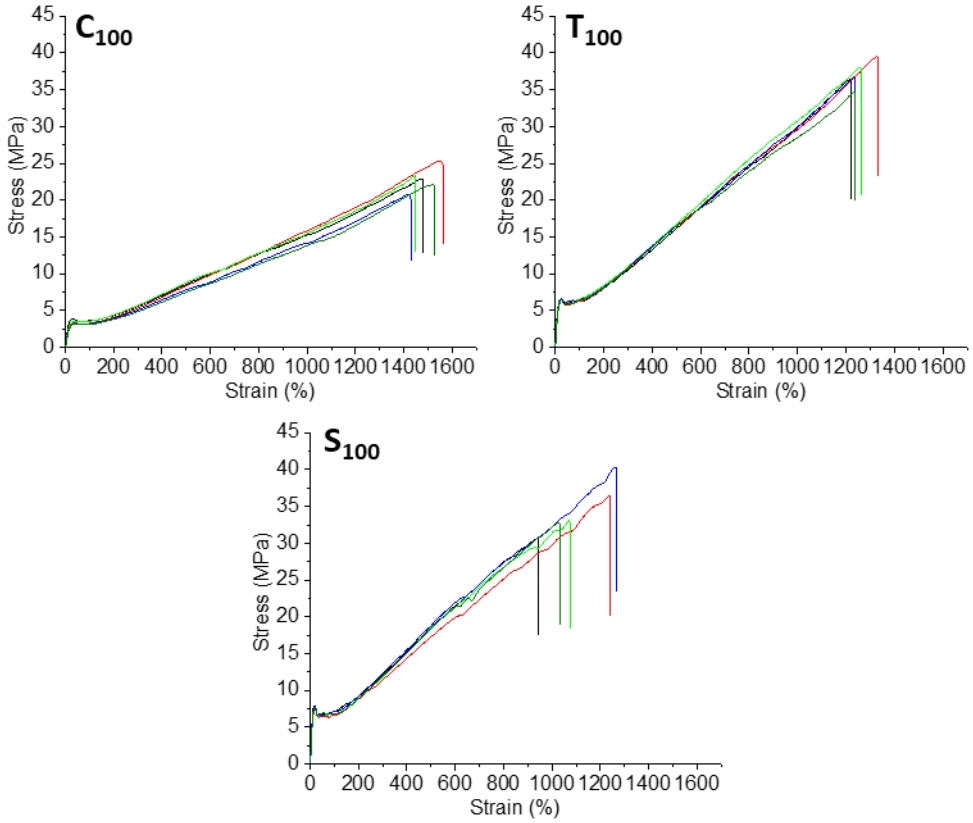


Figure S37. Stress *vs* strain curve for 7 day annealed polymer samples *via* uniaxial extension until failure

n=5 for all data sets. All curves used in uncertainty and average calculations are shown.

Tensile data of copolymers and blend

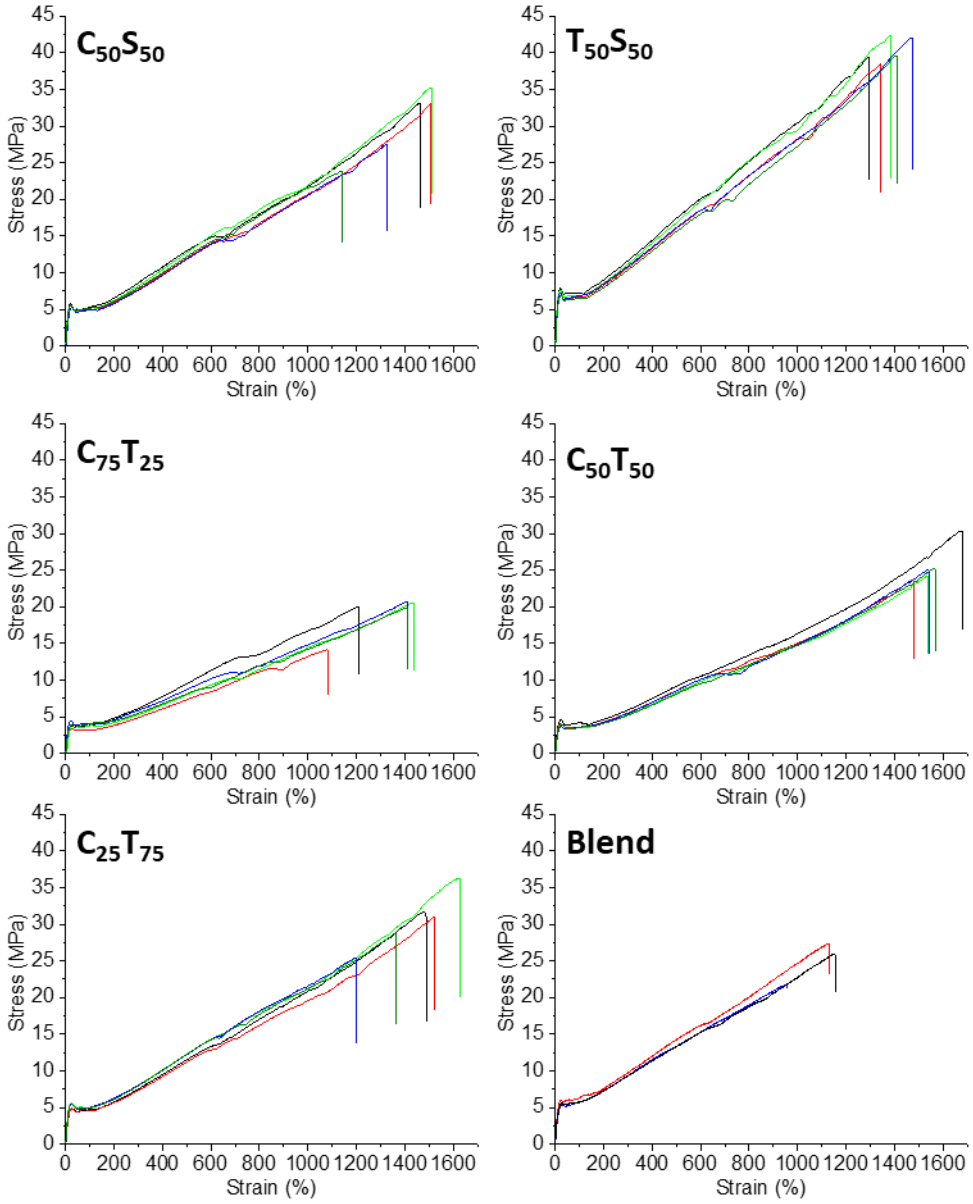


Figure S38. Stress *vs* strain curve for 7 day annealed polymer samples *via* uniaxial extension until failure

n=5 for all data sets except the blended sample of which n=3. All curves used in uncertainty and average calculations are shown.

Dynamic Mechanical Thermal Analysis (DMTA) of homopolymers

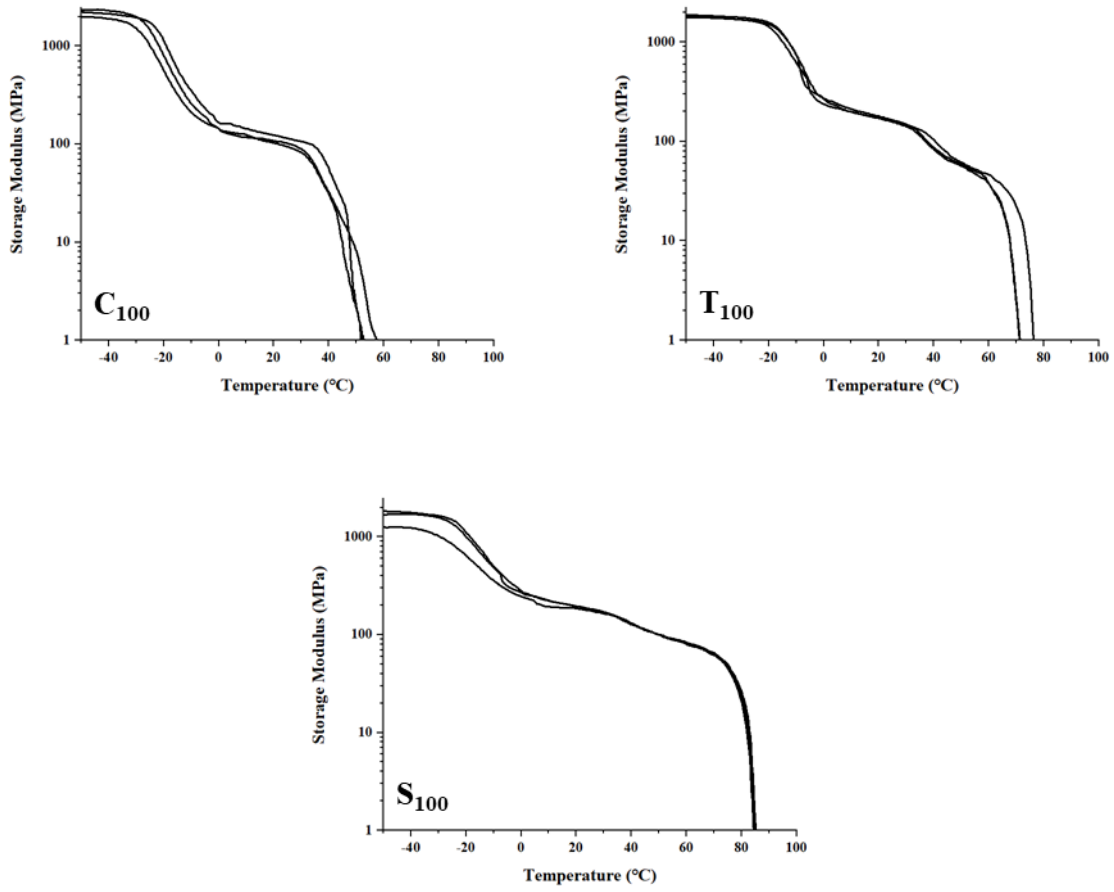


Figure S39. Storage modulus *vs* Temperature DMTA of 7 day annealed homopolymer film in tensile configuration

Dynamic Mechanical Thermal Analysis (DMTA) of copolymers

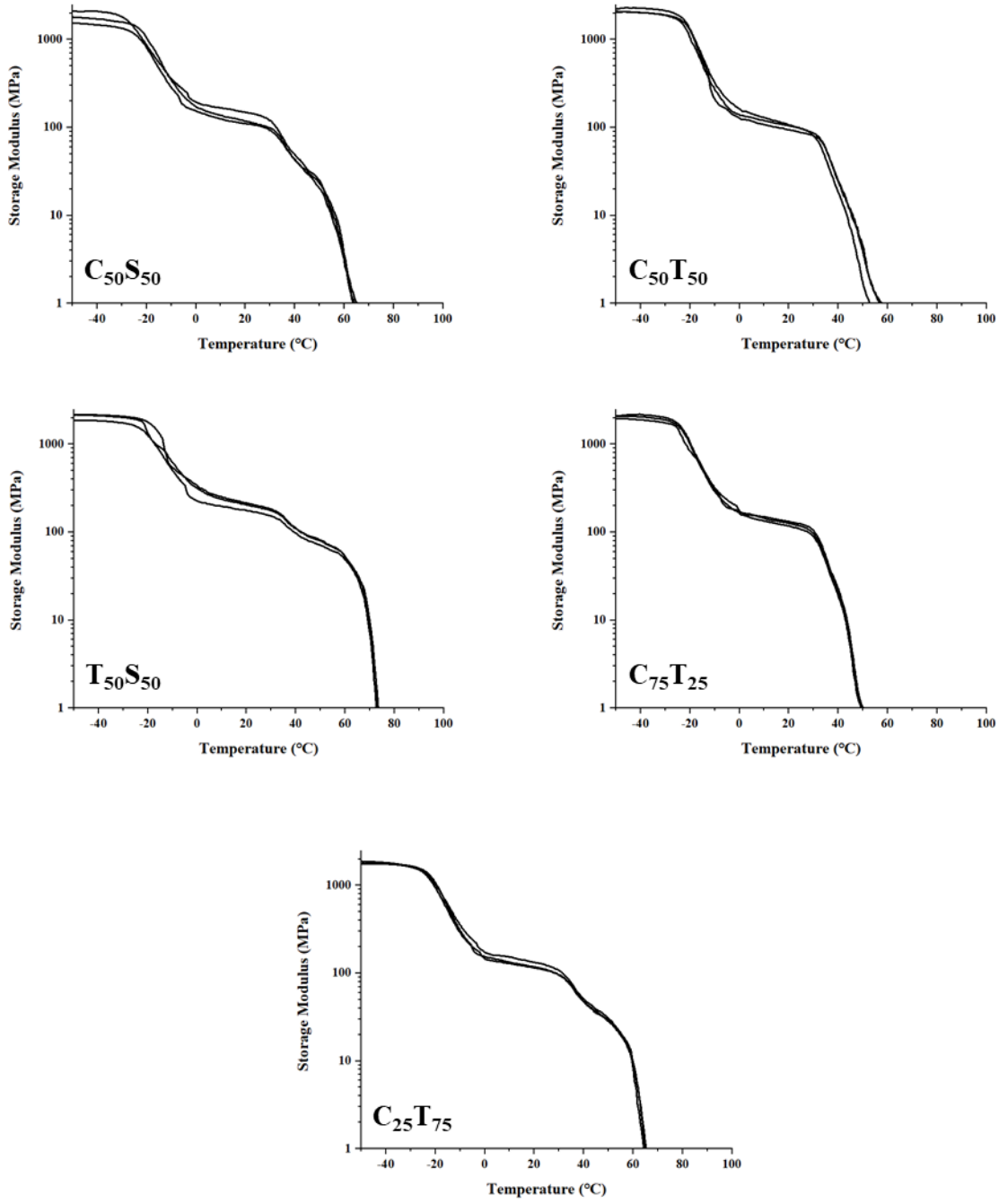


Figure S40. Storage modulus *vs* Temperature DMTA of 7 day annealed polymer film in tensile configuration

References

1. Kiran, Y. B.; Wakamatsu, H.; Natori, Y.; Takahata, H.; Yoshimura, Y., Design and synthesis of a nucleoside and a phosphonate analogue constructed on a branched-threo-tetrofuranose skeleton. *Tetrahedron Lett.* **2013,** *54*, 3949-3952.

2. Vorselaars, B., "Theory documentation: Polydisperse double reptation," Rheology of Entangled Polymers: Toolbox for the Analysis of Theory and Experiments (Reptate, http://www.reptate.com).

Chapter 3 – Understanding structure–property relationships of main chain cyclopropane in linear polyesters

3.1 Manuscript details and overview

Title: Understanding structure–property relationships of main chain cyclopropane in linear polyesters

Authors: **Connor J. Stubbs**[1], and Andrew P. Dove[1]*

Affiliations: [1]School of Chemistry, University of Birmingham, Edgbaston, Birmingham B15 2TT, United Kingdom.

Journal: Polymer chemistry

Year: 2020

Volume: 11

Page numbers: 6251-6258

DOI: 10.1039/D0PY01004A

Submitted: 14th of July 2020

Published: 28th of August 2020

Copyright statement: Adapted with permission from "C. J. Stubbs and A. P. Dove, *Polym. Chem.,* 2020, *11*, 6251-6258". This article is licensed under a Creative Commons Attribution 3.0 Unported Licence.

Permissions: This article and its supporting information are available, free of charge, at https://doi.org/10.1039/D0PY01004A.

Co-author contributions: Prof. Andrew P. Dove (University of Birmingham) supervised the project as well as providing guidance and editing the manuscript.

Overview:

Following on from Chapter 2, we wanted to investigate linear polymers containing a similar *cis/trans* geometry around a rigid ring. Whilst there is some significant study in the area of rigid rings in polymers, particularly 6-membered rings, there lacked detailed study into the simplest 3-membered ring. Hence, we decided to investigate the stereochemistry around a 1,2-cyclopropane ring.

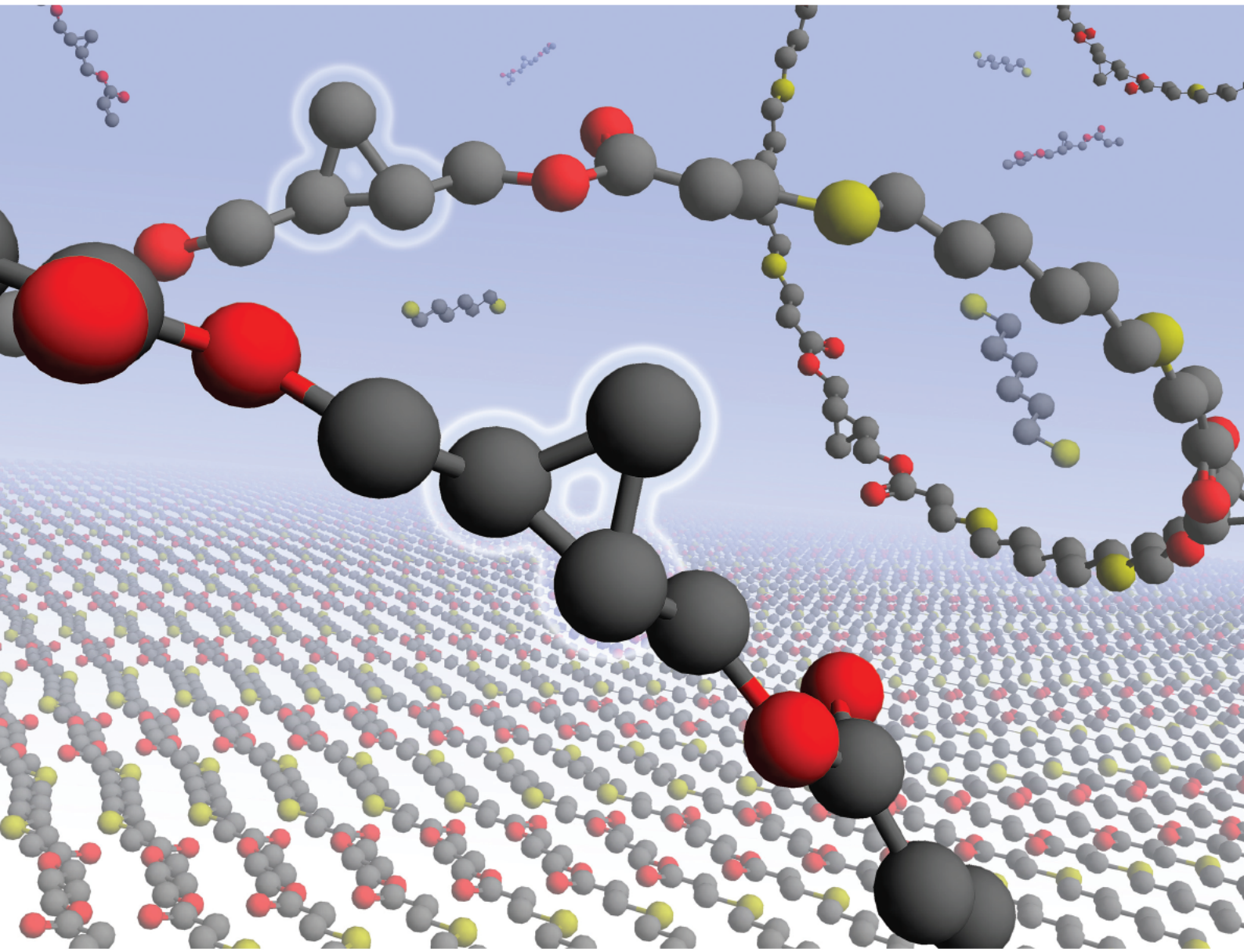
We adapted the thiol-ene step-growth polyaddition used in Chapter 2 to create polyesters with 3-membered rings in the backbone. We found modest thermal differences between the *cis/trans* analogues and both samples resembled a tacky gum at ambient temperature. However, a linear-chained analogue without the cyclopropane ring formed a semi-crystalline material and could be processed into a flexible film. We hypothesised the cyclopropane ring was inhibiting chain packing and movement, whereas the linear derivative had freer rotation and could pack more efficiently.

Considering the stereochemistry of 1,2-cyclopropane had a minimal impact on the thermal and bulk properties of the polymer, we investigated how copolymerising the cyclopropane structure with the linear derivative could tune the properties. In a similar technique described in chapter 2, feed ratios of the linear and cyclopropane monomer in the polymerisation could be varied to yield polymers with a controlled composition. We found that even low loadings of the cyclopropane monomer (10 - 25%) had a significant impact on the crystallinity of the final polymer. This translated to the tensile properties where a higher content of the cyclopropane moiety led to a lower stiffness and strength of the polymer. Whilst the stereochemistry had a small impact on the thermal properties, the cyclopropane unit itself could be used to tune the properties of a linear polyester.

Volume 11
Number 39
21 October 2020
Pages 6233-6388

Polymer Chemistry

rsc.li/polymers



ISSN 1759-9962

ROYAL SOCIETY OF CHEMISTRY

PAPER
Connor J. Stubbs and Andrew P. Dove
Understanding structure–property relationships of main chain cyclopropane in linear polyesters

Polymer Chemistry

ROYAL SOCIETY OF CHEMISTRY

PAPER

View Article Online
View Journal | View Issue

Check for updates

Cite this: *Polym. Chem.*, 2020, **11**, 6251

Understanding structure–property relationships of main chain cyclopropane in linear polyesters†

Connor J. Stubbs and Andrew P. Dove *

Rigid ring structures have gained increasing interest in the polymer materials community as an effective means to manipulate bulk properties. Despite this, little work has focussed on the smallest ring: cyclopropane. Herein, we report a polymerisation that enables incorporation of stereopure *cis* and *trans* 1,2-cyclopropanedimethanol through the thiol-Michael "click" reaction between dithiol and diacrylate monomers. Polyesters containing a cyclopropane backbone were found to be amorphous, whilst comparable polymers with a 1,4-butanediol backbone were semi-crystalline. By copolymerising cyclopropane monomers at varying ratios with 1,4-butanediol monomers, the crystalinity of the resulting polymer could be effectively tuned. Successfully adjusting the resulting crystallinity resulted in control over the ultimate tensile strength (UTS) and the Young's modulus (*E*) of the material. Generally, it was found that increasing cyclopropane content led to a decreased UTS and *E* as a result of lower polymer crystalinity. Effects of cyclopropane stereochemistry on thermomechanical properties were found to be minimal at low cyclopropane backbone ratios.

Received 14th July 2020,
Accepted 28th August 2020

DOI: 10.1039/d0py01004a

rsc.li/polymers

Open Access Article. Published on 28 August 2020. Downloaded on 7/26/2021 3:31:43 PM.
This article is licensed under a Creative Commons Attribution 3.0 Unported Licence.

Introduction

Conformationally-locked ring structures have recently garnered considerable attention in the design of new thermoplastic materials.[1–3] This derives from the ability to manipulate and predict bulk properties from their incorporation into linear polymer systems. Typically, property manipulation is achieved by altering functionalities within a polymer, which can require synthetically demanding steps. Conformationally locked rings offer simple and convenient control of bulk properties in linear polymers. Hence, continual understanding into the influence of rigid ring structures on the thermomechanical properties of the resultant polymers is vital to designing the next generation of high-performance materials.

Oil-sourced cyclohexylene rings have been extensively investigated in various thermoplastic systems, including polyesters, polyamides and polycarbonates.[3–6] By incorporating and controlling the ratios of cyclohexane units in polymers, numerous bulk properties can be manipulated. For example, the ratio of 1,4-cyclohexanedimethanol in polymer materials has been reported to impact bulk properties such as glass transition temperature (T_g), bulk crystallinity, tensile strength and gas permeability.[7–9] More recently bio-based bicyclic diols have gained significant attention in thermoplastic polymers.[10–13] Wang and co-workers reported that incorporation of isosorbide, a simple isohexide unit, in polyesters led to a higher T_g and lower polymer crystallinity.[14] Increasing isosorbide content also correlated with the speed at which hydrolytic degradation occurred.[15]

An additional structural feature to these ring systems is stereochemistry. Most rigid rings, including isohexides and cyclohexylenes, are geometrically locked which gives rise to multiple stereoisomers. There has been a recent surge in interest in leveraging stereochemistry in linear polymers to alter bulk properties.[16] The stereochemical contribution of isohexides and cyclohexylene in polymer backbones has already been briefly investigated.[8,17] Nevertheless, further investigation in the influence of stereochemistry on the physical and mechanical properties of the resultant materials remains a requirement for future polymer systems containing ring structures.

Despite the recent attention into cyclic structures in polymer materials, there lacks considerable investigation into the smallest cycle, cyclopropane. Previous works have focussed on cyclopropane within the polymer side chains.[18] This is typically achieved *via* post-polymerisation modification of unsaturated polymers with diazo species.[19] Mecking and co-workers have demonstrated that an increase in the side chain cyclopropane content within polybutadiene led to a higher T_g and a decrease in bulk crystallinity.[20] Whilst this effectively manipulated thermal properties, the focus was on side chain functionality. As a result of this, the architectural and stereochemical influence that could have resulted from main chain cyclopropane was not examined.

School of Chemistry, University of Birmingham, Birmingham, B15 2TT, UK.
E mail:

†Electronic supplementary information (ESI) available: NMR spectra and thermomechanical characterisation data included. See DOI: 10.1039/d0py01004a

Open Access Article. Published on 28 August 2020. Downloaded on 7/26/2021 3:31:43 PM.
This article is licensed under a Creative Commons Attribution 3.0 Unported Licence.

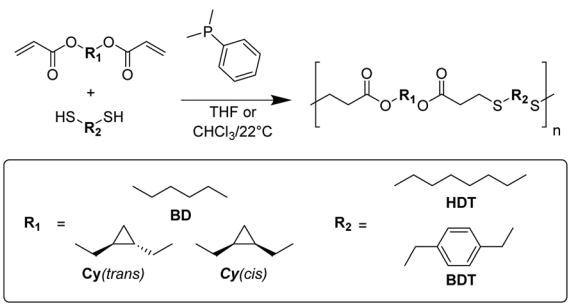
Few studies have focussed on cyclopropane in the main chain of the polymer. One notable example from Takao and co-workers demonstrated the synthesis of a range of polyesters, polyamides and polyurethanes containing cyclopropane in the main chain.[21] Di-functional 1,2-cyclopropanes were synthesised and subsequently polymerised; initial observations suggested that these polymers could be compressed into free-standing films. However, no further analysis was carried out. An extensive study into cyclopropane-containing polymers is needed to further our understanding of the 3-membered structure.

Herein, we present a study into the thermomechanical properties of polyesters containing main chain cyclopropane. Polymers are synthesised in step-growth fashion using mild thiol-Michael addition between multiple dithiols and cyclopropane diacrylate monomers. The effect of stereochemistry in the chain is also investigated.

Results and discussion

In order to fully understand how cyclopropane units in the polymer main chain affects bulk properties, both *cis* and *trans* stereoisomers need to be examined independently to elucidate the stereochemical contribution. Stereopure *cis* and *trans* 1,2-cyclopropane were obtained from established literature procedures (Fig. S1†).[22] The diols were functionalised with acryloyl chloride to afford diacrylate-containing monomers: **Cy**(*trans*) and **Cy**(*cis*) (Fig. S1†). An additional commercially available diacrylate monomer, 1,4-butanedioldiacrylate (**BD**), was also used to serve as a linear comparison to the cyclopropane-containing polymers. Nucleophilic thiol-Michael addition was selected because the mild and efficient conditions can afford high molecular weight polymers without causing isomerisation or other potential side reactions.[23,24] A range of polyesters were synthesised from the diacrylate monomers through a phosphine catalysed polyaddition with commercially available dithiols (Scheme 1, Table 1).

Initial polymerisations used 1,6-hexanedithiol (**HDT**) with the three diacrylate monomers (**BD**, **Cy**(*cis*) and **Cy**(*trans*)) to produce comparable homopolymers. Relatively high molecular weights were achieved (35 kDa < M_w) that possessed modest dispersities (4.5 > $Đ_M$, Table 1). ^{1}H NMR spectroscopy confirmed the reaction conditions had not impacted the stereochemistry or cyclopropane structure of the resulting polymers (Fig. 1a). Most noticeably, the polymers displayed vastly different physical appearances. Both cyclopropane polyesters (**Cy**(*trans*)-*co*-**HDT** and **Cy**(*cis*)-*co*-**HDT**) were translucent and possessed a tacky consistency, even after aging for multiple



Scheme 1 General scheme for linear polyesters synthesised from phosphine catalysed thiol Michael addition of diacrylate and dithiol monomers.

Table 1 Characterisation of linear polyesters

	M_w [a] (kDa)	$Đ_M$ [a]	T_g [b] (°C)	ΔH_m [b] (J g^{-1})	$T_{d,5\%}$ [c] (°C)
Cy(*trans*) *co* **HDT**	38.0	4.30	52		276
Cy(*cis*) *co* **HDT**	37.4	4.08	47		293
BD *co* **HDT**	52.7	3.13	66	64.0	315
Cy(*trans*) *co* **BDT**	23.5	6.58	17		256
BD *co* **BDT**	22.0	7.78	27	58.7	273

[a] M_w and $Đ_M$ were determined by size exclusion chromatography (THF, 2% v/v NEt_3) analysis against polystyrene (PS) standards. [b] Glass transition temperature obtained from second heating scan. Total enthalpy of melting calculated from integration of all melt transitions. [c] Temperature after 5% weight loss obtained from thermogravimetric analysis.

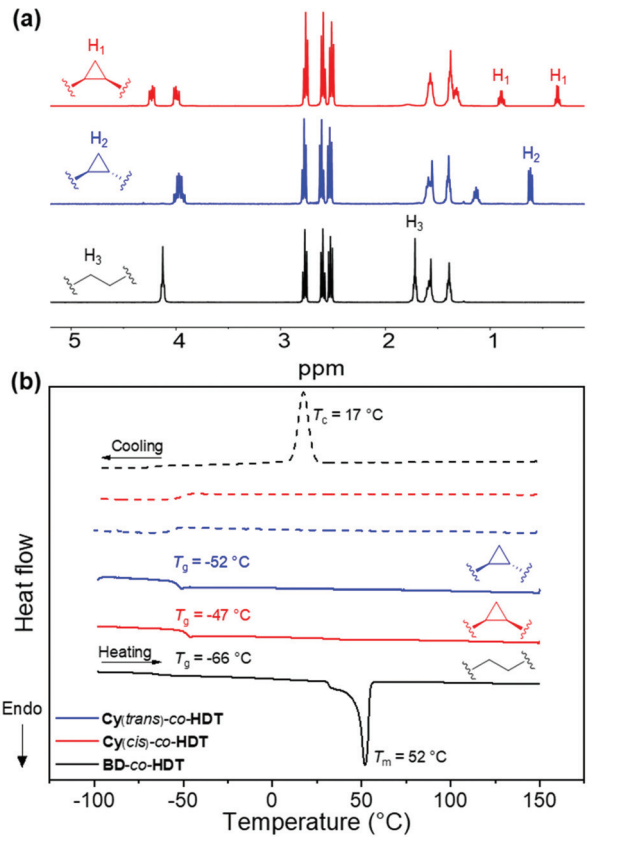


Fig. 1 (a) ^{1}H NMR spectra of polymers synthesised using **HDT** in $CDCl_3$ (400 MHz, 298 K) (b) normalised DSC thermograms of polymers synthesised using **HDT** at a heating and cooling rate of 10 K min^{-1} (solid line = heating run, dashed line = cooling run).

This journal is © The Royal Society of Chemistry 2020

Open Access Article. Published on 28 August 2020. Downloaded on 7/26/2021 3:31:43 PM.
This article is licensed under a Creative Commons Attribution 3.0 Unported Licence.

months at benchtop conditions. Whilst the linear control (**BD-*co*-HDT**) was an opaque white solid. This observation indicated that the cyclopropane structure had significantly impacted bulk properties: crystallinity in particular.

To quantify the thermal properties and gain insight into the crystallinity, differential scanning calorimetry (DSC) was performed (Fig. 1b). The T_gs of all the polymers were well below ambient temperature (−66 to −47 °C). There was a small deviation in the T_g observed between the *cis* and *trans* cyclopropane polyesters, where **Cy**(*cis*)-*co*-**HDT** had a T_g 5 °C higher than **Cy**(*trans*)-*co*-**HDT**. This could be ascribed to a higher free volume in **Cy**(*trans*)-*co*-**HDT** caused by the *trans* isomer. Copolymer **BD**-*co*-**HDT** had the lowest T_g which is attributed to more efficient chain packing of the butyl-group in comparison to the cyclopropane ring. However, the most striking observation from the DSC thermograms was the lack of melt transitions (T_m). Both cyclopropane-containing polyesters lacked a melt transition, while **BD**-*co*-**HDT** possessed a sharp melting peak at 52 °C. This indicates that the cyclopropane polymers are amorphous whereas **BD**-*co*-**HDT** is crystalline, which is in agreement with the observed physical differences. It was clear that the irregularity of the cyclopropane structure had inhibited chain alignment and, therefore, negated any possible crystallisation that would have otherwise occurred. Consequently, the polymers produced were excessively tacky and unable to produce free-standing films.

In attempts to produce a polymer suitable for heat-pressing and forming a stable film, a rigid aromatic dithiol was used as comonomer. 1,4-Benzenedimethanethiol (**BDT**) was reacted with the diacrylate monomers, **Cy**(*trans*) and **BD**. The polymerisation produced polyesters of a notably lower M_w and higher $Đ_M$ than the previously synthesised polymers. A similar physical difference was observed in this aromatic system in comparison to the **HDT** polymers: **Cy**(*trans*)-*co*-**BDT** produces a tacky texture whilst **BD**-*co*-**BDT** system produces an opaque white solid (Fig. 2a). It was observed that the **BD**-*co*-**BDT** visibly changed over the course of ~12 h at room temperature after melting which was hypothesised to be slow crystallisation. In efforts to produce comparable data, both polymers were melted until liquid-like flow was achieved (~100 °C) then cooled to room temperature (22 °C) and annealed in a thermostated incubator at 22 °C for 48 h. DSC was then performed on the annealed polymers to elucidate the thermal properties (Fig. 2b).

Both **Cy**(*trans*)-*co*-**BDT** and **BD**-*co*-**BDT** polymers possessed a higher T_g (−17 and −27 °C respectively) than the previous **HDT** system, which was expected as a consequence of increased planarity and rigidity. It was also evident that **Cy**(*trans*)-*co*-**BDT** had a higher T_g than **BD**-*co*-**BDT** resulting from the increased rigidity of the cyclopropane ring. The physical appearances of these polymers were further corroborated by the DSC thermograms. **BD**-*co*-**BDT** possessed multiple melt transitions which indicates that the material has multiple crystalline domains.[25] Interestingly there was also an absence of a crystallisation peak (T_c) in **BD**-*co*-**BDT**, which we attributed to inefficient crystallisation under cooling run conditions. This corroborates the slow

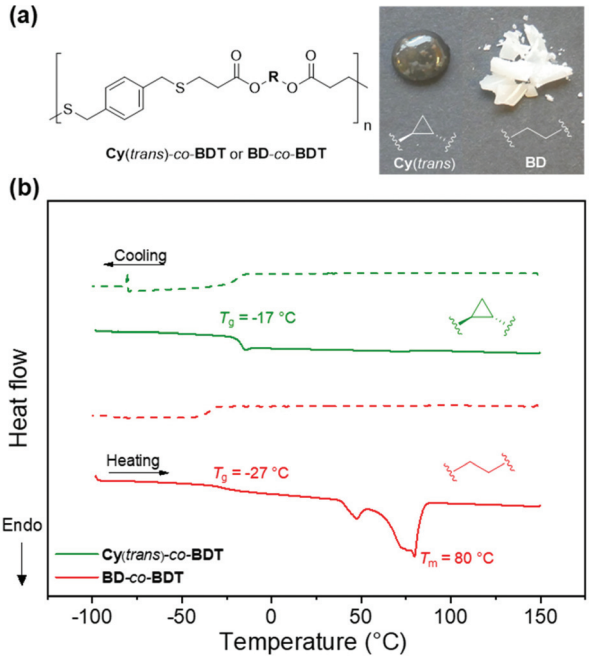


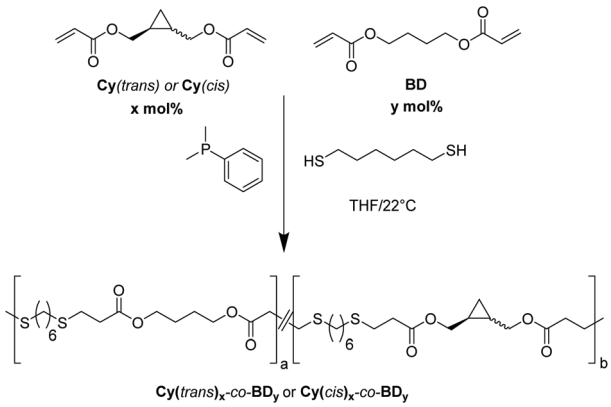
Fig. 2 (a) Polyester architecture with variable structure from diacrylate monomer with **BDT**. Image of annealed polyesters illustrating differences in physical appearance (b) normalised DSC thermograms of 2 day annealed polymers made using **BDT** at a heating and cooling rate of 10 K min ^{1} (solid line = heating run, dashed line = cooling run).

physical change to a white solid observed after melting. In contrast, the **Cy**(*trans*)-*co*-**BDT** does not display a T_m peak, indicative of an amorphous polymer. Despite the higher chain ordering promoted by **BDT**'s planarity, **Cy**(*trans*)-*co*-**BDT** was unable to produce a free-standing film. This has further demonstrated the lack of chain-packing, and subsequent crystallisation in polymers that contain the cyclopropane structure. We postulate that the geometry of 1,2-cyclopropanes can prevent packing in two ways: (i) the rigidity of the ring prevents the rotation and flexibility that aids chain packing and (ii) the 1,2-substitution of the rigid cyclopropane geometry induces a "kink" in the linear chain that further disadvantages facile chain packing and hence crystallisation.

In order to create cyclopropane-containing polymers that could be processed into a flexible free-standing film, we leveraged the efficient thiol–ene polyaddition to introduce cyclopropane units into **BD**-containing copolymers. By polymerising **BD** and **Cy** monomers with **HDT**, random copolymers could be accessed. Additionally, this method allowed total control over the backbone content through varying monomer ratios within the feedstock (Scheme 2).

The three copolymerised polyesters were of comparable M_w (63.5 to 91.8 kDa) and $Đ_M$ (4.28 to 4.62, Table 2). ^{1}H NMR spectroscopic analysis indicated that the initial feed ratio of the monomers had been successfully translated into the resulting polymers (ESI†). By keeping the cyclopropane content in the polymer low (<30%), the polymers could be heat-pressed to produce non-tacky free-standing films. It was noted that some

Open Access Article. Published on 28 August 2020. Downloaded on 7/26/2021 3:31:43 PM.
This article is licensed under a Creative Commons Attribution 3.0 Unported Licence.



Scheme 2 Scheme illustrating the co polymerisation of cyclopropane diacrylates and 1,4 butanediol diacrylate (**BD**) with 1,6 hexanedithiol (**HDT**) to create random co polymers.

Table 2 Characterisation table of random copolymers containing cyclopropane

	M_w [a] (kDa)	$Đ_M$ [a]	T_g [b] (°C)	$T_{d,\,5\%}$ [c] (°C)
$BD_{90}Cy(trans)_{10}$ *co* HDT	63.5	4.28	64	315
$BD_{90}Cy(cis)_{10}$ *co* HDT	76.9	4.62	63	314
$BD_{75}Cy(trans)_{25}$ *co* HDT	91.8	4.54	62	313

[a] M_w and $Đ_M$ were determined by size exclusion chromatography (THF, 2% v/v NEt_3) analysis against polystyrene (PS) standards. [b] Glass transition temperature obtained from second heating scan. [c] Temperature after 5% weight loss obtained from thermogravimetric analysis.

of the films visibly became more opaque and stiffer at room temperature (22 °C) a few hours after heat-pressing; particularly polymers containing cyclopropane. This was attributed to slow crystallisation. Therefore, to ensure the polymers had reached thermal equilibrium and were comparable, they were heat-pressed and annealed for 2 days at 22 °C in a thermostated incubator. These samples were then characterised by uniaxial tensile testing until breakage (Fig. 3).

The newly synthesised random co-polymers were compared alongside **BD**-*co*-**HDT** to assess the impact cyclopropane had on tensile properties. All the samples displayed tensile curves that are consistent with a tough thermoplastic and possessed a similar strain at break (Table S1†). All samples also displayed periodic drops in stress which was most apparent in **BD**-*co*-**HDT**. This is characteristic of stress-oscillation behaviour observed in numerous polymer systems, however origins of this phenomenon are often disputed.[26,27] A possible explanation is the formation of "voids" in the amorphous regions during elongation which leads to a stress drop and the reorientation of polymer crystallites leading to a stress increase.[28] Remarkably, this behaviour was considerably reduced in samples containing cyclopropane. This is attributed to a reduction in chain packing caused by the cyclopropane geometry, and subsequent impact on the size and spacing between the crystallites which are typically responsible for stress-oscillation behaviour.

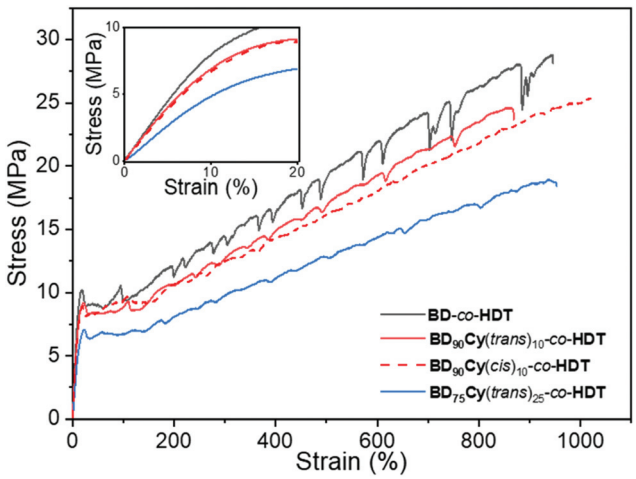


Fig. 3 Representative stress *vs.* strain curves of the random copolymers *Inset* data between 0 and 20% strain illustrating the difference in Young's modulus.

BD-*co*-**HDT** displayed the highest strength at break (UTS) and Young's Modulus (E). Upon incorporation of either cyclopropane isomer: the tensile strength and Young's modulus slightly decreased. Reduction of strength and stiffness is expected as a result of cyclopropane inhibiting chain crystallisation which ultimately leads to a weaker material. Interestingly, there appeared to be negligible tensile difference between the *cis* and *trans* cyclopropane isomers at 10% backbone content (Table S1†). Whilst this is a contrast to several previously reported *cis*/*trans* polymer systems, the low cyclopropane content within this system could inhibit the influence of stereochemistry.[29,30] Further increase of the *trans*-cyclopropane content to 25% led to a more flexible and weaker material. $BD_{75}Cy(trans)_{25}$-*co*-**HDT** possessed an average Young's modulus of 60 MPa in comparison to **BD**-*co*-**HDT** which was 105 MPa. A similar reduction in UTS was also observed between these two polymers (19.2 MPa from 29.7 MPa). This clear manipulation of tensile properties as a result of cyclopropane indicates that efforts to control polymer crystallinity were successful.

To quantify the impact of cyclopropane incorporation on polymer crystallinity in these random co-polymers, DSC analysis was performed (Fig. 4a). Incorporation of cyclopropane led to slight increases in the co-polymer T_g (Table 2). Unlike **Cy**(*trans*)-*co*-**HDT** and **Cy**(*cis*)-*co*-**BDT**, the butyl/cyclopropane random co-polymers all possessed a T_m and a T_c intuitive of a semi-crystalline material. This indicates that the large **BD** content was able to drive chain crystallisation within the polymer material. To quantify the extent of crystallinity, the melt transitions were normalised and integrated to obtain the total enthalpy of melting (ΔH_m). A higher value for ΔH_m indicates more extensive polymer crystallinity. As hypothesised, increasing the content of cyclopropane led to a lower ΔH_m indicating a loss of crystallinity. The other striking observation of these DSC thermograms is the shift seen in the T_c to lower temperatures with an increasing cyclopropane content. Both of

 This journal is © The Royal Society of Chemistry 2020

Open Access Article. Published on 28 August 2020. Downloaded on 7/26/2021 3:31:43 PM.
This article is licensed under a Creative Commons Attribution 3.0 Unported Licence.

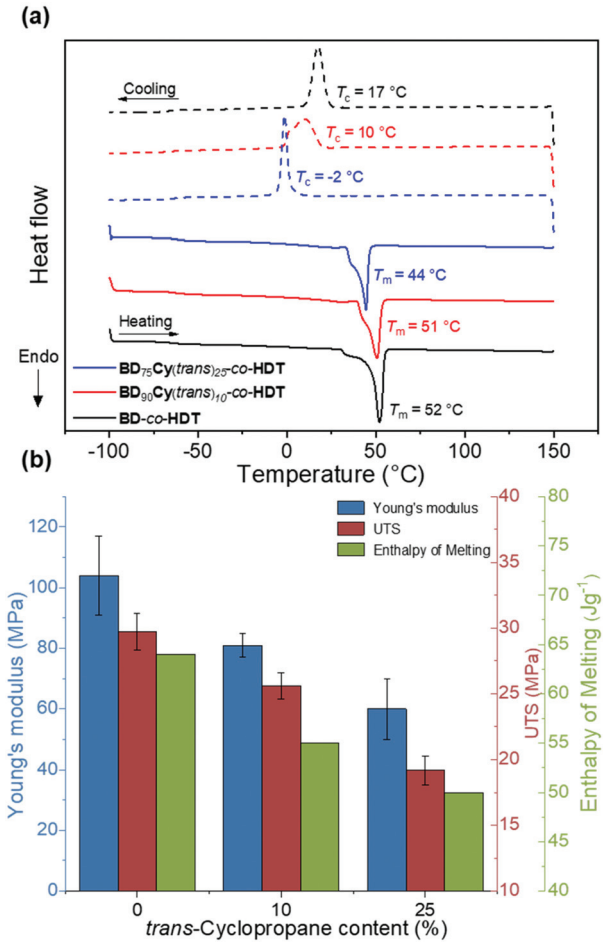


Fig. 4 (a) Normalised DSC thermograms of 2 day annealed polymers synthesised using different feed ratios of *trans* cyclopropane **Cy**(*trans*) at a heating and cooling rate of 10 K min ^{1} (solid line = heating run, dashed line = cooling run). (b) Bar chart of Young's modulus (*E*), ultimate tensile strength (UTS) and Enthalpy of Melting *vs. trans* cyclopropane content (%) in polyester backbone.

these observations corroborate the amorphous nature of the cyclopropane structure and its ability to impede crystallinity when implemented into highly ordered polymers. This loss in crystallinity could be directly correlated with strength and Young's modulus of the resulting copolymer (Fig. 4b). Thus, the tensile properties of the polymers can not only be modulated but can be predicted from the thermal transitions.

There were minimal differences in T_g, T_m and ΔH_m between the *cis* and *trans* stereochemistry at 10% backbone content (Table S1†). This was expected given the comparable tensile properties of **BD$_{90}$Cy**(*trans*)$_{10}$-*co*-**HDT** and **BD$_{90}$Cy**(*cis*)$_{10}$-*co*-**HDT**. However, previous investigations report that changing the *cis*/*trans* content of linear polymers led to a control of bulk crystallinity, and hence, tensile properties could be tuned.[29,31] The lack of crystallinity in the initial cyclopropane-containing polymers demonstrates that neither stereochemistry promotes crystallisation. Therefore, we observe minimal differences in tensile properties between the *cis* and *trans* stereochemistry in this cyclopropane system. It was clear that controlling the content of either cyclopropane isomer in a polymer backbone led to manipulation of thermomechanical properties. Future investigation is required to understand the full extent main chain cyclopropane has on further bulk properties.

Conclusion

A polymer system has been designed to incorporate both isomers of 1,2-cyclopropane into the main chain of a polyester using nucleophilic thiol–ene addition chemistry. Cyclopropane backbones were found to be unusually amorphous. However, used as a comonomer, cyclopropane could effectively manipulate polymer crystallinity. Through the control of polymer crystallinity, it was demonstrated that Young's modulus and UTS could be decreased by ~40% with as little as 25% cyclopropane content. This demonstrates an effective and simple means to control polymer crystallinity. Typically, elucidation and design of polymers with specific properties is a laborious experimental task. But through detailed understanding of structure–property relationships, design of polymers that satisfy diverse applications can be straightforward. Further study into cyclopropanes in polymers and networks are still required to understand its future potential in the synthesis of high-performance materials.

Experimental

Materials

1,6-Hexanedithiol was distilled under vacuum before use and stored under N_2 in a Schlenk-flask. All other chemicals were used as received.

Measurements

All NMR experiments were performed at 298 K on a Bruker DPX-400 NMR instrument equipped operating at 400 MHz for ^{1}H (100.57 MHz for ^{13}C). ^{1}H NMR spectra are referenced to residual proton solvent (δ 7.26 for $CDCl_3$ δ 2.50 for DMSO) and ^{13}C NMR spectra are referenced to the solvent signal (δ 77.2 for $CDCl_3$ δ 39.52 for DMSO). The resonance multiplicities are described as s (singlet), d (doublet), t (triplet), q (quartet) or m (multiplet).

Mass spectrometry was performed by University of Birmingham school of Chemistry on a Waters GCT Premier for compounds **2** and **3**. Mass spectrometry was performed on compounds **4** and **5** using Waters Xevo G2-XS QTof.

Size Exclusion Chromatography (SEC) in THF was performed on a system composed of an Agilent 1260 Infinity II LC system equipped with an Agilent guard column (PLGel 5 μM, 50 × 7.5 mm) and two Agilent Mixed-C columns (PLGel 5 μM, 300 × 7.5 mm). The mobile phase used was THF (HPLC grade) containing 2% v/v NEt_3 at 40 °C at flow rate of 1.0 mL min^{-1} (polystyrene (PS) standards used for calibration). Number average molecular weights (M_n), weight average molecular

Open Access Article. Published on 28 August 2020. Downloaded on 7/26/2021 3:31:43 PM.
This article is licensed under a Creative Commons Attribution 3.0 Unported Licence.

weights (M_w) and dispersities ($Đ_M = M_w/M_n$) were determined using Agilent SEC software.

Determination of the thermal characteristics of the polymers were carried out using a STARe system DSC3 with autosampler (Mettler Toledo, Switzerland). Samples were added to 40 μL aluminum pans. Thermograms obtained with a heating rate of 10 K min^{-1} were recorded from −100–150 °C with a 10 K min^{-1} heating and cooling rate over two cycles. The glass transition temperature (T_g) was determined by the minimum of the first derivative in the second heating cycle. Total enthalpy of melting (ΔH_m) was calculated from integration and normalization of all endothermic peaks present using the STARe software.

Thermal degradation was quantified using a Q550 Thermogravimetric analyser (TA instruments). Thermograms were recorded under an N_2 atmosphere at a heating rate of 10 K min^{-1} from 25–600 °C. Decomposition temperatures were reported at the 5% weight loss temperature ($T_{d,\ 5\%}$).

Thin polymer films were fabricated using a Specac Atlas™ Manual Hydraulic Press 15 T fitted with Specac heated plates. Films with a thickness of 0.3 ± 0.1 mm were prepared by melt compressing the polymers under *ca.* 5 kN of force in a hot press followed by cooling to ambient temperature in the press whilst under compression. Polymer samples were in an aluminium rectangular spacer (20 × 40 × 0.5 mm) between PTFE sheets and placed between heated plates at 90 °C unless stated otherwise and then cooled to ambient temperature maintaining 5 kN of force. Film samples were visually inspected for deformation and bubbles before annealing for 2 days at 25 °C. Dogbones ASTM Type IV were cut out of the films and subjected to uniaxial tensile testing on a Testometric M350-5CT fitted with a load cell of 10 kN. Each specimen was clamped into the tensile holders and subjected to an elongation rate of 10 mm min^{-1} until failure ($n = 3$). The data was averaged, and the standard deviation is posed as the uncertainty.

Synthesis of racemic diethyl-1,2-cyclopropanedicarboxylate (1)

A dry 3-necked 1000 mL round bottom flask fitted with a Suba-Seal®, dropping funnel and gas adapter with light nitrogen flow and was then charged with sodium hydride 60% dispersion in mineral oil (24 g, 0.6 mol, 1.5 equiv.) and cooled 0 °C with an ice bath. The sodium hydride was then suspended in dry toluene (400 mL). Ethyl acrylate (40 g, 0.4 mol, 1 equiv.) and ethyl chloroacetate (49 g, 0.4 mol, 1 equiv.) were mixed in a beaker and charged to the dropping funnel. Approximately 5 mL of this mixture was added to the cooled sodium hydride solution. Nitrogen flow was increased whilst ethanol (2 mL) was charged *via* needle to the reaction whilst maintaining vessel at 0 °C with an ice bath. Once bubbling had ceased, the remaining ethyl acrylate and ethyl chloroacetate mixture was added dropwise through the dropping funnel over the course of 3 h to maintain the reaction temperature at 0 °C. The reaction was stirred and allowed to warm to room temperature over *ca.* 16 h. The reaction was quenched over crushed ice (~400 mL) then extracted with ethyl acetate (3 × 200 mL) before removal of solvent *in vacuo*. The remaining orange oil was distilled under vacuum to obtain a crude mixture containing title compound (15% *trans* isomer and 85% *cis* isomer calculated by ^{1}H NMR spectroscopy) as a colourless oil (31.8 g, 170 mmol, 42% overall yield). This was used as obtained in further reactions (crude NMR shown Fig. S2†). Spectral data consistent with previous work.[32]

Synthesis of *cis*-1,2-cyclopropanedimethanol (2)

A dry 3-necked 500 mL round bottom flask fitted with a condenser and gas adapter with light nitrogen flow was then charged with $LiAlH_4$ (7.1 g, 186 mmol, 1.5 equiv.). The vessel was cooled to 0 °C and dry THF (~200 mL) was added and stirred. A mixture of **1** (23.3 g, 125 mmol, 1.0 equiv.) in THF (~40 mL) was added dropwise over 30 minutes. The reaction was then heated at reflux for 2 h and allowed to cool to ambient temperature and stirred for *ca.* 16 h. The reaction was then quenched with saturated NH_4Cl solution (42 mL) and diluted with EtOAc (42 mL). Remaining salts are removed by filtration and the filtrate was concentrated yielding a crude orange oil. The oil was further purified by column chromatography (100% EtOAc) yielding title compound as a colourless oil (7.3 g, 71 mmol, 57% yield). ^{1}H NMR (400 MHz; 298 K; DMSO-*d*6) δ 4.46 (dd, J = 6.1, 4.6 Hz, 2H), 3.56 (m, 2H), 3.33–3.22 (m, 2H), 1.13–0.97 (m, 2H), 0.62 (td, J = 8.2, 4.5 Hz, 1H), 0.11 (m, 1H) ^{13}C NMR (101 MHz; 298 K; DMSO-*d*6) δ 61.0, 17.8, 8.2. MS (CI-TOF) calculated for $C_5H_{10}O_2NH_4$ 120.10; found 120.03.

Synthesis of *trans*-1,2-cyclopropanedimethanol (3)

A dry 3-necked 500 mL round bottom flask fitted with a condenser and gas adapter with light nitrogen flow was then charged with $LiAlH_4$ (3.1 g, 81 mmol, 1.5 equiv.). The vessel was cooled to 0 °C and dry THF (~60 mL) was added and stirred. *trans*-Diethyl-1,2-cyclopropanedicarboxylate (10 g, 54 mmol, 1 equiv.) in THF (~20 mL) was added dropwise over 30 minutes. The reaction was then heated at reflux for 2 h and allowed to cool to ambient temperature and stirred for *ca.* 16 h. The reaction was then quenched with saturated NH_4Cl solution (20 mL) and diluted with EtOAc (20 mL). Remaining salts are removed by filtration and the filtrate is concentrated yielding a crude orange oil. The oil was further purified by column chromatography (100% EtOAc) to yield title compound as colourless oil (3.47 g, 34 mmol, 63% yield) ^{1}H NMR (400 MHz, DMSO-d6) δ 4.37 (d, J = 11.1 Hz, 1H), 3.35–3.23 (m, 2H), 3.26–3.14 (m, 2H), 2.08 (s, 1H), 0.86–0.72 (m, 2H), 0.33–0.25 (m, 2H). ^{13}C NMR (101 MHz; 298 K; DMSO-*d*6) δ 64.0, 18.9, 7.7. Spectral data consistent with previous work.[33] MS (CI-TOF) calculated for $C_5H_{10}O_2NH_4$ 120.1025; found 120.005.

Synthesis of *cis*-Cy diacrylate (4)

A 2-necked flask 100 mL round bottom flask fitted with a gas adapter and a dropping funnel was charged with **2** (2.0 g, 19 mmol, 1 equiv.), dry THF (~30 mL) and acryloyl chloride (4.4 g, 49 mmol, 2.5 equiv.). Triethylamine (5.9 g, 59 mmol, 3 equiv.) was added dropwise slowly over the course of 1 h at

 This journal is © The Royal Society of Chemistry 2020

Open Access Article. Published on 28 August 2020. Downloaded on 7/26/2021 3:31:43 PM.
This article is licensed under a Creative Commons Attribution 3.0 Unported Licence.

0 °C whilst stirring. The reaction was allowed to warm to ambient temperature and stirred for *ca.* 16 h. The reaction was then quenched with water (~50 mL) and was extracted with EtOAc (3 × 30 mL). The organic layer was dried with Mg_2SO_4 and concentrated to an orange oil. The oil was subject to further purification by column chromatography (3 : 1 hexanes to ethyl acetate) yielding title compound as a colourless oil (2.3 g,11 mmol, 58% yield). ^{1}H NMR (400 MHz, $CDCl_3$) δ 6.41 (dd, J = 17.3, 1.5 Hz, 2H), 6.11 (dd, J = 17.3, 10.4 Hz, 2H), 5.82 (dd, J = 10.4, 1.5 Hz, 2H), 4.45–4.28 (m, 2H), 4.13–3.96 (m, 2H), 1.50–1.30 (m, 2H), 0.94 (td, J = 8.4, 5.3 Hz, 1H), 0.40 (q, J = 5.6 Hz, 1H). ^{13}C NMR (101 MHz; 298 K; $CDCl_3$) δ 166.3, 131.0, 128.6, 64.7, 14.9, 8.9. MS (CI-TOF) calculated for $C_{11}H_{14}O_4NH_4$ 228.1236; found 228.1241.

Synthesis of *trans*-Cy diacrylate (5)

A 2-necked flask 100 mL round bottom flask fitted with a gas adapter and a dropping funnel was charged with **3** (2.0 g, 19 mmol, 1 equiv.), dry THF (~30 mL) and Acryloyl chloride (4.4 g, 49 mmol, 2.5 equiv.). Triethylamine(5.9 g, 59 mmol, 3 equiv.) was added dropwise slowly over the course of 1 h at 0 °C whilst stirring. The reaction was allowed to warm to ambient temperature and stirred for *ca.* 16 h. The reaction was then quenched with water (~50 mL) and was extracted with EtOAc (3 × 30 mL). The organic layer was dried with Mg_2SO_4 and concentrated to an orange oil. The oil was subject to further purification by column chromatography (3 : 1 hexanes to ethyl acetate) yielding title compound as a colourless oil (2.1 g, 10 mmol, 53% yield). ^{1}H NMR (400 MHz, $CDCl_3$) δ 6.40 (dd, J = 17.3, 1.5 Hz, 2H), 6.19–6.04 (m, 2H), 5.82 (dd, J = 10.4, 1.5 Hz, 2H), 4.14–4.00 (m, 2H), 4.05–3.91 (m, 2H), 1.24–1.18 (m, 2H), 0.70–0.59 (m, 2H). ^{13}C NMR (101 MHz; 298 K; DMSO-*d*6) δ 166.4, 130.9, 128.6, 67.7, 16.3, 9.1. MS (CI-TOF) calculated for $C_{11}H_{14}O_4H$ 211.0970; found 211.0978.

General polymerisation procedure (BD-*co*-HDT)

A scintillation vial was charged with 1,4-butanedioldiacrylate (0.1696 g, 0.856 mmol, 1 equiv.) and another scintillation vial was charged with 1,6-hexanedithiol (0.1285 g, 0.856 mmol, 1 equiv.). The contents of both scintillation vials were dissolved in THF (1.8 mL) and quantitatively transferred to a 25 mL scintillation vial and stirred at ambient temperature. Whilst stirring, polymerization was initiated with DMPP (2.4 μL, 2%mol) and left to stir. Initially an exotherm was observed with a visible increase in viscosity. After *ca.* 16 h the polymer solution was precipitated in MeOH (100 mL) and left to stir for 1 h before decanting the supernatant. Polymer was then dried under vacuum for approximately 2 h. SEC analysis (THF + 2% v/v NEt_3) M_w = 52.7, $Đ_M$ = 3.13, DSC analysis T_g = −66 °C, ^{1}H NMR (400 MHz, $CDCl_3$) δ 4.21–4.05 (m, 4H), 2.77 (t, J = 7.5 Hz, 4H), 2.60 (t, J = 7.5 Hz, 4H), 2.57–2.49 (m, 4H), 1.77–1.66 (m, 4H), 1.64–1.51 (m, 6H), 1.46–1.34 (m, 4H). ^{13}C NMR (101 MHz; 298 K; $CDCl_3$) δ 172.2, 64.3, 35.0, 32.3, 29.6, 28.6, 27.2, 25.5.

Cy(*trans*)-*co*-HDT. SEC analysis (THF + 2% v/v NEt_3) M_w = 38.0, $Đ_M$ = 4.30, DSC analysis T_g = −52 °C, ^{1}H NMR (400 MHz, $CDCl_3$) δ 4.03–3.87 (m, 4H), 2.76 (t, J = 6.7 Hz, 4H), 2.59 (t, J = 7.3 Hz, 4H), 2.52 (t, J = 7.2 Hz, 2H), 1.63–1.51 (m, 4H), 1.40–1.36 (m, 4H), 1.21–1.01 (m, 2H), 0.64–0.53 (t, J = 6.8 Hz, 2H). ^{13}C NMR (101 MHz; 298 K; $CDCl_3$) δ 172.1, 67.7, 35.1, 32.2, 29.6, 28.6, 27.1, 16.2, 9.2.

Cy(*cis*)-*co*-HDT. SEC analysis (THF + 2% v/v NEt_3) M_w = 37.4, $Đ_M$ = 4.08, DSC analysis T_g = −47 °C ^{1}H NMR (400 MHz, $CDCl_3$) δ 4.23 (m, 2H), 4.00 (m, 2H), 2.76 (t, J = 7.5 Hz, 4H), 2.59 (t, J = 7.2 Hz, 4H), 2.51 (t, J = 7.5 Hz, 4H), 1.63–1.52 (m, 4H), 1.40–1.37 (m, 4H), 1.34–1.28 (m, 2H), 0.93–0.85 (m, 1H), 0.36 (q, J = 5.6 Hz, 1H). ^{13}C NMR (101 MHz; 298 K; $CDCl_3$) 172.1, 64.8, 35.1, 32.2, 29.6, 28.6, 27.1, 14.8, 9.0.

Cy(*trans*)-*co*-BDT. SEC analysis (THF + 2% v/v NEt_3) M_w = 23.5, $Đ_M$ = 6.58, DSC analysis T_g = −17 °C, ^{1}H NMR (400 MHz, $CDCl_3$) 7.26 (s, overlaps with residual $CHCl_3$, 4H), 3.97–3.93 (m, 4H), 3.71 (s, 4H), 2.68 (t, J = 6.6 Hz, 4H), 2.56 (t, J = 7.4 Hz, 4H), 1.19–1.02 (m, 2H), 0.60 (t, J = 7.4 Hz, 2H). ^{13}C NMR (101 MHz; 298 K; $CDCl_3$) δ 172.0, 137.1, 129.2, 129.2, 67.8, 36.1, 34.7, 26.5, 16.2, 16.2, 9.2.

BD-*co*-BDT. SEC analysis (THF + 2% v/v NEt_3) M_w = 22.0, $Đ_M$ = 7.78, DSC analysis T_g = −27 °C, ^{1}H NMR (400 MHz, $CDCl_3$) δ 7.25 (s, overlaps with residual $CHCl_3$, 4H), 4.16–4.04 (m, 4H), 3.71 (s, 4H), 2.68 (t, J = 7.7 Hz, 4H), 2.55 (t, J = 7.4 Hz, 4H), 1.76–1.65 (m, 4H). ^{13}C NMR (101 MHz; 298 K; $CDCl_3$) δ 172.0, 137.1, 129.2, 64.3, 36.2, 34.6, 26.5, 25.4.

$BD_{90}Cy(trans)_{10}$-*co*-HDT. SEC analysis (THF + 2% v/v NEt_3) M_w = 63.5, $Đ_M$ = 4.28, DSC analysis T_g = −64 °C, ^{1}H NMR (400 MHz, $CDCl_3$) δ 4.21–4.04 (m, 1.8 H), 3.99–3.94 (m, 0.2 H), 2.77 (t, J = 7.4 Hz, 2H), 2.60 (t, J = 7.1 Hz, 2H), 2.53 (t, J = 7.3 Hz, 2H), 1.81–1.65 (m, 2H), 1.62–1.58 (m, overlapping with HDO, 2H), 1.42–1.38 (m, J = 5.4 Hz, 2H), 1.18–1.08 (m, 0.1 H), 0.65–0.58 (m, 0.1 H). ^{13}C NMR (101 MHz; 298 K; $CDCl_3$) δ 172.2, 67.8, 64.3, 35.0, 32.3, 29.6, 28.6, 27.2, 25.5, 16.2.

$BD_{90}Cy(cis)_{10}$-*co*-HDT. SEC analysis (THF + 2% v/v NEt_3) M_w = 76.9, $Đ_M$ = 4.62, DSC analysis T_g = −63 °C, ^{1}H NMR (400 MHz, $CDCl_3$) δ 4.27–4.23 (m, 0.1 H), 4.17–4.09 (m, 1.8 H), 4.04–3.99 (m, 0.1 H), 2.77 (t, J = 7.4 Hz, 2H), 2.60 (t, J = 7.3 Hz, 1H), 2.53 (t, J = 7.9 Hz, 2H), 1.80–1.66 (m, 2H), 1.65–1.48 (m, 2H), 1.40 (t, J = 5.3 Hz, 2H), 0.96–0.87 (m, 0.05 H), 0.38 (q, J = 5.5 Hz, 0.05 H). ^{13}C NMR (101 MHz; 298 K; $CDCl_3$) δ 172.1, 64.9, 64.3, 35.0, 32.3, 29.6, 28.6, 27.2, 25.4, 14.9, 9.1.

$BD_{75}Cy(trans)_{25}$-*co*-HDT. SEC analysis (THF + 2% v/v NEt_3) M_w = 91.8, $Đ_M$ = 4.54, DSC analysis T_g = −62 °C, ^{1}H NMR (400 MHz, $CDCl_3$) δ 4.21–4.04 (m, 1.5 H), 3.99–3.94 (m, 0.5 H), 2.77 (t, J = 7.4 Hz, 2H), 2.60 (t, J = 7.1 Hz, 2H), 2.53 (t, J = 7.3 Hz, 2H), 1.81–1.65 (m, 2H), 1.62–1.58 (m, overlapping with HDO, 2H), 1.42–1.38 (m, J = 5.4 Hz, 2H), 1.18–1.08 (m, 0.25 H), 0.65–0.58 (m, 0.25 H). ^{13}C NMR (101 MHz; 298 K; $CDCl_3$) δ 172.2, 67.8, 64.3, 35.0, 32.3, 29.6, 28.6, 27.2, 25.5, 16.2, 9.2.

Conflicts of interest

There are no conflicts to declare.

Acknowledgements

This project has received funding from the European Research Council (ERC) under the European Union's Horizon 2020 research and innovation programme under grant agreement No 681559.

Open Access Article. Published on 28 August 2020. Downloaded on 7/26/2021 3:31:43 PM.
This article is licensed under a Creative Commons Attribution 3.0 Unported Licence.

Notes and references

1 J. A. Galbis, M. d. G. García-Martín, M. V. de Paz and E. Galbis, *Chem. Rev.*, 2016, **116**, 1600–1636.
2 D. J. Saxon, A. M. Luke, H. Sajjad, W. B. Tolman and T. M. Reineke, *Prog. Polym. Sci.*, 2020, **101**, 101196.
3 X. Li and A. F. Yee, *Macromolecules*, 2003, **36**, 9421–9429.
4 C.-W. Chen, C.-W. Lin, Y.-H. Chen, T.-F. Wei, S.-P. Rwei and R. Sasikumar, *Polym. Bull.*, 2020, **77**, 235–253.
5 N. Sánchez-Arrieta, A. M. de Ilarduya, A. Alla and S. Muñoz-Guerra, *Eur. Polym. J.*, 2005, **41**, 1493–1501.
6 X. Li and A. F. Yee, *Macromolecules*, 2004, **37**, 7231–7239.
7 J. Wang, X. Liu, Y. Zhang, F. Liu and J. Zhu, *Polymer*, 2016, **103**, 1–8.
8 F. Liu, J. Zhang, J. Wang, X. Liu, R. Zhang, G. Hu, H. Na and J. Zhu, *J. Mater. Chem. A*, 2015, **3**, 13637–13641.
9 A. Celli, P. Marchese, L. Sisti, D. Dumand, S. Sullalti and G. Totaro, *Polym. Int.*, 2013, **62**, 1210–1217.
10 S.-A. Park, J. Choi, S. Ju, J. Jegal, K. M. Lee, S. Y. Hwang, D. X. Oh and J. Park, *Polymer*, 2017, **116**, 153–159.
11 C. Lavilla and S. Muñoz-Guerra, *Green Chem.*, 2013, **15**, 144–151.
12 L. M. Lillie, W. B. Tolman and T. M. Reineke, *Polym. Chem.*, 2017, **8**, 3746–3754.
13 N. G. Moon, F. Mazzini, A. M. Pekkanen, E. M. Wilts and T. E. Long, *Macromol. Chem. Phys.*, 2018, **219**, 1800177.
14 D.-D. Xing, Y.-W. Jia, D.-F. Li, X.-L. Wang and Y.-Z. Wang, *ACS Sustainable Chem. Eng.*, 2017, **5**, 7040–7051.
15 J. Qi, J. Wu, J. Chen and H. Wang, *Polym. Degrad. Stab.*, 2019, **160**, 229–241.
16 J. C. Worch, H. Prydderch, S. Jimaja, P. Bexis, M. L. Becker and A. P. Dove, *Nat. Rev. Chem.*, 2019, **3**, 514–535.
17 R. J. Kieber, S. A. Silver and J. G. Kennemur, *Polym. Chem.*, 2017, **8**, 4822–4829.
18 A. B. Glazyrin, M. I. Abdullin, E. R. Atnabaeva, R. M. Sultanova, V. P. Volodina and V. A. Dokichev, *Polym. Bull.*, 2019, **76**, 3643–3657.
19 Á. Beltrán, B. P. Gómez-Emeterio, C. Marco, G. Ellis, M. D. Parellada, M. M. Díaz-Requejo, S. Corona-Galván and P. J. Pérez, *Macromolecules*, 2012, **45**, 9267–9274.
20 J. Urbano, B. Korthals, M. M. Díaz-Requejo, P. J. Pérez and S. Mecking, *J. Polym. Sci., Part A: Polym. Chem.*, 2010, **48**, 4439–4444.
21 R. Oda, T. Shono, A. Oku and H. Takao, *Makromol. Chem.*, 1963, **67**, 124–131.
22 L. L. McCoy, *J. Am. Chem. Soc.*, 1958, **80**, 6568–6572.
23 J. W. Chan, C. E. Hoyle, A. B. Lowe and M. Bowman, *Macromolecules*, 2010, **43**, 6381–6388.
24 J. Vandenbergh, K. Ranieri and T. Junkers, *Macromol. Chem. Phys.*, 2012, **213**, 2611–2617.
25 A. Frick and A. Rochman, *Polym. Test.*, 2004, **23**, 413–417.
26 H. Ebener, B. Pleuger and J. Petermann, *J. Appl. Polym. Sci.*, 1999, **71**, 813–817.
27 K. K. Childress, M. D. Alim, J. J. Hernandez, J. W. Stansbury and C. N. Bowman, *Polym. Chem.*, 2020, **11**, 39–46.
28 C. Wan, E. L. Heeley, Y. Zhou, S. Wang, C. T. Cafolla, E. M. Crabb and D. J. Hughes, *Soft Matter*, 2018, **14**, 9175–9184.
29 C. J. Stubbs, J. C. Worch, H. Prydderch, M. L. Becker and A. P. Dove, *Macromolecules*, 2020, **53**, 174–181.
30 Y. Yu, Z. Wei, X. Leng and Y. Li, *Polym. Chem.*, 2018, **9**, 5426–5441.
31 C. A. Bell, J. Yu, I. A. Barker, V. X. Truong, Z. Cao, A. V. Dobrinyin, M. L. Becker and A. P. Dove, *Angew. Chem., Int. Ed.*, 2016, **55**, 13076–13080.
32 R. Csuk and Y. von Scholz, *Tetrahedron*, 1994, **50**, 10431–10442.
33 W. S. McDonald, C. A. Verbicky and C. K. Zercher, *J. Org. Chem.*, 1997, **62**, 1215–1222.

This journal is © The Royal Society of Chemistry 2020

3.2 Supporting Information

Electronic Supplementary Material (ESI) for Polymer Chemistry.
This journal is © The Royal Society of Chemistry 2020

Understanding Structure-property relationships of main chain cyclopropanes in linear polyesters

Connor J. Stubbs[§], *Andrew P. Dove*[§*]

[§]School of Chemistry, University of Birmingham, Edgbaston, Birmingham, B15 2TT, UK

Contents of PDF

Synthetic scheme for cyclopropane diacrylate preparation 2
NMR Spectra of monomers and precursors.....3-7
NMR Spectra of Homopolymers 8-12
NMR Spectra of Copolymers 13-15
SEC Chromatograms of Homopolymers 16
SEC Chromatograms of Copolymer 17
DSC Thermograms of Homopolymers 18
DSC Thermograms of Copolymers.....19
Stress *vs* Strain Tensile Curves 20
Thermogravimetric analysis.....21
Summary of Data Table 22

Synthetic scheme for cyclopropane diacrylate preparation

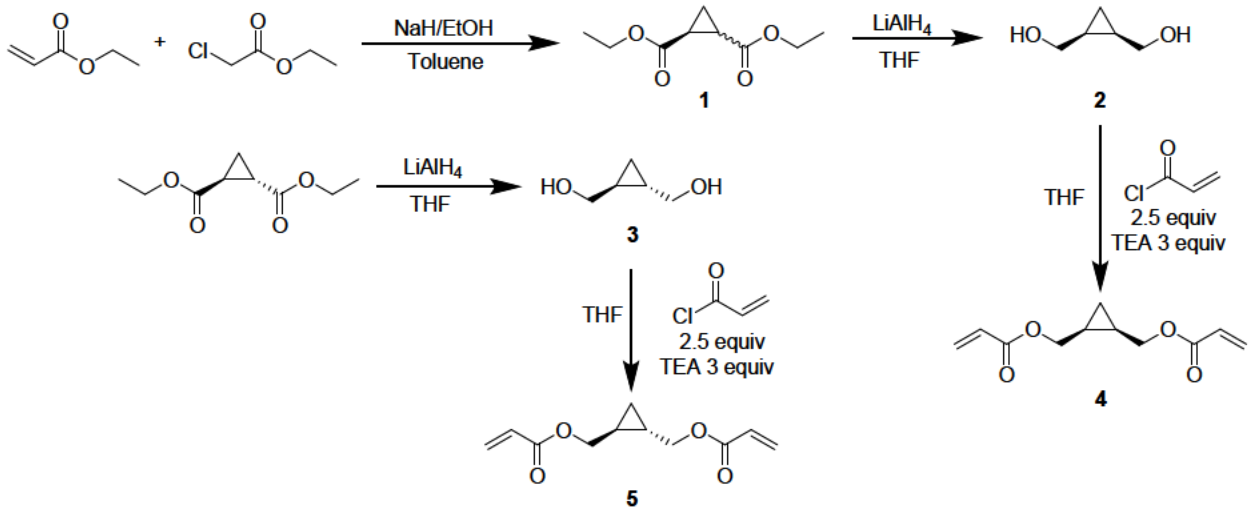


Figure S1 Synthetic scheme for the preparation of cyclopropane diacrylate monomers

NMR spectra of monomers and precursors

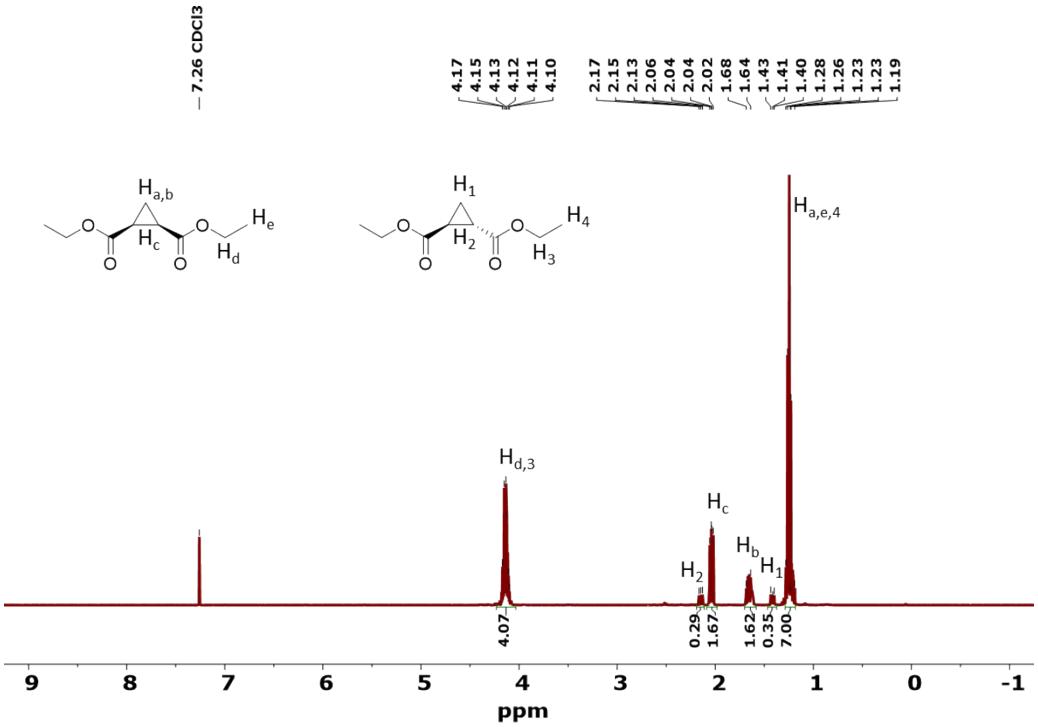


Figure S2 ^{1}H NMR spectrum of racemic diethyl-1,2-cyclopropane dicarboxylate in $CDCl_3$ (400 MHz, 298 K) **(1)**

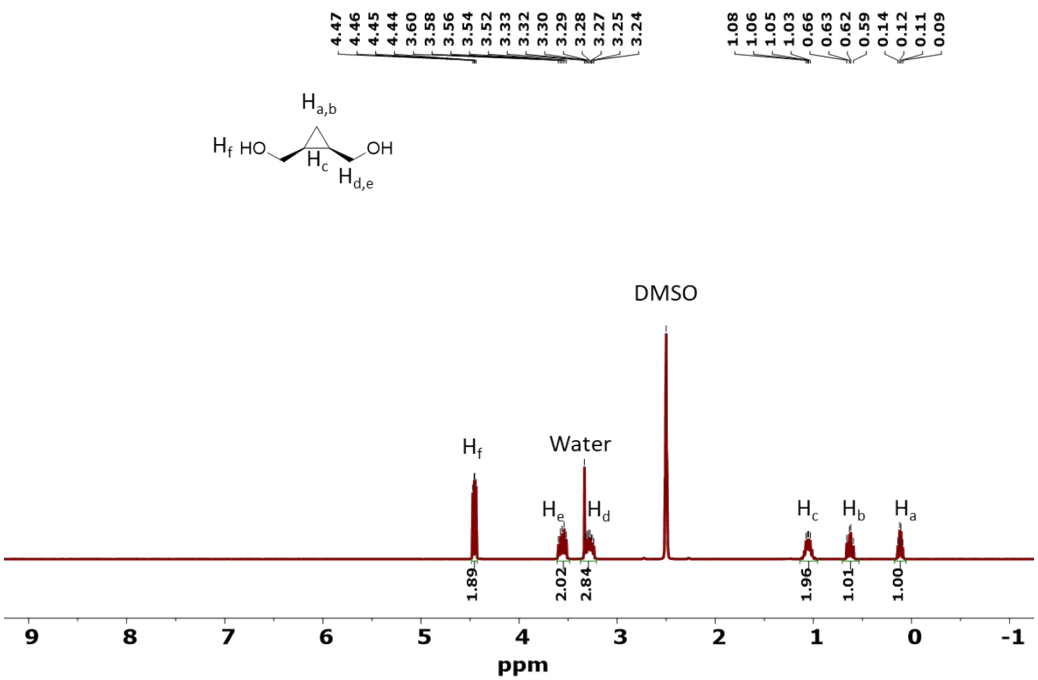


Figure S3 [1]H NMR spectrum of *cis*-1,2-cyclopropanedimethanol **(2)** in DMSO-d6 (400 MHz, 298 K)

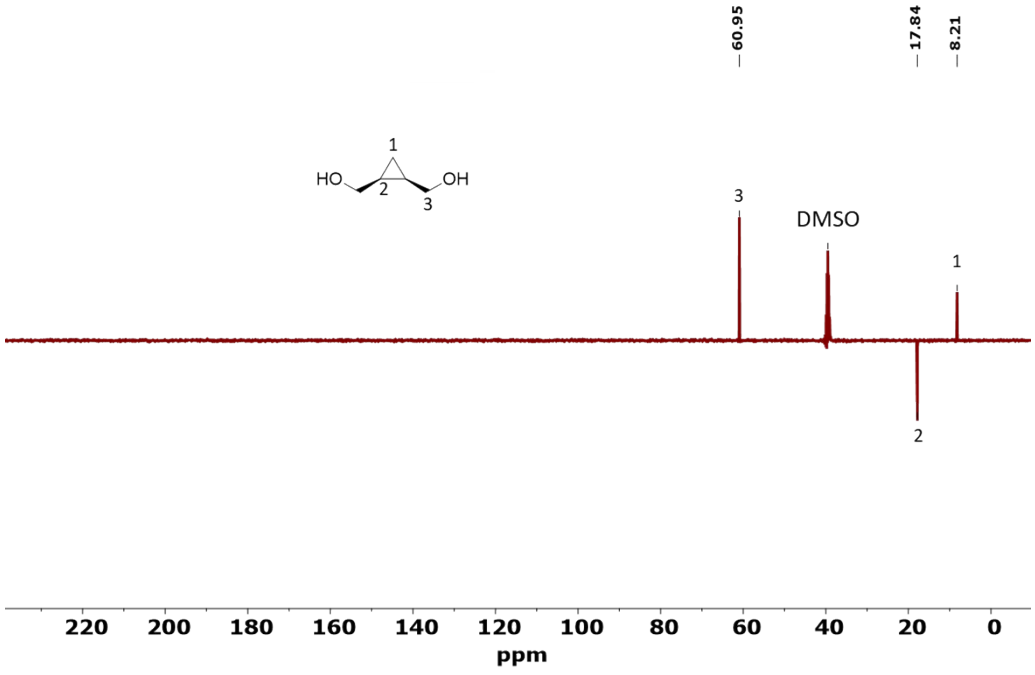


Figure S4 [13]C NMR spectrum of *cis*-1,2-cyclopropanedimethanol **(2)** in DMSO-d6 (400 MHz, 298 K)

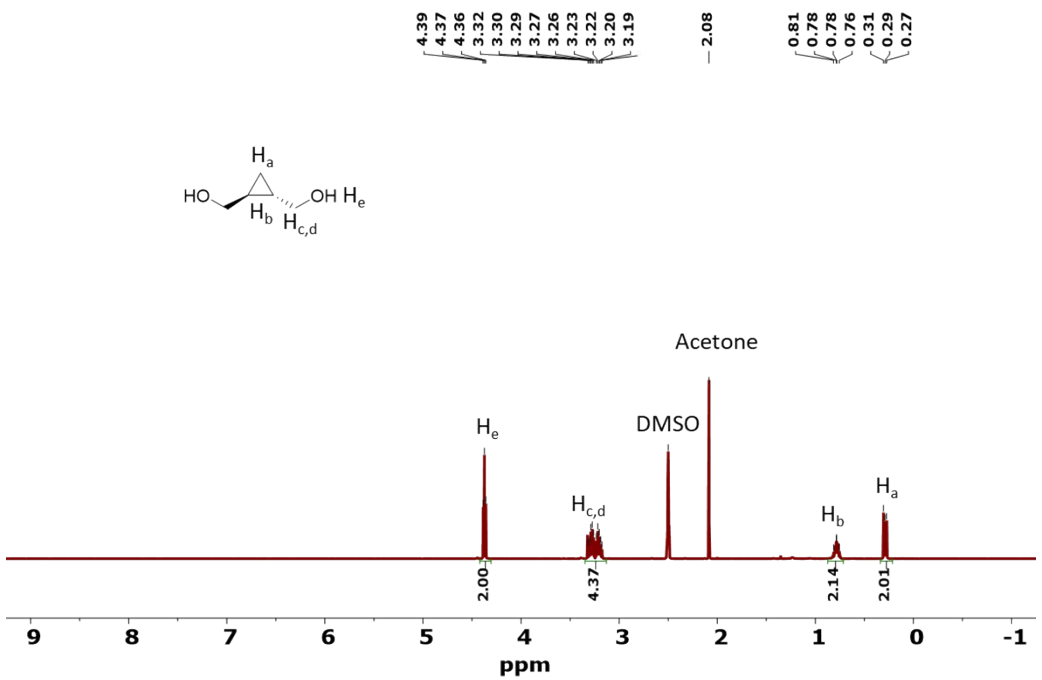


Figure S5 [1]H NMR spectrum of *trans*-1,2-cyclopropanedimethanol **(3)** in DMSO-d6 (400 MHz, 298 K)

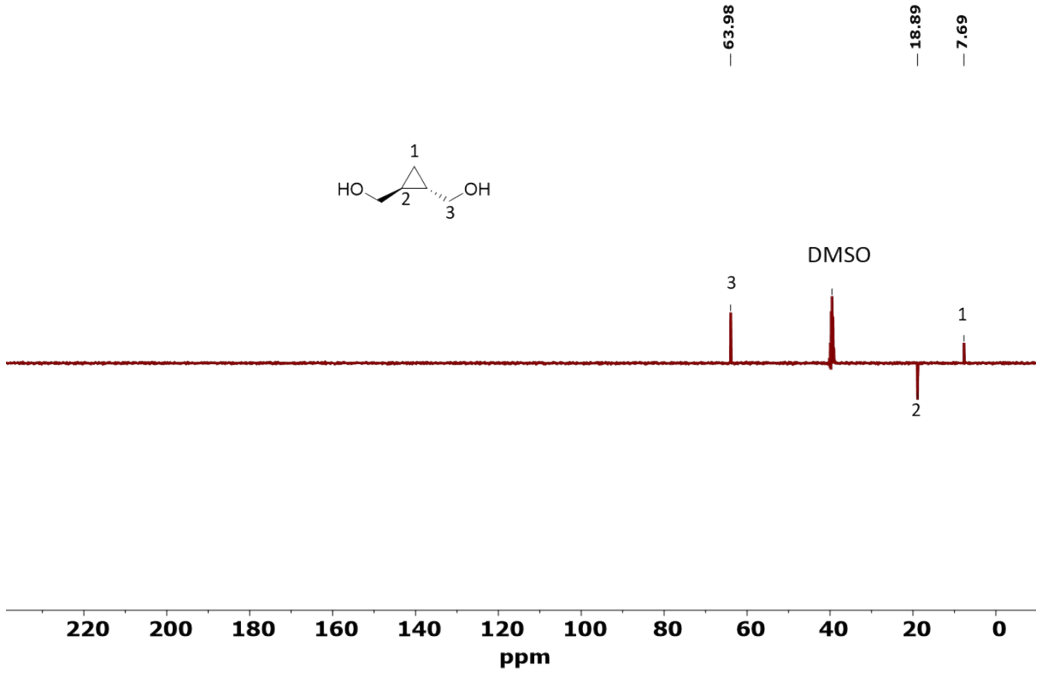


Figure S6 [13]C NMR spectrum of *trans*-1,2-cyclopropanedimethanol **(3)** in DMSO-d6 (400 MHz, 298 K)

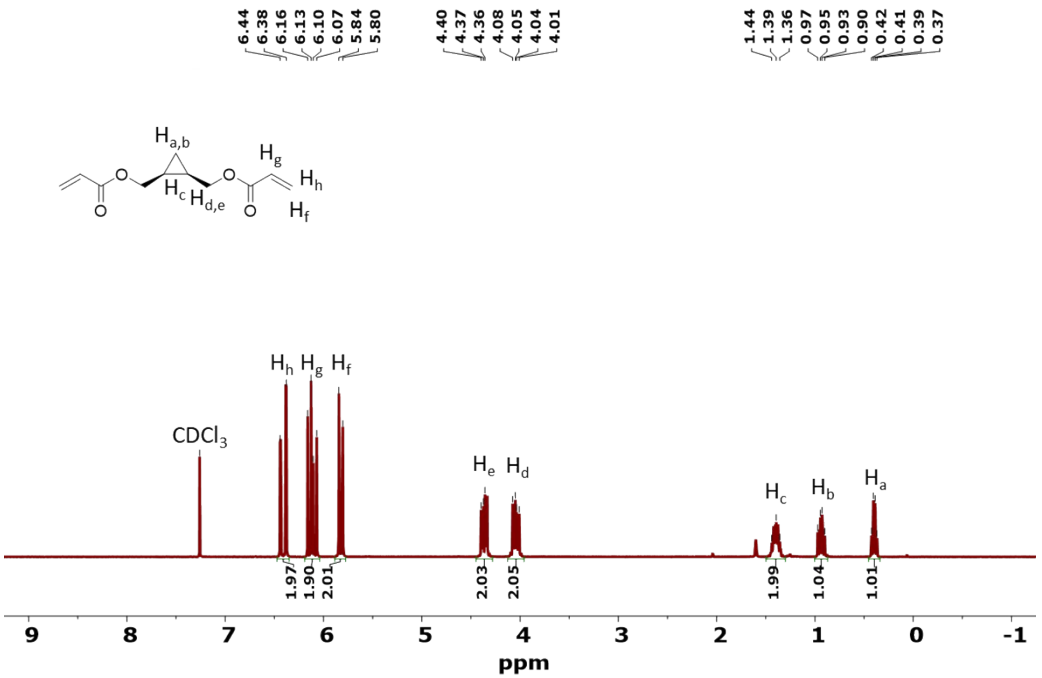


Figure S7 ^{1}H NMR spectrum of *cis* Cy-diacrylate monomer **(4)** in $CDCl_3$ (400 MHz, 298 K)

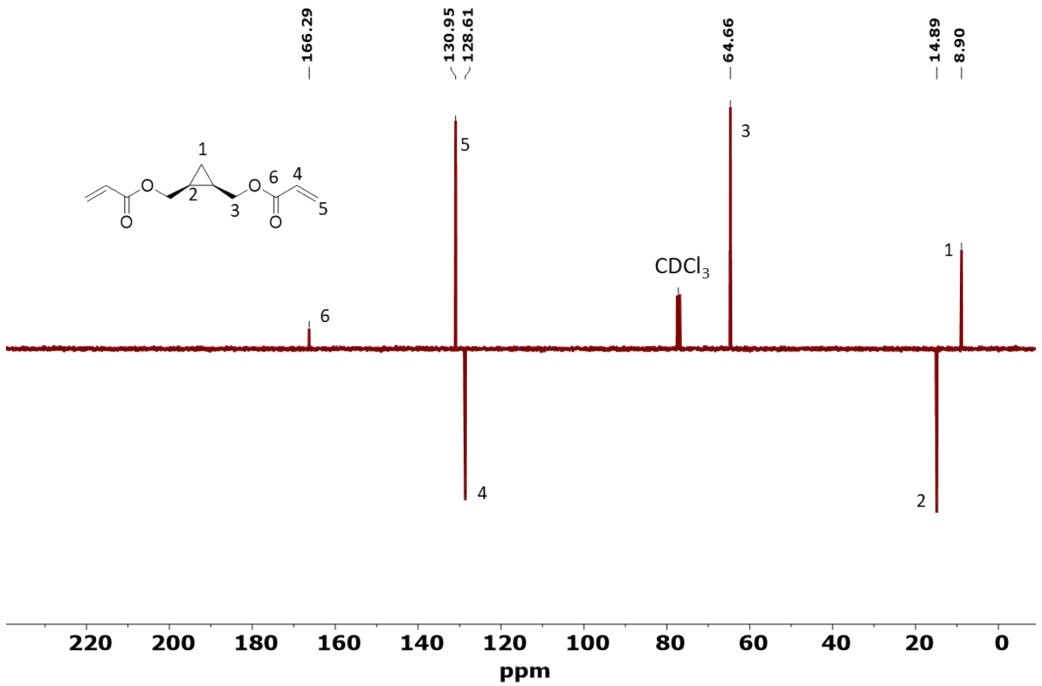


Figure S8 ^{13}C NMR spectrum of *cis* Cy-diacrylate monomer **(4)** in $CDCl_3$ (400 MHz, 298 K)

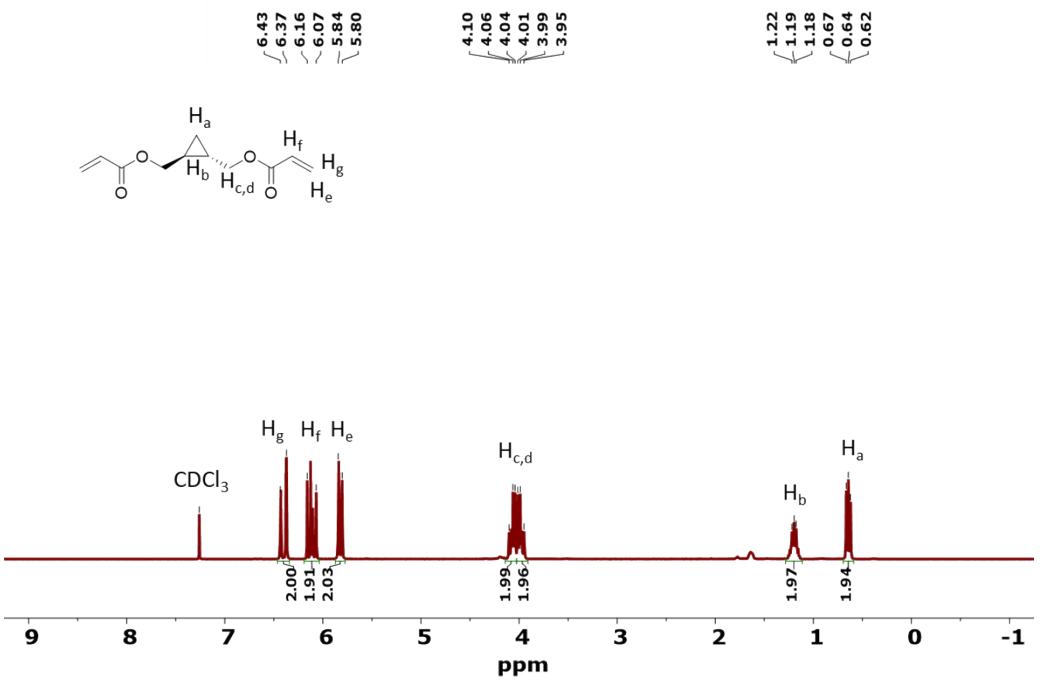


Figure S9 ^{1}H NMR spectrum of *trans* Cy-diacrylate monomer **(5)** in $CDCl_3$ (400 MHz, 298 K)

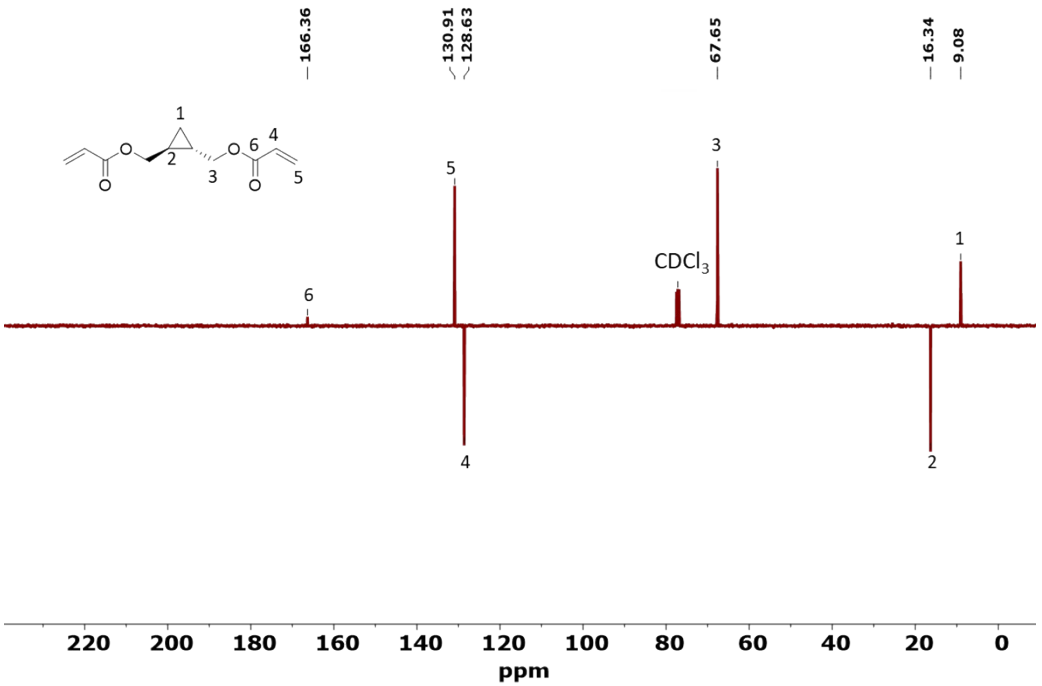


Figure S10 ^{13}C NMR spectrum of *trans* Cy-diacrylate monomer **(5)** in $CDCl_3$ (400 MHz, 298 K)

NMR spectra of Homopolymers

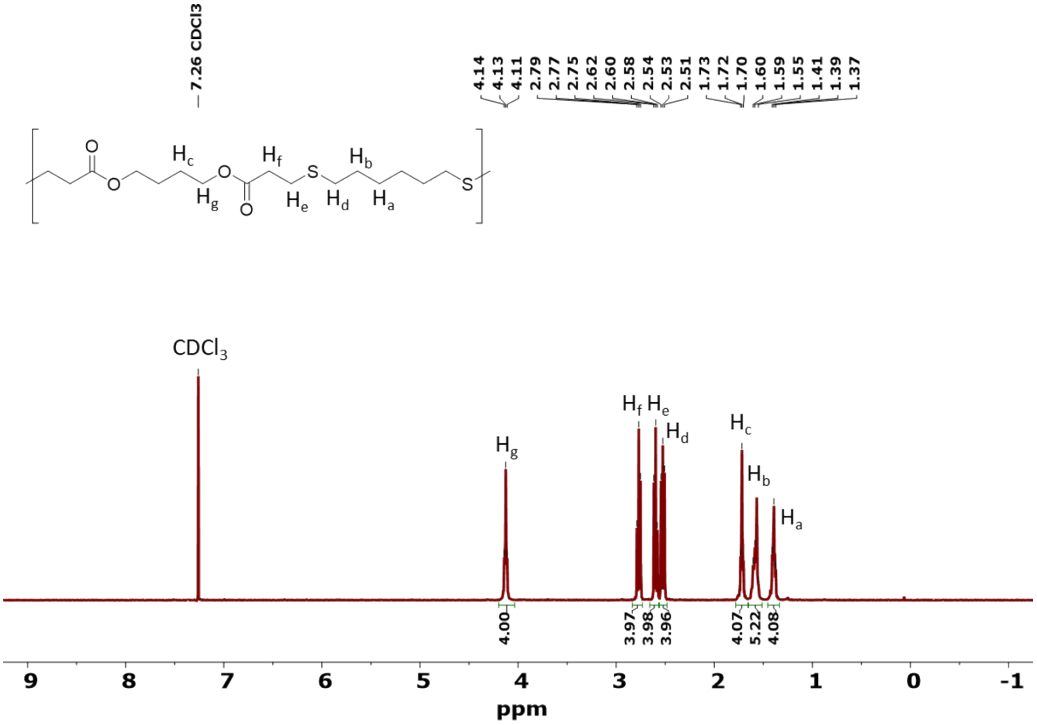


Figure S11 ^{1}H NMR spectrum of **BD-*co*-HDT** in $CDCl_3$ (400 MHz, 298 K)

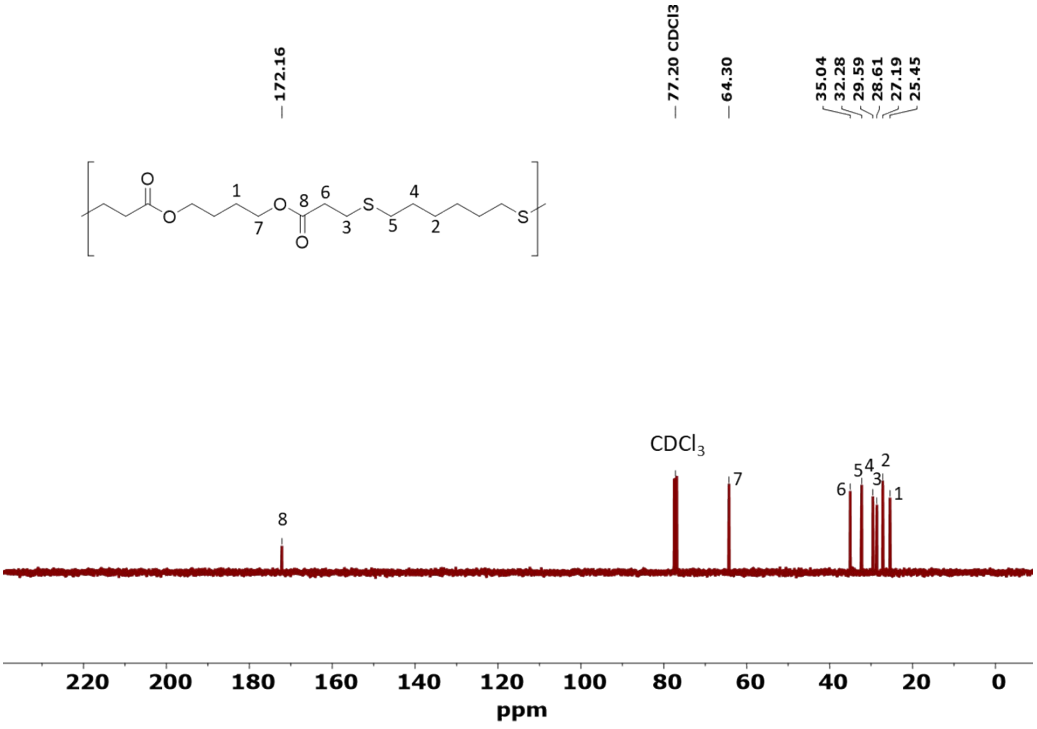


Figure S12 ^{13}C NMR spectrum of **BD-*co*-HDT** in $CDCl_3$ (400 MHz, 298 K)

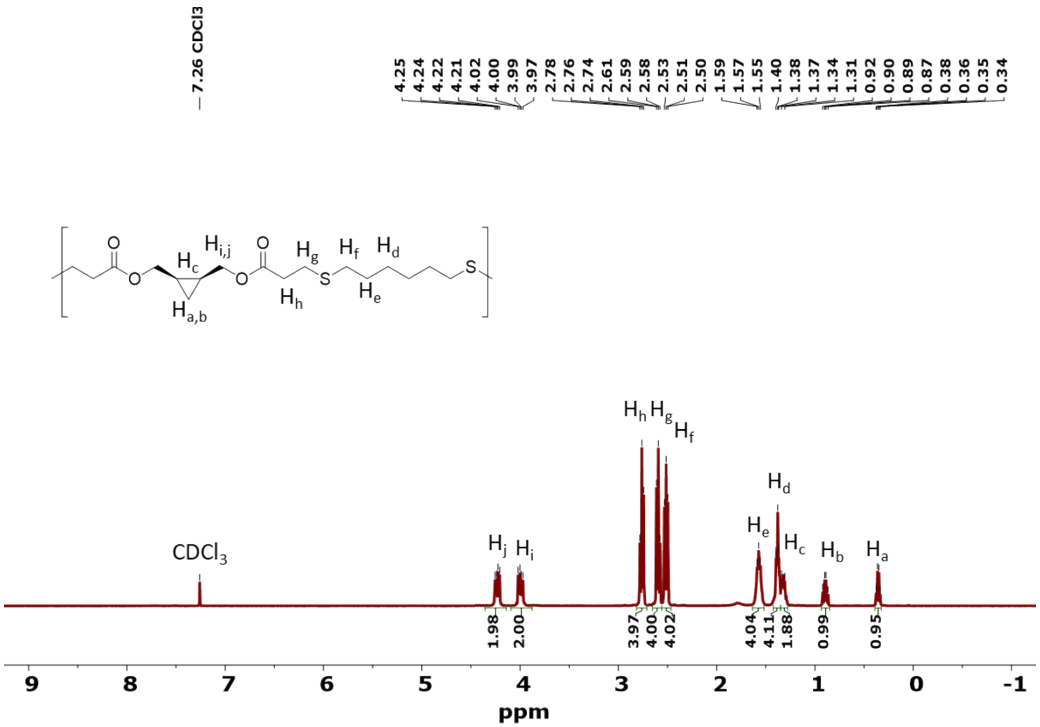


Figure S13 ^{1}H NMR spectrum of **Cy**(*cis*)-*co*-**HDT** in $CDCl_3$ (400 MHz, 298 K)

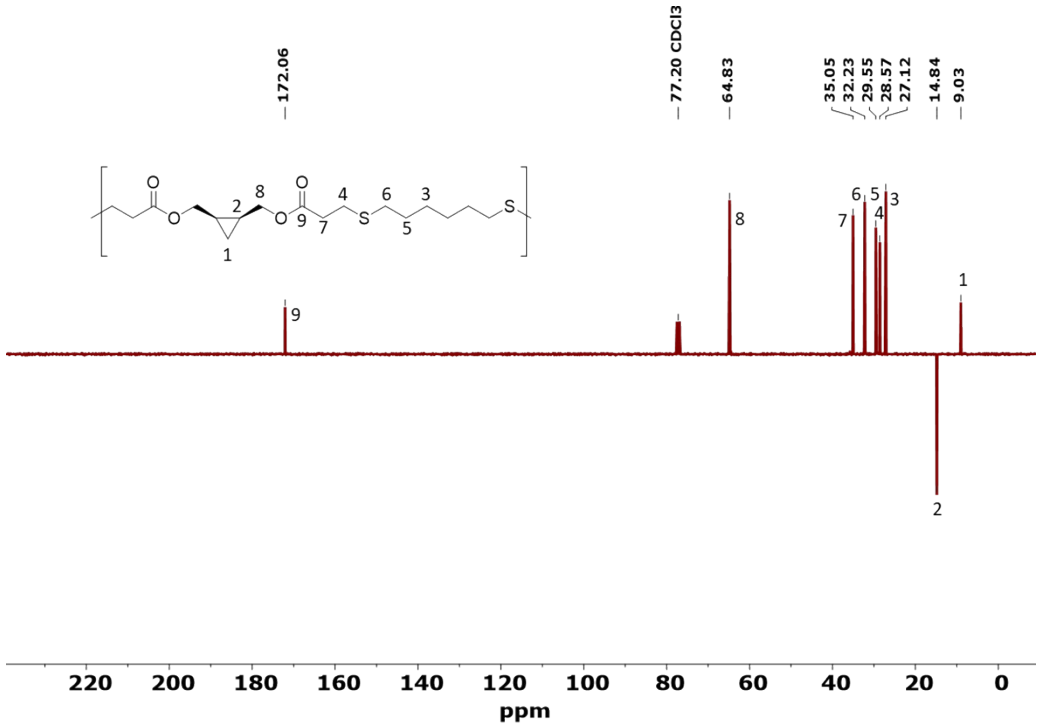


Figure S14 ^{13}C NMR spectrum of **Cy**(*cis*)-*co*-**HDT** in $CDCl_3$ (400 MHz, 298 K)

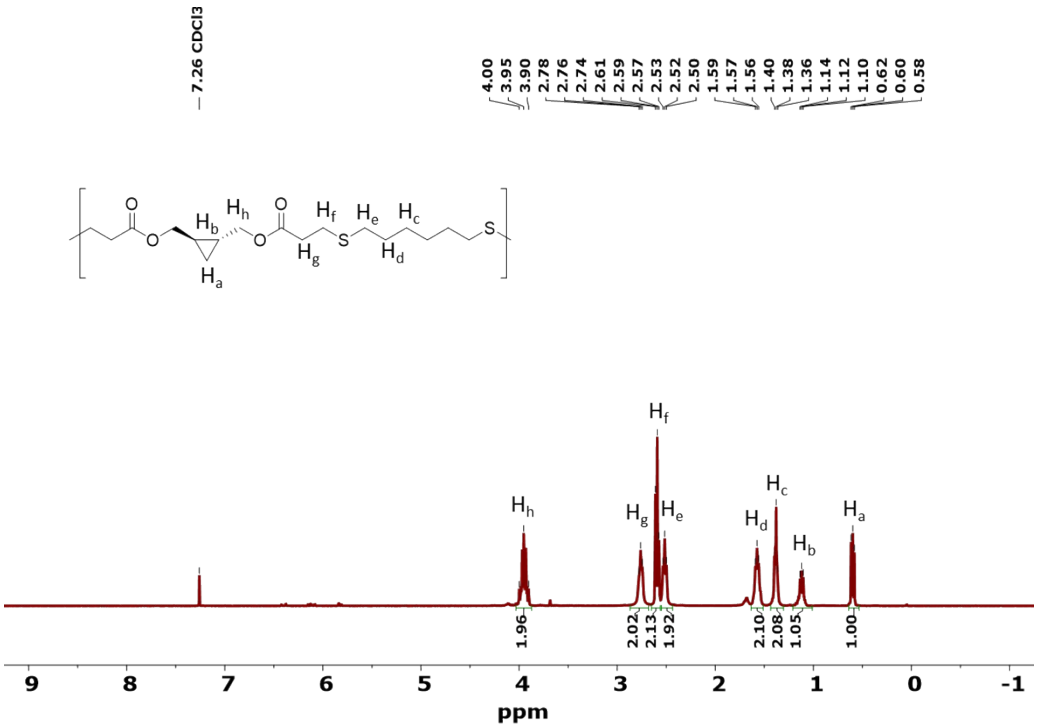


Figure S15 ^{1}H NMR spectrum of **Cy**(*trans*)-*co*-**HDT** in $CDCl_3$ (400 MHz, 298 K)

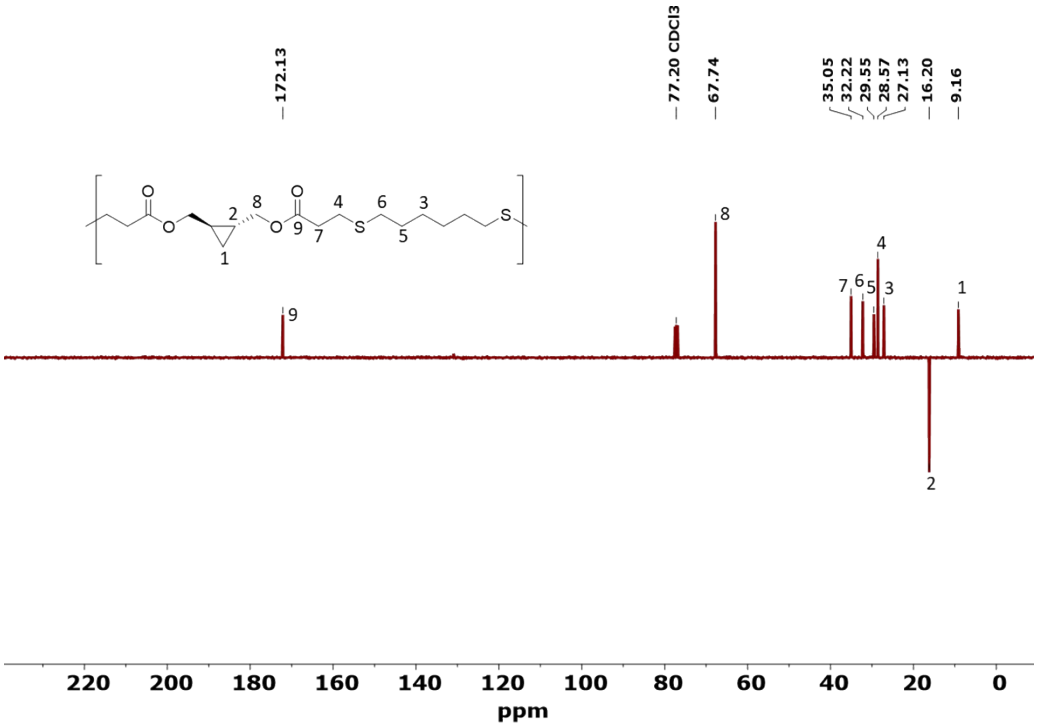


Figure S16 ^{13}C NMR spectrum of **Cy**(*trans*)-*co*-**HDT** in $CDCl_3$ (400 MHz, 298 K)

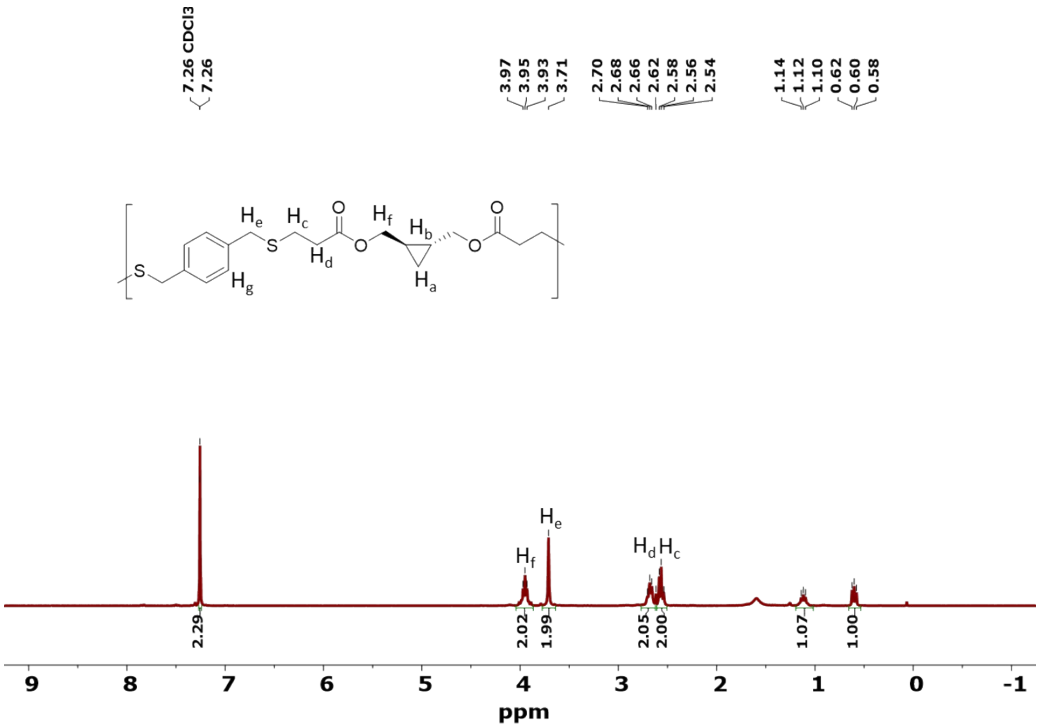


Figure S17 ^{1}H NMR spectrum of **Cy**(*trans*)-*co*-**BDT** in $CDCl_3$ (400 MHz, 298 K)

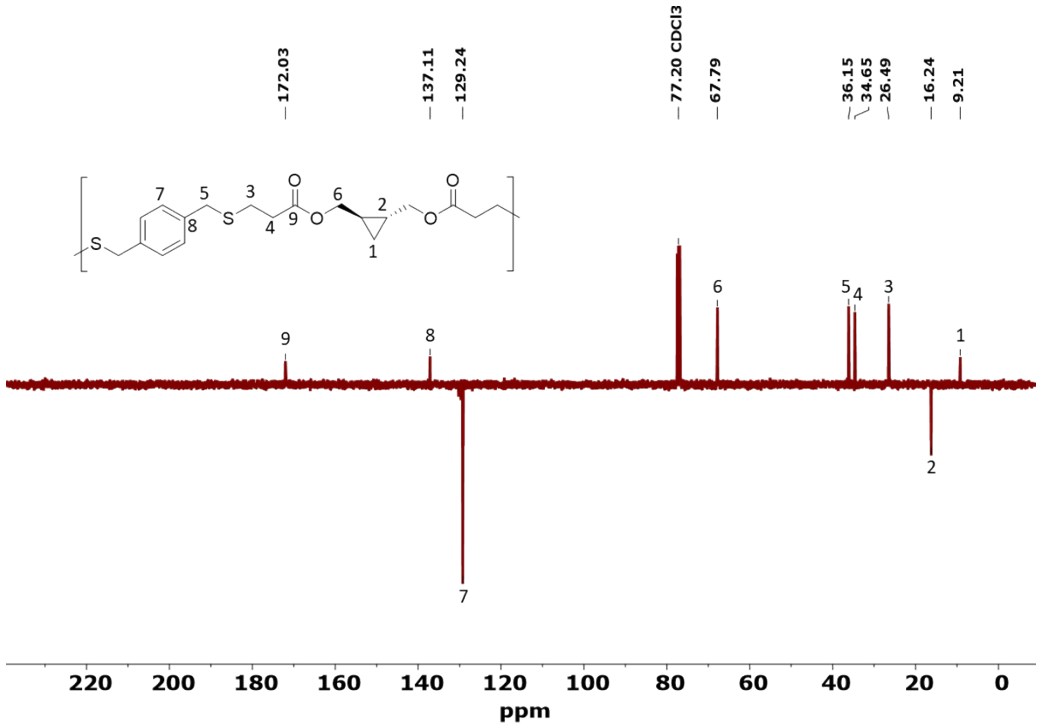


Figure S18 ^{13}C NMR spectrum of **Cy**(*trans*)-*co*-**BDT** in $CDCl_3$ (400 MHz, 298 K)

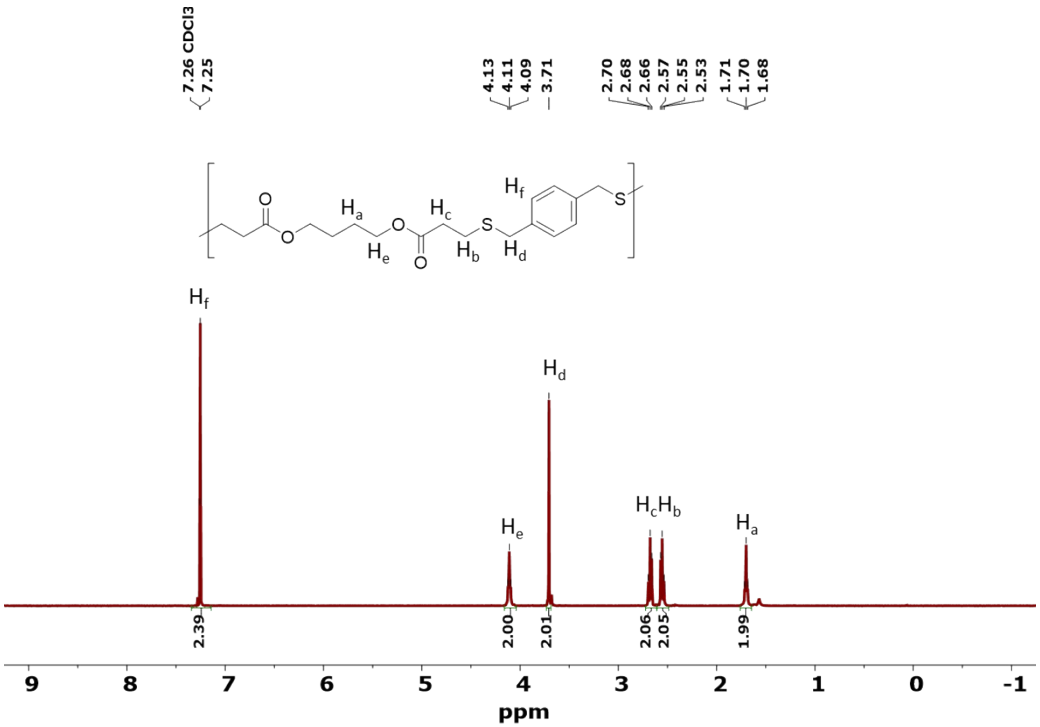


Figure S19 ^{1}H NMR spectrum of **BD-*co*-BDT** in $CDCl_3$ (400 MHz, 298 K)

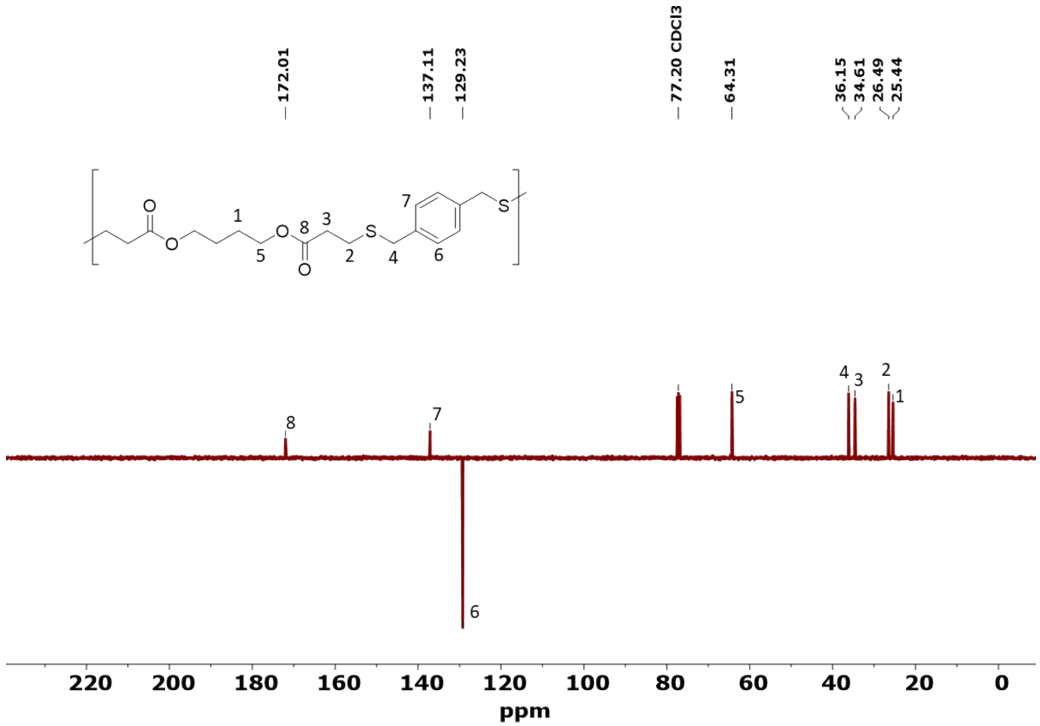


Figure S20 ^{13}C NMR spectrum of **BD-*co*-BDT** in $CDCl_3$ (400 MHz, 298 K)

NMR spectra of copolymers

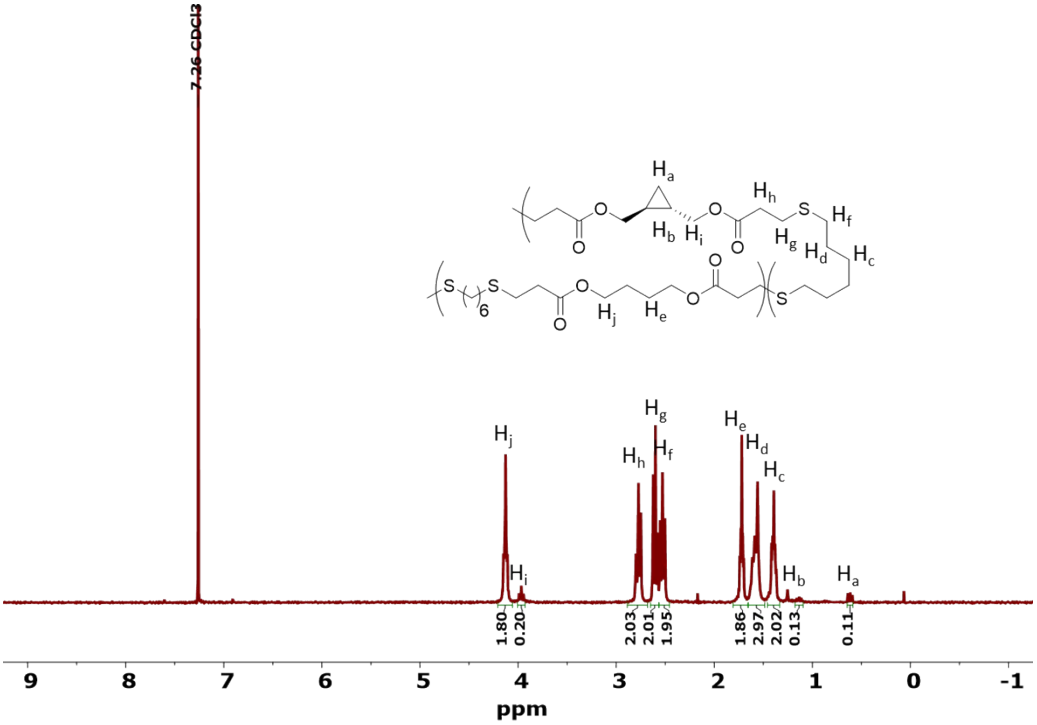


Figure S21 ^{1}H NMR spectrum of **BD$_{90}$Cy(*trans*)$_{10}$-*co*-HDT** in $CDCl_3$ (400 MHz, 298 K)

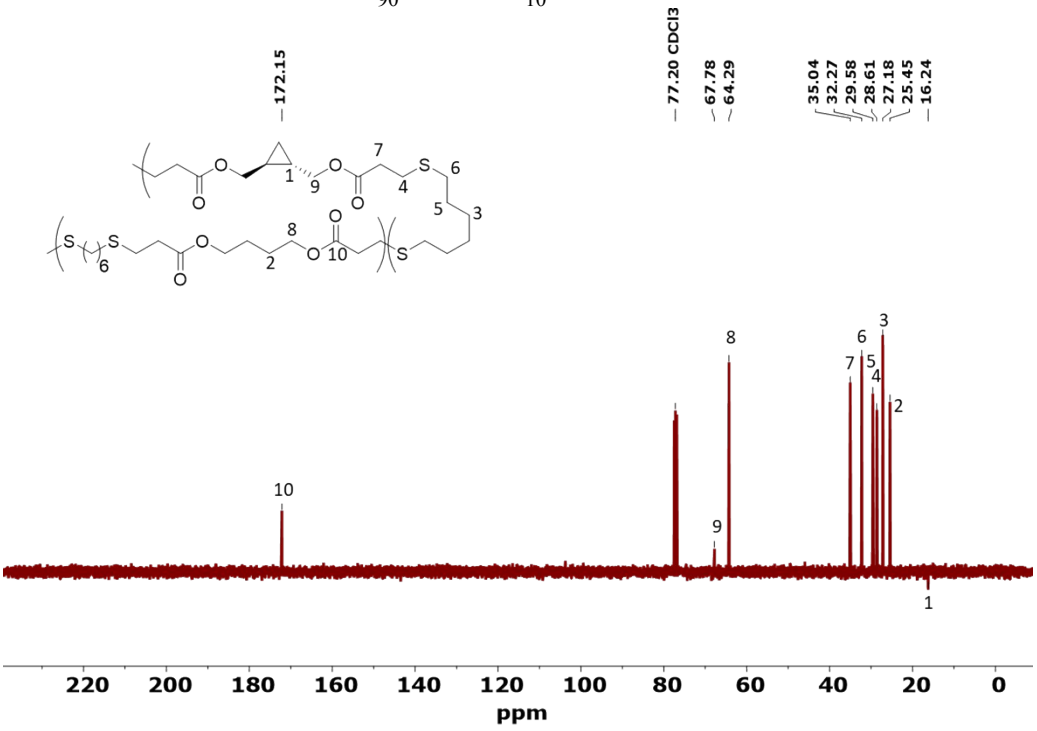


Figure S22 ^{13}C NMR spectrum of **BD$_{90}$Cy(*trans*)$_{10}$-*co*-HDT** in $CDCl_3$ (400 MHz, 298 K)

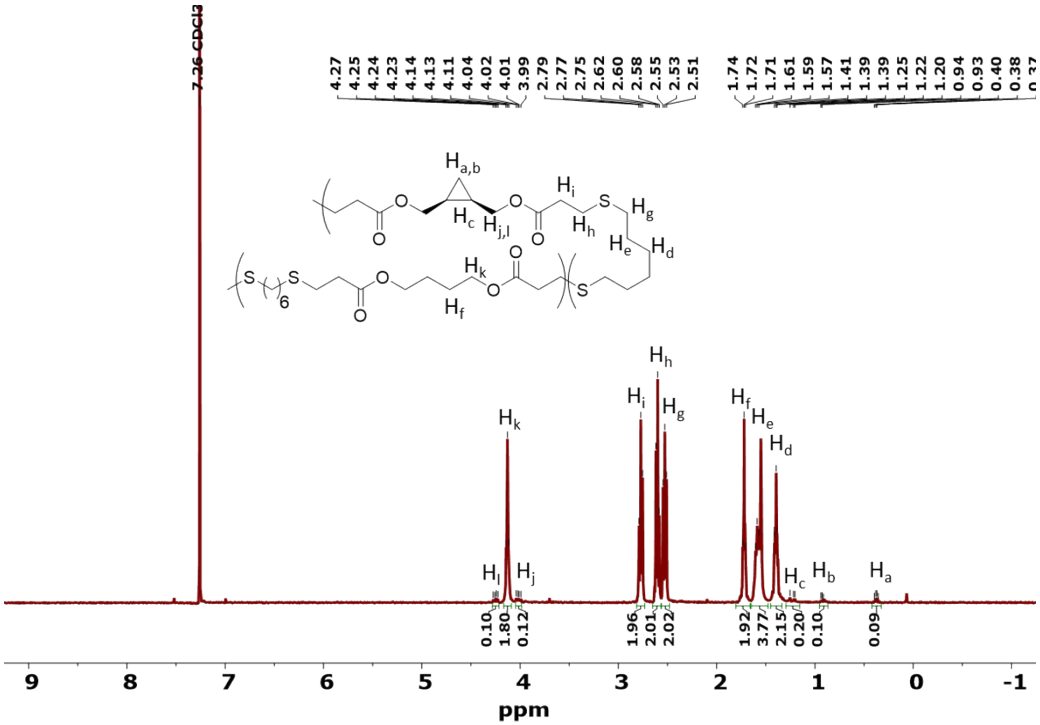


Figure S23 ^{1}H NMR spectrum of **BD$_{90}$Cy(*cis*)$_{10}$-*co*-HDT** in $CDCl_3$ (400 MHz, 298 K)

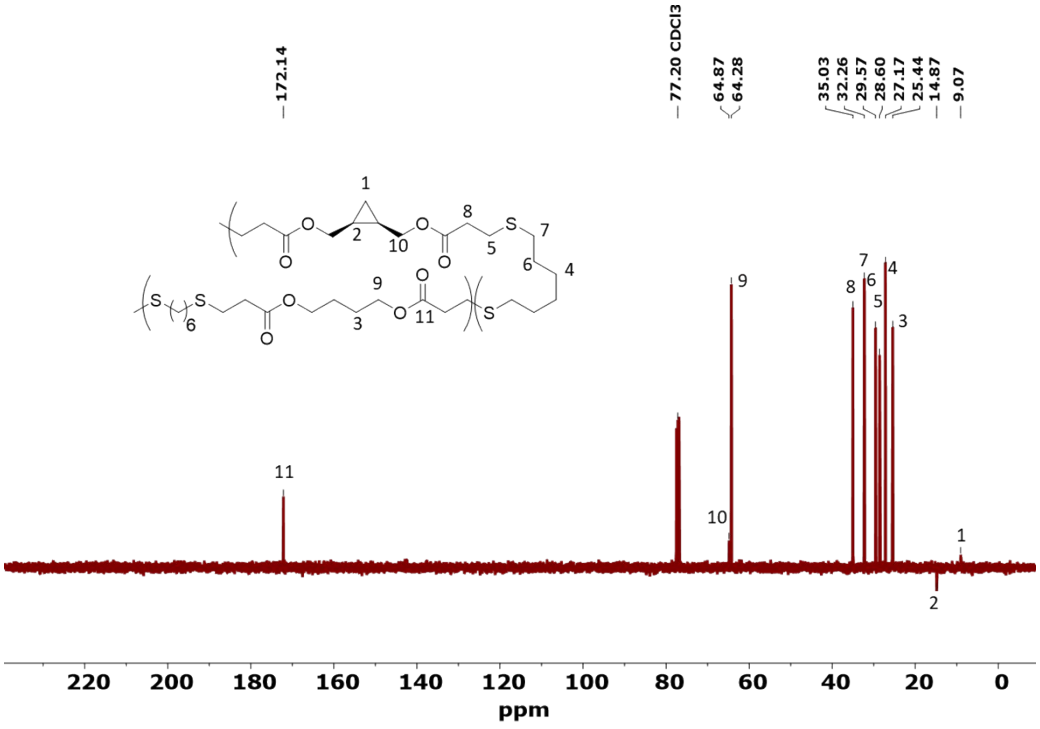


Figure S24 ^{13}C NMR spectrum of **BD$_{90}$Cy(*cis*)$_{10}$-*co*-HDT** in $CDCl_3$ (400 MHz, 298 K)

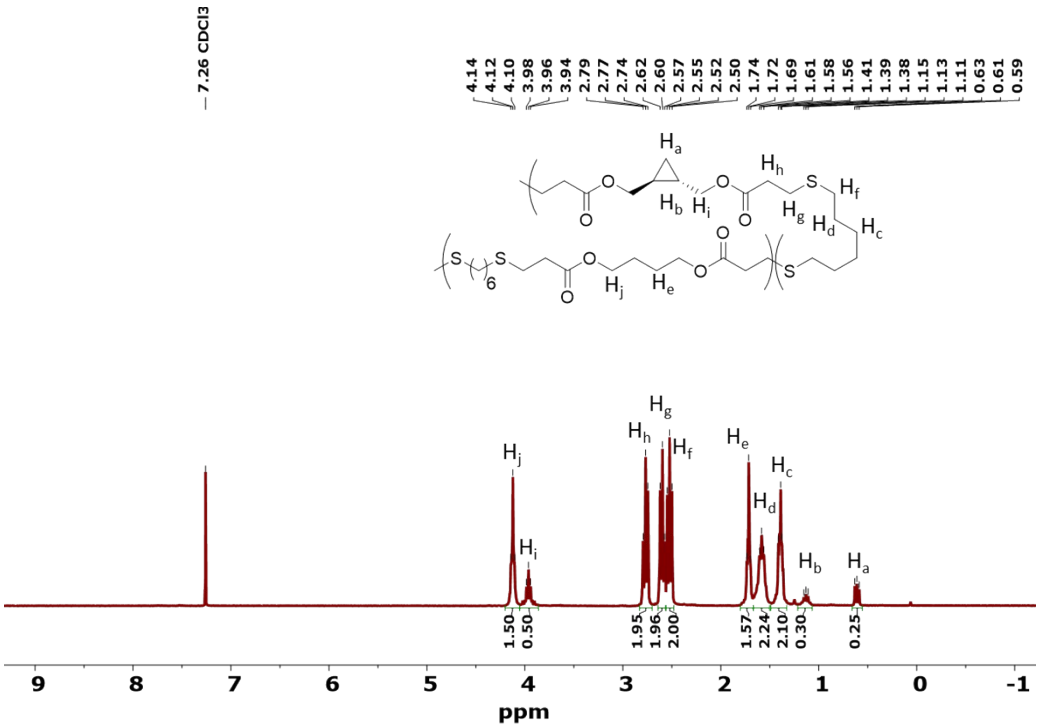


Figure S25 ^{1}H NMR spectrum of **BD**$_{75}$**Cy**(*trans*)$_{25}$-*co*-**HDT** in $CDCl_3$ (400 MHz, 298 K)

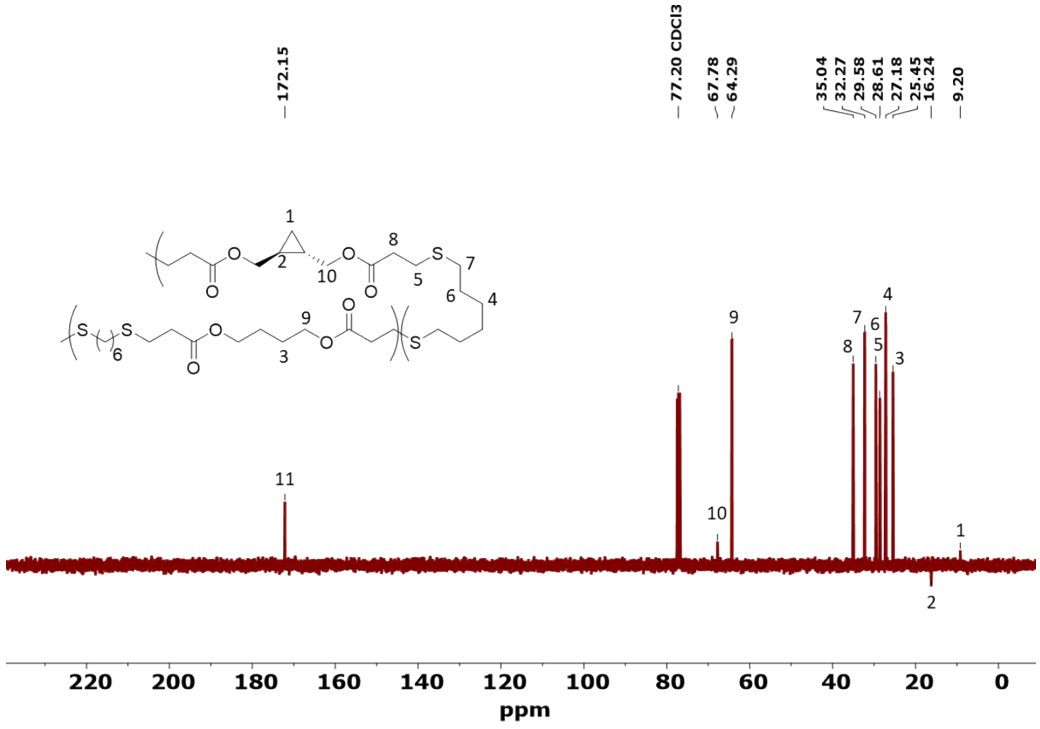


Figure S26 ^{13}C NMR spectrum of **BD**$_{75}$**Cy**(*trans*)$_{25}$-*co*-**HDT** in $CDCl_3$ (400 MHz, 298 K)

SEC chromatograms of Homopolymers

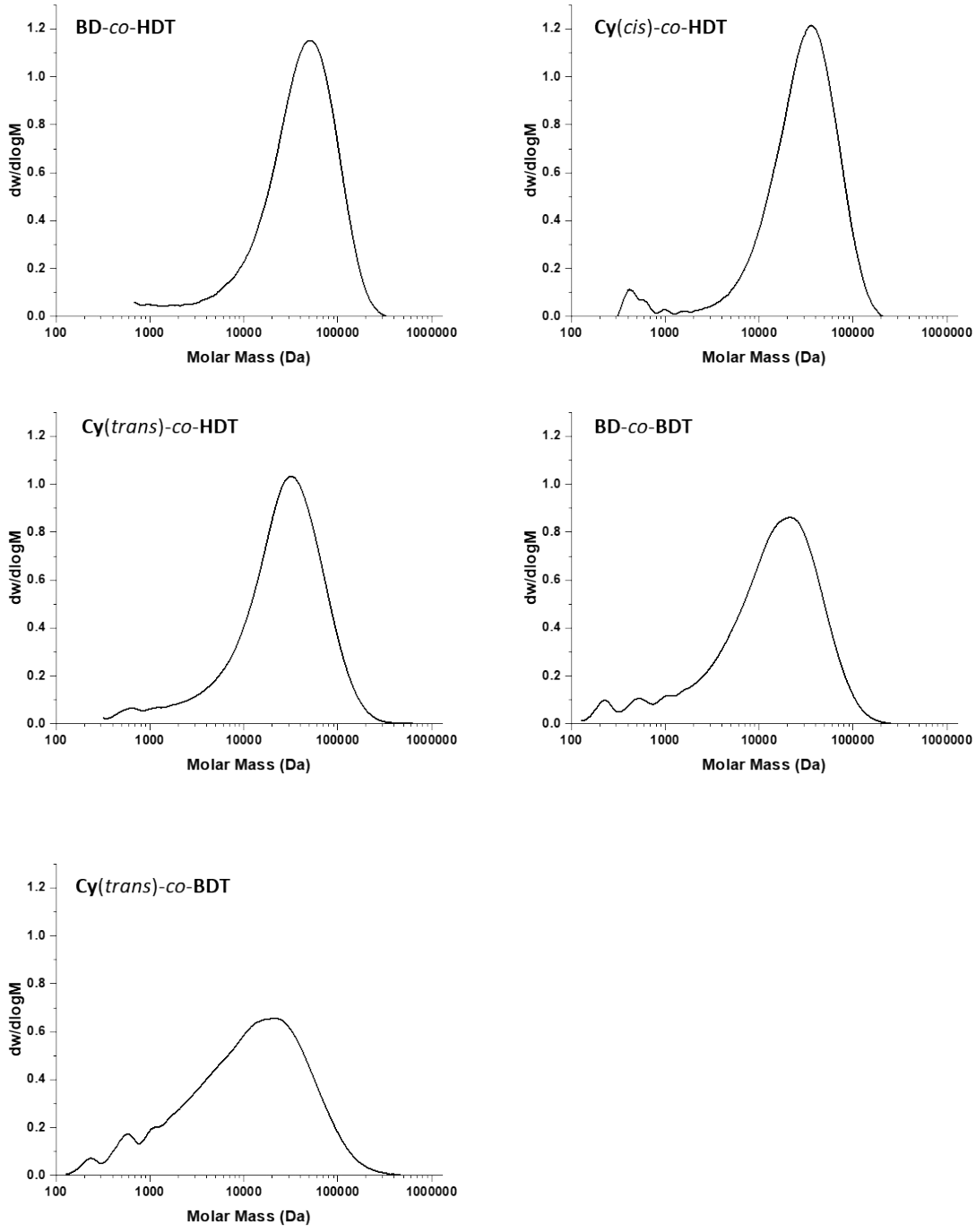


Figure S27 SEC chromatograms of homopolymers calculated against polystyrene standards in THF + 2% v/v NEt_3.

SEC chromatograms of Copolymers

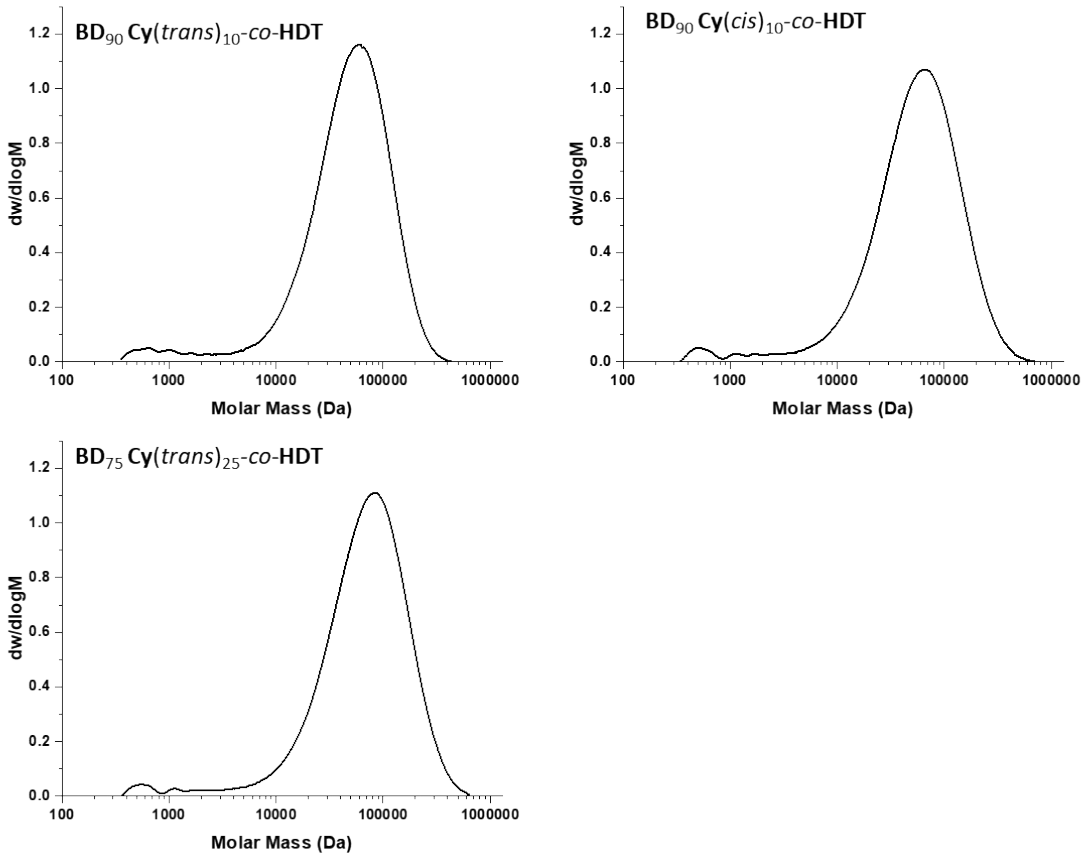


Figure S28 SEC chromatograms of Copolymers calculated against polystyrene standards in THF + 2% v/v NEt_3.

DSC thermograms of Homopolymers

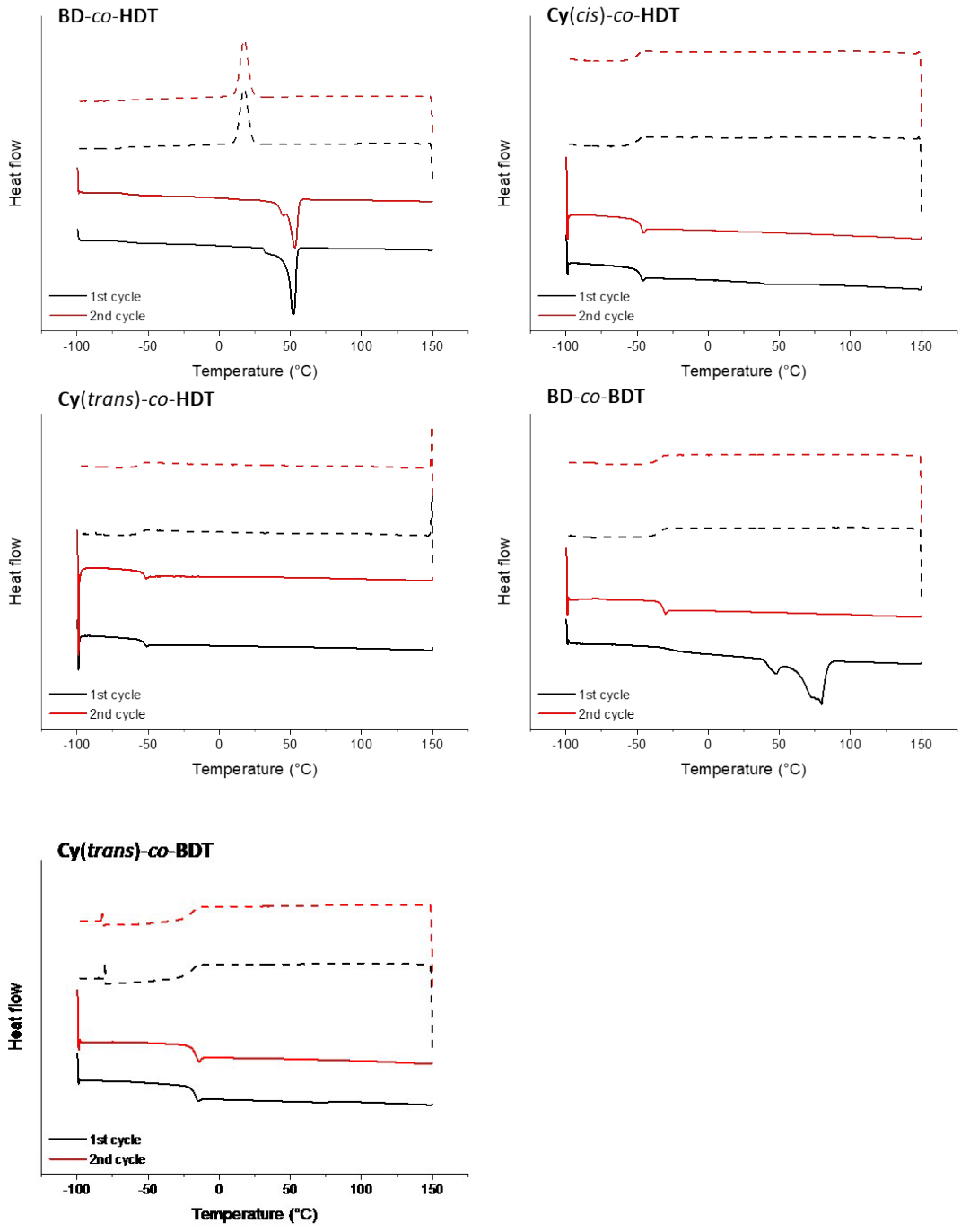


Figure S29 DSC thermograms of Homopolymers 10 K·min^{-1} heating and cooling rate.

DSC thermograms of Copolymers

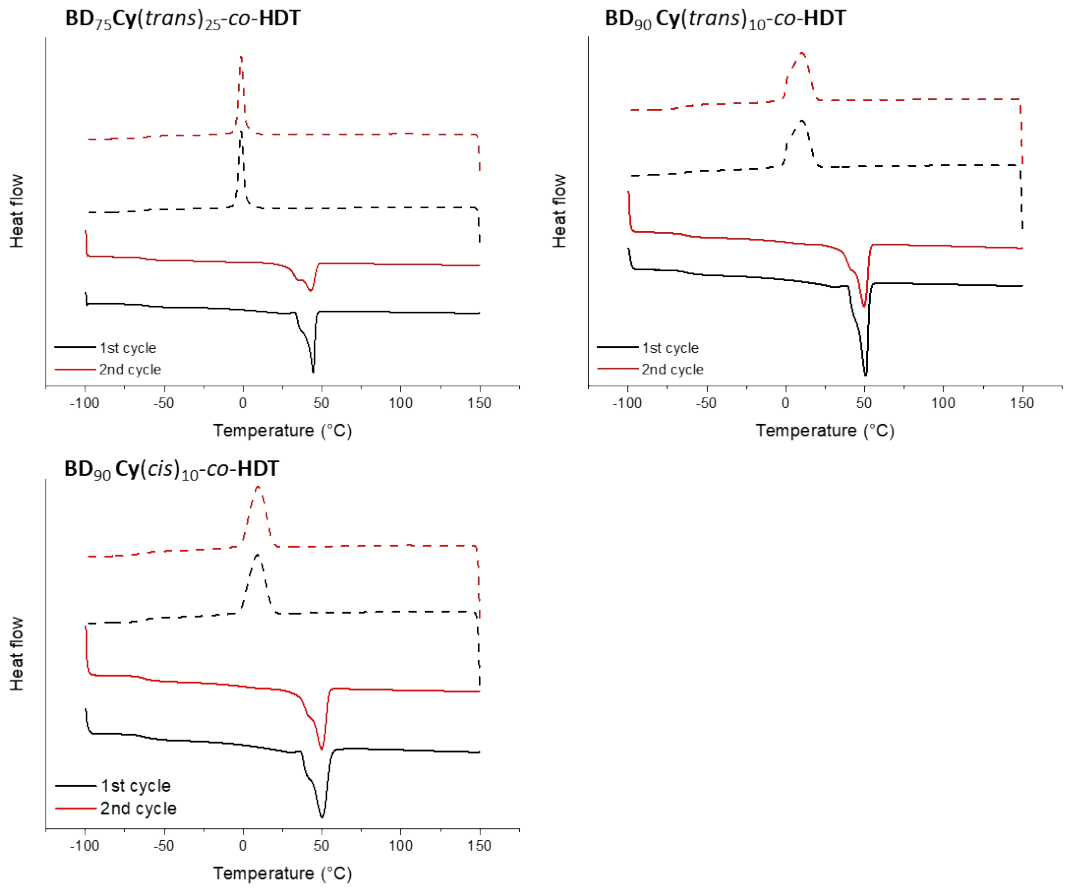


Figure S30 DSC thermograms of Copolymers 10 K·min^{-1} heating and cooling rate

Tensile stress *vs* strain Curves

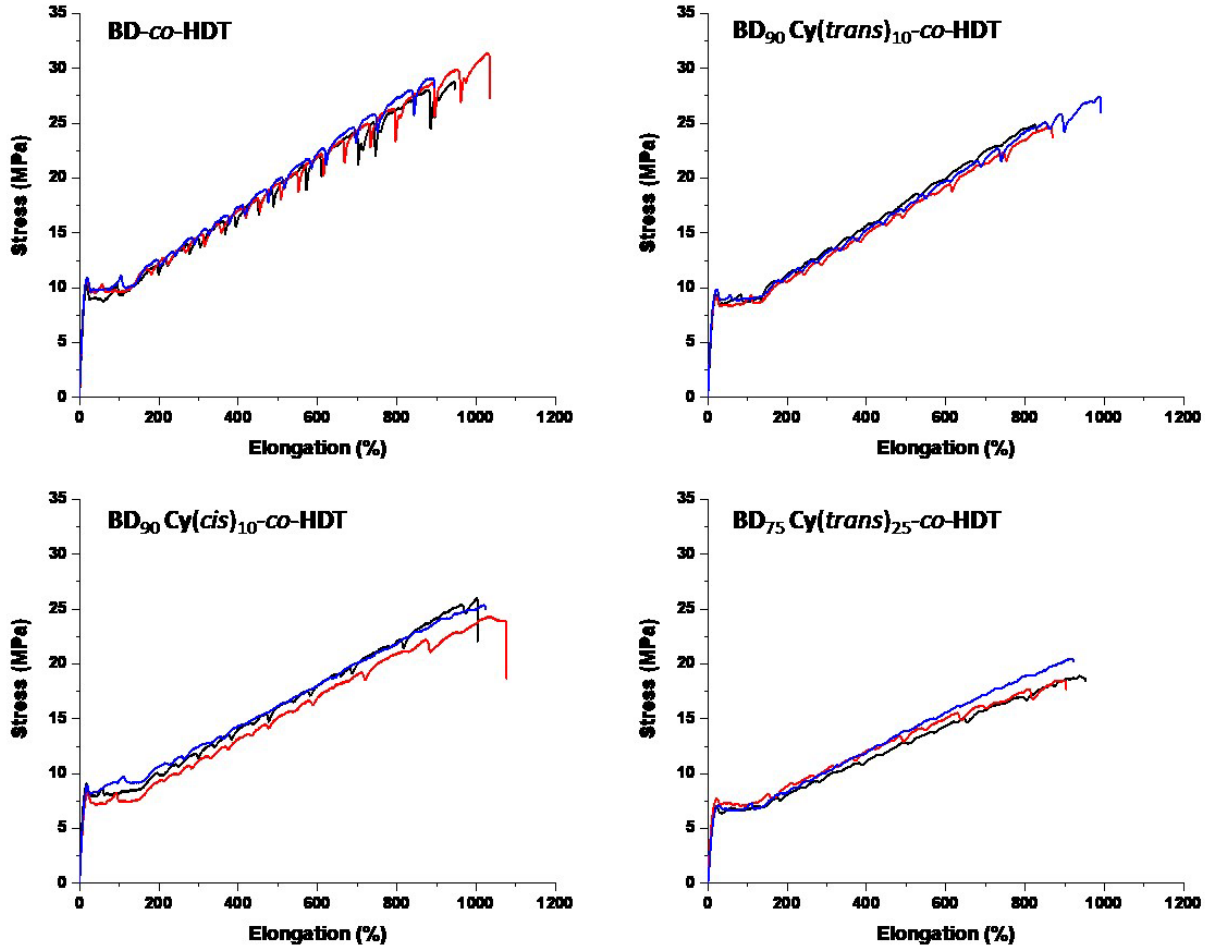


Figure S31 Stress *vs* strain tensile curves of 2 day annealed polyester films

Thermogravimetric analysis (TGA)

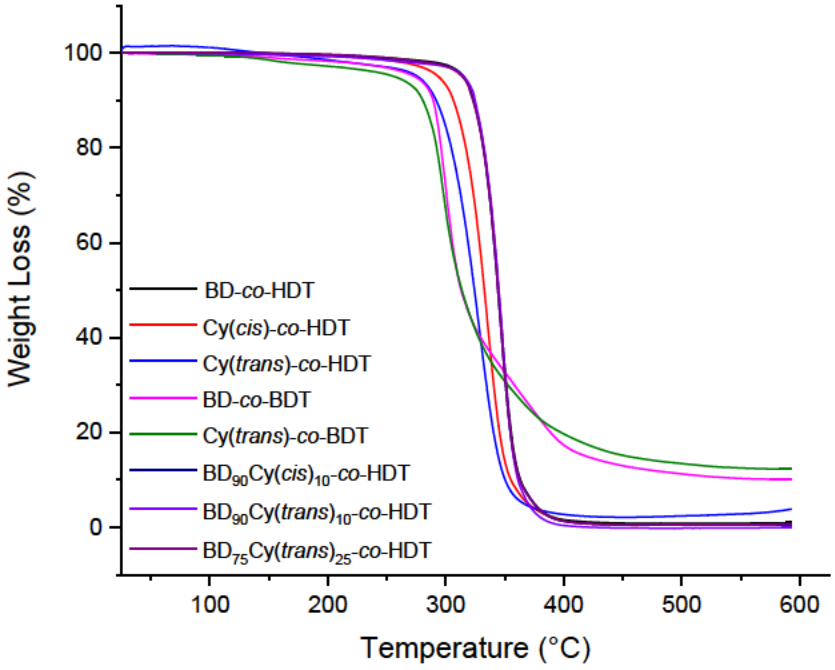


Figure S32 Thermogravimetric analysis of polymers at a 10 $K \cdot min^{-1}$

Sample	M_w (kDa)	$Đ$	T_g (°C)	T_m (°C)	T_c (°C)	ΔH_m (J g^{-1})	E (MPa)ǂ	UTS (MPa)ǂ	ε_b (%)ǂ	U_T (MJm^{-3})ǂ
BD-*co*-HDT	52.7	3.13	-66	52	17	-64.0	105±13	30±2	952±72	180±20
Cy(*cis*)-*co*-HDT	37.4	4.08	-47	-	-	-	-	-	-	-
Cy(*trans*)-*co*-HDT	38.0	4.30	-52	-	-	-	-	-	-	-
BD-*co*-BDT	22.0	7.78	-27	80	-	-58.7	-	-	-	-
Cy(*trans*)-*co*-BDT	23.5	6.58	-17	-	-	-	-	-	-	-
Cy(*cis*)$_{10}$BD$_{90}$-*co*-HDT	76.9	4.62	-63	50	9	-53.3	87±2	25±1	1028±31	167±1
Cy(*trans*)$_{10}$BD$_{90}$-*co*-HDT	63.5	4.28	-64	51	10	-55.0	81±4	26±2	890±84	147±22
Cy(*trans*)$_{25}$BD$_{75}$-*co*-HDT	91.8	4.54	-62	44	-2	-50.0	60±10	19±1	920±26	117±4

Table S1 Summary of the reported thermomechanical properties for all polyesters. ǂ Uncertainty taken as standard deviation (n=3).

Chapter 4 – Stereochemistry Dependent Mechanical Properties in Sugar-Based Degradable Polymers

4.1 Manuscript details and overview

Title: Stereochemistry Dependent Mechanical Properties in Sugar-Based Degradable Polymers

Authors: C. J. Stubbs†[1], J. C. Worch†[1], H. Prydderch[1], Z. Wang[2], R. T. Mathers[3], A. V. Dobrynin[2], M. L. Becker[4], A. P. Dove[1]

† denotes equal contribution

Affiliations:

[1] School of Chemistry, The University of Birmingham, Edgbaston, Birmingham, B15 2TT, UK.

[2] Department of Chemistry, University of North Carolina-Chapel Hill, Chapel Hill, NC, 27599, United States

[3] Department of Chemistry, Pennsylvania State University, University Park, Pennsylvania, 15068, United States.

[4] Department of Chemistry, Department of Mechanical Engineering & Materials Science, Department of Orthopaedic Surgery, Duke University, 308 Research Drive, Durham, North Carolina 27708, United States

Submitted article

Co-author contributions: Dr Josh Worch (University of Birmingham) synthesised and characterised the monomers and polymers for the project, in addition to performing the hydrolytic degradation experiment. Dr Hannah Prydderch (University of Birmingham)

provided technical and synthetic advice including troubleshooting some of the initial synthetic pathways. Prof. Andrey Dobrynin (University of North Carolina-Chapel Hill) and Zilu Wang (University of North Carolina-Chapel Hill) performed Molecular dynamic calculations and polymer chain simulations. Prof. Robert Mathers (Pennsylvania State University) performed ocean degradation simulations. Prof. Matthew Becker (Duke University) and Prof. Andrew Dove (University of Birmingham) supervised the project, in addition to providing guidance and editing the manuscript.

Overview: Isosorbide is a product of biomass fermentation that is expected to replace common crude oil derivatives in polymer synthesis. Despite the plethora of study into the influence of the isosorbide structure in polymer materials, there is limited work on the other stereoisomers: isomannide and isoidide. The goal of this chapter was to elucidate how the isomannide and isoidide stereoisomers impact the thermal, mechanical and hydrolytic degradation in linear polymers.

We adapted the polymerisation technique described in chapter 2 and 3 to incorporate the isoidide and isomannide structures into polyester-urethanes. To our surprise, the materials displayed an almost two orders of magnitude difference in the Young's modulus and each possessed a unique stress *vs* strain profile. The crystalline isoidide polymer behaved as tough plastic material with a characteristic yield point with a high stiffness and UTS. Whereas the amorphous isomannide polymer displayed similar behaviour to a traditional elastomer with no observable yield point and a strain hardening regime that produces a UTS comparable to the isoidide polymer. Molecular Dynamic simulations of the polymers suggested the difference arose from inter- and intra- molecular hydrogen bonding, where the isoidide polymer favoured intermolecular interactions.

To further exploit the divergent mechanical properties of the isohexides, co-polymers of isoidide and isomannide were fabricated in a similar fashion to chapter 2 and 3. Furthermore, we blended the isomannide and isoidide polymers at varying quantities to

elucidate the impact of stereochemistry in polymer blends. We found that blending and copolymerising the same quantity of each stereoisomer led to the same divergent property relationship. The blended sample maintained a high stiffness and stress *vs* strain profile as a plastic material, whilst the copolymer maintained a low stiffness the characteristic elastomer curve shape.

The final aspect of the chapter was to understand how the stereochemistry in homopolymers, copolymers and blends influenced environmental degradation. An accelerated degradation study revealed isomannide (elastomer) degraded more rapidly than the isoidide polymer (plastic), whilst the blend (plastic) degraded faster than the copolymer (elastomer). To summarise: the hydrolytic degradation rate of either the elastomer or plastic material could be independently tuned by incorporating the stereoisomers in different ways. This opens the possibility of designing polymers with similar mechanical properties but different rates of environmental degradation.

Stereochemistry Dependent Mechanical Properties in Sugar-Based Degradable Polymers

Connor J. Stubbs,[1]† Joshua C. Worch,[1]† Hannah Prydderch,[1] Zilu Wang,[2] Robert T. Mathers,[3] Andrey V. Dobrynin,[2] Matthew L. Becker,[4]* Andrew P. Dove[1]**

[1] School of Chemistry, The University of Birmingham, Edgbaston, Birmingham, B15 2TT, UK.

[2] Department of Chemistry, University of North Carolina-Chapel Hill, Chapel Hill, NC, 27599, United States.

[3] Department of Chemistry, Pennsylvania State University, University Park, Pennsylvania, 15068, United States.

[4] Department of Chemistry, Mechanical Engineering and Materials Science, Biomedical Engineering and Orthopaedic Surgery, Duke University, Durham, NC, 20899, United States.

†Authors contributed equally

* Correspondence:

**Correspondence:

ABSTRACT

Replacing non-degradable petrochemically-derived commercial plastics with renewably-sourced, biodegradable surrogates presents an appealing option for increasing the sustainability of our plastic use. Such substitution however remains challenging as non-degradable plastics typically possess superior thermomechanical properties. Here we show that stereochemical differences in sugar-based monomers can yield a family of polyurethanes that can be either strong amorphous thermoplastic elastomers with properties that exceed most crosslinked rubbers, or robust, semi-crystalline thermoplastics with toughness higher than that of high-density polyethylene or nylon-6. The difference in stereochemistry directs distinct intra- and inter-chain supramolecular hydrogen-bonding interactions in the bulk materials to define their behaviour. The chemical similarity of the isohexide-based polymers that we report enables: copolymerisation, that allows the design of useful materials in which the degradability can be controlled independently of the mechanical properties and, blending which yields materials with comparable properties to the homopolymers and offers opportunities in mechanical recycling of mixed polymer feeds.

KEY WORDS

Polymer materials, sustainability, degradable plastics, stereochemistry.

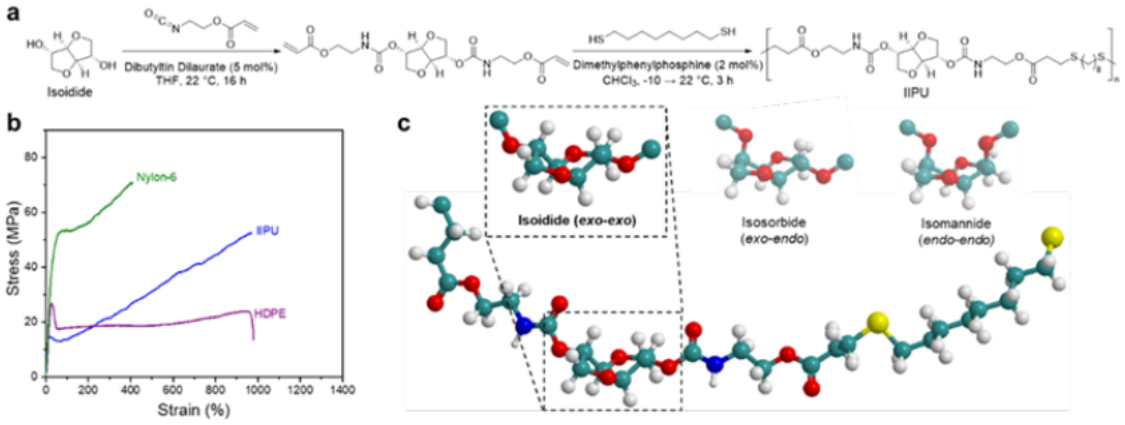
INTRODUCTION

Commercial plastics have been optimised over decades to be robust, lightweight materials that satisfy countless demands as a consequence of their excellent mechanical strength, flexibility and toughness.[1] Despite the interest in renewably-sourced monomers to increase the sustainability of our plastic use, the plastic materials that result typically lack the mechanical integrity to compete effectively in diverse application settings.[2-6] While there are a few exceptions,[7-11] they are typically more complex block copolymer structures. The intricate structures and stereoisomerism found in natural compounds, however, provides researchers with a strategic advantage in their endeavour towards creating mechanically robust materials.[12, 13] Indeed, the stereochemistry within synthetic polymer backbones is already known to be critical to materials' performance.[14] Polypropylene (PP), for example, possesses a methyl group at each repeat unit and the stereochemical relationship of neighbouring substituents (tacticity) significantly impacts chain packing behaviour. By increasing the stereoregularity of these neighbouring units along the backbone (such as for isotactic polypropylene), polymer chains can pack more efficiently, increasing material crystallinity, which in turn results in dramatic improvements of the materials' strength and toughness.[15] The same tacticity phenomenon is also observed in leading bioplastics such as polylactic acid (PLA), which has an elastic modulus that ranges from 1.2 to 4 GPa, depending on the polymer stereochemistry.[16-18] As highlighted by these examples, stereoregularity in these plastic materials typically produces an increase in strength (concomitant with a decrease in extensibility) that results from more efficient crystallisation, that is driven by more facile ordering of the chains in the polymer backbone. However, all stereoisomers of these polymers remain plastic materials that deform irreversibly under load; their fundamental behaviour (plastic *vs* elastic) remains the same, irrespective of the stereochemistry.

Rigid-ring bicyclic ethers, obtained from the dehydrative cyclisation of sugar alcohols, have garnered substantial attention as monomers because of their unique structural complexity, imparting planar geometric isomerism, and inherent degradability (*via* hydrolytic and/or enzymatic pathways).[19-34] While there has been substantial focus on isosorbide, relatively little work has focussed on its accompanying diastereomers, isomannide and isoidide.[35-41] Inspired by the stereochemical differences between natural rubber (*cis*-1,4-polyisoprene) and Gutta percha (*trans*-1,4-polyisoprene)[42], we hypothesised that the stereochemistry of the isohexide unit would significantly affect their toughness and ductility. Recent work has described a scalable 1-step synthesis of isoidide from its sustainably produced stereoisomer, isosorbide,[43] making it an interesting starting material for polymer synthesis.

RESULTS AND DISCUSSION

Incorporation of the isoidide stereoisomer into a well-defined, high molar mass polymer was achieved by step-growth polymerisation of an isoidide-containing diacrylate with 1,8-octanedithiol using previously reported phosphine-catalysed thiol-Michael polyaddition chemistry (**Figure 1a**)[44] to yield an alternating non-crosslinked polymer structure (IIPU). Key to our monomer design were internal urethane units positioned adjacent to the sugar unit which we reasoned would enhance thermomechanical properties by promoting a strong hydrogen bonding network,[45] complementing the rigidity of the isohexide unit. The polymer was isolated as a high molecular weight white, fibrous material (M_w = 117 kDa, $Đ_M$ = 8.12) with a high dispersity that may be expected to result from irreversible formation of cyclic oligomers in the step-growth process.[46] Nevertheless, this approach offers synthetic versatility to fine tune the properties of the polymers in the future.



d Sample	T_g (°C)	ΔH_m (Jg^{-1})	E^a (MPa)	UTS^b (MPa)	$\varepsilon_b{}^c$ (%)	$U_T{}^d$ (MJ·m^{-3})
IIPU	15	24	320 ± 65	56 ± 5	989 ± 115	329 ± 62
HDPE	-	170	599 ± 46	28 ± 2	1145 ± 117	234 ± 29
Nylon-6	60	87	215 ± 11	67 ± 4	336 ± 60	186 ± 37
iPPO†	-	-	295 ± 10	75 ± 3	-	-

Figure 1. (a) Synthesis of acrylate terminated isoidide monomer and step-growth polyaddition to afford IIPU (b) Representative stress *vs* strain curves of IIPU, HDPE and Nylon-6 tested at 10 mm min^{-1} and 22 °C. HDPE (Alfa Aesar, product no. 41731, lot no. S02D047, d = 0.95) and Nylon-6 (Aldrich, product no. 181110, lot no. MKCB9179, *d* = 1.084) were received from commercial suppliers as pellets and then pressed into thin films for thermomechanical analysis. (c) Three-dimensional energy optimized structure of one repeat unit of IIPU showing different orientation of polymer backbone according to relative stereochemistries (d) Bottom – summary of thermomechanical properties for reported plastics. [a]Young's modulus [b]Ultimate tensile strength [c]Strain at breakage [d]Tensile toughness. †Recently reported example of a degradable Nylon mimic, isotactic polypropylene oxide (iPPO).[47]

The isolated polymer sample possessed high thermal stability ($T_{d,5\%}$ = 286 °C, Figure S1, Table S2) that enabled facile processing (heated compression moulding) into a flexible, free-standing film that was suitable for mechanical analysis. We observed that thermally-processed films became less transparent (indicative of crystallization) within hours of processing, so the

films were annealed for three days before testing to ensure a thermal equilibrium had been reached. The mechanical properties of the annealed IIPU sample were assessed using uniaxial tensile testing and compared with commodity polymer samples – Nylon-6 and high-density polyethylene, HDPE − that were also tested under the same conditions (**Figure 1b**). IIPU possessed a high Young's modulus (320 ± 66 MPa) and a distinct yield point when the material entered the plastic deformation region, which is a general feature of most thermoplastic materials. The stiffness and ductility of IIPU was comparable to common plastics such as LDPE and HDPE, however the strain hardening phenomenon exhibited in IIPU (onset near ~100% strain) resulted in a substantially larger ultimate tensile strength (UTS). In fact, the UTS of IIPU is more analogous to engineering plastics such as Nylon-6.

Recyclability is an essential aspect for any modern plastic. In order to address potential concerns over the mechanical recyclability due to the thermal stability of the sugar-based isoidide backbone, we reprocessed and tested a sample of IIPU. IIPU displays excellent retention of mechanical properties upon recycling (Figure S2). Shredded and thermally reprocessed samples maintained a high toughness (initial 312 ± 49 $MJ \cdot m^{-3}$, reprocessed 295 ± 25 $MJ \cdot m^{-3}$) with mechanical values within error of the initially processed polymer film. Hence, IIPU is a recyclable thermoplastic that merges the ductility of polyolefins with the strength of nylons. These observations highlight the significant potential of isoidide as a bio-derived building block in polymer materials.

The unique bowl-shaped structure that is presented in isoidide results from the two fused tetrahydrofuranyl rings and presents three possible stereoisomers with two hydroxyl groups. Polymers incorporating isosorbide (one *exo*, one *endo* relative to the plane through the rings) typically have regio-irregular polymer backbones (*endo-endo versus endo-exo versus exo-exo* connectivities) as a result of non-selective reactivity. While this can be overcome by regiocontrolled ring-opening polymerisation[48] or by polymerising asymmetrical isosorbide-based A-B monomers,[49] we sought to compare polymers with more analogous chemistry and hence focused our study on the isomannide (*endo-endo*) derivative to eliminate the effects of regiochemistry that are associated with the isosorbide derivative. Hence, a well-defined alternating isomannide-polyurethane (IMPU) was prepared in a protocol analogous to IIPU synthesis to afford an optically transparent and rubbery material with comparable molecular weight and dispersity (M_w = 95 kDa, $Đ_M$ = 9.69). In contrast to what may be expected by varying stereochemistry in synthetic polymers such as PP, PLA or other sugar-based materials,[19] the isomannide-based material displayed elastic behaviour against the isoidide-based material (**Figure 2a)**.

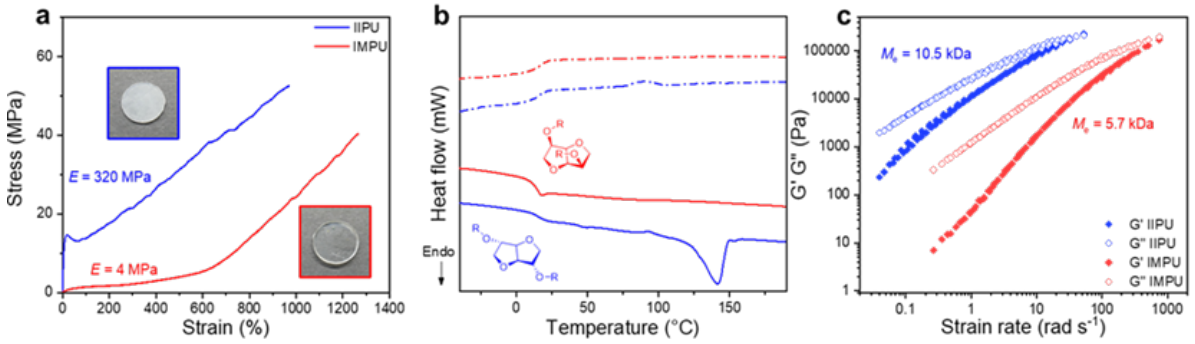


Figure 2. (a) Representative stress *vs* strain curves obtained at 10 mm min^{-1}, 22 °C for annealed IIPU and IMPU with Young's modulus (*E*) displayed (Inset: photographs of pressed films of IIPU and IMPU). (b) DSC thermogram cycles of annealed (3 day) IIPU and IMPU (solid line = heating scan and dashed line = cooling scan) (c) Time-temperature superposition of rheological frequency sweeps of IIPU and IMPU overlaid at 130 °C. Chain entanglement molecular weight (M_e) of IIPU and IMPU is displayed.

For both IIPU and IMPU, tensile testing showed significant strain hardening leading to high UTS and toughness (Table S2). The tough plastic behaviour of IIPU was starkly contrasted against the soft elastomeric behaviour of IMPU, underlined by a difference in the Young's moduli of almost two orders of magnitude (IIPU *E* = 320 MPa, IMPU *E* = 4 MPa, **Figure 2a**). In addition, IMPU displayed excellent recoverability after deformation, evidenced by the absence of a yield point in the tensile curve, whereas the IIPU was irreversibly deformed above the yield point. This mechanical phenomenon is starkly contrasted by a recently reported unsaturated polyurethane system, where strength and stiffness changed between *cis/trans* stereoisomers but both polymers displayed characteristically plastic behaviour.[44] Typically, creating materials with mechanical properties that are as divergent as IIPU and IMPU requires significant microstructure changes to the polymer architecture (such as altering composition, topology and/or cross-linking), *i.e.* one must 'redesign' the polymer. Here, the profound difference in thermomechanical properties appears to be solely attributed to the stereochemical differences between the isohexide moieties. Even though we envisioned that the configurational differences between the isohexide diastereomers would affect the polymer chain packing, consequently their crystallinity and, in turn, bulk thermomechanical properties of the polymer, we were still surprised by the obvious difference in fundamental behaviour between the two polymers. To date, there is insufficient data to enable accurate prediction of which stereoisomer will pack better in the solid state or that stereochemical changes to the polymer would result in changing from plastic to elastic deformation behaviour. Among the few systems in which both geometric isomers have been reported, some have more rigid or crystalline *cis*-isomers,[50-52] and in some polymers the *trans*-isomer is the most rigid or crystalline.[44, 53]

The stark contrast in mechanical behaviour displayed by IIPU to its structural analogue derived from isomannide (IMPU) inspired us to determine the influence of stereochemistry on

the physical properties of the polymers that manifested such large macroscopic differences. Annealed thin films of IIPU and IMPU were compared using differential scanning calorimetry (**Figure 2b**). Despite IIPU and IMPU possessing similar, single, glass transition temperatures (T_g ~ 15 °C) which suggest that the alternating polymer structure prevents phase separation, the DSC thermogram indicates a distinct difference at higher temperatures. The sharp endothermic peak (140 °C) observed in the IIPU heating run is characteristic of a first-order phase transition (T_m) but is absent in IMPU. This confirms that IIPU is semi-crystalline while IMPU appears to be amorphous. To further understand how the isohexide structure influenced the polymer chain interactions, rheological frequency sweeps were performed on IIPU and IMPU at various temperatures (**Figure 2c**). From this measurement, the molecular weight between polymer entanglements (M_e) can be calculated from fitting the data to a reptation model. IIPU was calculated to have a larger M_e (M_e = 10.5 kDa, G_e = 1.8 MPa) than IMPU (M_e = 5.7 kDa, G_e = 5.3 MPa), which indicates that the isoidide stereochemistry causes chains to be more linear and less tangled chains in comparison in isommanide.

We performed detailed molecular dynamics simulations to highlight the origin of the opposing mechanical properties of the IIPU and IMPU polymers. Evolution of the macromolecular conformations of two intertwined IIPU macromolecules upon deformations (snapshots shown in **Figure 3a**) revealed that the IIPU macromolecules have a large number of both inter- and intra- molecular H-bonds in the undeformed state (**Figure 3b**). In fact, an almost equal number of intra- and inter-molecular H-bonds is indicated by the observed ratio close to unity. A similar analysis of the effect of the macromolecular elongation on intermolecular interactions demonstrates striking differences between structural transformations in IIPU and IMPU (**Figure 3b and 3c**). Specifically, while with increasing deformation, the number of intramolecular H-bonds decreases for both systems while the number of inter-molecular bonds remains constant for IIPU systems and increases for IMPU polymers. We postulated that this preference for formation of the intermolecular associations for IIPU macromolecules could be the reason that these polymers crystallise. To further understand the origin of crystallinity in the IIPU polymer materials, we performed detailed molecular dynamics simulations of the bulk systems consisting of 75 IIPU repeat units with a degree of polymerization, DP = 16, at polymer density 0.97 g·cm^{-3}, temperature T = 300 K and pressure P = 1.0 atm (**Figure 3d**) and compared them to the equivalent for IMPU chains. These simulations show that IIPU forms approximately 50% more H-bonds than IMPU and is a direct consequence of the differences in the local molecular conformations (Figure S3). Furthermore, unlike IMPU, IIPU is capable of forming strong H-bonded associations (Figure S3) which could be viewed as precursors of IIPU chain crystallization that is responsible for the plastic behaviour observed in the bulk material. The differences between isoidide and

isomannide-based materials, as well as their exceptional inherent mechanical features, are testament to the potential of leveraging stereochemistry to influence supramolecular interactions (especially ring-induced geometric isomerism) in bio-sourced monomer feedstocks.

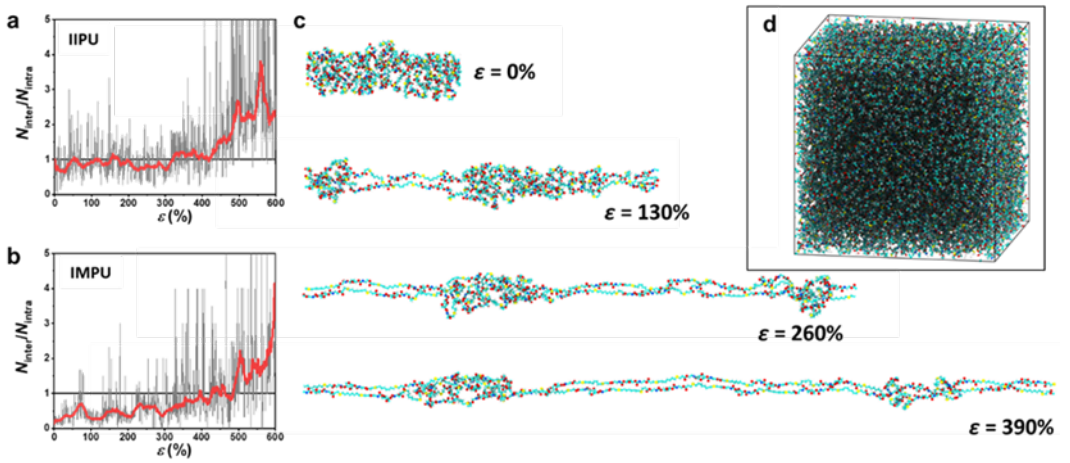
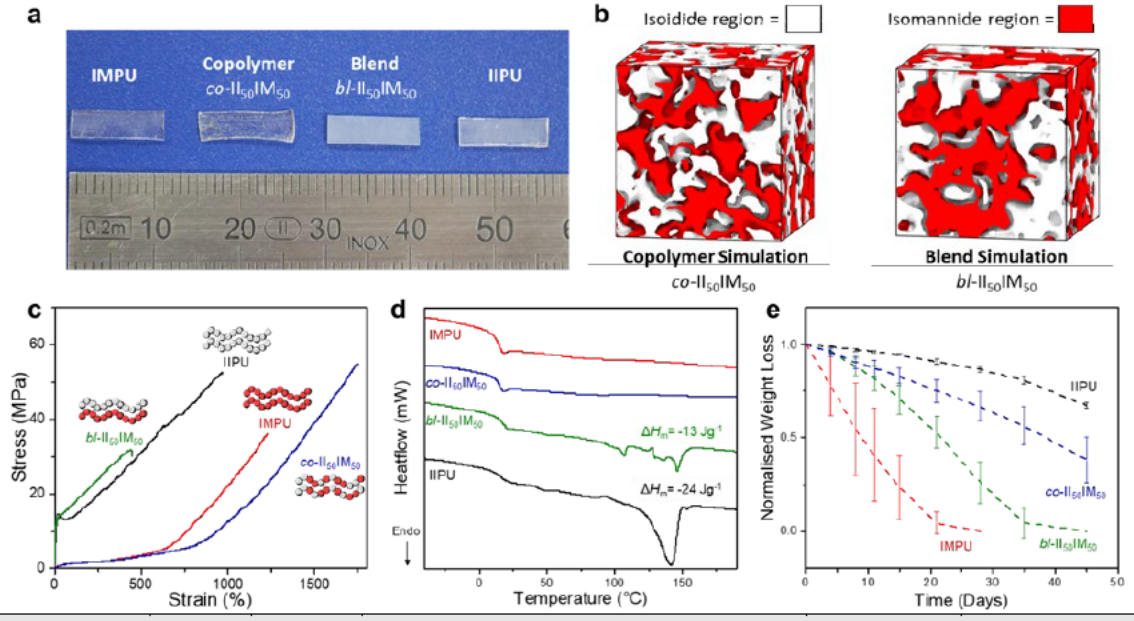


Figure 3. Dependence of the ratio of the intermolecular (N_{inter}) hydrogen bonds to intramolecular (N_{intra}) hydrogen bonds on deformation for IIPU (a) and IMPU (b) systems. Data averaged over 20 different simulation runs from undeformed state. (c) Snapshots illustrating conformational changes of IIPU macromolecules under deformation. (d) Snapshot of the IIPU bulk system.

The disparity of mechanical properties juxtaposed against the chemical similarity between IIPU and IMPU presented the opportunity to finely manipulate material mechanical properties by combining the stereoisomers either in physical blends or by copolymerization. Random copolymers (*co*-II_xIM_y) with controlled stereochemical composition were obtained by varying the relative quantity of isoidide and isomannide monomer in the feed and copolymerizing with 1,8-octanedithiol to afford polymers suitable for DSC and tensile testing. The copolymer with 75% isoidide content, *co*-$II_{75}IM_{25}$, was semi-crystalline albeit with a significant reduction in overall crystallinity evidenced by a decrease of 4 $J \cdot g^{-1}$ in the total enthalpy of melting (ΔH_m), compared to IIPU, and a decrease in the overall T_m (Δ17 °C, Table S2). Below 75% isoidide content, copolymer thermal properties were more influenced by isomannide than isoidide (Figure S4) and resulted in a series of amorphous thermoplastic elastomers that displayed a notable increase in strength and toughness compared to IMPU. These differences in crystallinity are reflected in the respective tensile properties for each copolymer. The semi-crystalline *co*-$II_{75}IM_{25}$ behaved like a tough plastic, which demonstrated a reduction in material toughness and modulus as compared to IIPU (Figure S4). Likewise, both *co*-$II_{50}IM_{50}$ and *co*-$II_{25}IM_{75}$ presented with a similar tensile profile (J-shaped curve) to the elastomeric IMPU. This suggests that the presence of isoidide enhanced the mechanical performance of *co*-$II_{50}IM_{50}$ and *co*-$II_{25}IM_{75}$ without imparting the crystallinity that is observed in the stereopure IIPU or

75% II formulation. This feature also adds to the capacity of isoidide as an attractive sustainable comonomer.



Sample	T_g (°C)	ΔH_m (Jg^{-1})	E^a (MPa)	UTS^b (MPa)	$\sigma_y{}^c$ (MPa)	$\varepsilon_b{}^d$ (%)	$U_T{}^e$ (MJ·m^{-3})
IIPU	15	24	320 ± 65	56 ± 5	16 ± 1	990 ± 120	329 ± 62
IMPU	15	-	5.7 ± 0.3	39 ± 5	-	1285 ± 70	187 ± 18
bl-II$_{50}$IM$_{50}$	18	14	272 ± 10	37 ± 5	13 ± 1	460 ± 100	218 ± 24
co-II$_{50}$IM$_{50}$	16	-	3.0 ± 0.3	55 ± 3	-	1660 ± 85	279 ± 24

Figure 4. (a) Image of heat compressed IIPU, IMPU, *co*-II$_{50}$IM$_{50}$ and *bl*-II$_{50}$IM$_{50}$ to illustrate crystallinity differences. (b) Bulk system simulations of *co*-II$_{50}$IM$_{50}$ and *bl*-II$_{50}$IM$_{50}$ illustrating the separation of isoidide (white) and isomannide (red) regions. (c) Representative stress *vs* strain tensile curves of annealed IIPU, IMPU and both random copolymers and physical blend at 50/50 II/IM ($n > 3$) Mechanical testing was performed at 10 mm·min^{-1}. (d) DSC thermograms of 1st heating cycle of annealed IIPU, IMPU, *co*-II$_{50}$IM$_{50}$ and *bl*-II$_{50}$IM$_{50}$ at 10 K·min^{-1}. Total enthalpy of melting (ΔH_m) calculated from integration of all thermal transitions. (e) Normalized weight loss of IIPU, IMPU, *co*-II$_{50}$IM$_{50}$ and *bl*-II$_{50}$IM$_{50}$ discs in 1 M NaOH$_{(aq)}$ over 45 days at 25 °C. n = 3. [a]Young's modulus, [b]Ultimate tensile strength (UTS) [c]Stress at yield point [d]Strain at breakage [e]Tensile toughness.

Physical blending of polymers provides a rapid and convenient method to access a range of properties between two or more distinctly different polymers, however it can be practically challenging to achieve desirable physical properties in the resultant material. In many cases, immiscibility between polymers dominates, even where the structures are very similar (i.e. polypropylene and polyethylene) unless targeted compatibilization efforts are applied, thus leading to phase separation in the blended sample.[54] These miscibility difficulties are particularly notorious in binary blends derived from a semi-crystalline/amorphous polymers,[55] but could offer advantages in mechanical recycling of these materials. Despite IIPU and IMPU possessing distinctly different thermomechanical properties (IIPU – semicrystalline, plastic; IMPU – amorphous elastomer), blending of these two polymers was simple and yielded

macroscopically homogeneous blended films, presumably as a result of the isomeric nature of the polymers. Polymer blends with varying quantities of IMPU and IIPU were made by a simple dissolution-precipitation and then melt processed into uniform films after drying. Notably, the physical blends display multifeatured DSC profiles (Figure S5). Surprisingly, the ΔH_m for the blended films is greater than expected when normalised to the molar content of isoidide in the sample (Table S2). The presence of IMPU homopolymer actually enhances the crystallisation efficiency of IIPU, which is a similar phenomenon previously reported in *cis*- or *trans*-rich polyisoprene blends.[56] In contrast to the copolymer samples, all physical blends were semi-crystalline, but they exhibited more complex melting behaviours compared to IIPU. This manifests in all the blended IIPU/IMPU samples being tough plastic materials, irrespective of composition. Many polymerisation methods prevent the copolymerisation of monomers that produce materials with dramatically different mechanical properties and commonly, blending of the resulting materials results in bulk phase separation to produce plastics that have inferior properties to the homopolymers.[57-63] Here, however, the post-blending compatibility, yielding materials with good mechanical properties, offers further opportunity to retain the excellent materials properties of IIPU, even after recycling mixed polymer feeds.

To understand this behaviour, we undertook further molecular dynamics simulations of bulk systems. In both cases, there was a distinct regional separation between the isoidide and isomannide domains (**Figure 4b**). The copolymer simulations showed the formation of a greater number of smaller domains which indicates that this microstructure facilitates better separation between II and IM regions than is possible in the physical blends. This was further quantified by calculating the interfacial surface area per unit volume between the II and IM domains (**Figure 4b** and Figure S6) with a lower surface area being calculated in each case for physical blends (*i.e. bl*-$II_{50}IM_{50}$ = 0.9297 $Å^{-1}$) in comparison to the copolymers (*i.e. co*-$II_{50}IM_{50}$ = 1.4399 $Å^{-1}$) at the same II/IM molar ratio. We postulate that the larger IIPU domains in the physical blends facilitates crystallisation of the IIPU regions and hence promotes the plastic, IIPU-based behaviour (Figure S6).

Petroleum-derived plastics are notorious for their environmental persistence, even under extreme conditions, due to the hydrophobicity and homogeneity imparted by their all carbon-based backbones.[1] Without useful chemical ‘trigger’ points (such as oxygen and nitrogen) in the backbone of polymers,[7] environmental degradation processes are limited and slow and hence we also sought to demonstrate that hydrolytic degradation could provide a further advantage for this new sustainable thermoplastic over traditional petrochemical-derived plastics. A simple accelerated degradation experiment using 1 M $NaOH_{(aq)}$ was performed on thin discs (ca. 0.5 mm thickness) of IIPU and IMPU to assess the influence of stereochemistry

and composition on the rate of hydrolytic degradation (**Figure 4e**). Polymer crystallinity is known to inhibit hydrolytic degradation by restricting water penetration into the bulk sample,[64] and hence we theorised that differences in degradation behaviour between IIPU and IMPU would be largely regulated by crystallinity. Although IIPU degraded at a slower rate than amorphous IMPU, the sample still exhibited significant mass loss within the timeframe of the study (~25% mass loss within 45 d) showing its potential to degrade by hydrolysis should it be released into the environment or for chemical depolymerisation methods such as those used for chemical recycling of PET.

To quantify the contribution of abiotic hydrolysis to degradation, we screened physical property data, relative rates (k_{rel}) for degradation experiments in NaOH(aq), and insight from a degradation database, which contains similar functional groups as those found in IIPU and IMPU,[65] to propose a simple model to predict k_{rel} values (Figure S42). As such, the predicted rate of degradation of IIPU in seawater is comparable to PCL and is faster by approximately an order of magnitude when compared to PLA (Figure S43, Table S1). Furthermore, IMPU is predicted to degrade approximately an order of magnitude faster than IIPU (i.e. 2 orders of magnitude greater than PLA).

Exploration of the hydrolytic degradation of the copolymers and physical blends revealed that the mechanical behaviour (plastic vs elastic) could be decoupled from the inherent hydrolytic degradation. Studying the accelerated hydrolysis (1M NaOH, 25 °C) of the crystalline polymer blend (*bl*-$II_{50}IM_{50}$) and the analogous amorphous copolymer (*co*-$II_{50}IM_{50}$) under the same conditions, revealed that *bl*-$II_{50}IM_{50}$ degraded far more rapidly than IIPU, even though the thermomechanical properties were similar (**Figure 4e**). On the contrary, *co*-$II_{50}IM_{50}$ degraded significantly slower than the IMPU despite both materials being amorphous and possessing similar T_gs. These results were mirrored in the computational prediction of ocean degradation (Figure S42-43). These contrasting behaviours are consistent with the separation of II and IM domains within copolymers and physical blends, such that the slower degradation of the II-based domains has a more significant effect in the copolymer where they are smaller and more dispersed throughout the bulk system; the higher separation in the blended system leads to a lower impact on the degradation rate. Previous systems with degradability control based on microstructure have required precision-made sequences,[66-69] however the simplicity of the approach herein lends to the opportunity to tune mechanical properties independent of degradation.

Conclusion

Satisfying the broad range of properties that common petrol plastics achieve using sustainable sources is a monumental hurdle in tackling the global plastics crisis. Historically,

degradable plastics made from sustainable sources are mechanically limited to a narrow range of mechanical properties. However, our study emphasizes how stereochemistry, a common motif of sustainably derived feedstocks, can be leveraged to create mechanically divergent materials with minimal changes to the overall polymer structure. A future focus into stereochemistry will be crucial to unlocking the full potential of bio-sourced derivatives.

References

1. Chamas, A.; Moon, H.; Zheng, J.; Qiu, Y.; Tabassum, T.; Jang, J. H.; Abu-Omar, M.; Scott, S. L.; Suh, S., Degradation rates of plastics in the environment. *ACS Sustain. Chem. Eng.* **2020,** *8* (9), 3494-3511.
2. Wang, Z.; Ganewatta, M. S.; Tang, C., Sustainable polymers from biomass: Bridging chemistry with materials and processing. *Prog. Polym. Sci.* **2020,** *101*, 101197.
3. Haider, T. P.; Völker, C.; Kramm, J.; Landfester, K.; Wurm, F. R., Plastics of the future? The impact of biodegradable polymers on the environment and on society. *Angew. Chem. Int. Edit.* **2019,** *58* (1), 50-62.
4. Tang, X.; Chen, E. Y. X., Chemical synthesis of perfectly isotactic and high melting bacterial poly(3-hydroxybutyrate) from bio-sourced racemic cyclic diolide. *Nat. Commun.* **2018,** *9* (1), 2345.
5. Lambert, S.; Wagner, M., Environmental performance of bio-based and biodegradable plastics: the road ahead. *Chem. Soc. Rev.* **2017,** *46* (22), 6855-6871.
6. Vert, M., Aliphatic polyesters: Great degradable polymers that cannot do everything. *Biomacromolecules* **2005,** *6* (2), 538-546.
7. Häußler, M.; Eck, M.; Rothauer, D.; Mecking, S., Closed-loop recycling of polyethylene-like materials. *Nature* **2021,** *590* (7846), 423-427.
8. Gregory, G. L.; Sulley, G. S.; Carrodeguas, L. P.; Chen, T. T. D.; Santmarti, A.; Terrill, N. J.; Lee, K.-Y.; Williams, C. K., Triblock polyester thermoplastic elastomers with semi-aromatic polymer end blocks by ring-opening copolymerization. *Chem. Sci.* **2020,** *11* (25), 6567-6581.
9. Tang, X.; Westlie, A. H.; Caporaso, L.; Cavallo, L.; Falivene, L.; Chen, E. Y. X., Biodegradable polyhydroxyalkanoates by stereoselective copolymerization of racemic diolides: Stereocontrol and polyolefin-like properties. *Angew. Chem. Int. Edit.* **2020,** *59* (20), 7881-7890.
10. Sangroniz, A.; Zhu, J.-B.; Tang, X.; Etxeberria, A.; Chen, E. Y. X.; Sardon, H., Packaging materials with desired mechanical and barrier properties and full chemical recyclability. *Nat. Commun.* **2019,** *10* (1), 3559.
11. Wanamaker, C. L.; Bluemle, M. J.; Pitet, L. M.; O'Leary, L. E.; Tolman, W. B.; Hillmyer, M. A., Consequences of polylactide stereochemistry on the properties of polylactide-polymenthide-polylactide thermoplastic elastomers. *Biomacromolecules* **2009,** *10* (10), 2904-2911.
12. Schneiderman, D. K.; Hillmyer, M. A., 50th Anniversary perspective: There is a great future in sustainable polymers. *Macromolecules* **2017,** *50* (10), 3733-3749.
13. Zhu, Y.; Romain, C.; Williams, C. K., Sustainable polymers from renewable resources. *Nature* **2016,** *540* (7633), 354-362.
14. Worch, J. C.; Prydderch, H.; Jimaja, S.; Bexis, P.; Becker, M. L.; Dove, A. P., Stereochemical enhancement of polymer properties. *Nat. Rev. Chem.* **2019,** *3* (9), 514-535.
15. Natta, G.; Pino, P.; Corradini, P.; Danusso, F.; Mantica, E.; Mazzanti, G.; Moraglio, G., Crystalline high polymers of α-olefins. *J. Am. Chem. Soc.* **1955,** *77* (6), 1708-1710.
16. Chile, L.-E.; Mehrkhodavandi, P.; Hatzikiriakos, S. G., A comparison of the rheological and mechanical properties of isotactic, syndiotactic, and heterotactic Poly(lactide). *Macromolecules* **2016,** *49* (3), 909-919.
17. Farah, S.; Anderson, D. G.; Langer, R., Physical and mechanical properties of PLA, and their functions in widespread applications — A comprehensive review. *Adv. Drug Deliver. Rev.* **2016,** *107*, 367-392.
18. Garlotta, D., A literature review of poly(lactic acid). *J. Polym. Environ.* **2001,** *9* (2), 63-84.
19. Galbis, J. A.; García-Martín, M. d. G.; de Paz, M. V.; Galbis, E., Synthetic polymers from sugar-based monomers. *Chem. Rev.* **2016,** *116* (3), 1600-1636.
20. Lavilla, C.; Muñoz-Guerra, S., Sugar-based aromatic copolyesters: A comparative study regarding isosorbide and diacetalized alditols as sustainable comonomers. *Green Chem.* **2013,** *15* (1), 144-151.
21. Vijjamarri, S.; Hull, M.; Kolodka, E.; Du, G., Renewable isohexide-based, hydrolytically degradable poly(silyl ether)s with high thermal stability. *ChemSusChem* **2018,** *11* (17), 2881-2888.
22. Ji, X.; Wang, Z.; Wang, Z.; Yan, J., Bio-based poly(ether imide)s from isohexide-derived isomeric dianhydrides. *Polymers* **2017,** *9* (11).
23. Legrand, S.; Jacquel, N.; Amedro, H.; Saint-Loup, R.; Pascault, J.-P.; Rousseau, A.; Fenouillot, F., Synthesis and properties of poly(1,4-cyclohexanedimethylene-co-isosorbide terephthalate), a biobased copolyester with high performances. *Eur. Polym. J.* **2019,** *115*, 22-29.
24. Wroblewska, A.; Zych, A.; Thiyagarajan, S.; Dudenko, D.; van Es, D.; Hansen, M. R.; Koning, C.; Duchateau, R.; Jasinska-Walc, L., Towards sugar-derived polyamides as environmentally friendly materials. *Polym. Chem.* **2015,** *6* (22), 4133-4143.
25. Javni, I.; Bilić, O.; Bilić, N.; Petrović, Z. S.; Eastwood, E. A.; Zhang, F.; Ilavský, J., Thermoplastic polyurethanes with isosorbide chain extender. *J. Appl. Polym. Sci.* **2015,** *132* (47).

26. Bachmann, F.; Reimer, J.; Ruppenstein, M.; Thiem, J., Synthesis of novel polyurethanes and polyureas by polyaddition reactions of dianhydrohexitol configurated diisocyanates. *Macromol. Chem. Phys.* **2001,** *202* (17), 3410-3419.
27. Saxon, D. J.; Luke, A. M.; Sajjad, H.; Tolman, W. B.; Reineke, T. M., Next-generation polymers: Isosorbide as a renewable alternative. *Prog. Polym. Sci.* **2020,** *101*, 101196.
28. Hu, C.; Bourbigot, S.; Delaunay, T.; Collinet, M.; Marcille, S.; Fontaine, G., Synthesis of isosorbide based flame retardants: Application for polybutylene succinate. *Polym. Degrad. Stabil.* **2019,** *164*, 9-17.
29. Gallagher, J. J.; Hillmyer, M. A.; Reineke, T. M., Acrylic triblock copolymers incorporating isosorbide for pressure sensitive adhesives. *ACS Sustain. Chem. Eng.* **2016,** *4* (6), 3379-3387.
30. Gallagher, J. J.; Hillmyer, M. A.; Reineke, T. M., Isosorbide-based polymethacrylates. *ACS Sustain. Chem. Eng.* **2015,** *3* (4), 662-667.
31. Qian, W.; Liu, L.; Zhang, Z.; Su, Q.; Zhao, W.; Cheng, W.; Dong, L.; Yang, Z.; Bai, R.; Xu, F.; Zhang, Y.; Zhang, S., Synthesis of bioderived polycarbonates with adjustable molecular weights catalyzed by phenolic-derived ionic liquids. *Green Chem.* **2020,** *22* (8), 2488-2497.
32. Park, S.-A.; Jeon, H.; Kim, H.; Shin, S.-H.; Choy, S.; Hwang, D. S.; Koo, J. M.; Jegal, J.; Hwang, S. Y.; Park, J.; Oh, D. X., Sustainable and recyclable super engineering thermoplastic from biorenewable monomer. *Nat. Commun.* **2019,** *10* (1), 2601.
33. Nelson, A. M.; Long, T. E., A perspective on emerging polymer technologies for bisphenol-A replacement. *Polym. Int.* **2012,** *61* (10), 1485-1491.
34. Park, S.-A.; Im, C.; Oh, D. X.; Hwang, S. Y.; Jegal, J.; Kim, J. H.; Chang, Y.-W.; Jeon, H.; Park, J., Study on the synthetic characteristics of biomass-derived isosorbide-based poly(arylene ether ketone)s for sustainable super engineering plastic. *Molecules* **2019,** *24* (13).
35. Fenouillot, F.; Rousseau, A.; Colomines, G.; Saint-Loup, R.; Pascault, J. P., Polymers from renewable 1,4:3,6-dianhydrohexitols (isosorbide, isomannide and isoidide): A review. *Prog. Polym. Sci.* **2010,** *35* (5), 578-622.
36. Braun, D.; Bergmann, M., 1,4:3,6-Dianhydrohexite als bausteine für polymere. *J. Prak. Chem-Chem. ZTG* **1992,** *334* (4), 298-310.
37. Kieber, R. J.; Silver, S. A.; Kennemur, J. G., Stereochemical effects on the mechanical and viscoelastic properties of renewable polyurethanes derived from isohexides and hydroxymethylfurfural. *Polym. Chem.* **2017,** *8* (33), 4822-4829.
38. Beldi, M.; Medimagh, R.; Chatti, S.; Marque, S.; Prim, D.; Loupy, A.; Delolme, F., Characterization of cyclic and non-cyclic poly-(ether-urethane)s bio-based sugar diols by a combination of MALDI-TOF and NMR. *Eur. Polym. J.* **2007,** *43* (8), 3415-3433.
39. Okada, M.; Okada, Y.; Tao, A.; Aoi, K., Biodegradable polymers based on renewable resources: Polyesters composed of 1,4 : 3,6-dianhydrohexitol and aliphatic dicarboxylic acid units. *J. Appl. Polym. Sci.* **1996,** *62* (13), 2257-2265.
40. Storbeck, R.; Ballauff, M., Synthesis and properties of polyesters based on 2,5-furandicarboxylic acid and 1,4:3,6-dianhydrohexitols. *Polymer* **1993,** *34* (23), 5003-5006.
41. Thiem, J.; Lüders, H., Synthesis of polyterephthalates derived from dianhydrohexitols. *Polym. Bull.* **1984,** *11* (4), 365-369.
42. Bunn, C. W.; Bragg, W. L., Molecular structure and rubber-like elasticity - III. Molecular movements in rubber-like polymers. *Proc. R. Soc. Lond. A Mat.* **1942,** *180* (980), 82-99.
43. Le Nôtre, J.; van Haveren, J.; van Es, D. S., Synthesis of isoidide through epimerization of isosorbide using ruthenium on carbon. *ChemSusChem* **2013,** *6* (4), 693-700.
44. Stubbs, C. J.; Worch, J. C.; Prydderch, H.; Becker, M. L.; Dove, A. P., Unsaturated poly(ester-urethanes) with stereochemically dependent thermomechanical properties. *Macromolecules* **2020,** *53* (1), 174-181.
45. Tang, D.; Chen, Z.; Correa-Netto, F.; Macosko, C. W.; Hillmyer, M. A.; Zhang, G., Poly(urea ester): A family of biodegradable polymers with high melting temperatures. *J. Polym. Sci. Pol. Chem.* **2016,** *54* (24), 3795-3799.
46. Yong Choi, K. M., Kim B. , Step-Growth Polymerization. In *Polymer Reaction Engineering*, 2007; pp 273-314.
47. Lipinski, B. M.; Morris, L. S.; Silberstein, M. N.; Coates, G. W., Isotactic poly(propylene oxide): A photodegradable polymer with strain hardening properties. *J. Am. Chem. Soc.* **2020,** *142* (14), 6800-6806.
48. Saxon, D. J.; Nasiri, M.; Mandal, M.; Maduskar, S.; Dauenhauer, P. J.; Cramer, C. J.; LaPointe, A. M.; Reineke, T. M., Architectural control of isosorbide-based polyethers via ring-opening polymerization. *J. Am. Chem. Soc.* **2019,** *141* (13), 5107-5111.
49. Besset, C.; Binauld, S.; Ibert, M.; Fuertes, P.; Pascault, J.-P.; Fleury, E.; Bernard, J.; Drockenmuller, E., Copper-catalyzed vs thermal step growth polymerization of starch-derived α-azide−ω-alkyne dianhydrohexitol stereoisomers: To click or not to click? *Macromolecules* **2010,** *43* (1), 17-19.
50. Worch, J. C.; Weems, A. C.; Yu, J.; Arno, M. C.; Wilks, T. R.; Huckstepp, R. T. R.; O'Reilly, R. K.; Becker, M. L.; Dove, A. P., Elastomeric polyamide biomaterials with stereochemically tuneable mechanical properties and shape memory. *Nat. Commun.* **2020,** *11* (1), 3250.
51. McGuire, T. M.; Pérale, C.; Castaing, R.; Kociok-Köhn, G.; Buchard, A., Divergent catalytic strategies for the *cis*/*trans* stereoselective ring-opening polymerization of a dual cyclic carbonate/olefin monomer. *J. Am. Chem. Soc.* **2019,** *141* (34), 13301-13305.
52. Bell, C. A.; Yu, J.; Barker, I. A.; Truong, V. X.; Cao, Z.; Dobrinyin, A. V.; Becker, M. L.; Dove, A. P., Independent control of elastomer properties through stereocontrolled synthesis. *Angew. Chem. Int. Edit.* **2016,** *55* (42), 13076-13080.

53. Phuphuak, Y.; Bonnet, F.; Stoclet, G.; Bria, M.; Zinck, P., Isoprene chain shuttling polymerisation between cis and trans regulating catalysts: straightforward access to a new material. *Chem. Commun.* **2017,** *53* (38), 5330-5333.
54. Utracki, L. A., Introduction to Polymer Blends. In *Polymer Blends Handbook*, Utracki, L. A., Ed. Springer Netherlands: Dordrecht, 2003; pp 1-122.
55. Qiu, Z., Chapter 8 - Crystallization behavior of miscible semicrystalline polymer blends. In *Crystallization in Multiphase Polymer Systems*, Thomas, S.; Arif P, M.; Gowd, E. B.; Kalarikkal, N., Eds. Elsevier: 2018; pp 213-237.
56. Yao, K.; Nie, H.; Liang, Y.; Qiu, D.; He, A., Polymorphic crystallization behaviors in *cis*-1,4-polyisoprene/*trans*-1,4-polyisoprene blends. *Polymer* **2015,** *80*, 259-264.
57. Schyns, Z. O. G.; Shaver, M. P., Mechanical recycling of packaging plastics: A review. *Macromol. Rapid Comm.* **2021,** *42* (3), 2000415.
58. Karaagac, E.; Koch, T.; Archodoulaki, V.-M., The effect of PP contamination in recycled high-density polyethylene (rPE-HD) from post-consumer bottle waste and their compatibilization with olefin block copolymer (OBC). *Waste Manage.* **2021,** *119*, 285-294.
59. Xu, J.; Eagan, J. M.; Kim, S.-S.; Pan, S.; Lee, B.; Klimovica, K.; Jin, K.; Lin, T.-W.; Howard, M. J.; Ellison, C. J.; LaPointe, A. M.; Coates, G. W.; Bates, F. S., Compatibilization of isotactic polypropylene (*i*PP) and high-density polyethylene (HDPE) with *i*PP–PE multiblock copolymers. *Macromolecules* **2018,** *51* (21), 8585-8596.
60. Eagan, J. M.; Xu, J.; Di Girolamo, R.; Thurber, C. M.; Macosko, C. W.; LaPointe, A. M.; Bates, F. S.; Coates, G. W., Combining polyethylene and polypropylene: Enhanced performance with PE/iPP multiblock polymers. *Science* **2017,** *355* (6327), 814.
61. Kallel, T.; Massardier-Nageotte, V.; Jaziri, M.; Gérard, J.-F.; Elleuch, B., Compatibilization of PE/PS and PE/PP blends. I. Effect of processing conditions and formulation. *J. Appl. Polym. Sci.* **2003,** *90* (9), 2475-2484.
62. Macosko, C. W.; Guégan, P.; Khandpur, A. K.; Nakayama, A.; Marechal, P.; Inoue, T., Compatibilizers for melt blending: Premade block copolymers. *Macromolecules* **1996,** *29* (17), 5590-5598.
63. Xanthos, M.; Dagli, S. S., Compatibilization of polymer blends by reactive processing. *Polym. Eng. Sci.* **1991,** *31* (13), 929-935.
64. Brannigan, R. P.; Dove, A. P., Synthesis, properties and biomedical applications of hydrolytically degradable materials based on aliphatic polyesters and polycarbonates. *Biomater. Sci.* **2017,** *5* (1), 9-21.
65. Min, K.; Cuiffi, J. D.; Mathers, R. T., Ranking environmental degradation trends of plastic marine debris based on physical properties and molecular structure. *Nat. Commun.* **2020,** *11* (1), 727.
66. Nowalk, J. A.; Swisher, J. H.; Meyer, T. Y., Influence of short-range scrambling of monomer order on the hydrolysis behaviors of sequenced degradable polyesters. *Macromolecules* **2019,** *52* (12), 4694-4702.
67. Swisher, J. H.; Nowalk, J. A.; Meyer, T. Y., Property impact of common linker segments in sequence-controlled polyesters. *Polym. Chem.* **2019,** *10* (2), 244-252.
68. Washington, M. A.; Swiner, D. J.; Bell, K. R.; Fedorchak, M. V.; Little, S. R.; Meyer, T. Y., The impact of monomer sequence and stereochemistry on the swelling and erosion of biodegradable poly(lactic-co-glycolic acid) matrices. *Biomaterials* **2017,** *117*, 66-76.
69. Li, J.; Rothstein, S. N.; Little, S. R.; Edenborn, H. M.; Meyer, T. Y., The effect of monomer order on the hydrolysis of biodegradable poly(lactic-co-glycolic acid) repeating sequence copolymers. *J. Am. Chem. Soc.* **2012,** *134* (39), 16352-16359.

Associated Content

Complete descriptions of experimental procedures including monomer and polymer synthesis, NMR spectra, SEC chromatograms, DSC & TGA thermograms, tensile testing, and computational descriptions.

Author Information

Corresponding Authors: *Andrew P. Dove, email: [redacted] and *Matthew L. Becker, email: [redacted]

Acknowledgment

J.C.W. acknowledges funding from the European Union's Horizon 2020 research and innovation programme under the Marie Sklodowska-Curie grant agreement No 751150. MLB acknowledges the Biomaterials Division of the National Science Foundation (DMR-1507420) for funding these efforts.

A.P.D. and C.J.S thank the European Research Council (Grant Number 681559) for funding. H.P. acknowledges funding from the Leverhulme Trust (RPG-2015-120).

Author Contributions

J.C.W., C.J.S, A.P.D. and M.L.B. conceived and designed the project idea. J.C.W. and H.P. synthesized and characterized the materials. C.J.S. performed thermal, rheological, and mechanical analyses. J.C.W performed degradation analyses. A.V.D. and Z.W. performed computational analysis. R.T.M. performed degradation calculations. The manuscript was written through contributions of J.C.W., C.J.S, M.L.B., A.V.D and A.P.D. All authors have edited and given approval to the final version of the manuscript. Data and materials availability: All data is available in the main text or the supplementary materials.

4.2 Supporting Information

Supplementary Information

Stereochemistry Dependent Mechanical Properties in Sugar-Based Degradable Polymers

Connor J. Stubbs,† Joshua C. Worch,† Hannah Prydderch, Zilu Wang, Robert T. Mathers, Andrey V. Dobrynin, Matthew L. Becker,* Andrew P. Dove*

Correspondence to: [redacted]

Materials and methods

All manipulations of air sensitive compounds were carried out under a dry nitrogen atmosphere using standard Schlenk techniques. All compounds, unless otherwise indicated were purchased from commercial sources and used as received. The following chemicals were vacuum distilled prior to use and stored in Young's tapped ampoules under N_2: 1,8-octanedithiol (Sigma-Aldrich, ≥ 97%). All solvents and chemicals used for recrystallisation were used as received. All polymer reactions were precipitated into methanol and dried in vacuo at ambient temperature for 24 h and then at 100 °C overnight (ca. 16 h). After processing, all samples were annealed for 3 d at ambient temperature before analysis.

Characterisation techniques

All NMR spectroscopy experiments were performed at 298 K on a Bruker DPX-400 NMR instrument equipped operating at 400 MHz for ^{1}H (100.57 MHz for ^{13}C). ^{1}H NMR spectra are referenced to residual protic solvents ($CHCl_3$ at δ = 7.26 ppm, DMSO–d_5 at δ = 2.50) and ^{13}C NMR spectra are referenced to the residual solvent signal ($CDCl_3$ at δ = 77.16 ppm, δ = 39.52 for DMSO–d_6). The resonance multiplicities are described as s (singlet), d (doublet), t (triplet), q (quartet) or m (multiplet).

Mass spectrometry was performed by University of Birmingham school of Chemistry on a Waters GCT Premier using electrospray ionization and on Waters Xevo G2-XS using chemical H+ ionization.

FTIR spectroscopy was carried out using an Agilent Technologies Cary 630 FTIR spectrometer. 16 Scans from 600 to 4000 cm^{-1} were taken at a resolution of 2 cm^{-1}, and the spectra were corrected for background absorbance.

SEC measurements were performed in $CHCl_3$ on an Agilent 1260 Infinity II Multi-Detector GPC/SEC System fitted with RI, ultraviolet (UV, λ = 309 nm), and viscometer detectors. The polymers were eluted through an Agilent guard column (PLGel 5 μM, 50 × 7.5 mm) and two Agilent mixed-C columns (PLGel 5 μM, 300 × 7.5 mm) using $CHCl_3$ (buffered with 0.5% NEt_3) as the mobile phase (flow rate = 1 $mL \cdot min^{-1}$, 40 °C). Number average molecular weight (M_n), weight average molecular weight (M_w) and dispersity ($Đ_M = M_w/M_n$) were determined using Agilent GPC/SEC software (vA.02.01) against a 15-point calibration curve (M_p = 162 – 3,187,000 $g \cdot mol^{-1}$) based on polystyrene standards (Easivial PS-M/H, Agilent).

Thermal characterisation

Determination of the thermal characteristic of the polymer were carried out using a STARe system DSC3 with an auto-sampler (Mettler Toledo, Switzerland). Disc shapes measuring 5 mm in diameter and 0.4 − 0.6 mm in thickness and weighing between 9 − 14 mg were cut from annealed polymer films. Thermograms were obtained in 40 μL aluminum pans from −50 − 150 °C (0 – 280 °C for Nylon-6) at a heating rate of 10 $K \cdot min^{-1}$ for two heating/cooling cycles unless otherwise specified. The glass transition temperature (T_g) was determined by the minimum of the first derivative in the second heating cycle of DSC. Total enthalpy of melting (ΔH_m) was calculated from integration and normalization of all endothermic peaks present.

Thermal degradation was quantified using a Q550 Thermogravimetric analyser (TA instruments). Thermograms were recorded under an N_2 atmosphere at a heating rate of 10 $K \cdot min^{-1}$ from 25 – 600 °C. Decomposition temperatures were reported at the 5% weight loss temperature ($T_{d,\,5\%}$).

Mechanical characterization

Uniaxial tensile testing was performed using a Testometric M350-5CT universal mechanical testing instrument fitted with a load cell of 100 kN. Samples were prepared into thin polymer films using Specac Atlas™ Manual Hydraulic Press 15T fitted with Specac heated plates.* The polymer was added into a 40 × 50 × 0.50 mm stainless steel mold and placed into pre-heated press at 160 °C. The sample was heated for 10 min (with no pressure) before degassing 5 × (500 kg pressure/release). Next, 4000 kg pressure was applied, and the sample was held at 160 °C for 5 min before cooling to ~ 25 °C under the same pressure. Film samples were visually inspected for deformation and bubbles before annealing for 3 days at 23 °C. Finally, dumbbell shaped samples were cut using custom ASTM Die D-638 Type 5. Each specimen was clamped into the tensile holders and subjected to an elongation rate of 10 mm·min^{-1} until failure. All tensile tests were repeated at least 5 times (unless otherwise indicated), and an average of the data was taken to find the ultimate tensile stress and strain. Data was analyzed using winTest™ Analysis software (v.5.0.34) and OriginPro® software. *Data obtained for mechanical recycling was performed using films that were fabricated using an automated Carver CMG 30H-12 ASTM floor standing model.

Rheology experiments were performed on an Anton Paar MCR 302 using a PP8 geometry on discs (8 × 1 mm) cut out of films fabricated using a Specac Atlas™ Manual Hydraulic Press 15T fitted with Specac heated plates (as detailed in tensile testing method). Temperature was controlled with a P-PTD 200/AIR Peltier and a P-PTD 200 hood. Frequency sweeps were performed at 1% strain from 0.1 to 100 rad·s^{-1} at 5 °C intervals between the temperatures of 140 °C to 170 °C and 100 °C to 130 °C for IMPU. G' and G'' of IIPU and IMPU were overlayed to a single spectrum at a reference temperature of 130 °C by applying a Williams-Landel-Ferry (WLF) time-temperature superposition. Molecular entanglement was extracted by fitting polydisperse double reptation theory in the REPTATE software package.[1] Molecular weights obtained from SEC, were discretized to 20 values per decade and used as theory input. The adjustable parameters in the fitting were G_e (Entanglement modulus) M_e (entanglement molecular weight) τ_e (Rouse time of one entangled segment) and the value of M_0 was kept to a value of 0.001 kg·mol^{-1} as recommended.[1]

Moleculecular dynamics simulation details

Atomistic molecular dynamics simulations were performed using the General Amber Force Field[2] (GAFF) to model the isohexide-containing polyurethanes. The forces on the atoms were calculated by differentiating the potential energy of the system, which consisted of bonded (bonds, angle, dihedral, and improper potentials) interactions as well as nonbonded interactions (van de Waals and electrostatic):

$$U = \sum_{Bonds} k_r (r - r_{eq})^2 + \sum_{Angles} k_\theta (\theta - \theta_{eq})^2 + \sum_{Dihedrals} k_d [1 + \mathrm{dcos}(n\phi)] + \sum_{i<j} \left(4\epsilon_{ij} \left[\left(\frac{\sigma}{r_{ij}} \right)^{12} - \left(\frac{\sigma}{r_{ij}} \right)^{6} \right] + \frac{q_i q_j}{4\pi\varepsilon_0 \varepsilon r_{ij}} \right) \quad \text{(S1)}$$

where $\varepsilon_0 = 8.85 \times 10^{-12}\ F\ m^{-1}$ is dielectric permittivity of the vacuum, ε is a medium relative dielectric constant.

In GAFF, the van de Waals interactions are represented by the Lennard-Jones (*LJ*) potentials with parameters given for each homogeneous atomic pairs (r_{ii} and ϵ_{ii}), while the parameters for heterogeneous pairs are determined as $r_{ij} = r_i + r_j$ and $\epsilon_{ij} = \sqrt{\epsilon_i \epsilon_j}$. The *LJ*-

potential is truncated at a cutoff distance of 10 Å. The weighting coefficient for the 1-4 interaction was set to 0.5 for the *LJ*-interactions and 0.833 for the Columbic interactions. Partial charge distributions were obtained from DFT calculations using B3LYP 6-31G* (d,p) basis set for AM1 optimized structures (Figure S7). These simulations were done by using Gaussian 09. The interaction parameters for non-bonded/bonded interactions are summarized in Table S5. Each polymer chain has n=16 repeat units. Information about macromolecular structure (list of bonds, angles, dihedrals, improper dihedrals) was generated by Topotools plugins in VMD.[3]

Simulations of chain deformation

The two ends of each polymer chain were connected across the periodic boundary along x direction forming a loop representing an infinitely long polymer chain. There were two identical chains in the periodic simulation box with equilibrium dimensions L_x=80 Å and L_y=L_z=40 Å. The system was equilibrated for 5000 *ns*. After equilibration, two polymer chains adopted a bundle-like conformation. The equilibration step followed by simulations of chain deformation. During these simulations, simulation box was deformed along x-direction at a constant strain rate 2.5×10^{-6} fs^{-1}. The system temperature was maintained by coupling the system to the thermostat applied in y and z directions. All simulations were performed using the following setup: PPPM[4,5] method for calculations of the electrostatic interactions with targeted accuracy 10^{-4}, vacuum dielectric constant ε = 1.0, T = 300 K, Langevin thermostat (damping parameter 10 fs), and time step dt = 0.5 fs. All simulations were performed using LAMMPS with GPU acceleration.[6]

Simulations of IIPU, IMPU, copolymers and physical blends bulk systems

The bulk systems of pure polymer components, polymer blends and copolymers were prepared by implementing the following procedure: (i) 75 polymer chains with degree of polymerization n = 16 were randomly distributed in a cubic box with the side length of 300 Å and with partial charges on the atoms switched off; (ii) the simulation box was slowly compressed to achieve equilibrium system density $\rho \approx 1$ $g \cdot cm^{-3}$ over time 1.0 ns at constant temperature T = 600 K; (iii) after achieving required density, the system was relaxed for 1.0 ns under NVT ensemble conditions; (iv) with partial charges on the atoms switched on, the system was relaxed for 1.0 ns at fixed volume and temperature; (v) system was annealed to room temperature, T = 300 K, during 1.0 ns time interval; (vi) this followed by NPT ensemble simulation run lasting 5 ns with target temperature T = 300 K and pressure P = 1.0 atm. Data collection was done during additional 2 ns long simulation run under NPT ensemble conditions. All simulations were performed using LAMMPS with GPU acceleration.[6] The final system densities are summarised in Table S3.

The specific surface area, a, was calculated as a ratio of the surface area, $A_{interface}$, of the interface between the isoidide and isommanide regions to the total system volume V_{sample} :

$$a = \frac{A_{interface}}{V_{sample}}$$

for the copolymer melts and polymer blends. The interfacial area was determined by calculating the area of interface between 3D density distribution of atoms belonging to IMPU and IIPU (or *vice versa*) assigned to the discrete grid points. The data are summarized in Table S4.

Physical Degradation Studies

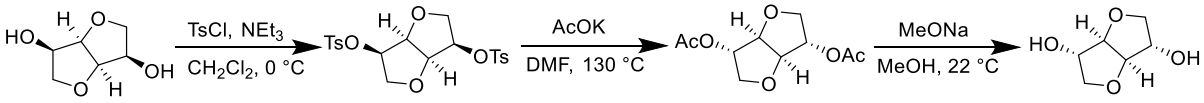
Accelerated degradation studies were conducted under conditions previously reported by Lam *et al*.[7] Polymer films were annealed for 3 d and then cut into "degradation disks" (*ca.* 0.1 g) and subjected to 1 M aq. NaOH at 25 °C. The disks were placed in individual vials containing 20 mL of the corresponding solution and incubated at 25 °C with constant agitation at 60 rpm. The surfaces of the disks were dried in order to remove excess water before the weight was measured periodically using an analytical balance.

Quantitative Degradation Studies

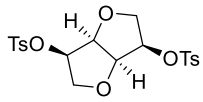
Hydrophobicity (i.e. *LogP/SA* values) was calculated with Materials Studio 2019. *LogP* values were extracted from the QSAR menu using the ALogP98 option. Connolly surface area (*SA*) was calculated with a 1.40 Å probe after conducting a Molecular Dynamics simulation of molecular models. The Forcite Geometry Optimization employed a Smart algorithm and COMPASS II forcefield to minimize the energy below certain specifications. Convergence tolerance for the Smart algorithm included a 1.0 x 10^{-3} kcal/mol energy convergence, a 0.005 kcal/mol/Å force convergence, and a 5.0 x 10^{-5} Å displacement convergence. To improve accuracy of *LogP/SA* values, multiple models ranging from 10, 12, and 14-monomer units were averaged.

Synthetic procedures

Overview for the 3-step synthesis of isoidide from isomannide

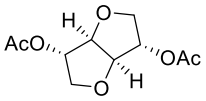


Synthesis of isomannide tosylate



A 250 mL round bottom flask was charged with isomannide (68.4 mmol, 10.0 g, 1.0 equiv), triethylamine (171.1 mmol, 23.8 mL, 2.5 equiv), dimethylaminopyridine (6.8 mmol, 0.84 g, 0.1 equiv) and dichloromethane (100 mL). The reaction mixture was cooled to 0 °C and then *p*-toluenesulfonyl chloride (143.7 mmol, 27.4 g, 2.1 equiv) was added portion-wise over several minutes. After the addition was complete, the reaction was stirred at 22 °C overnight (*ca.* 16 h). The mixture was transferred a 500 mL separatory funnel and washed with 1 M HCl (1 × 50 mL), water (2 × 50 mL), $NaHCO_3$ (1 × 50 mL) and brine (1 × 50 mL). The remaining organic phase was dried with $MgSO_4$ and concentrated *in vacuo* to afford an off-white solid (60.3 mmol, 27.4 g, 88% yield). The crude product was recrystallized in ethanol to produce a white crystalline solid (24.5 g, 79%). ^{1}H NMR (400 MHz, Chloroform-*d*) δ 7.84 – 7.76 (m, 4H), 7.38 – 7.30 (m, 4H), 4.84 (dddd, J = 7.7, 6.7, 3.8, 1.5 Hz, 2H), 4.50 – 4.43 (m, 2H), 3.91 (dd, J = 9.6, 6.7 Hz, 2H), 3.72 (dd, J = 9.5, 7.6 Hz, 2H), 2.45 (s, 6H). ^{13}C NMR (101 MHz, Chloroform-*d*) δ 145.46, 133.14, 130.07, 128.13, 80.07, 77.95, 70.23, 21.85. HRMS (TOF-MS-El$^+$) (*m*/*z*): $[M]^+$ calculated for $C_{20}H_{22}O_8S_2$, 454.0756; found, 454.0770.

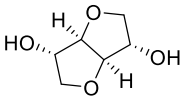
Synthesis of isoidide acetate



An oven-dried 500 mL 2-neck round bottom flask was charged with isomannide tosylate (66.0 mmol, 30.0 g, 1.0 equiv), potassium acetate (396.0 mmol, 38.9 g, 6.0 equiv) and 100 mL anhydrous DMF. The reaction was

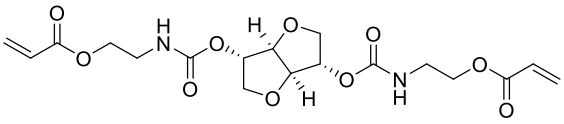
heated to 140 °C and checked by TLC after 4 h to reveal remaining tosylate starting material. Another portion of potassium acetate (15.0 g) was added and the mixture was stirred overnight (*ca*. 16 h total) after which TLC analysis revealed complete consumption of the tosylate compound. Note: we observed batch-to-batch variability for complete consumption of starting material ranging from 2 h at 130 °C to 24 h at 140 °C. The reaction was poured into 100 mL ice-water while it was warm (*ca*. 60 - 80 °C) and then transferred to a 500 mL separatory funnel. The mixture was extracted with EtOAc (4 × 75 mL) and the combined organic fractions were washed with water (5 × 50 mL), 5 % LiCl (5 × 50 mL) and brine (1 × 50 mL). The resultant organic phase was dried over $MgSO_4$ and concentrated in vacuo to afford an off-white solid (12.7 g, 84%) that darkened to a brown solid upon standing. The product was used without further purification. ^{1}H NMR (400 MHz, Chloroform-*d*) δ 5.27 – 5.13 (m, 2H), 4.63 (s, 2H), 4.00 – 3.84 (m, 4H), 2.08 (s, 6H). ^{13}C NMR (101 MHz, Chloroform-*d*) δ 170.09, 85.50, 77.74, 72.72, 21.06. HRMS (TOF-MS) (m/z): [M + H]+ calculated for $C_{10}H_{14}O_6$ + H, 231.0869; found, 231.0872.

Synthesis of isoidide



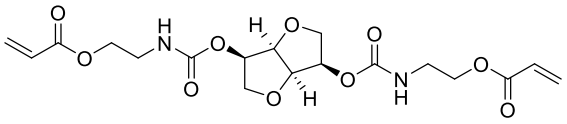
An oven-dried 100 mL 2-neck round bottom flask was charged with *isoidide acetate* (60.8 mmol, 14.0 g, 1.0 equiv), 50 mL anhydrous MeOH, and sodium methoxide (25 wt% solution in methanol) (5 mL, ~ 0.33 equiv). The reaction was stirred at 22 °C for 24 h and checked by TLC to confirm consumption of the acetate. Dowex® 50W X8 (3.0 g) was added and the mixture was stirred for 24 h. The reaction mixture was filtered into a 100 mL round bottom flask and the DOWEX resin was rinsed with MeOH (10 mL) and concentrated *in vacuo* to reveal a viscous oil. The oil was further dried overnight (*ca*. 16 h) at 100 mTorr pressure to afford a white solid (8.4 g, 95%) that was used without further purification. ^{1}H NMR (400 MHz, DMSO-d_6) δ 5.13 (d, J = 3.7 Hz, 2H), 4.31 (s, 2H), 4.02 (td, J = 3.5, 1.3 Hz, 2H), 3.61 (qd, J = 9.4, 2.4 Hz, 4H). ^{13}C NMR (101 MHz, DMSO-d_6) δ 87.14, 74.76, 74.01. HRMS (TOF-MS-ES$^+$) (m/z): [M]$^+$ calculated for $C_6H_{10}O_4$, 146.0579; found, 146.0565.

Synthesis of isoidide-urethane monomer



A 250 mL round bottom flask was charged with *isoidide* (27.3 mmol, 4.0 g, 1.0 equiv), 2-isocyanatoethyl acrylate (66.2 mmol, 9.34 g, 2.4 equiv), 50 mg BHT (to inhibit radical crosslinking) and 50 mL THF. Dibutyltin dilaurate (0.16 mmol, 97.3 µL, 0.006 equiv) was added in one portion to the reaction mixture, causing a mild exotherm. The mixture stirred at 22 °C overnight (*ca*. 16 h) and checked by TLC to confirm consumption of isoidide. Approximately half the solvent volume was removed *in vacuo* causing some precipitate to form. The reaction was diluted with 200 mL of cyclohexane and stirred for 1 h causing more precipitate to form. The precipitate was filtered and washed with cyclohexane (2 × 100 mL) to afford a white solid. The crude solid was purified using flash column chromatography (R_f = 0.6, EtOAc), eluting with 100% EtOAc to afford a white crystalline solid (8.3 g, 71%). ^{1}H NMR (400 MHz, Chloroform-*d*) δ 6.44 (dd, J = 17.3, 1.4 Hz, 2H), 6.13 (dd, J = 17.3, 10.4 Hz, 2H), 5.88 (dd, J = 10.5, 1.4 Hz, 2H), 5.17 – 5.11 (m, 2H), 5.04 (s, 2H), 4.61 (minor rotamer), 4.25 (t, J = 5.2 Hz, 4H), 3.98 – 3.86 (m, 4H), 3.50 (q, J = 5.5 Hz, 4H). ^{13}C NMR (101 MHz, Chloroform-*d*) δ 166.20, 155.19, 131.77, 128.02, 85.47, 78.29, 72.77, 63.55, 40.40. HRMS (TOF-MS) (m/z): [M + H]$^+$ calculated for $C_{18}H_{24}O_{10}N_2$ + H, 429.1509; found, 429.1504. Anal. Calcd for $C_{18}H_{24}O_{10}N_2$: C, 50.47; H, 5.65; N, 6.54. Found: C, 50.39; H, 5.68; N, 6.77. FTIR 3332 cm^{-1} (N-H) 1725 cm^{-1} (C=O ester) 1696 cm^{-1} (C=O urethane).

Synthesis of isomannide-urethane monomer



A 250 mL round bottom flask was charged with *isomannide* (51.3 mmol, 7.5 g, 1.0 equiv), 2-isocyanatoethyl acrylate (123.1 mmol, 15.9 g, 2.4 equiv), 50 mg BHT (to inhibit radical crosslinking), 40 mL THF and 10 mL DMF. Dibutyltin dilaurate (0.10 mmol, 61.1 μL, 0.002 equiv) was added in one portion to the reaction mixture, causing a mild exotherm. The mixture stirred at 22 °C overnight (*ca*. 16 h) and checked by TLC to confirm consumption of isomannide. Approximately half of the solvent volume was removed *in vacuo* and then the mixture was cooled to 0 °C, causing the product to precipitate. The product was filtered and washed with diethyl ether (2 × 100 mL) to reveal a white solid. The crude product was recrystallized from a mixture of *n*-hexane/EtOAc to yield white needles (17.5 g, 80 %). ^{1}H NMR (400 MHz, Chloroform-*d*) δ 6.43 (dd, J = 17.3, 1.4 Hz, 2H), 6.12 (dd, J = 17.3, 10.4 Hz, 2H), 5.87 (dd, J = 10.4, 1.4 Hz, 2H), 5.16 (s, 2H) 5.13 – 5.06 (m, 2H), 4.83 (minor rotamer), 4.67 (d, J = 4.2 Hz, 1H), 4.25 (t, J = 5.3 Hz, 2H), 4.07 (dd, J = 9.2, 6.5 Hz, 1H), 3.82 – 3.74 (m, 1H), 3.51 (p, J = 5.5 Hz, 2H). ^{13}C NMR (101 MHz, Chloroform-*d*) δ 166.14, 155.56, 131.70, 128.03, 80.95, 74.42, 70.65, 63.57, 40.42. HRMS (TOF-MS) (*m*/*z*): $[M + H]^+$ calculated for $C_{18}H_{24}O_{10}N_2$ + H, 429.1509; found, 429.1510. Anal. Calcd for $C_{18}H_{24}O_{10}N_2$: C, 50.47; H, 5.65; N, 6.54. Found: C, 50.97; H, 5.61; N, 6.60. FTIR 3321 cm^{-1} (N-H) 1731 cm^{-1} (C=O ester) 1691 cm^{-1} (C=O urethane).

Representative step-growth polymerization procedure

A 50 mL round bottom flask was charged with isohexide-urethane (2.40 g, 5.61 mmol, 1.00 equiv) and a separate 20 mL scintillation vial was charged with 1,8-octanedithiol (1.00 g, 5.61 mmol, 1.00 equiv). The thiol was quantitatively transferred to the round bottom flask containing isohexide-urethane monomer using $CHCl_3$ (11 mL) for a final monomer concentration of ~0.5 M. The reaction mixture was cooled to −10 °C in a brine ice-bath and dimethylphenylphosphine (8.0 μL, 0.56 mmol, 0.01 equiv) was injected in one portion causing an exotherm. After the exotherm, the reaction was stirred at 22 °C for 3 h and then diluted to approximately 50 mL with $CHCl_3$. The polymer solution was precipitated into methanol and dried *in vacuo* at ambient temperature for 24 h and then at 100 °C overnight for *ca*. 16 h.

IIPU

Yield = 2.74 g, 84%. SEC analysis ($CHCl_3$ + 0.5% NEt_3) M_w = 117.1 kDa, M_n = 14.4 kDa, M_p = 103.8 kDa, $Đ_M$ = 8.12. ^{1}H NMR (400 MHz, Chloroform-*d*) δ 5.26 (t, J = 6.0 Hz, 2H), 5.12 (s, 2H), 4.60 (s, 2H), 4.19 (t, J = 5.2 Hz, 4H), 3.92 (d, J = 2.9 Hz, 4H), 3.45 (q, J = 5.6 Hz, 4H), 2.78 (td, J = 7.2, 0.8 Hz, 4H), 2.63 (td, J = 7.2, 0.8 Hz, 4H), 2.57 – 2.46 (m, 4H), 1.61 – 1.53 (m, 4H), 1.44 – 1.25 (m, 8H). ^{13}C NMR (101 MHz, Chloroform-*d*) δ 172.04, 155.30, 85.47, 78.27, 72.73, 63.62, 40.27, 34.79, 32.23, 29.58, 29.18, 28.86, 27.11.

IMPU

Yield = 3.07 g, 89%. SEC analysis ($CHCl_3$ + 0.5% NEt_3) M_w = 95.6 kDa, M_n = 9.9 kDa, M_p = 87.1 kDa, $Đ_M$ = 9.69. ^{1}H NMR (400 MHz, Chloroform-*d*) δ 5.34 (s, 2H), 5.09 (s, 2H), 4.77 – 4.57 (m, 2H), 4.28 – 4.12 (m, 4H), 4.06 (dd, J = 9.1, 6.6 Hz, 2H), 3.89 – 3.71 (m, 2H), 3.46 (p, J = 5.4 Hz, 4H), 2.77 (td, J = 7.2, 0.8 Hz, 4H), 2.62 (td, J = 7.2, 0.8 Hz, 4H), 2.57 – 2.48 (m, 4H), 1.63 – 1.51 (m, 5H), 1.44 – 1.24 (m, 8H). ^{13}C NMR (101 MHz, Chloroform-*d*) δ 172.01, 155.64, 80.90, 74.40, 70.57, 63.63, 40.29, 34.79, 32.24, 29.59, 29.18, 28.87, 27.04.

***co*-$\mathbf{II_{50}IM_{50}}$**

Yield = 2.84 g, 85%. SEC analysis ($CHCl_3$ + 0.5% NEt_3) M_w = 79.6 kDa, M_n = 10.2 kDa, M_p = 68.3 kDa, $Đ_M$ = 7.81. ^{1}H NMR (400 MHz, Chloroform-*d*) δ 5.33 (s, 2H), 5.25 (s, 2H), 5.10 (d, J = 18.7 Hz, 4H), 4.72 – 4.54 (m, 4H), 4.26 – 4.12 (m, 4H), 4.06 (dd, J = 9.1, 6.6 Hz, 2H), 3.91 (d, J = 2.8 Hz, 2H), 3.76 (t, J = 8.2 Hz, 1H), 3.46 (dq, J = 10.5, 5.5 Hz, 4H), 2.77 (tdd, J = 7.2, 2.4, 0.9 Hz, 4H), 2.67 – 2.58 (m, 4H), 2.52 (td, J = 7.4, 1.1 Hz, 4H), 1.57 (p, J = 7.7, 7.3 Hz, 4H), 1.44 – 1.26 (m, 8H). ^{13}C NMR (101 MHz, Chloroform-*d*) δ 172.01, 155.64, 85.46, 80.90, 78.26, 74.40, 72.73, 70.57, 63.62, 40.28, 34.79, 32.24, 29.58, 29.18, 28.87, 27.10, 27.04.

***co*-$\mathbf{II_{25}IM_{75}}$**

Yield = 2.92 g, 86%. SEC analysis ($CHCl_3$ + 0.5% NEt_3) M_w = 89.9 kDa, M_n = 9.0 kDa, M_p = 72.4 kDa, $Đ_M$ = 9.95.

***co*-$\mathbf{II_{75}IM_{25}}$**

Yield = 2.90 g, 86%. SEC analysis ($CHCl_3$ + 0.5% NEt_3) M_w = 81.1 kDa, M_n = 10.4 kDa, M_p = 74.5 kDa, $Đ_M$ = 7.77.

Physical blending procedure to make *bl*-$\mathbf{II_xIM_y}$

IIPU and IMPU were combined in the indicated ratios (1.2 g polymer total: 0.6 g IIPU + 0.6 g IMPU; 0.3 g IIPU + 0.9 g IMPU; 0.9 g IIPU + 0.3 g IMPU) in a 20 mL scintillation vial and dissolved in 10 mL $CHCl_3$. After the polymers were fully solubilized, the solution was poured onto a teflon sheet (~ 10 × 10 cm) where it evaporated to dryness over several hours to afford a blended homopolymer sample. The materials were then further dried *in vacuo* at 100 °C overnight (*ca*. 16 h) to ensure complete solvent removal before heated compression molding.

Thermogravimetric analysis of polymer samples

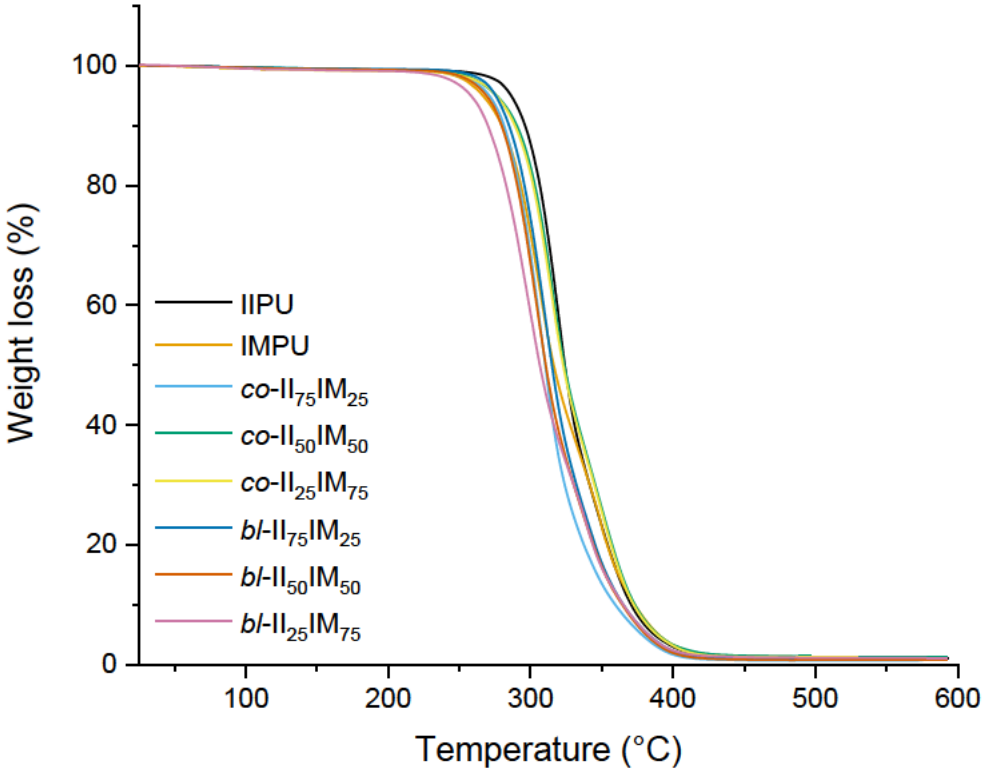
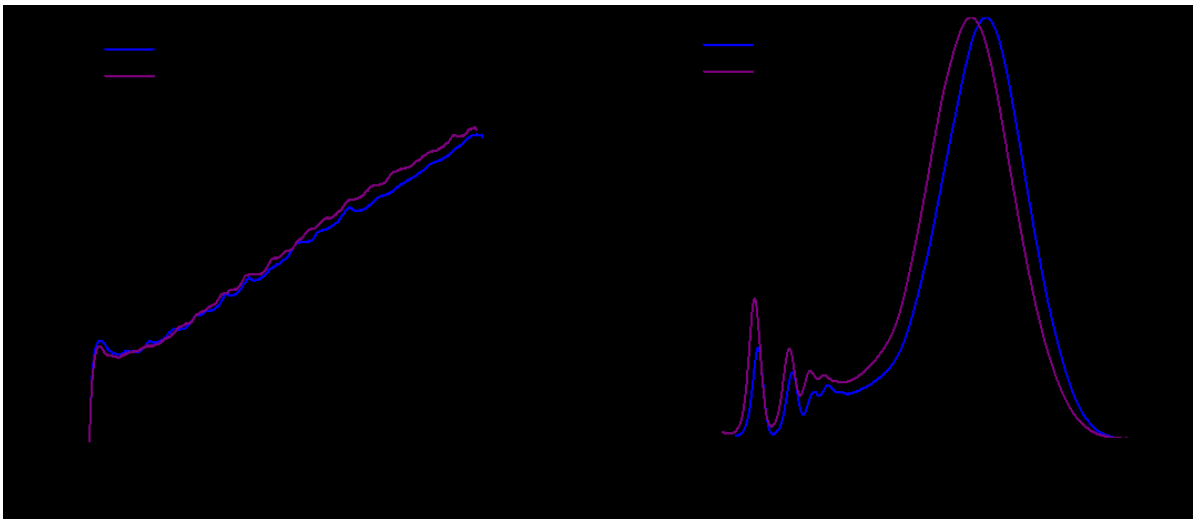


Figure S1.

Thermogravimetric analysis of polymer samples measured at a heating rate of 10 K·min^{-1} from ambient temperature (~22 °C) to 600 °C.

Mechanical recycling of IIPU



	M_w (kDa)	$Đ_M$	E (MPa)	σ_b (MPa)	ε_b(%)	U_T (MJm^{-3})
IIPU	98.0	7.71	255±37	46±4	1159±130	312±49
IIPU recycled	74.0	8.68	210±53	44±2	1088±70	295±25

Figure S2.

Summary of IIPU Mechanical recycling: Representative tensile curves of 3-day annealed IIPU and recycled IIPU n = 3 (left) Normalized size exclusion chromatograms of IIPU and recycled IIPU ($CHCl_3$, 0.5% NEt_3) analysis against poly(styrene) (PS) standards (right).

Simulation of the homopolymer conformations

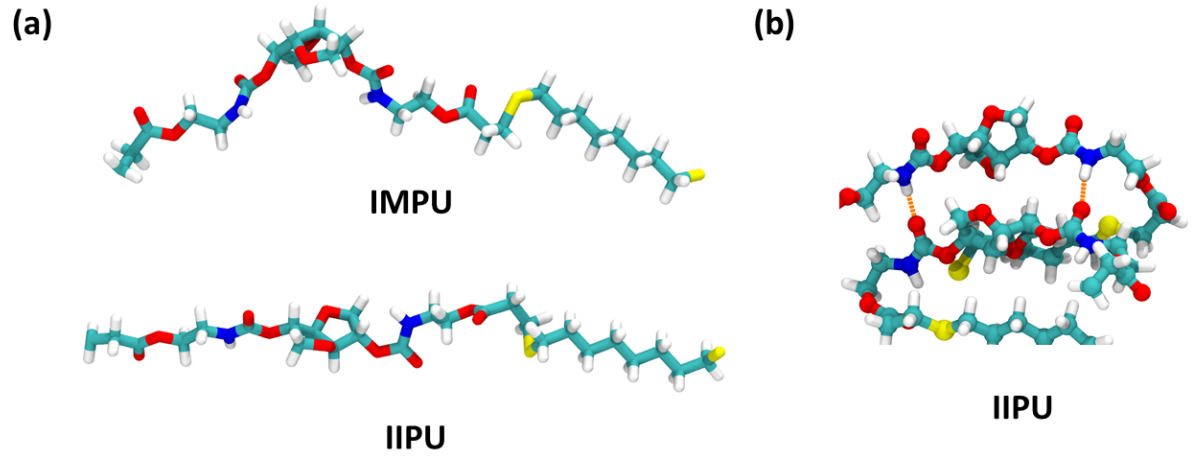


Figure S3.
(a) Local conformation differences of IIPU and IMPU as a direct result of the isohexide center. (b) Hydrogen bonding formed in the IIPU chain.

Thermomechanical characterization of copolymers

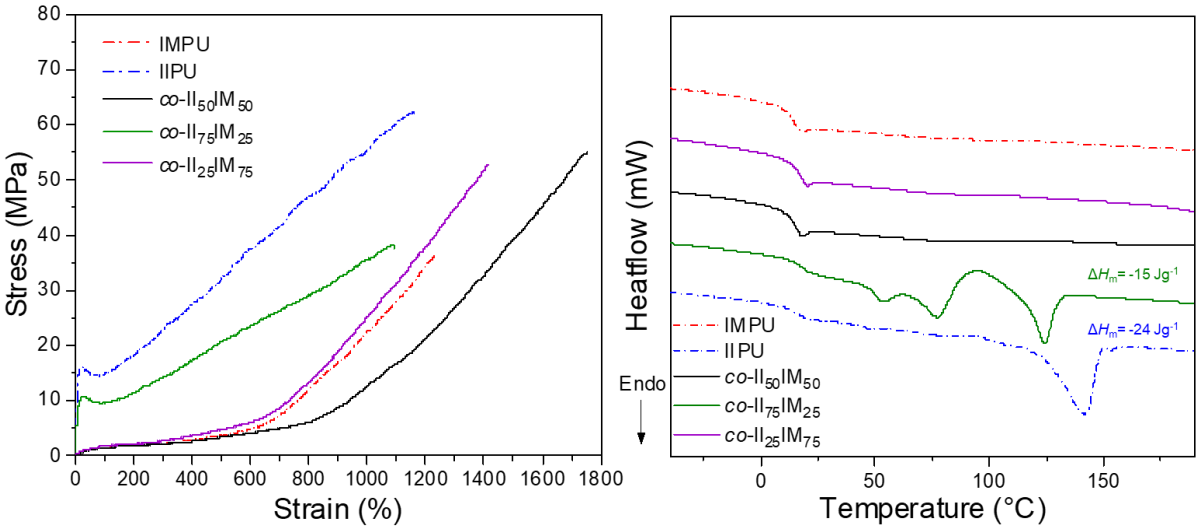


Figure S4.

Representative tensile curves of isoidide and isomannide homopolymers and copolymers at 10 mm·min^{-1} strain rate (left). Initial heating run of 3-day annealed isoidide and isomannide homopolymers and copolymers at a 10 K·min^{-1} heating rate (right).

Note: Complete tensile data and heating runs of each sample can be found below.

Thermomechanical characterization of physical blends

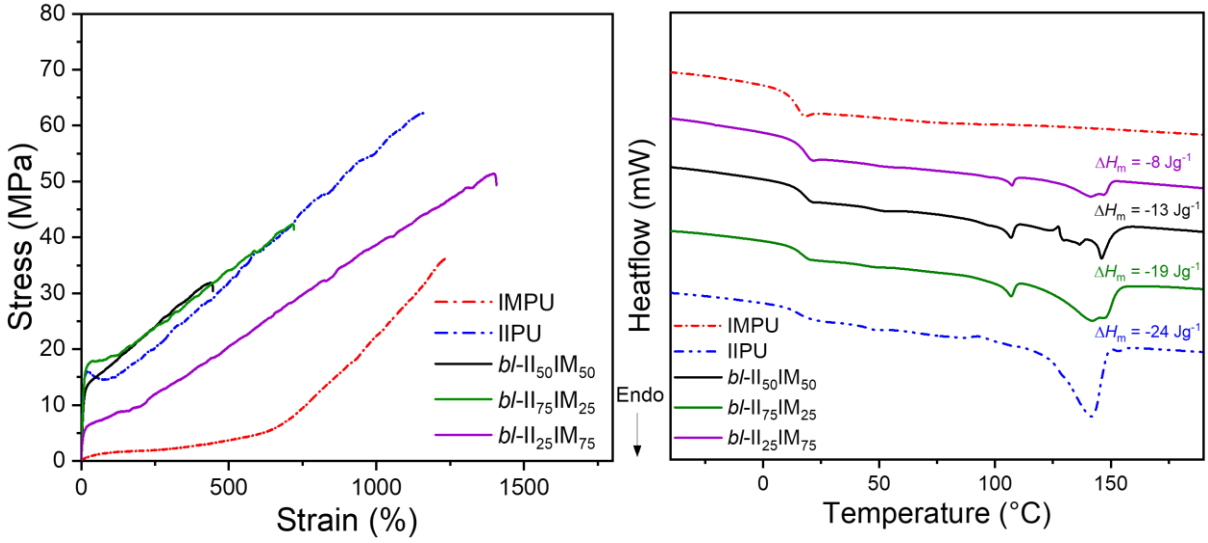


Figure S5.

Representative tensile curves of isoidide and isomannide homopolymers and physical blends at 10 mm·min^{-1} strain rate (left). Initial heating run of 3-day annealed isoidide and isomannide homopolymers and physical blends at a 10 K·min^{-1} heating rate (right).

Note: Complete tensile data and heating runs of each sample can be found below.

Bulk system molecular dynamics simulations

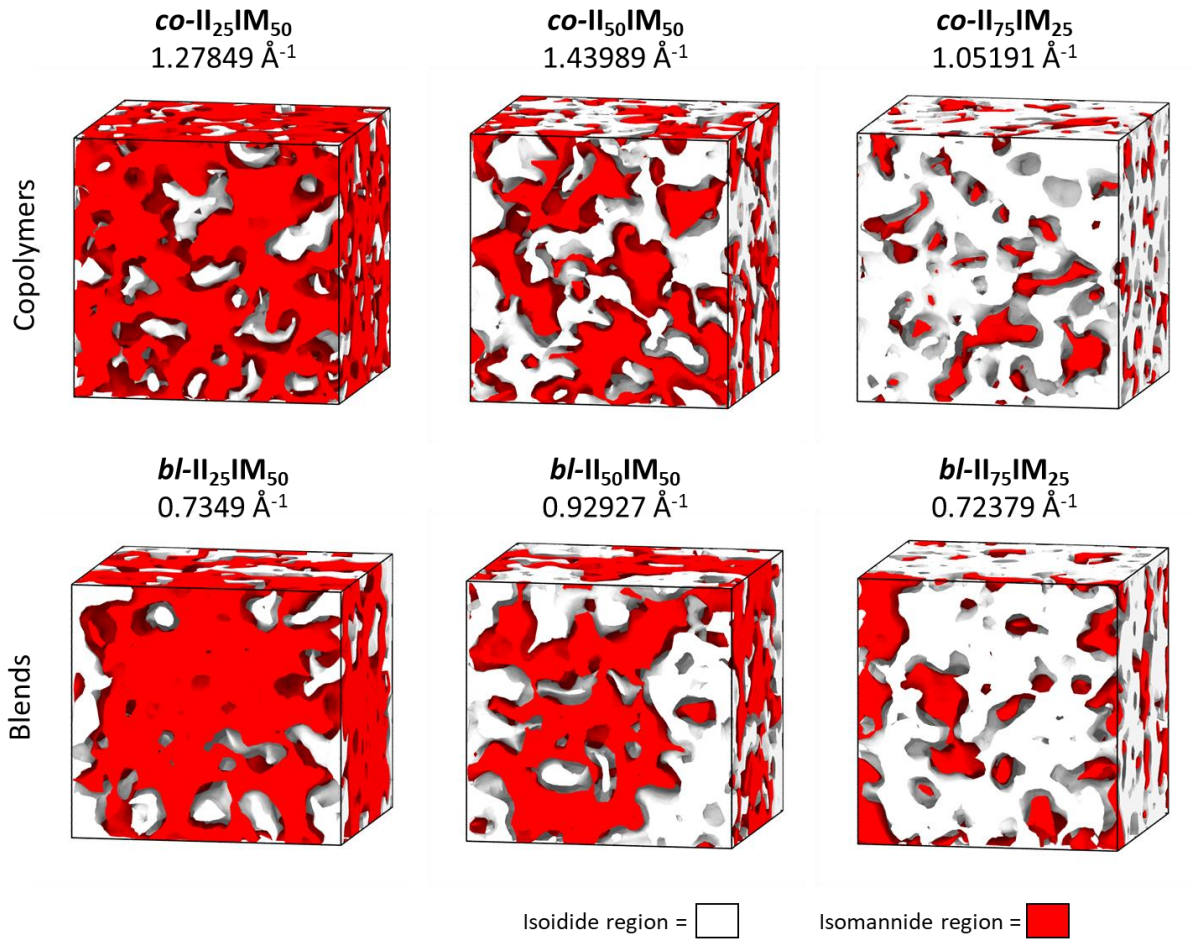


Figure S6.

Molecular dynamics bulk simulations of isoidide and isommanide copolymers and physical blends. Calculated interfacial surface area displayed.

Simulation details of polymer model

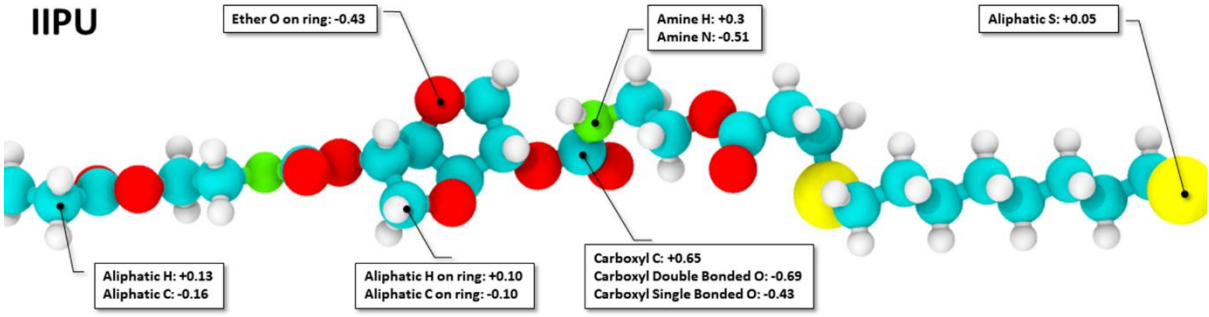


Figure S7.
Partial charge distribution on a polymer repeat unit (IIPU shown).

NMR Spectra

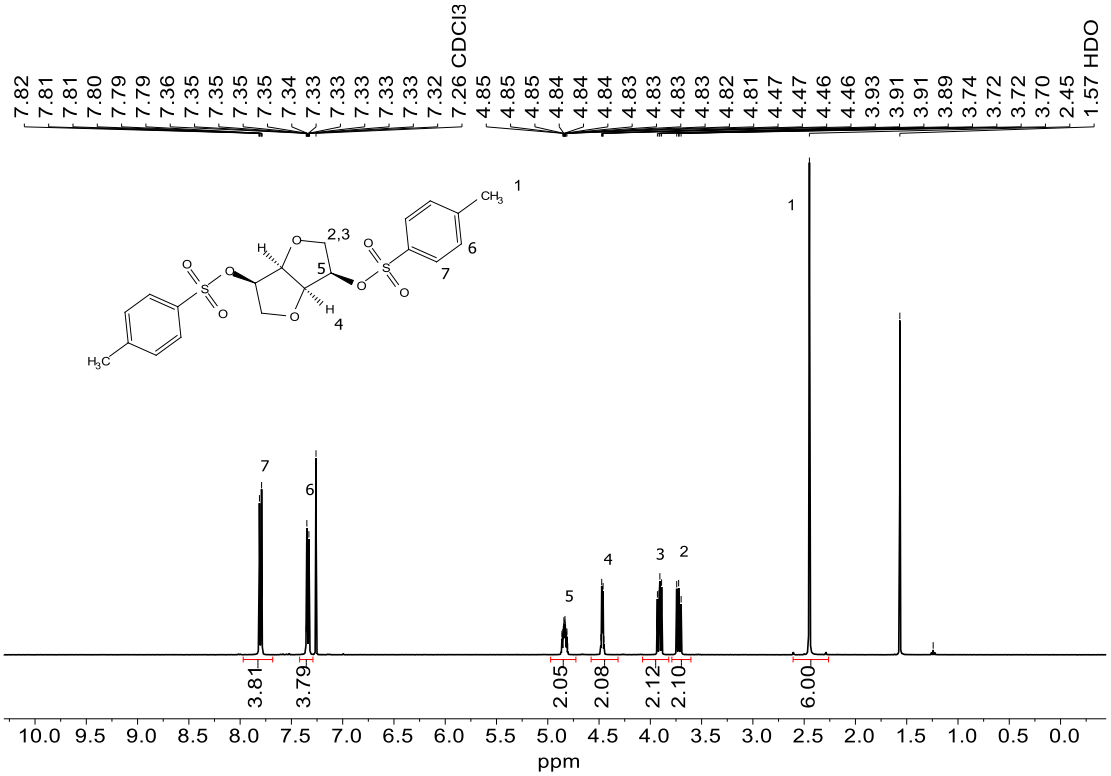


Figure S8.

^{1}H NMR spectrum of *isomannide tosylate* (400 MHz, 298 K, $CDCl_3$)

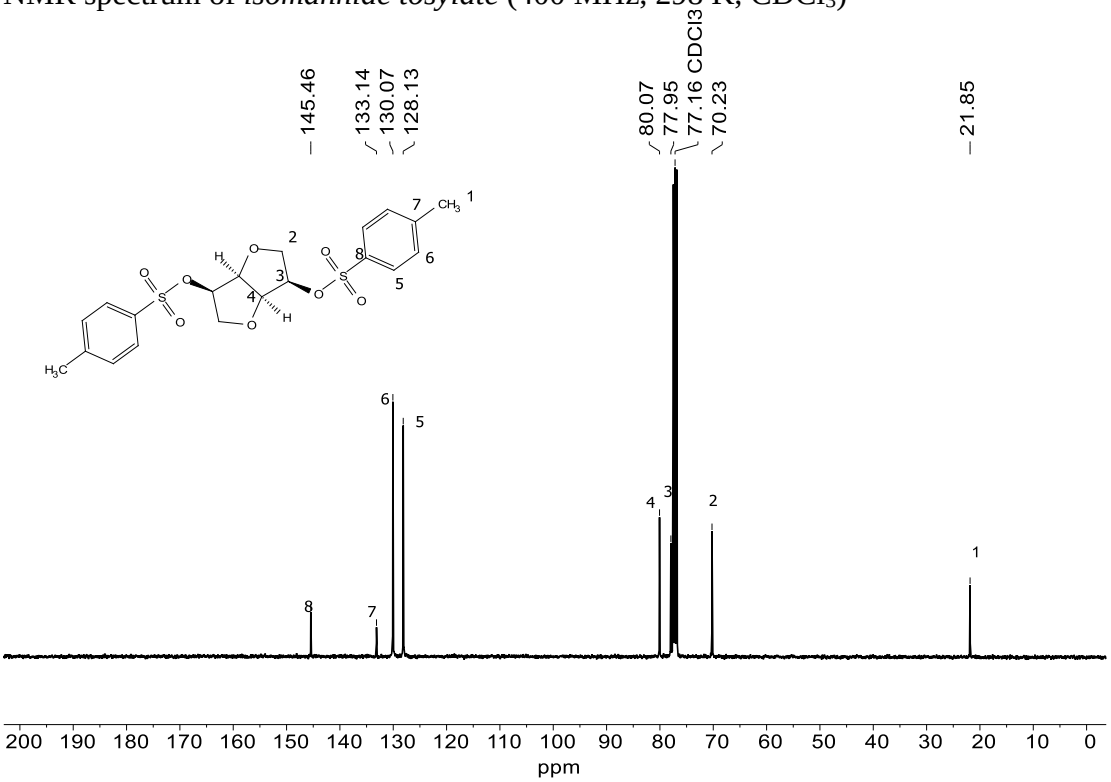


Figure S9.

^{13}C NMR spectrum of *isomannide tosylate* (100.57 MHz, 298 K, $CDCl_3$)

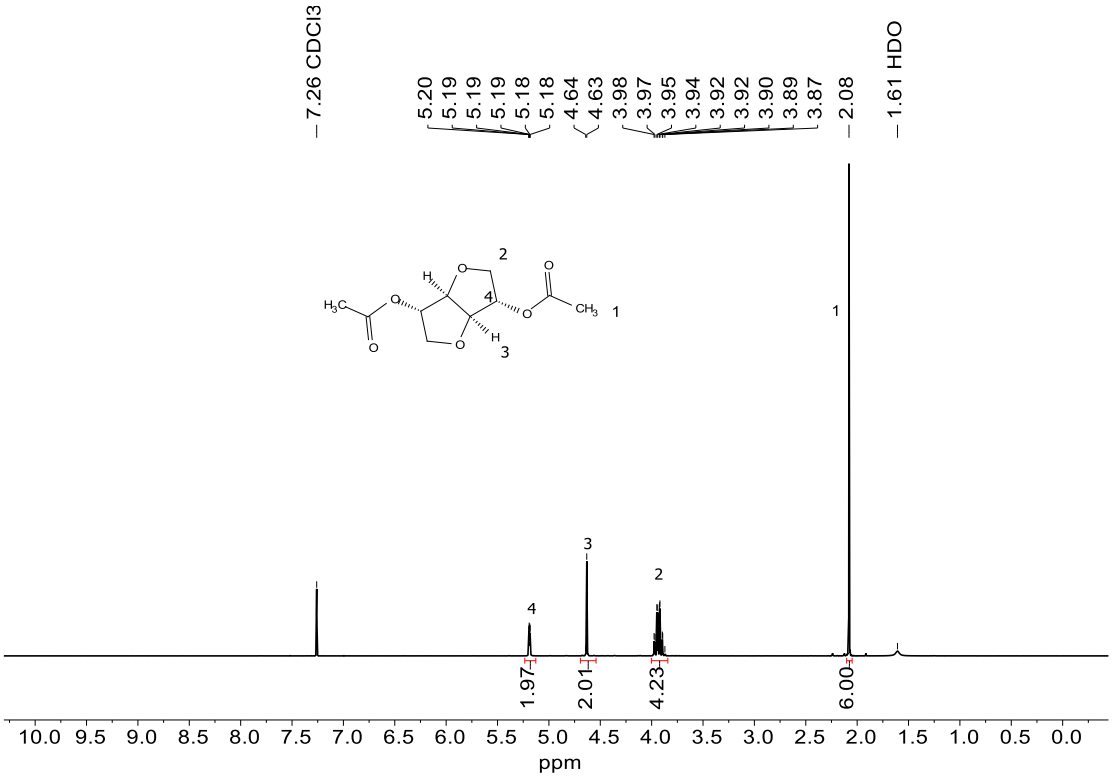


Figure S10.

^{1}H NMR spectrum of *isoidide acetate* (400 MHz, 298 K, $CDCl_3$)

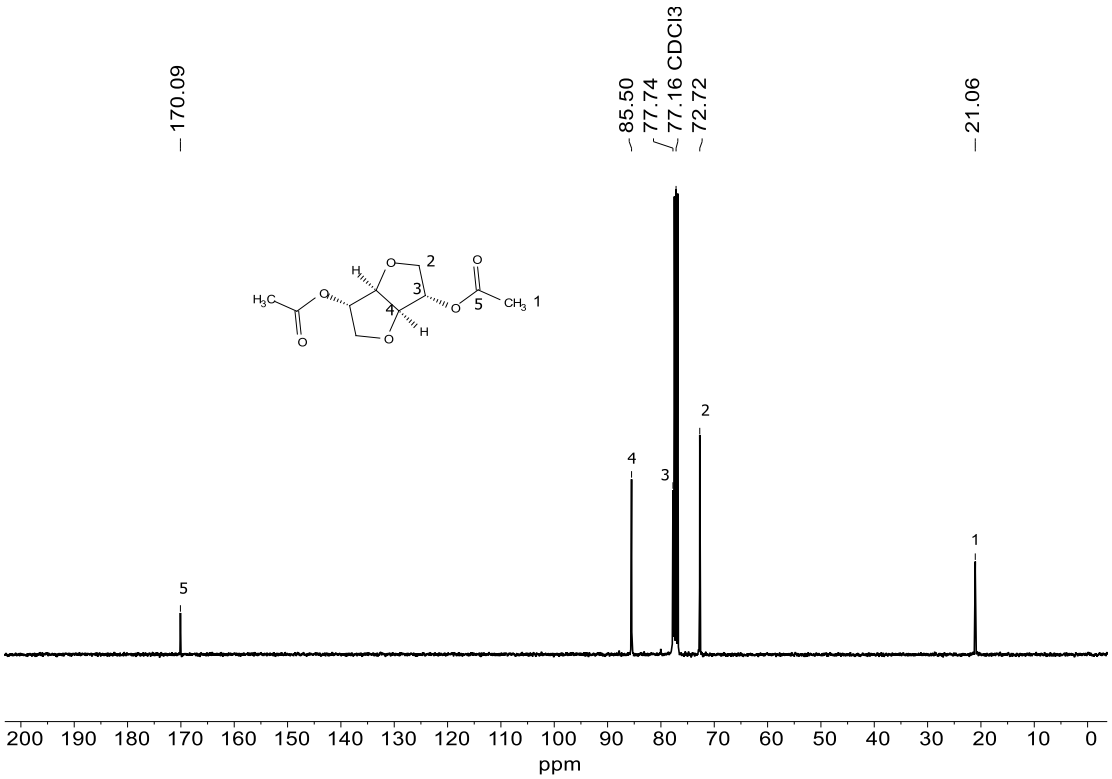


Figure S11.

^{13}C NMR spectrum of *isoidide acetate* (100.57 MHz, 298 K, $CDCl_3$)

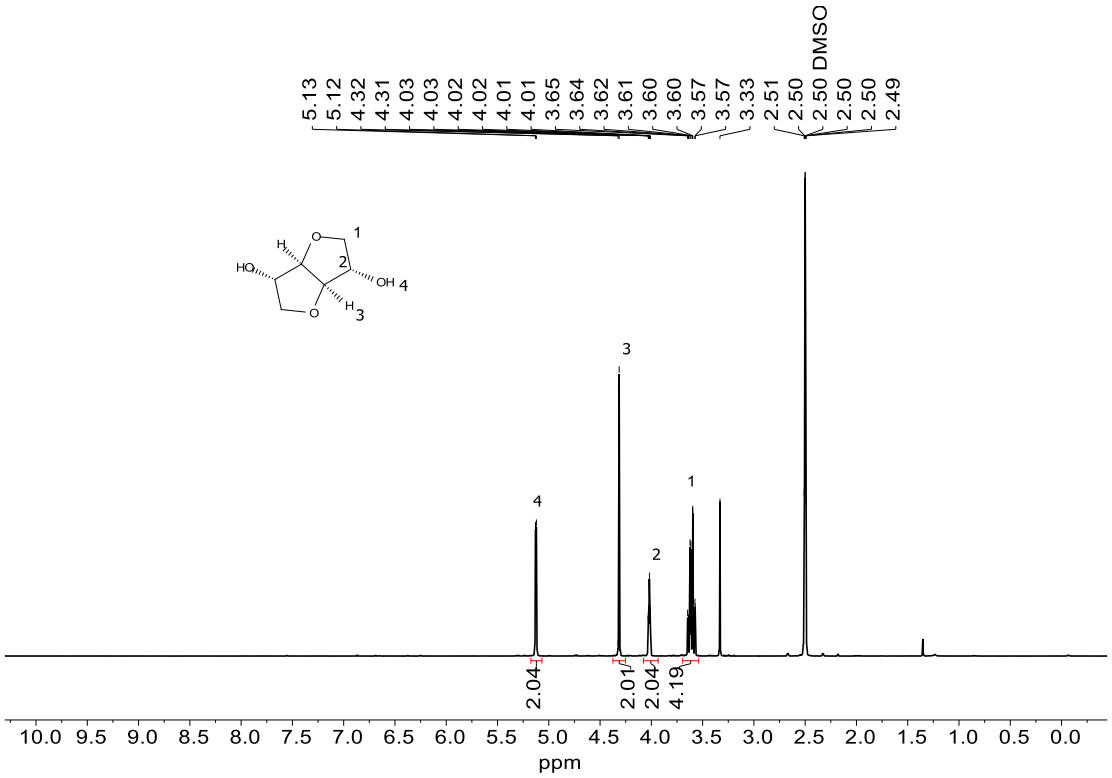


Figure S12.

^{1}H NMR spectrum of *isoidide* (400 MHz, 298 K, DMSO)

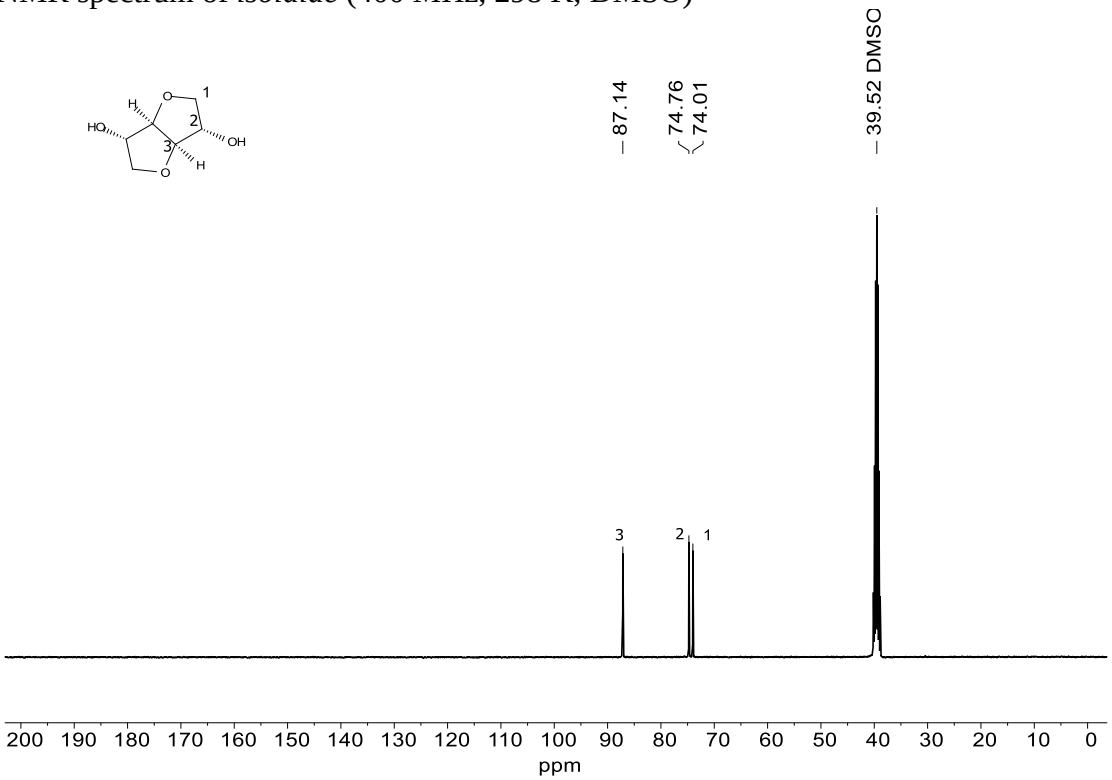


Figure S13.

^{13}C NMR spectrum of *isoidide* (100.57 MHz, 298 K, DMSO)

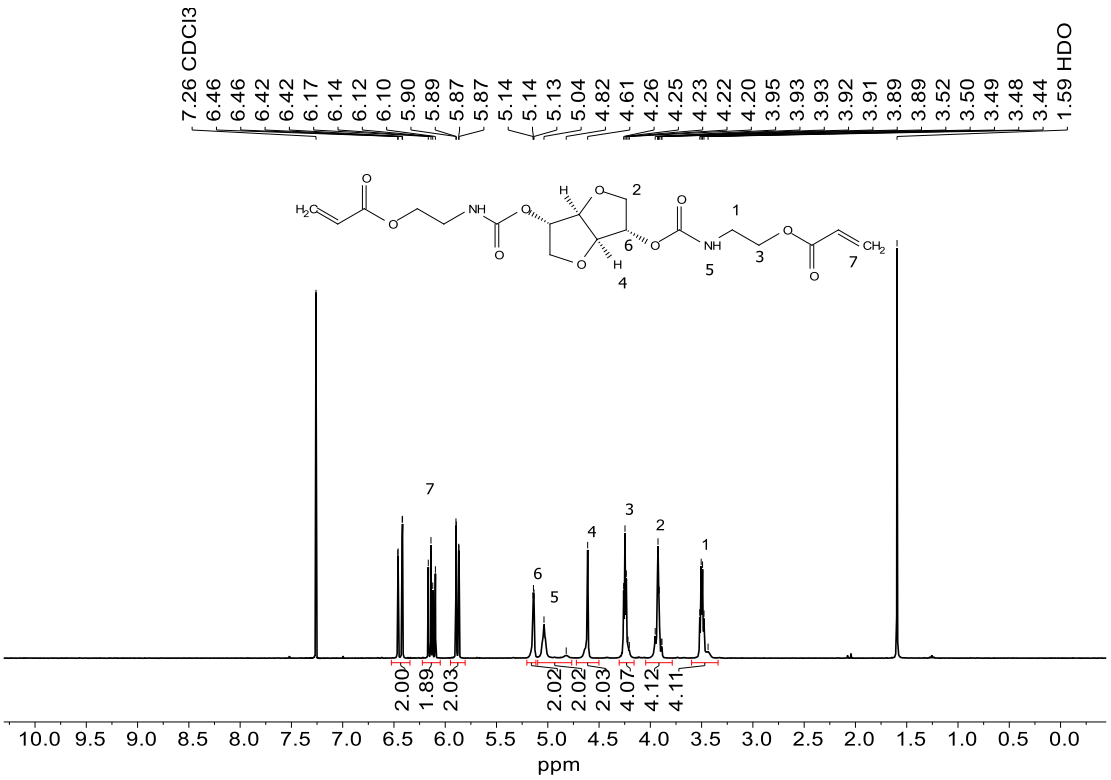


Figure S14.

^{1}H NMR spectrum of *isoidide urethane* (400 MHz, 298 K, $CDCl_3$)

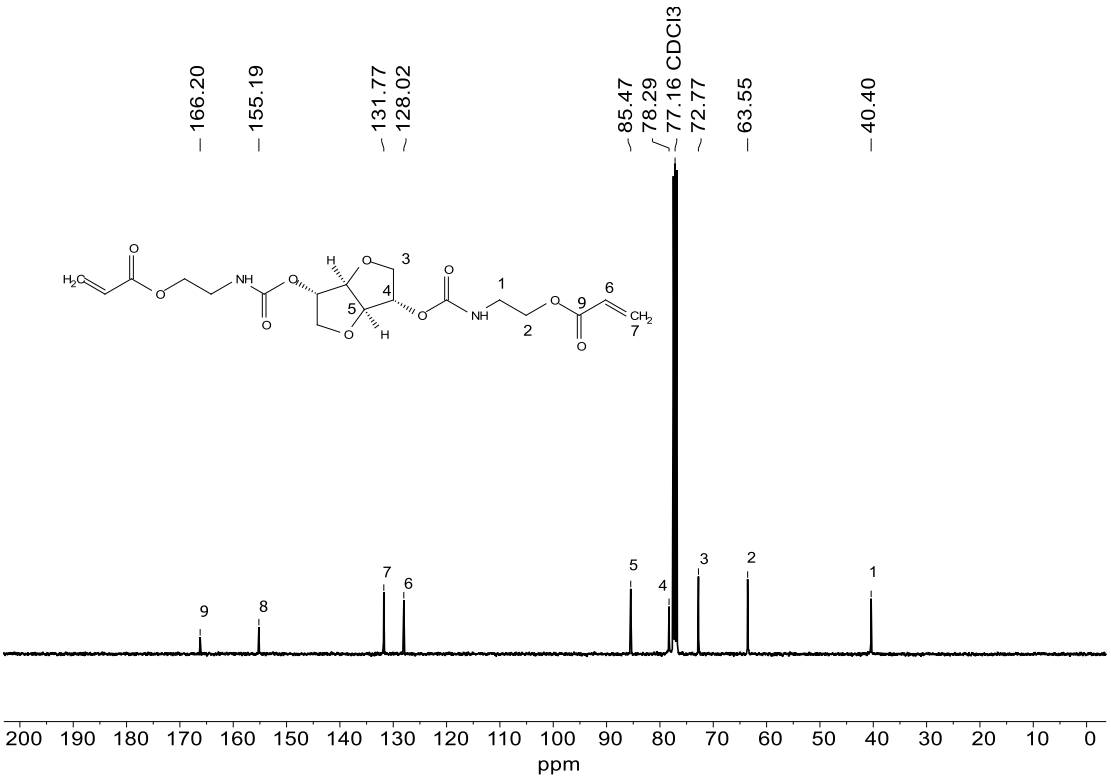


Figure S15.

^{13}C NMR spectrum of *isoidide urethane* (100.57 MHz, 298 K, $CDCl_3$)

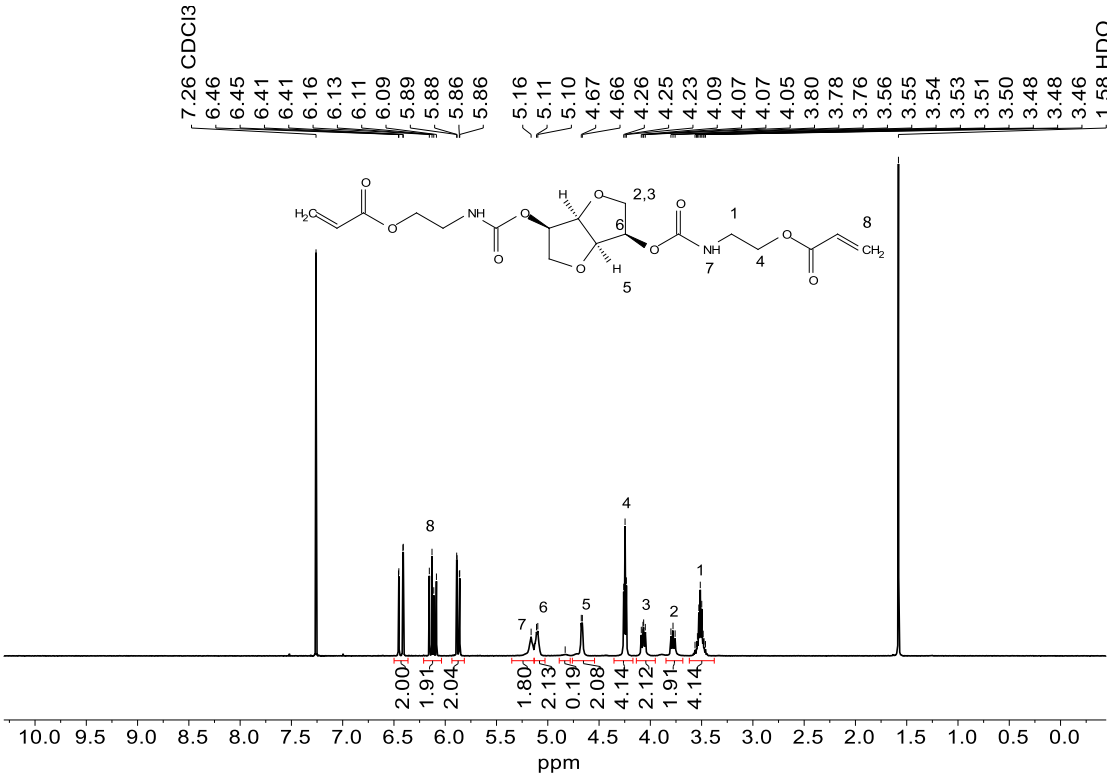


Figure S16.

^{1}H NMR spectrum of *isomannide urethane* (400 MHz, 298 K, $CDCl_3$).

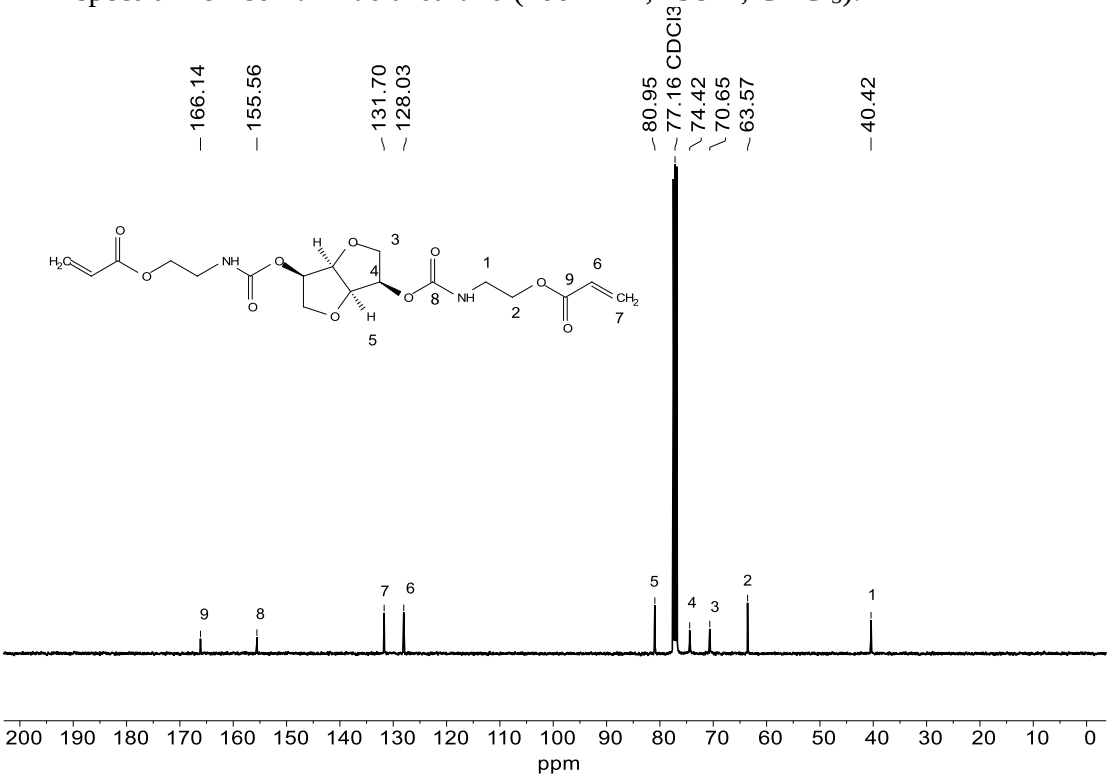


Figure S17.

^{13}C NMR spectrum of *isomannide urethane* (100.57 MHz, 298 K, $CDCl_3$).

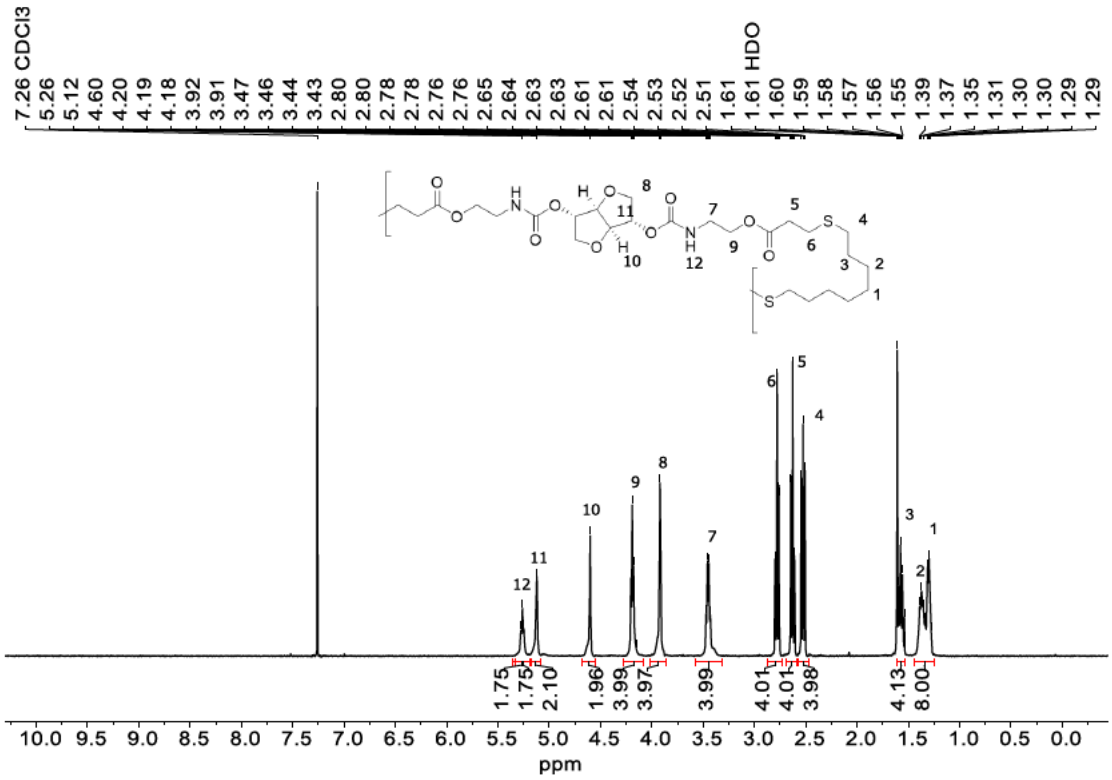


Figure S18.

^{1}H NMR spectrum of *IIPU* (400 MHz, 298 K, $CDCl_3$).

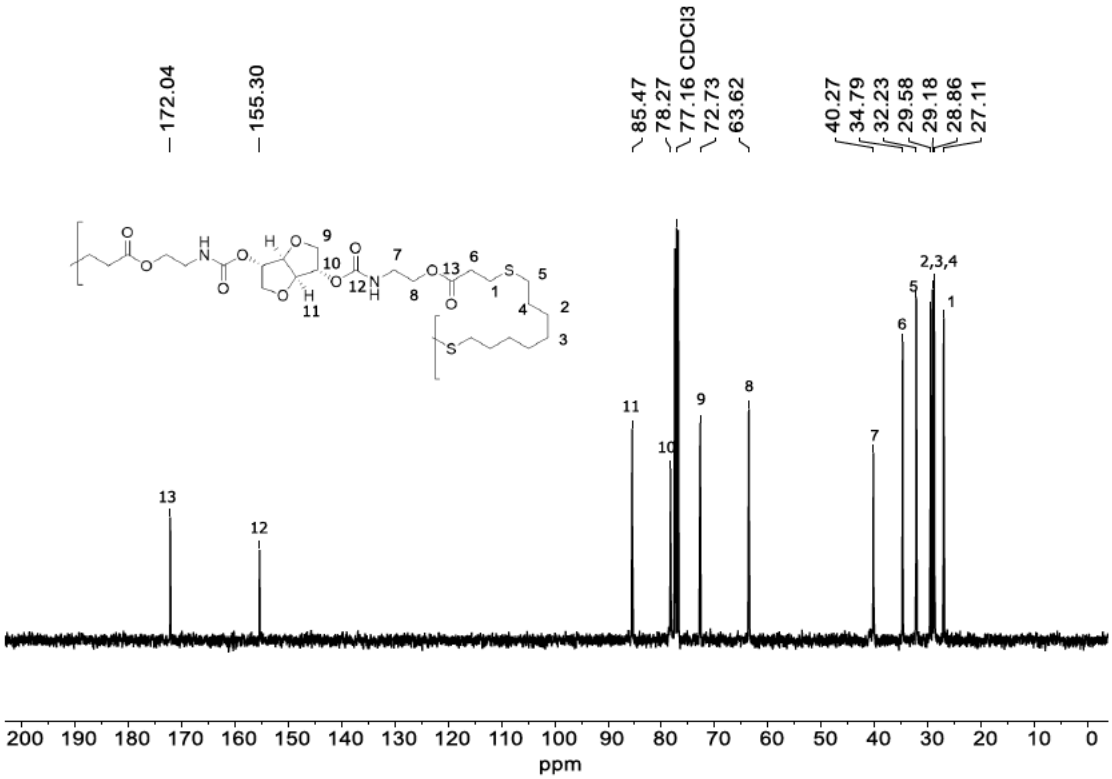


Figure S19.

^{13}C NMR spectrum of *IIPU* (100.57 MHz, 298 K, $CDCl_3$).

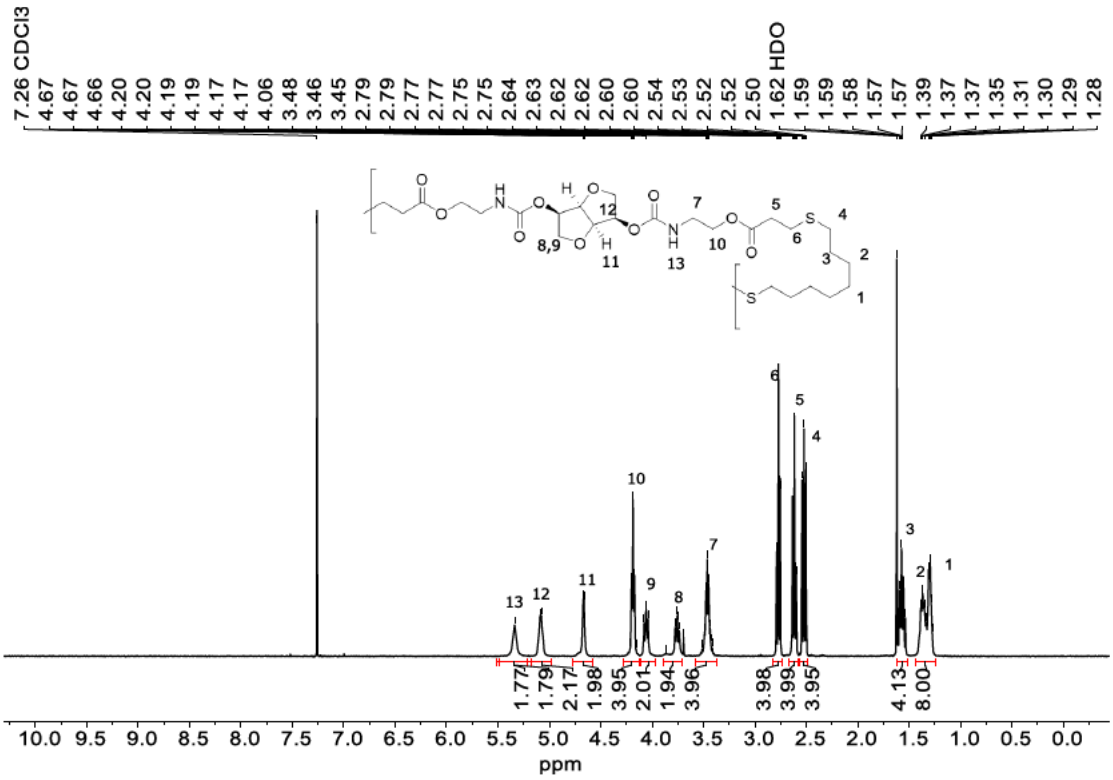


Figure S20.

^{1}H NMR spectrum of *IMPU* (400 MHz, 298 K, $CDCl_3$)

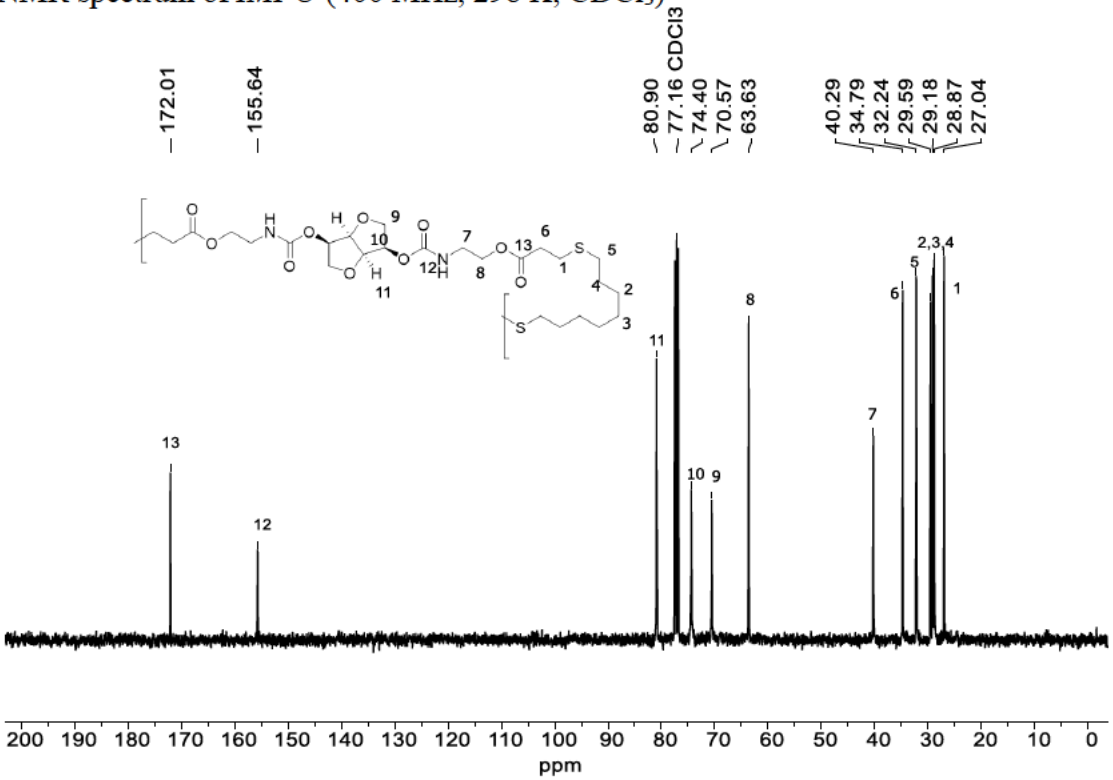


Figure S21.

^{13}C NMR spectrum of *IMPU* (100.57 MHz, 298 K, $CDCl_3$)

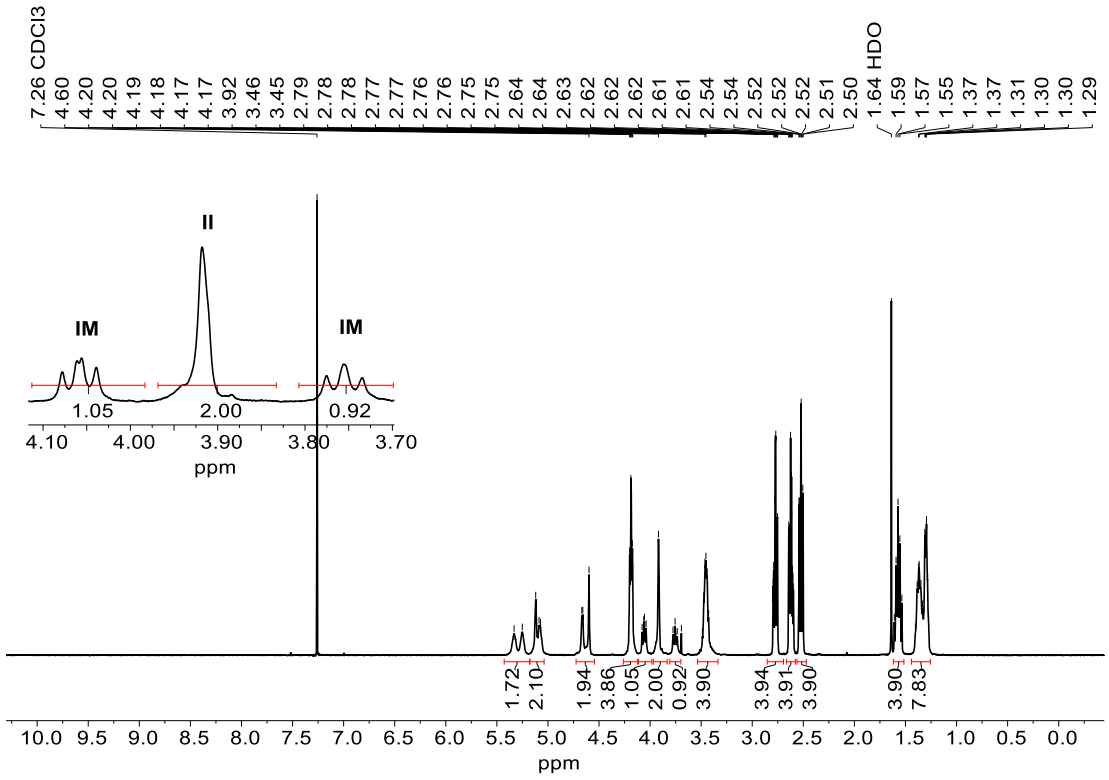


Figure S22.

^{1}H NMR spectrum of *co-II*$_{50}$*IM*$_{50}$ (400 MHz, 298 K, $CDCl_3$)

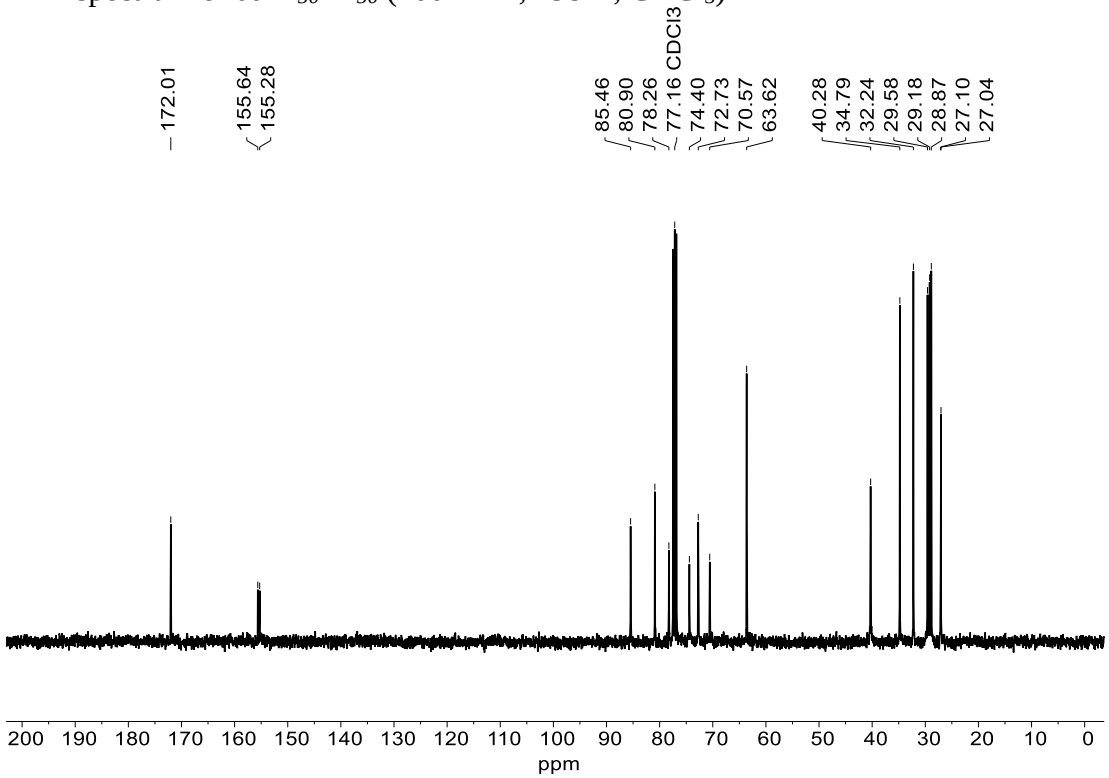


Figure S23.

^{13}C NMR spectrum of *co-II*$_{50}$*IM*$_{50}$ (100.57 MHz, 298 K, $CDCl_3$).

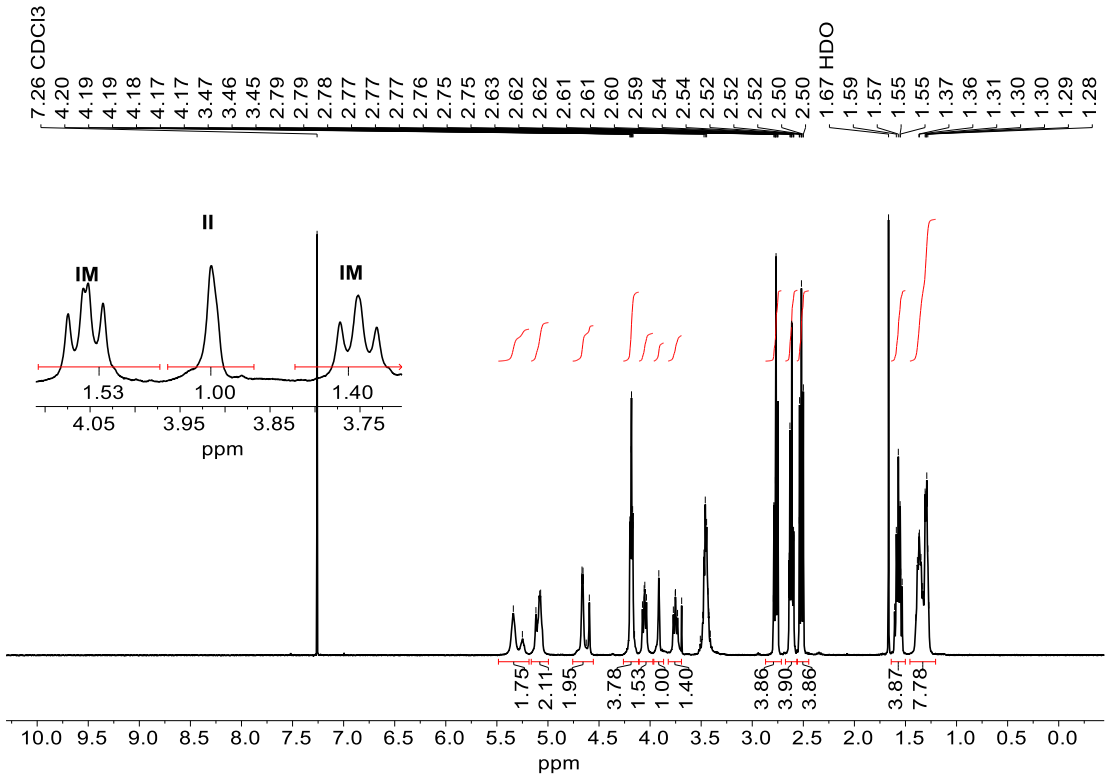


Figure S24.

^{1}H NMR spectrum of *co-II*$_{25}$*IM*$_{75}$ (400 MHz, 298 K, $CDCl_3$).

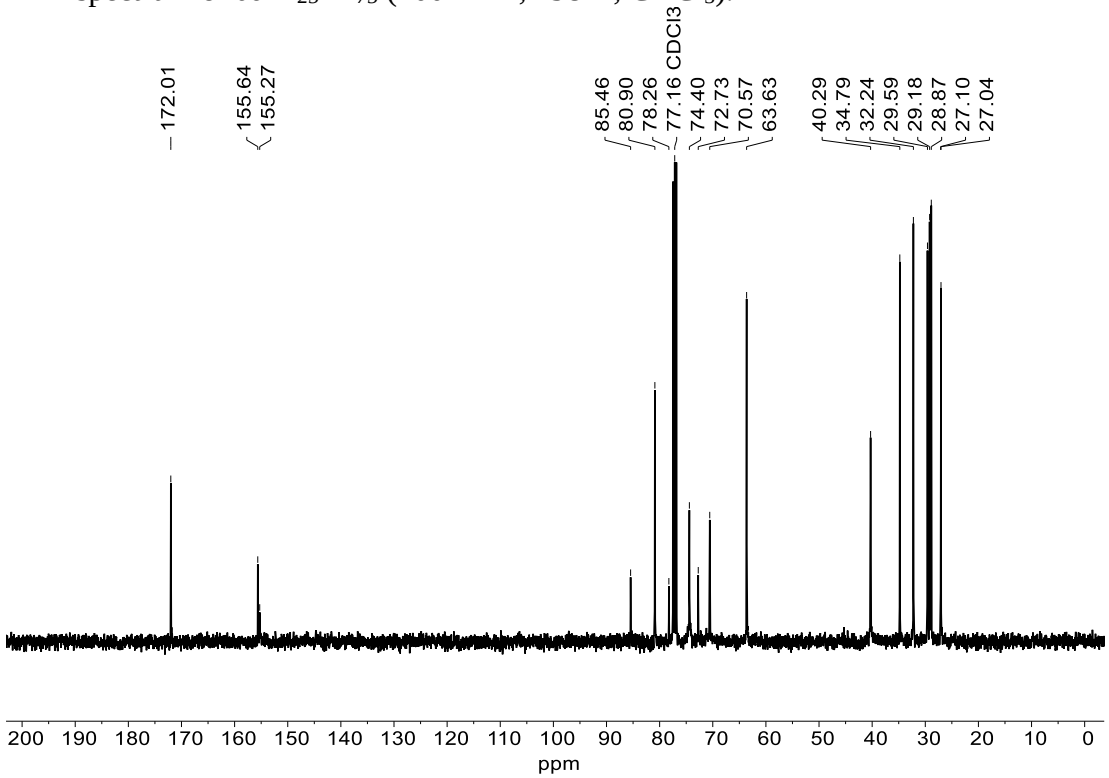


Figure S25.

^{13}C NMR spectrum of *co-II*$_{25}$*IM*$_{75}$ (100.57 MHz, 298 K, $CDCl_3$).

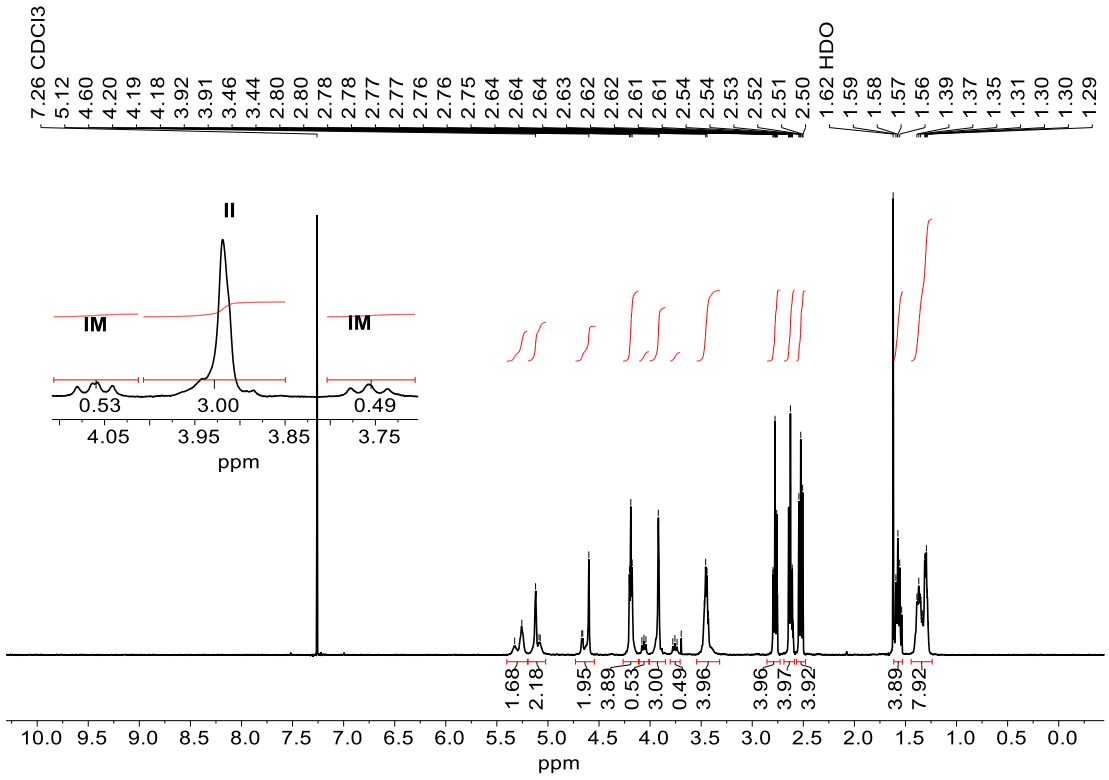


Figure S26.

^{1}H NMR spectrum of *co-II*$_{75}$*IM*$_{25}$ (400 MHz, 298 K, $CDCl_3$).

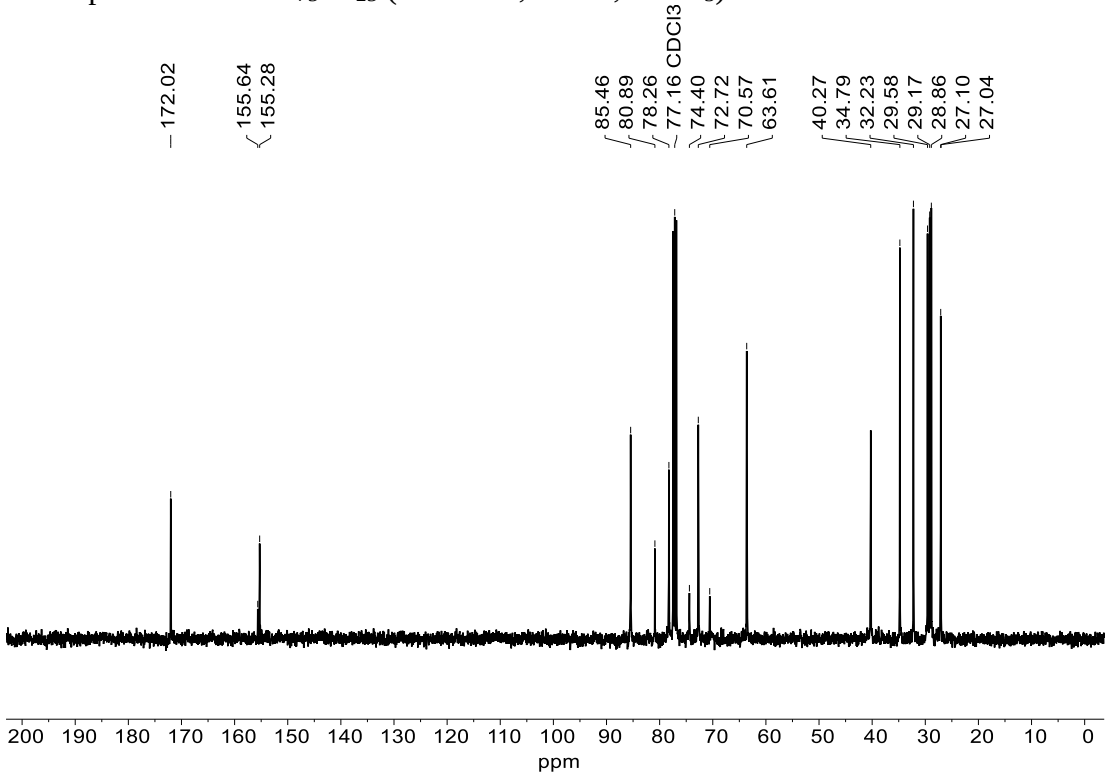


Figure S27.

^{13}C NMR spectrum of *co-II*$_{75}$*IM*$_{25}$ (100.57 MHz, 298 K, $CDCl_3$).

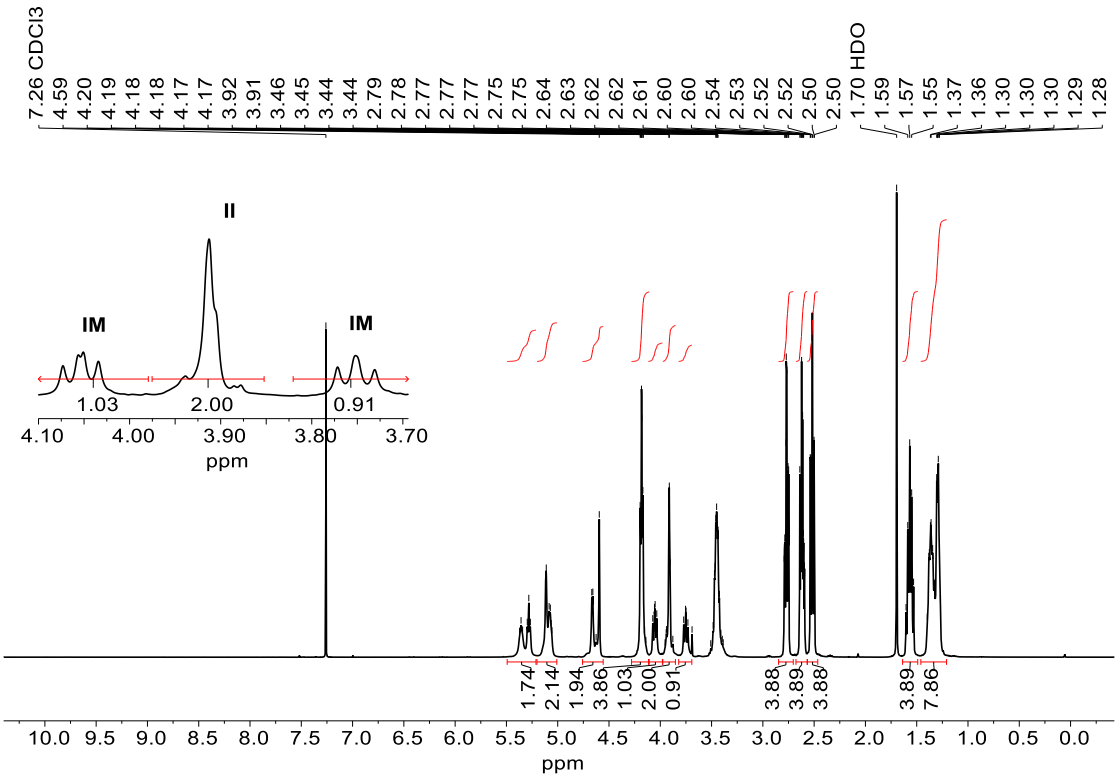


Figure S28.

^{1}H NMR spectrum of *bl-II*$_{50}$*IM*$_{50}$ (400 MHz, 298 K, $CDCl_3$).

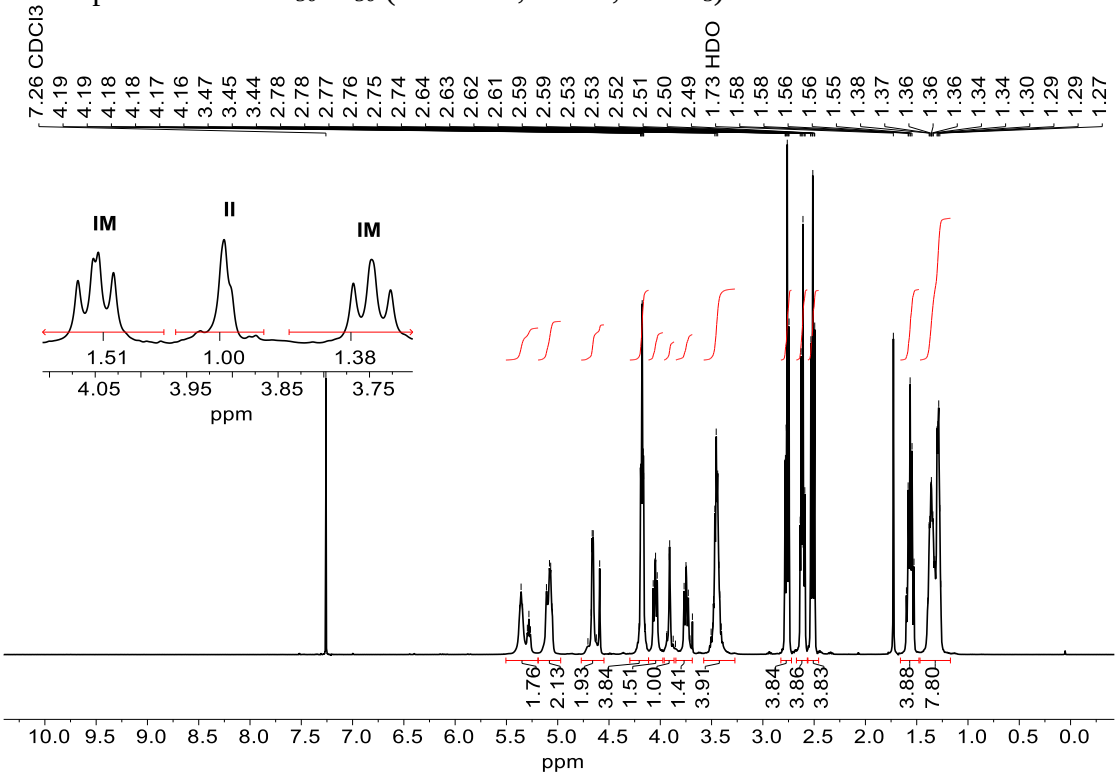


Figure S29.

^{1}H NMR spectrum of *bl-II*$_{25}$*IM*$_{75}$ (400 MHz, 298 K, $CDCl_3$).

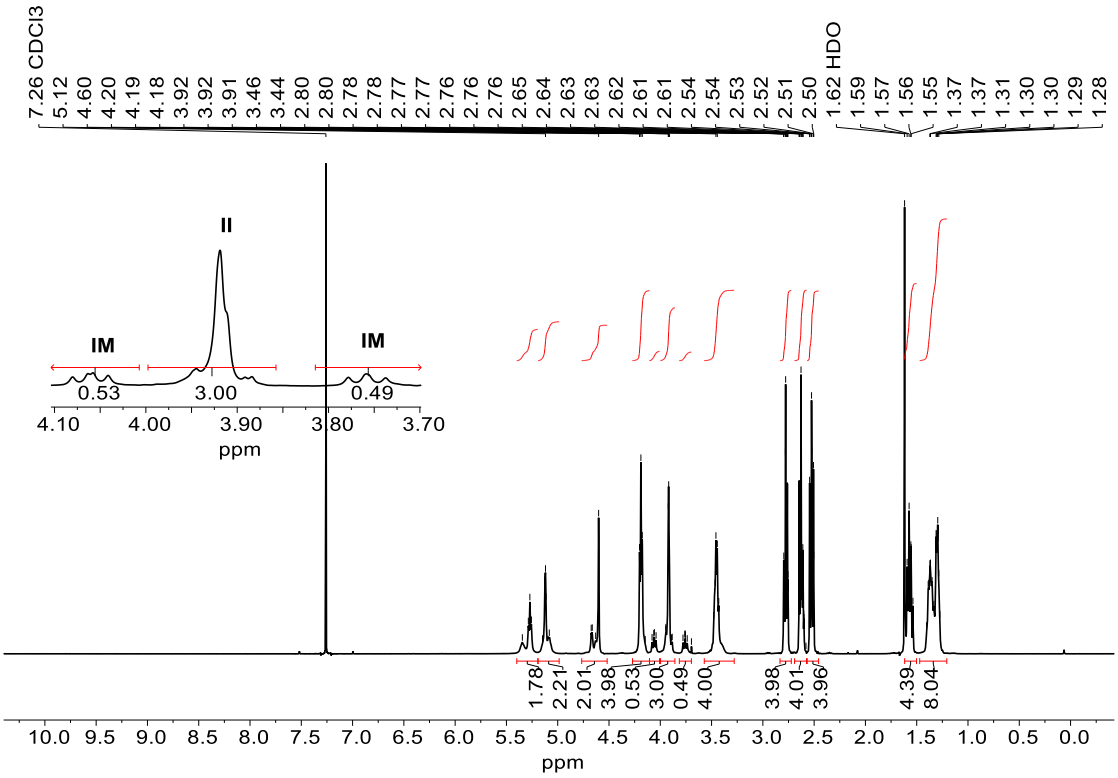


Figure S30.

^{1}H NMR spectrum of *bl-II*$_{75}$*IM*$_{25}$ (400 MHz, 298 K, $CDCl_3$).

SEC data of polymers

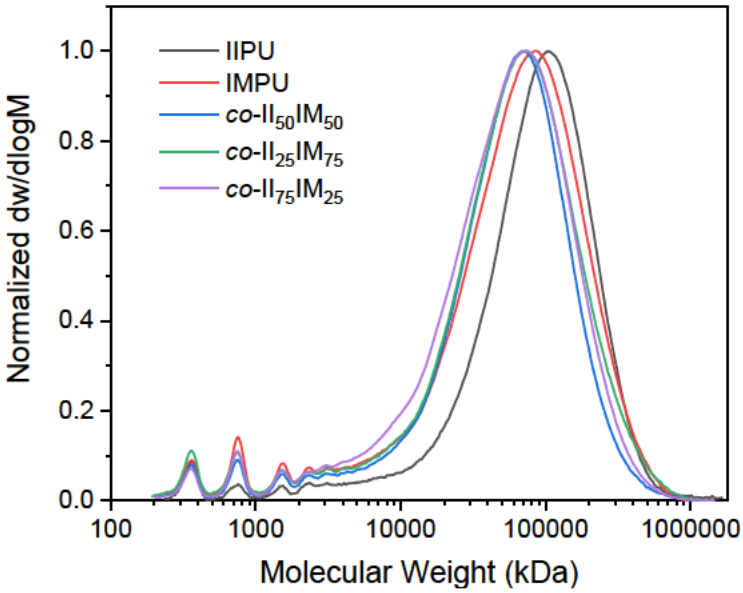


Figure S31.

Normalized size exclusion chromatograms of homopolymers and copolymers ($CHCl_3$, 0.5% NEt_3) analysis against poly(styrene) (PS) standards.

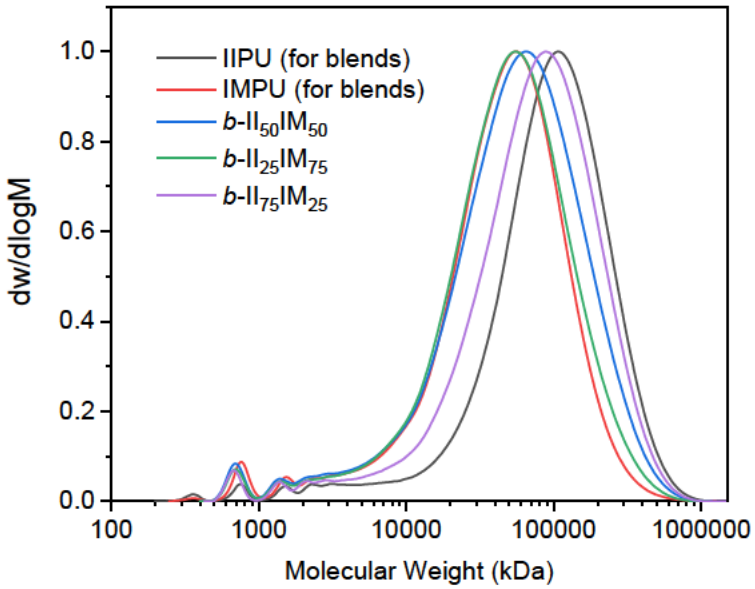


Figure S32.

Normalized size exclusion chromatograms of blended homopolymers and respective homopolymers ($CHCl_3$, 0.5% NEt_3) analysis against poly(styrene) (PS) standards.

Note. The molecular weight distributions of the blended samples have a slightly different profile than those in Figure S30 since a different batch of IIPU and IMPU were used for blending. The SEC profiles of the IIPU and IMPU used to prepare the blends are shown above and values are shown in Table S1.

Rheological frequency sweeps and WLF fitting

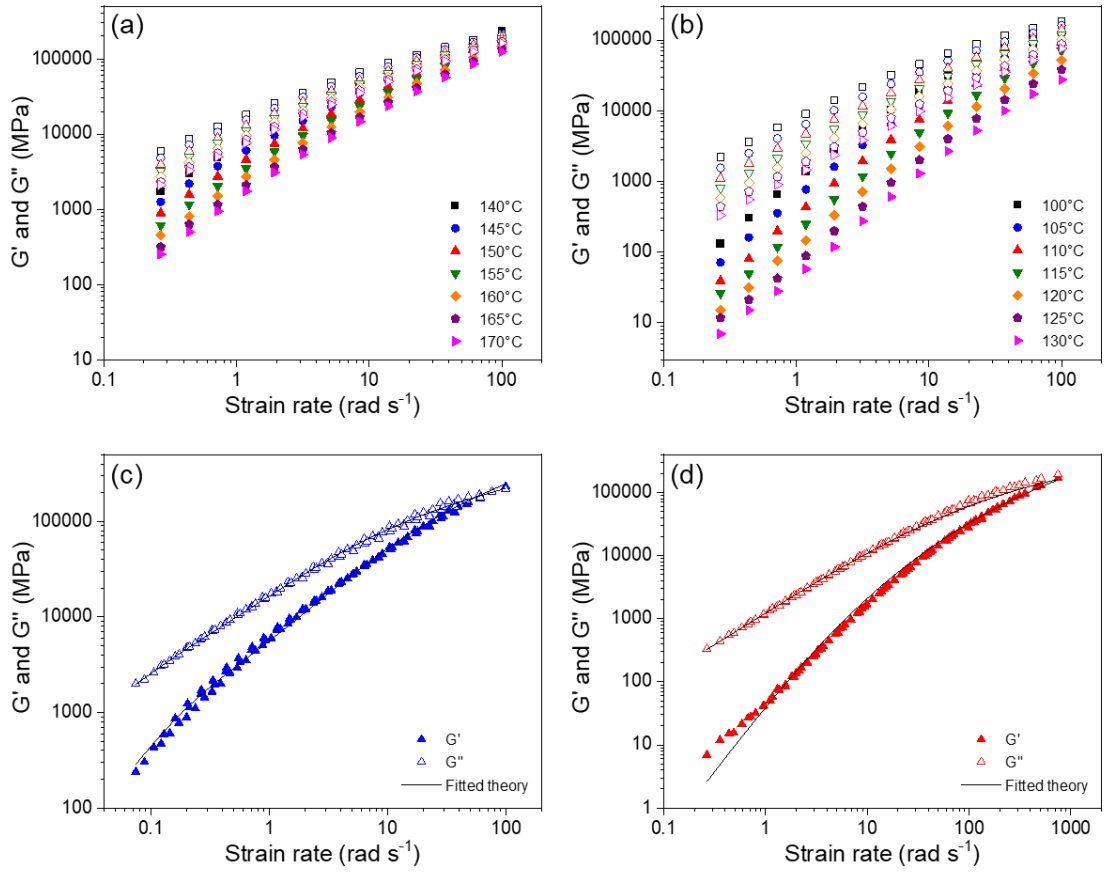


Figure S33.

(a) IIPU Storage and loss modulus plot of a frequency sweep between 140 °C and 170 °C (b) IMPU Storage and loss modulus plot of IIPU film between 100 °C and 130 °C (c) IIPU Time-temperature superposition (TTS) created from shifting data to 130 °C using WLF superposition. (d) IMPU Time-temperature superposition (TTS) created from shifting data to 130 °C using WLF superposition.

DSC thermograms of IIPU and IMPU

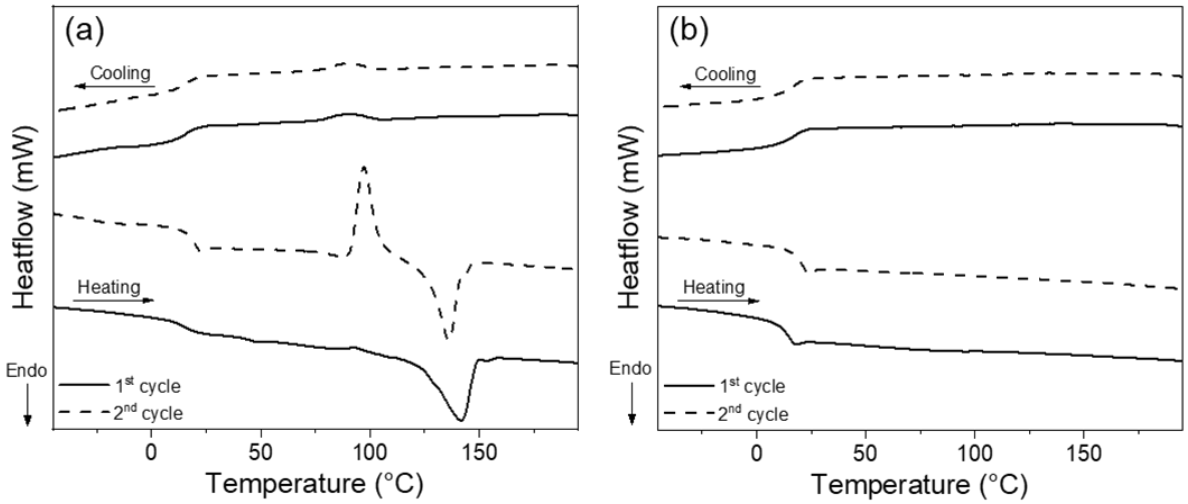


Figure S34.

DSC thermograms showing heating and cooling cycles of 3-day annealed polymers at a rate of 10 $K \cdot min^{-1}$ (a) IIPU (b) IMPU.

DSC thermograms of co-polymers

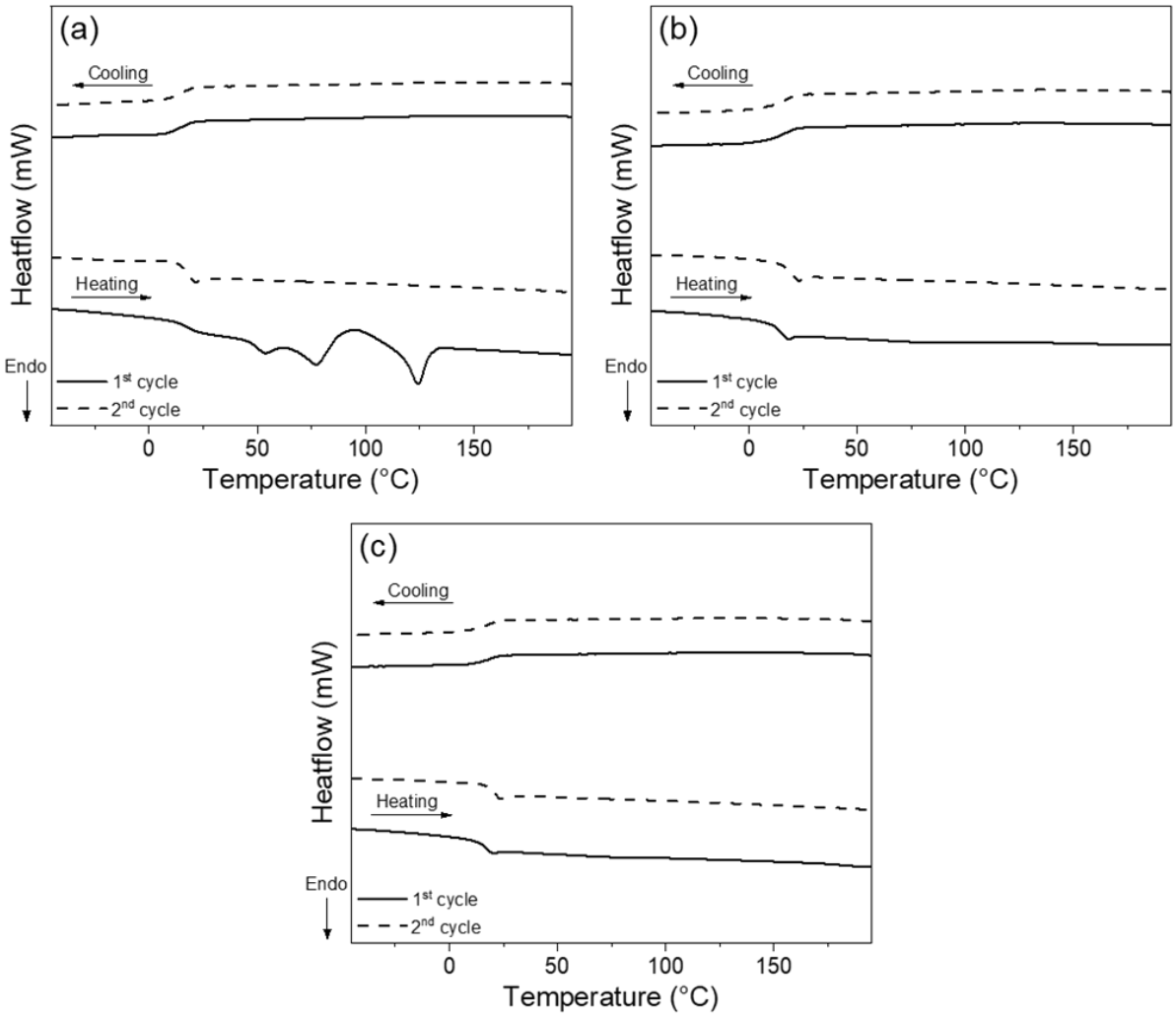


Figure S35.

DSC thermograms showing heating and cooling cycles of 3-day annealed copolymers at a rate of 10 K·min^{-1} (a) *co*-II$_{75}$IM$_{25}$ (b) *co*-II$_{50}$IM$_{50}$ (c) *co*-II$_{25}$IM$_{75}$.

DSC thermograms of physical blends

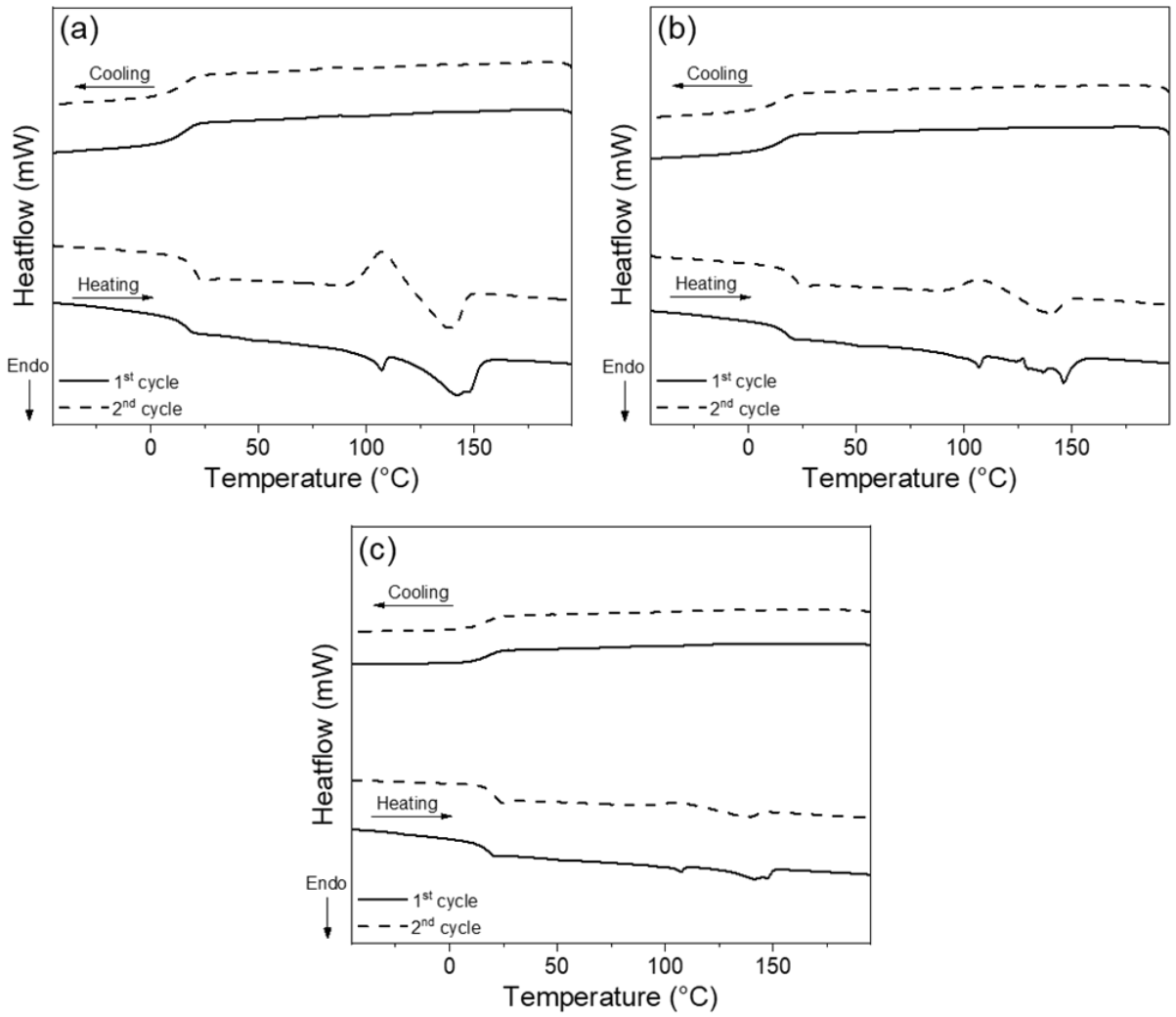


Figure S36.

DSC thermograms showing heating and cooling cycles of 3-day annealed copolymers at a rate of 10 K·min^{-1} (a) *bl*-II$_{75}$IM$_{25}$ (b) *bl*-II$_{50}$IM$_{50}$ (c) *bl*-II$_{25}$IM$_{75}$.

DSC thermograms of commercial polymer samples

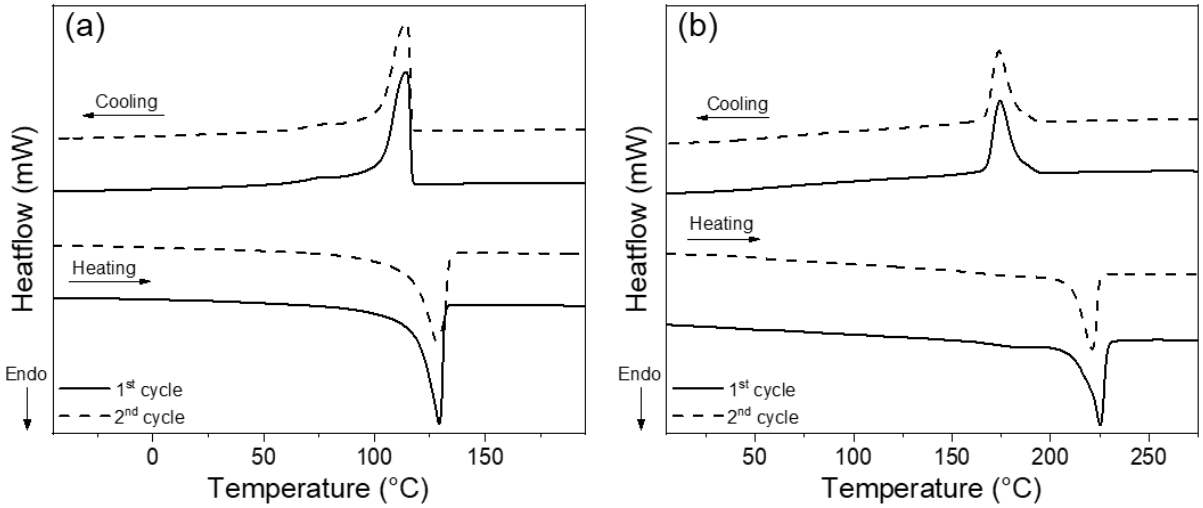


Figure S37.

DSC thermograms showing heating and cooling cycles of commercial polymer samples at a rate of 10 $K \cdot min^{-1}$ (a) HDPE (b) Nylon-6.

Tensile curves of IIPU and IMPU

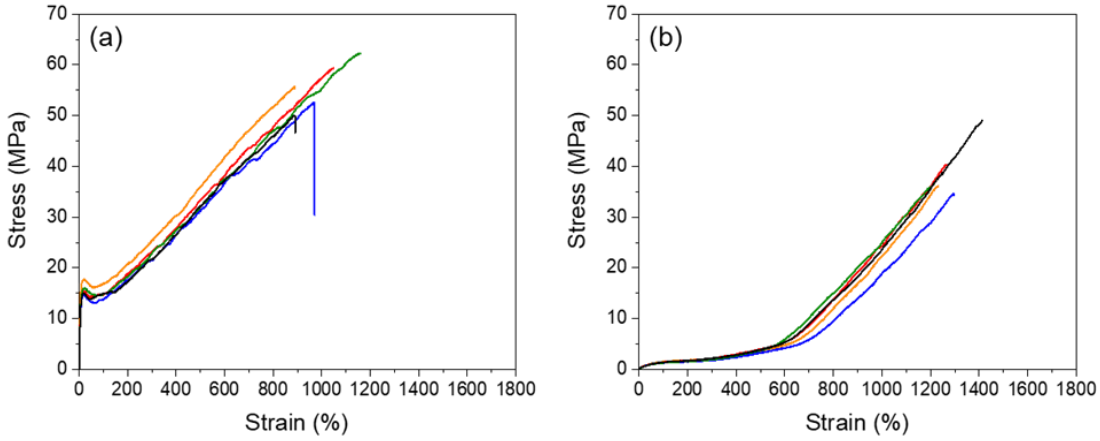


Figure S38.

Stress *vs* strain curve for 3-day annealed polymer samples (a) IIPU (b) IMPU. *n = 5*

Tensile curves of copolymers

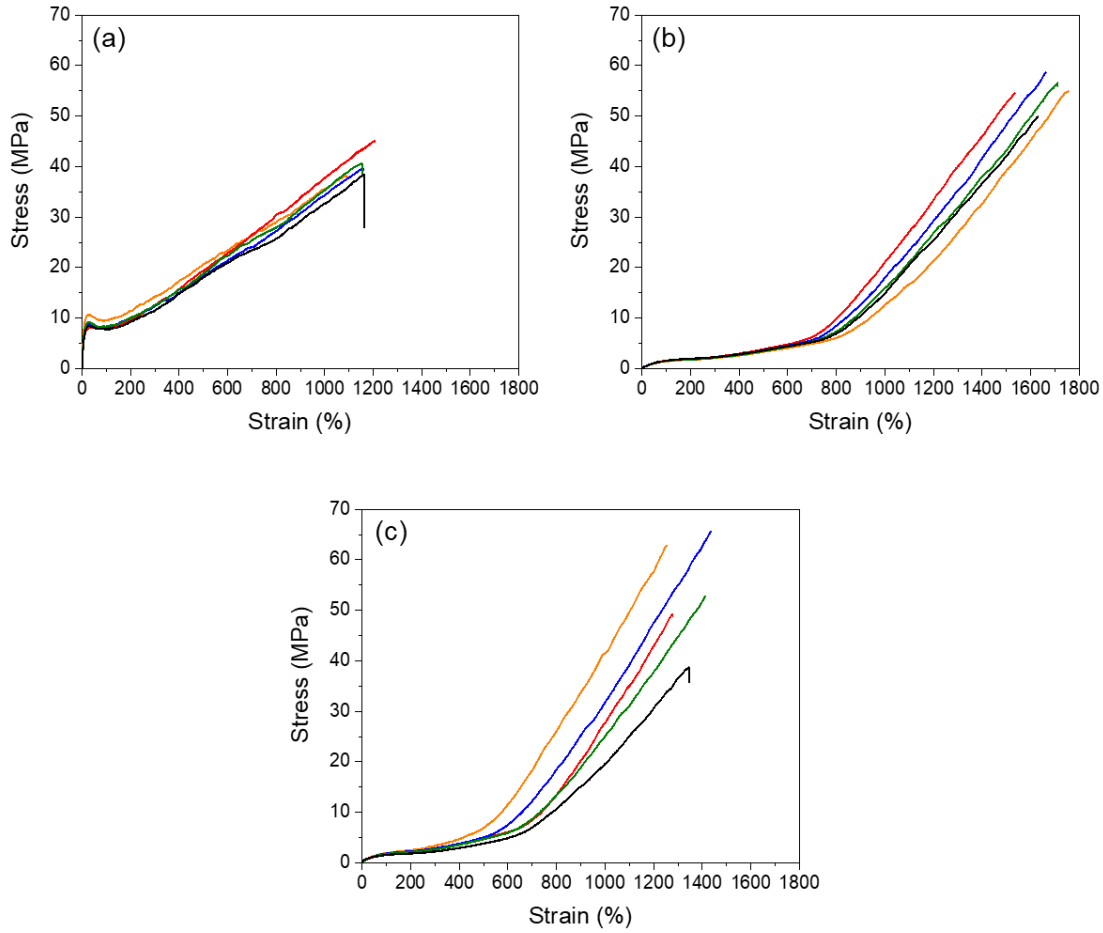


Figure S39.

Stress *vs* strain curves for 3-day annealed polymer samples (a) *co*-$II_{75}IM_{25}$ (b) *co*-$II_{50}IM_{50}$ (c) *co*-$II_{25}IM_{75}$. $n = 5$

Tensile curves of physical blends

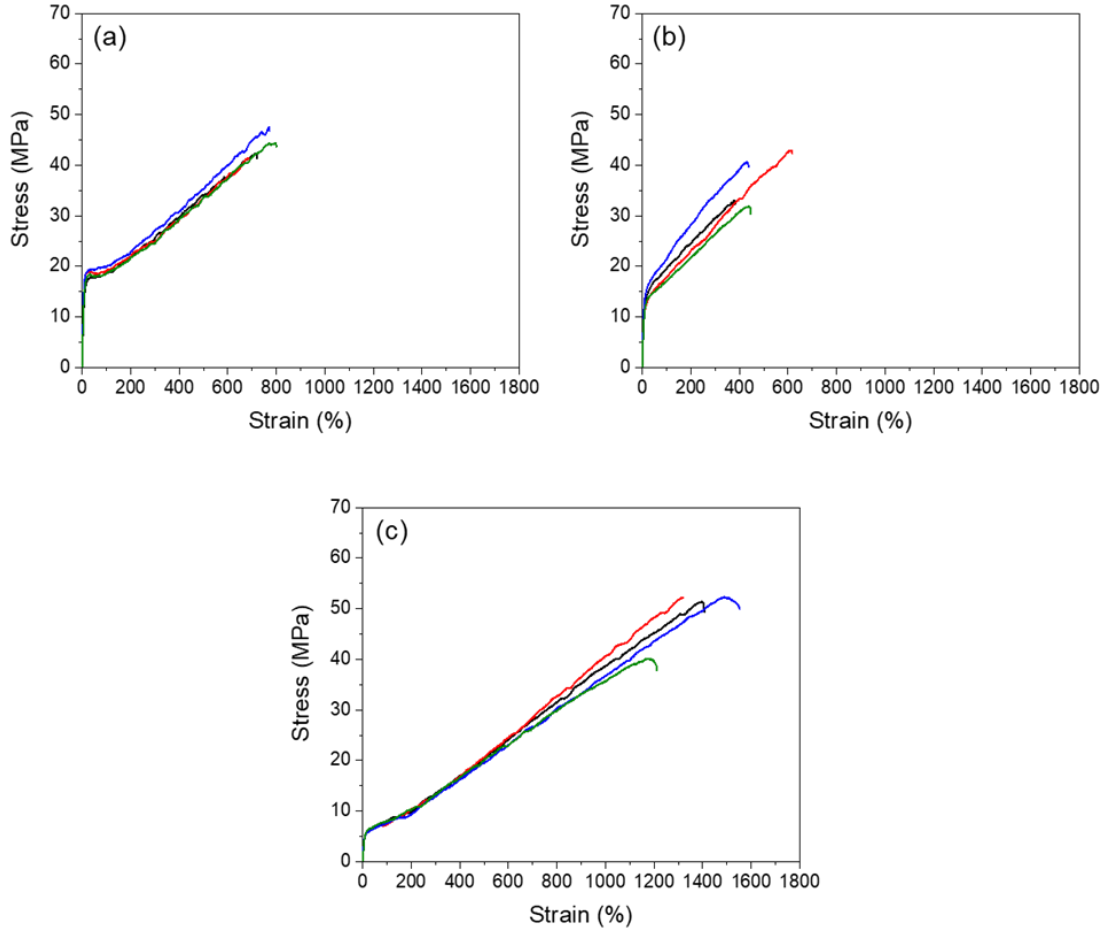


Figure S40.

Stress *vs* strain curves for 3-day annealed polymer samples (a) *bl*-$II_{75}IM_{25}$ (b) *bl*-$II_{50}IM_{50}$ (c) *bl*-$II_{25}IM_{75}$. $n = 4$

Tensile curves of commercial polymers

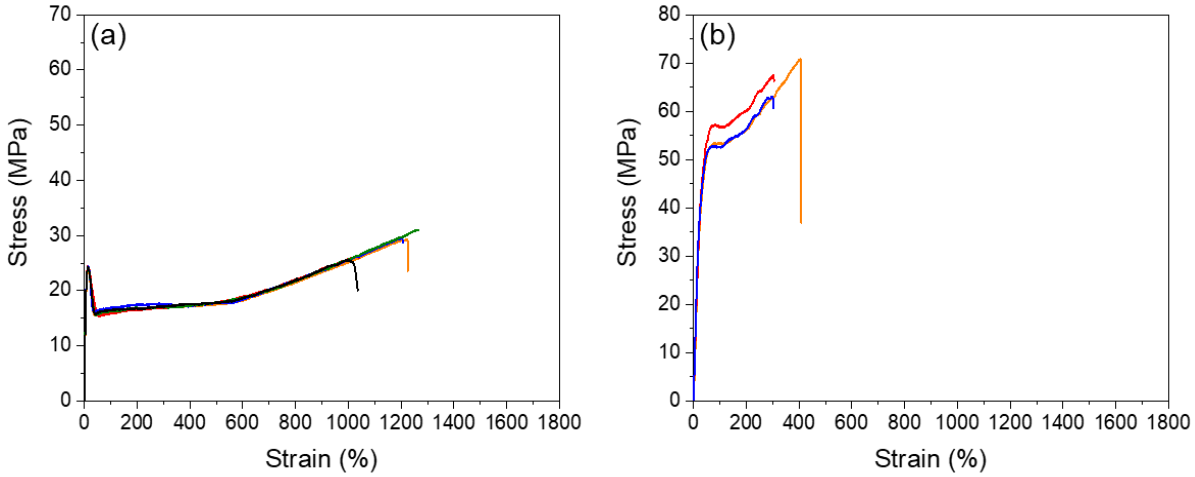


Figure S41.

Stress *vs* strain curves for commercial polymer samples (a) HDPE (b) Nylon-6.

Quantitative degradation calculations

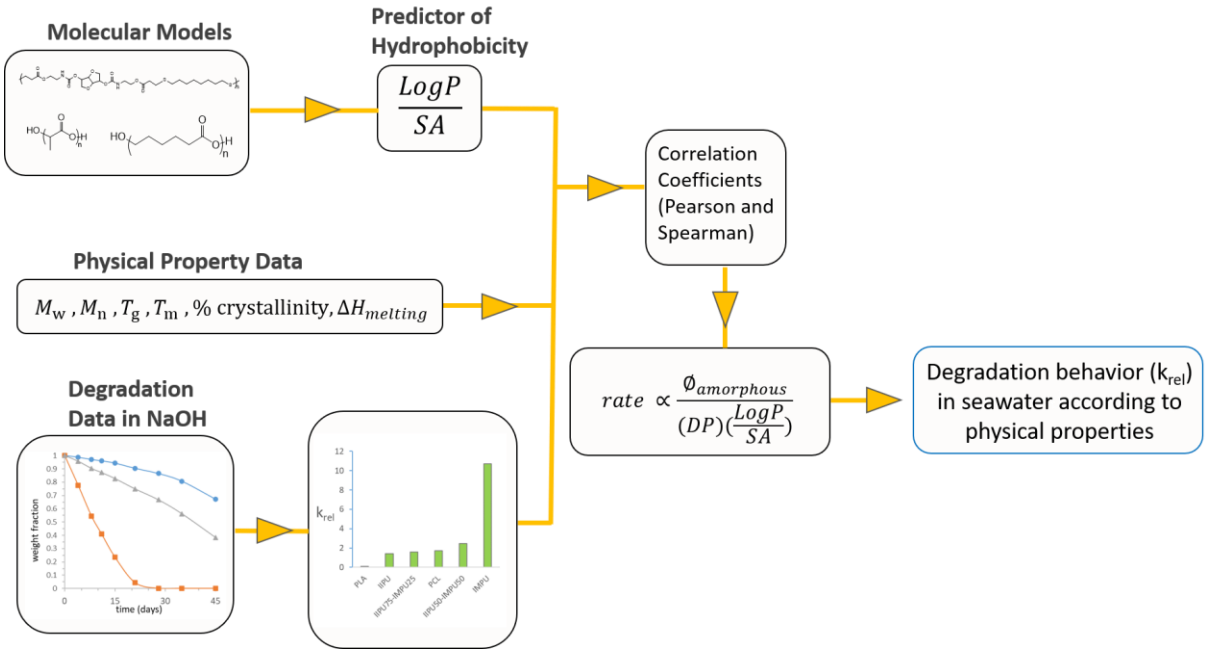


Figure S42.

Overview schematic that describes model used to predict relative degradation rate (k_{rel}) values.

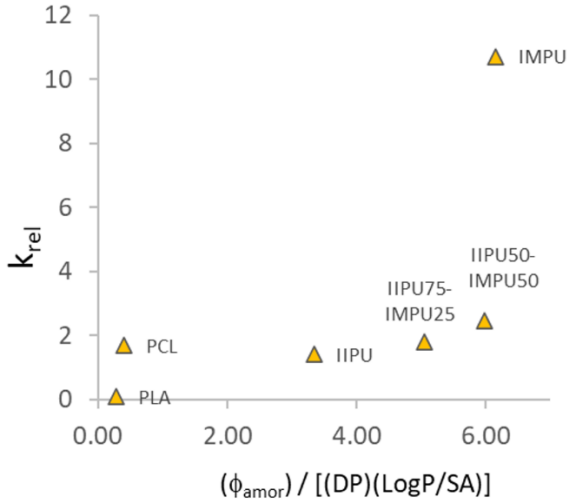


Figure S43.

The k_{rel} *vs* physical parameters for IIPU, IMPU and their copolymers as compared to PLA and PCL.

Table S1. Summary of key data values from quantitative model.

Polymer	**Hydrophobicity (*LogP/SA*)**	***k*rel**
PLA	0.0036	0.0967
IIPU	0.0059	1.42
PCL	0.0096	1.7
co-II$_{75}$IM$_{25}$	0.0059	1.8
co-II$_{50}$IM$_{50}$	0.0059	2.48
IMPU	0.0059	10.71

Table S2. Summary data table

	M_w *(kDa)*	$Đ_M$	T_g[a] (°C)	T_m[b] (°C)	ΔH_m[c] (J·g^{-1})	$T_{d,5\%}$ (°C)	E[d] (MPa)	σ_b[e] (MPa)	σ_y[f] (MPa)	ε_b[g] (%)	U_T[h] (MJm^{-3})
IIPU	117	8.12	15	141	23.9	286	320±66	56±5	16±1	989±114	329±63
IIPU-1‡	98	7.71	-	-	-	-	255±37	46±4	14±1	1159±130	312±49
IIPU-2‡	74	8.68	-	-	-	-	210±53	45±2	14±0.3	1088±70	295±25
IMPU	95	9.69	15	-	-	266	3.7±0.3	39±5	-	1285±68	187±18
co-II$_{75}$IM$_{25}$	81	9.95	18	124	15.1	271	134±5	40±3	9±1	1151±41	253±19
co-II$_{50}$IM$_{50}$	79	7.81	16	-	-	276	3.0±0.3	55±3	-	1658±84	279±24
co-II$_{25}$IM$_{75}$	89	7.77	17	-	-	276	3.5±0.6	54±11	-	1344±80	228±59
bl-II$_{75}$IM$_{25}$	-	-	17	147	18.9	276	350±43	44±3	19±1	740±51	218±24
bl-II$_{50}$IM$_{50}$	-	-	18	146	13.6	269	272±10	37±5	13±1	462±100	123±37
bl-II$_{25}$IM$_{75}$	-	-	19	147	7.9	258	139±32	49±6	5±0.5	1357±131	372±70
IIPU*	123	5.62	-	-	-	-	-	-	-	-	-
IMPU*	64	4.50	-	-	-	-	-	-	-	-	-
HDPE	-	-	-	128	170.5	-	599±46	28±2	24±1	1145±117	234±29
Nylon-6	-	-	60	224	87.0	-	215±11	67±4	55±2	336±60	186±37

(a) The T_g was obtained from 2nd heating cycle from the derivative (b) The T_m was taken as the minimum of the first transition (c) Total enthalpy of melting (ΔH_m) was calculated by integration of all endothermic transitions. (d) Young's modulus (e) Stress at break (f) Stress at yield (g) Strain at break (h) Tensile toughness n ≥ 4. Uncertainty presented as the standard deviation of samples. ‡ Polymers for mechanical recycling where IIPU-1 is initial pressing and IIPU-2 is a reprocessed sample. *Polymers used for physical blending.

Table S3. Equilibrium system densities

Polymer System	Density (g cm^{-3})
$\mathbf{II_{100}}$	**0.953**
$\mathbf{IM_{100}}$	**0.968**
***bl*-$\mathbf{II_{25}IM_{75}}$**	**0.964**
***bl*-$\mathbf{II_{50}IM_{50}}$**	**0.955**
***bl*-$\mathbf{II_{75}IM_{25}}$**	**0.954**
***co*-$\mathbf{II_{25}IM_{75}}$**	**0.958**
***co*-$\mathbf{II_{50}IM_{50}}$**	**0.958**
***co*-$\mathbf{II_{75}IM_{25}}$**	**0.955**

Table S4. Summary of data used to calculated the specific interfacial surface area of

Polymer System	L (Å)	$A_{interface}$ (Å^2)	V_{sample} (Å^3)	Specific Interfacial Area (Å^{-1})
***bl*-$\mathbf{II_{25}IM_{75}}$**	52.965	189960.6	148582.2	1.27849
***bl*-$\mathbf{II_{50}IM_{50}}$**	53.2169	217009.7	150712.3	1.43989
***bl*-$\mathbf{II_{75}IM_{25}}$**	53.4479	160608.8	152683.4	1.05191
***co*-$\mathbf{II_{25}IM_{75}}$**	51.7984	102135.7	138979	0.7349
***co*-$\mathbf{II_{50}IM_{50}}$**	53.2128	140019.6	150677.5	0.92927
***co*-$\mathbf{II_{75}IM_{25}}$**	53.6005	111460.2	153995	0.72379

Table S5. Interaction parameters of polymer repeat unit (names are consistent with GAFF)

id	Atom Types	Mass(g/mol)	ε_{LJ} (kCal/mol)	σ_{LJ}(Å)	Description
1	C	12.0107	0.086	3.39967	sp^2 C in Carboxyl group
2	C3	12.0107	0.1094	3.39967	sp^3 C in Aliphatic chain
3	HC	1.00794	0.0157	2.649533	H bonded to sp^3 C
4	HN	1.00794	0.0157	1.069078	H bonded to N
5	N	14.0067	0.17	3.249999	sp^2 N in amide groups
6	O	15.9994	0.21	2.959922	O double bonded in Carboxyl group
7	OS	15.9994	0.17	3.000012	O in ester/ether bond
8	SS	32.065	0.25	3.563595	sp^3 S in in thio-ester and thio-ether

id	Bond Types	k_r (kCal/mol Å^{-2})	r_{eq} (Å)	Description
1	C-C3	328.3	1.508	C-C bond between aliphatic C and carboxyl group
2	C3-N	478.2	1.345	N-C bond between aliphatic C to amino group N

3	C-O	648	1.214	O-C double bond in carboxyl group
4	C-OS	411.3	1.343	O-C single bond in carboxyl group
5	C3-C3	303.1	1.535	C-C bond between aliphatic C
6	C3-HC	337.3	1.092	C-H bond in aliphatic C chain
7	C3-N	330.6	1.46	C-N bond in amide group
8	C3-OS	301.5	1.439	C-O bond in ester bond
9	C3-SS	225.8	1.821	C-S bond in thio-ether bond
10	HN-N	410.2	1.009	N-H bond in amide group

id	Angle Types	k_θ (kCal/mol rad^{-2})	θ_{eq} (degree)	Description
1	C-C3-C3	63.8	110.53	
2	C-C3-HC	47.2	109.68	
3	C-N-C3	63.9	121.35	
4	C-N-HN	49.2	118.46	
5	C-OS-C3	63.6	115.14	
6	C3-C-O	68	123.11	
7	C3-C-OS	69.3	111.96	
8	C3-C3-C3	63.2	110.63	
9	C3-C3-HC	46.4	110.05	
10	C3-C3-N	65.9	112.13	
11	C3-C3-OS	67.8	108.42	
12	C3-C3-SS	61.1	112.69	
13	C3-N-HN	46	116.78	
14	C3-OS-C3	62.1	113.41	
15	C3-SS-C3	60.6	99.92	
16	HC-C3-HC	39.4	108.35	
17	HC-C3-N	49.8	109.5	
18	HC-C3-OS	50.9	108.7	
19	HC-C3-SS	42.5	108.76	
20	N-C-O	75.8	122.03	
21	N-C-OS	74.7	115.25	
22	O-C-OS	76.2	122.43	

id	Proper Dihedral Types	k_d (kCal/mol)	d	n	Description
1	C-C3-C3-HC	0.155556	1	3	

2	C-C3-C3-S	0.155556	1	3
3	C3-C-OS-C3	2.7	-1	2
4	C3-C3-C3-C3	0.155556	1	3
5	C3-C3-C3-C3	0.18	1	3
6	C3-C3-C3-C3	0.25	-1	2
7	C3-C3-C3-C3	0.2	-1	1
8	C3-C3-C3-HC	0.155556	1	3
9	C3-C3-C3-HC	0.16	1	3
10	C3-C3-C3-OS	0.155556	1	3
11	C3-C3-C3-S	0.155556	1	3
12	C3-C3-N-C	0	1	2
13	C3-C3-N-C	0.5	-1	4
14	C3-C3-N-C	0.15	-1	3
15	C3-C3-N-C	0.53	1	1
16	C3-C3-N-HN	0	1	2
17	C3-C3-OS-C	0.383333	1	3
18	C3-C3-OS-C	0.383	1	3
19	C3-C3-OS-C	0.8	-1	1
20	C3-C3-OS-C3	0.383333	1	3
21	C3-C3-OS-C3	0.383	1	3
22	C3-C3-OS-C3	0.1	-1	2
23	C3-C3-S-C3	0.333333	1	3
24	HC-C3-C3-HC	0.155556	1	3
25	HC-C3-C3-HC	0.15	1	3
26	HC-C3-C3-N	0.155556	1	3
27	HC-C3-C3-OS	0.155556	1	3
28	HC-C3-C3-OS	0.25	1	1
29	HC-C3-C3-S	0.155556	1	3
30	HC-C3-N-C	0	1	2
31	HC-C3-N-HN	0	1	2
32	HC-C3-OS-C	0.383333	1	3
33	HC-C3-OS-C3	0.383333	1	3
34	HC-C3-S-C3	0.333333	1	3
35	N-C-OS-C3	2.7	-1	2
36	N-C3-C3-OS	0.155556	1	3

37	O-C-C3-C3	0	-1	2	
38	O-C-C3-HC	0	-1	2	
39	O-C-C3-HC	0.8	1	1	
40	O-C-C3-HC	0.08	-1	3	
41	O-C-N-C3	2.5	-1	2	
42	O-C-N-HN	2.5	-1	2	
43	O-C-N-HN	2.5	-1	2	
44	O-C-N-HN	2	1	1	
45	O-C-OS-C3	2.7	-1	2	
46	O-C-OS-C3	2.7	-1	2	
47	O-C-OS-C3	1.4	-1	1	
48	OS-C-C3-C3	0	-1	2	
49	OS-C-C3-HC	0	-1	2	
50	OS-C-N-C3	2.5	-1	2	
51	OS-C-N-HN	2.5	-1	2	
52	OS-C3-C3-OS	0.155556	1	3	
53	OS-C3-C3-OS	0.144	1	3	
54	OS-C3-C3-OS	1.175	1	2	

id	Improper Dihedrals	k_d (kCal/mol)	d	n	Description
1	C-C3-N-HN	1.1	-1	2	
2	C3-O-C-OS	10.5	-1	2	
3	N-O-C-OS	10.5	-1	2	

References

1 Vorselaars, B. *Theory documentation: Polydisperse double reptation*, <http://www.reptate.com> (

2 Wang, J., Wolf, R. M., Caldwell, J. W., Kollman, P. A. & Case, D. A. Development and testing of a general amber force field. *J. Comput. Chem.* **25**, 1157-1174, (2004).

3 Humphrey, W., Dalke, A. & Schulten, K. VMD: Visual molecular dynamics. *J. Mol. Graph.* **14**, 33-38, (1996).

4 Brown, W. M., Kohlmeyer, A., Plimpton, S. J. & Tharrington, A. N. Implementing molecular dynamics on hybrid high performance computers – Particle–particle particle-mesh. *Comput. Phys. Commun.* **183**, 449-459, (2012).

5 Hockney, R. W. & Eastwood, J. W. *Computer simulation using particles*. 564 (Taylor & Francis Group, 1988).

6 Plimpton, S. Fast parallel algorithms for short-range molecular dynamics. *J. Comput. Phys.* **117**, 1-19, (1995).

7 Lam, C. X. F., Savalani, M. M., Teoh, S.-H. & Hutmacher, D. W. Dynamics of *in vitro* polymer degradation of polycaprolactone-based scaffolds: Accelerated versus simulated physiological conditions. *Biomed. Mater.* **3**, 034108, (2008).

Chapter 5 – Chemical Recycling of photocurable resins containing reversible thiol-Michael bonds

5.1 Manuscript details and overview

Title: Chemical Recycling of photocurable resins containing reversible thiol-Michael bonds

Authors: Connor J. Stubbs[1], A Khalfa[1], V. Chiaradia[1], Joshua C. Worch[1], and Andrew P. Dove[1]*

Affiliations: [1] School of Chemistry, The University of Birmingham, Edgbaston, Birmingham, B15 2TT, UK.

Manuscript Prepared

Co-author contributions: Anissa Khalfa (University of Birmingham) performed and characterised NMR spectra for the model reactions and prepolymers. Dr Viviane Chiaradia (University of Birmingham) performed stress relaxation experiments. Dr Josh Worch (University of Birmingham) performed swell testing and gel fraction experiments. Prof. Andrew Dove (University of Birmingham) supervised the project, in addition to providing guidance and editing the manuscript.

Overview:

The work in this chapter is very tangential from the preceding chapters. The idea arose from the combined influence of previous work in our group relating to photocurable terpene systems, and the reversibility of the thia-Michael reaction.

Crosslinked polymers, or networks, are an extremely important material class that offers chemical resistance, high elasticity, thermal stability, and resistance to stress relaxation. An increasingly growing sub-class is photocurable networks which generate a crosslinked

material from a liquid resin upon exposure to light (typically UV). However, the prevailing issue with networks is their lack of recyclability due to the same crosslinks that impart a material with their desirable properties. An emergent solution is producing crosslinked materials with dynamic bonds that can be activated upon a stimulus, called CANs (covalent adaptable networks). Previous examples of photocurable CANs enable a photocured structure to be re-shaped into a distinctly different shape when heated, however there currently lacks a technique to depolymerise and recure a sample using the same photochemical stimulus. This chapter is about the design and invention of a photocurable network that can be depolymerised and recured *via* the same stimulus without synthetic modification or addition of reactive diluents.

We designed a photocurable resin that crosslinked and forms a dynamic bond *in-situ* with the network formation. These dynamic bonds in the network are in constant equilibrium and as conditions that favour dissociation increase, such as heat, the quantity of bond dissociation also increases. Once the equilibrium is sufficiently shifted in favour of bond breakage, the network depolymerizes into soluble oligomers disrupting the infinite network. Importantly, the soluble oligomers bare the same functionality that was initially used in the curing, which enables the ability to recure.

The initial network demonstrated properties characteristic of crosslinked materials (insoluble in solvent, no observable flow temperature, good resistance to stress relaxation) in each of the 2 recures. There is an observed decrease in the properties between the initial and the first recure, however the first recure and second recure display a similar mechanical performance. Nevertheless, our findings present a modular, photocurable resin platform that can be fabricated, depolymerized and recured on-demand atleast 2 times.

Chemical Recycling of photocurable resins containing reversible thiol-Michael bonds

Connor J. Stubbs, Anissa Khalfa, Viviane Chiaradia, Josh C. Worch, Andrew P. Dove*

School of Chemistry, University of Birmingham, Birmingham, B15 2TT, UK. E-mail: [redacted]

Photocurable resins, Covalently Adaptable networks, Polymer networks, recycling, sustainability, dynamic bonds, Thiol-Michael addition.

ABSTRACT: The development of photocurable platforms that can both satisfy the mechanical demands of consumer application and display reversibility required for use in a circular framework has created a myriad of new challenges within this emerging field. A bio-sourced terpenoid structure, L-carvone, inspired the creation of a photocurable resin that formed a dynamic thiol-Michael bond *in situ*. Initially, small molecule model studies were performed to assess and optimize the curing and depolymerization conditions. The di-alkene containing L-carvone could be incorporated into a photocurable resin using a multi-arm thiol as a crosslinking agent with a photo-initiator. Upon UV exposure, the resin formed a mechanically robust network laden with reversible Michael bonds, which could be depolymerized into soluble oligomers regenerating the initial photocurable functionalities. The recovered oligomers could be reformulated and recured back into a networked material, which could then depolymerized again to demonstrate its repeated recyclability. The properties of each cycle were found to be consistent with conventional networks: insoluble in solvents, good resistance to stress relaxation, maintains shape up to 170 °C. There is an observed loss of crosslinking density and mechanical strength after the first recycle, however the second recycle displays similar properties to the first recycle. Our findings present a modular, photocurable resin platform from a sustainable source that can be fabricated, depolymerized and recured on-demand, which represents a significant advancement towards a circular materials economy.

Currently, polymer materials follow a linear pathway, with commercial plastic materials lacking efficient recycling routes to achieve a circular economy.[1] Polymer networks make up a considerable portion of the non-recyclable materials market with historic usage in thermosets, foams, rubbers, and coatings but, also, in the emergent photocurable resin industry.[2] Conventional photocurable resins are based on reactive polymers and/or monomers that undergo rapid covalent crosslinking upon initiation from a light stimulus to afford materials with excellent chemical resistance, dimensional stability, and recoverability. The combination of on-demand, light triggered fabrication and mechanically robust properties have made photocurable networks key to coatings, inks and even 3D printing applications.[3-5] As such, it is imperative to design new photocurable resin platforms that can contribute to a more circular economy whilst satisfying the mechanical demands that current networks fulfill.

To realize these targets, modern solutions have focused upon creating networks laden with dynamic bonds, commonly referred to as covalent adaptable networks (CANs).[6] Careful selection of the dynamic bonds used in CANs allow the network to retain the robust mechanical properties of an archetypal network material, whilst imparting thermal reprocessability. This technology was applied to a photocurable system, where the resin contained a *pre-formed* dynamic thiol-anhydride bond that once crosslinked could be reshaped into a new part at elevated temperatures.[7] An alternative recycling route that photocurable CANs offer is through the depolymerization of the dynamic network, which is usually driven by the entropy gain of bond breaking at elevated temperatures.[2, 8] However, these depolymerized networks regenerate functionalities unsuitable for photocuring and require synthetic modification or additional reactive diluents to be reused in a UV-active resin.[9, 10] Whilst both of these CANs technologies mark a considerable milestone in developing more recyclable photocuring resins, the ability to depolymerize to the original photocurable resin is yet to be fully realized.

The necessary innovation is to design a system where the dynamic network is formed *in situ* rather than *pre-formed*, thus enabling a photocured network to be degraded back into the original functionalities of the resin (Figure 1). The closest examples to this aim utilize reversible cycloadditions such as anthracene [4+4][11] and coumarin [2+2][12] dimerization as well as triazolinedione-napthalene [2+4][13] addition, however the mechanical properties of these systems are not conducive for universal consumer application.

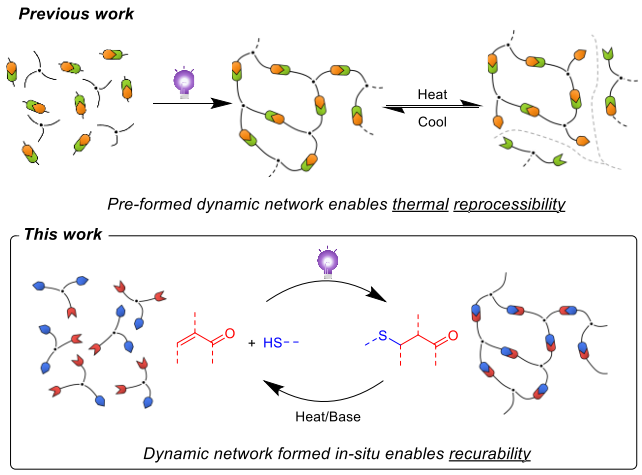


Figure 1. Previous work using *pre-formed* dynamic network versus *in-situ* formed dynamic network.

We envisioned a photocurable platform that featured a dynamic bond at each crosslink junction and could be reversed on-demand to re-form the original photocurable functionalities. The radical-mediated thiol-ene reaction was targeted as an optimal chemistry to achieve this aim due to its extensive use in photocurable resins and the various well-established dynamic sulfur-based bonds.[14] Specifically, the electron deficient β-thioether (or Michael bond)

has been reported as dynamic bond that proceeds *via* a dissociative mechanism that reforms the same functionalities.[15] We hypothesized a multifunctional compound containing an electron deficient alkene could be crosslinked with a multi-arm thiol under a UV stimulus to form the dynamic Michael bond *in situ*. A search of abundant bio-sourced derivatives revealed L-carvone, a remarkably underutilized terpenoid that fulfilled our requirements. The structure consists of two alkene functionalities: an *exo*- di-substituted alkene, or isopropenyl group, and an *endo*- tri-substituted enone group, suitably electron deficient to form the desired thiol-Michael bond. Using this bio-sourced derivative not only offers a cost-effective solution,[16] but shifts reliance from traditionally-used oil derivatives to a more sustainable source.

Model reactions

Initially, we assessed the suitability of carvone in our recyclable photocurable resin platform with a series of model reactions. L-carvone and methyl 3-mercaptopropionate (MMP) were mixed in bulk with a photo-initiator (TPO-L, 1 wt%) and exposed to UV light to simulate photocuring conditions (Figure 2a). Near visible (405 nm) UV was used to slow reaction kinetics, due to the diminished absorption of TPO-L at that wavelength. The reaction was periodically sampled to quantify the consumption of both alkenes *via* ^{1}H-NMR spectroscopy. Unsurprisingly, the less sterically hindered *exo*- alkene was consumed faster and achieved a higher conversion (99% after 30 minutes) than the enone, which was significantly slower and achieved a poorer overall conversion (17% after 180 minutes, Figure S1, Table S1). Whilst the steric barrier of the tri-substituted enone hindered addition, the stabilizing effect of ketone and the α-methyl also contributed to its poor reaction rate and overall conversion.[17, 18] Nevertheless, the observed reactivity of the enone highlighted its suitability in a photocurable system.

The radically mediated thiol-ene reaction typically favors the anti-Markovnikov adduct which would yield the desired β-ketone thioether for the carvone structure. However, the reversibility of the system depended upon the formation of β-ketone thioether where significant formation of the Markovnikov product (α-ketone thioether) could limit the recyclability of the network. Further analysis of the model reaction products identified ^{1}H-NMR peaks associated with the desired Michael adduct. The formation of these diagnostic peaks was plotted against the consumption of the enone and found to form equivalently, which indicates the desired Michael bond is the major product (Figure 2b, Figure S2).

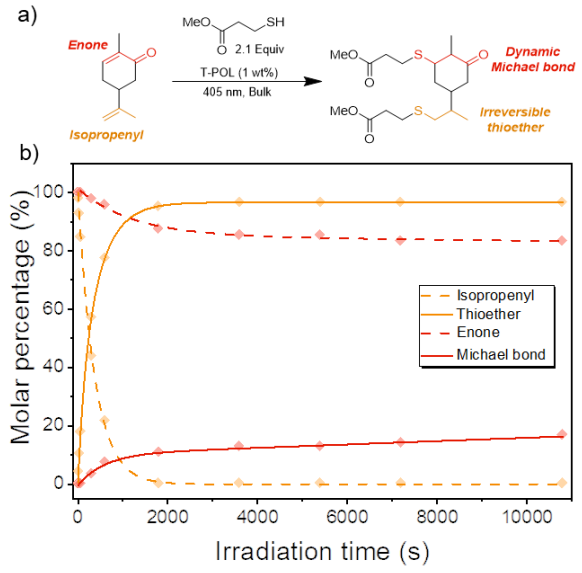


Figure 2. a) Scheme of the radical mediated addition of methy 3-mercaptopropionate to L-carvone using radical initiator TPO-L (1 wt%) under 405 nm UV irradiation. b) Plot of the molar percentage of each functionality over irradiation time monitored by ^{1}H-NMR spectroscopy.

A key goal to this project was to create a resin that forms a robust network material whilst maintaining the reversibility required for recycling. Historically, dissociative bonds, such as the Michael bonds, have been avoided in CANs due to concerns that the dynamic network could behave similarly to a thermoplastic, i.e. flowing at high temperatures and/or solubilizing in organic solvents.[19, 20] Although more recent work has suggested dissociative dynamic networks can be equally robust,[21] the reversibility of the Michael bond needed to be understood. A mono-functional thiol-Michael adduct of carvone (CarMMP) was synthesized from a conjugate addition of MMP to carvone. Alone, CarMMP displayed no dissociation in DMF-d_7, however upon addition of DBU (5 mol%) dissociation at room temperature occurred rapidly, before an initial time point could be taken (Figure 3a and Figure S3). Further time points taken suggested that the system equilibrated before the first time point (Figure S3). The equilibrium of CarMMP was further investigated using variable temperature ^{1}H-NMR spectroscopy (Figure 3b). The equilibrium constant at each temperature was calculated and used to construct a Van't Hoff plot (Figure 3b, Table S2). The calculated activation energy (49.3 kJ mol^{-1}) for CarMMP was comparable to previously reported dynamic Michael bonds.[15, 22, 23] CarMMP's observed stability in the absence of DBU suggested a carvone based network would likely be robust at ambient temperature, but could depolymerize readily upon addition of DBU.

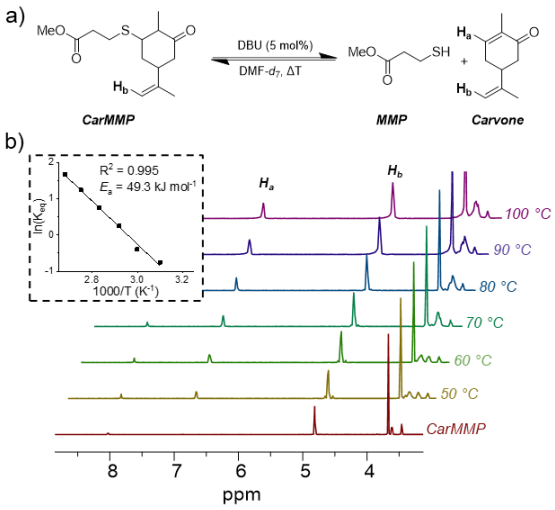


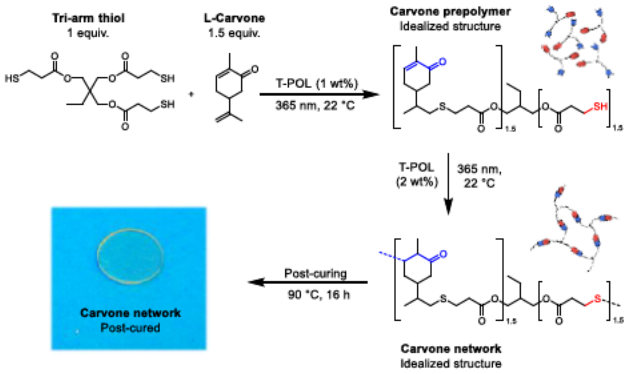
Figure 3. a) Scheme for the dissociation of CarMMP in the presence of DBU b) Variable temperature ^{1}H-NMR of CarMMP in DMF-d_7 with DBU (5 mol%) illustrating the regeneration of the enone functionality at increasing temperature *Inset* Van't Hoff plot of the dissociation of CarMMP.

Initial material fabrication

The model studies indicated L-carvone to be a suitable candidate for formulating a recyclable photocurable resin. For the resin system, a 3+2 network architecture was selected for its simplicity, where the difunctional carvone and a tri-arm thiol (trimethylolpropane tris(3-mercaptopropionate)) were combined at a ratio of 3:2 respectively, to ensure equimolar equivalents of alkene and thiol functionalities were present. It is typical to use a prepolymer within a photocuring resin to reduce the curing time since less crosslinks are required to form the infinite network.[24] Applying a modified technique from our previous work[24], the mixture of carvone (1.5 equiv.) and the tri-arm thiol (1 equiv.) were combined with a photo-

initiator (1 wt%) and irradiated under UV light (Scheme 1). The considerable reactivity difference between the carvone alkenes led to a total consumption of the propenyl functionality with only a partial consumption of the enone (6%) after 150 min of UV irradiation. As a result, the reaction could be quenched before crosslinking occurred, yielding a viscous liquid prepolymer.

Formulation of the carvone resin required dilution of the prepolymer with a non-reactive solvent to reduce the viscosity. The carvone prepolymer (70 wt%) was dissolved in dimethylcarbonate (DMC, 30 wt%) with photo-initiator (TPO-L, 2 wt%) to produce the initial carvone resin. Upon irradiation with UV light, source the resin transitioned from a viscous liquid to a freestanding solid structure, characteristic of a crosslinked polymer. Finally, the structure was post-cured in a vacuum oven at 90 °C to remove DMC and to maximize crosslinking, which finally yielded a flexible carvone network (Scheme 1).



Scheme 1. Schematic depiction of the thiol-ene reaction of L-carvone and trimethylolpropane tris(3-mercaptopropionate) to obtain the carvone prepolymer and its subsequent crosslinking to obtain the carvone network. The image shows the obtained network after curing.

Depolymerization and reformulation

In order to depolymerize the formed network, pieces of the post-cured network were added into a degassed solution (to inhibit unwanted oxidation) containing DBU (5 mol%) and DMF as a solvent, foreseeing the need for high temperature to promote depolymerization (Figure 4a). Dissolution of the carvone network readily occurred once a temperature of 140 °C was maintained for 4 h, however the reaction was left *ca.* 16 h to ensure equilibrium had been reached (Figure 4b). Even though the initial carvone network had visibly dissolved, a minor quantity of particulates could still be observed in the solution. These were assumed to be areas of high crosslink density that failed to depolymerize yet represented a trivial fraction of the initial material mass (*ca.* 0.5 wt%). Work-up of the depolymerization reaction required the removal of DBU and DMF, which can favor the forward Michael addition, hence it was imperative to remove them before re-crosslinking could occur.[25] Precipitation into methanol was found to be effective at removing the DBU and the majority of the DMF, however small quantities persisted even after drying (Figure 4d). The majority of the initial mass of the resin was recovered (55%) and resembled a slightly orange tack, likely caused by DBU and/or thiol oxidation. Further optimization of the depolymerization reaction and work-up procedure to increase yield were not investigated.

Finally, the depolymerized network was analyzed and compared with the initial prepolymer. ^{1}H-NMR spectroscopy confirmed the enone had been recovered (31%) and the depolymerized product resembled the initial prepolymer (Figure 4d). Gel Permeation Chromatography (GPC) was also used to estimate the molecular weight of the depolymerized and initial prepolymer (Figure 5a). However, since the depolymerization was driven through equilibrium, the molecular weight of the species is expected to be significantly larger than the initial prepolymer. As expected, the depolymerized network had a significantly higher molecular weight and dispersity (M_n = 5.8 kDa, $Đ$ = 6.3) than the initial prepolymer (M_n = 0.9 kDa, $Đ$ = 1.4). As a result, the recycled resin formulation needed to be adjusted to account for the higher molecular weight species. Further dilution in DMC (45 wt%) was required to fully dissolve the depolymerized network, but the quantity of photo-initiator (2 wt%) remained the same.

To further evidence the dissociative nature of the Michael bond, an analogous network was created without the electron deficient enone in carvone. As such, networks comprised of limonene, an equivalent terpenoid that lacks the ketone functionality, and tri-arm thiol were fabricated and subjected to the same depolymerization conditions. The network remained visually intact after heating at 140 °C overnight (Figure 4c), which further supports the role of the enone in the observed depolymerization of the carvone network.

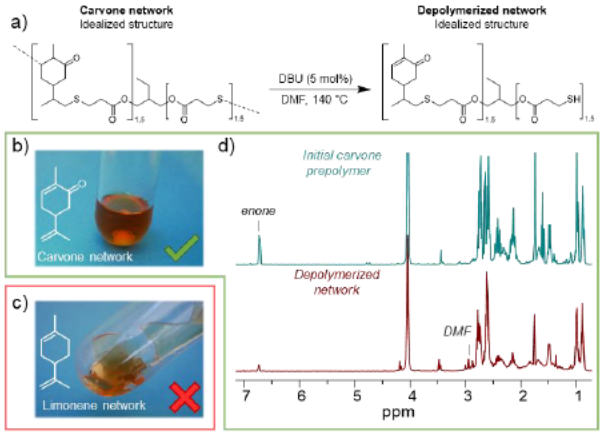


Figure 4. a) Scheme illustrating the depolymerization of the carvone network to regenerate the original functionalities. b) Image of depolymerized carvone network. c) Image of limonene network after depolymerization attempt. d) ^{1}H-NMR spectra of the initial carvone prepolymer (*top*) and depolymerized carvone network (*bottom*).

Initial curing vs Recure 1

After demonstrating that the initial resin could be cured and depolymerized into oligomers with similar composition to the original prepolymer, the recycled resin was recured. Photorheology was performed on the initial and recycled resins to assess their curing profiles. A low storage modulus is observed in both resins in their liquid phase, with a sudden increase in their stiffness upon exposure to UV light (Figure 5b). The storage modulus eventually reaches a plateau, characteristic of a sol-gel transition. Logically, the gelation time is faster for the recycled resin (9 s) *vs* the initial resin (85 s) since higher molecular weight prepolymers require fewer crosslinks to form the infinite network. The storage modulus at plateau is a good indicator of the network's mechanical stiffness. Recure 1 plateaued at a notably lower storage modulus than the initial cure, this was attributed to a comparatively lower crosslinking density. This was further supported by solvent swelling experiment, where Recure 1 had a higher degree of swelling in THF (315 ± 39% *vs* the initial cure 239 ± 3%), due to the increased distance between covalent crosslinks equating to a lower crosslink density within recure 1. We hypothesized that the lower observed crosslink density could arise from two different factors: unwanted thiol oxidation during depolymerization preventing the thiol-ene addition, or the formation of loop defects which could reduce the network elasticity. Quantifying these factors can be particularly challenging, and a

combination of different events are likely responsible for the observed lower crosslinking density in recure 1. Nevertheless, the carvone network could be effectively depolymerized and recured *via* the same UV stimulus without further chemical modification or dilution with additional reactive species.

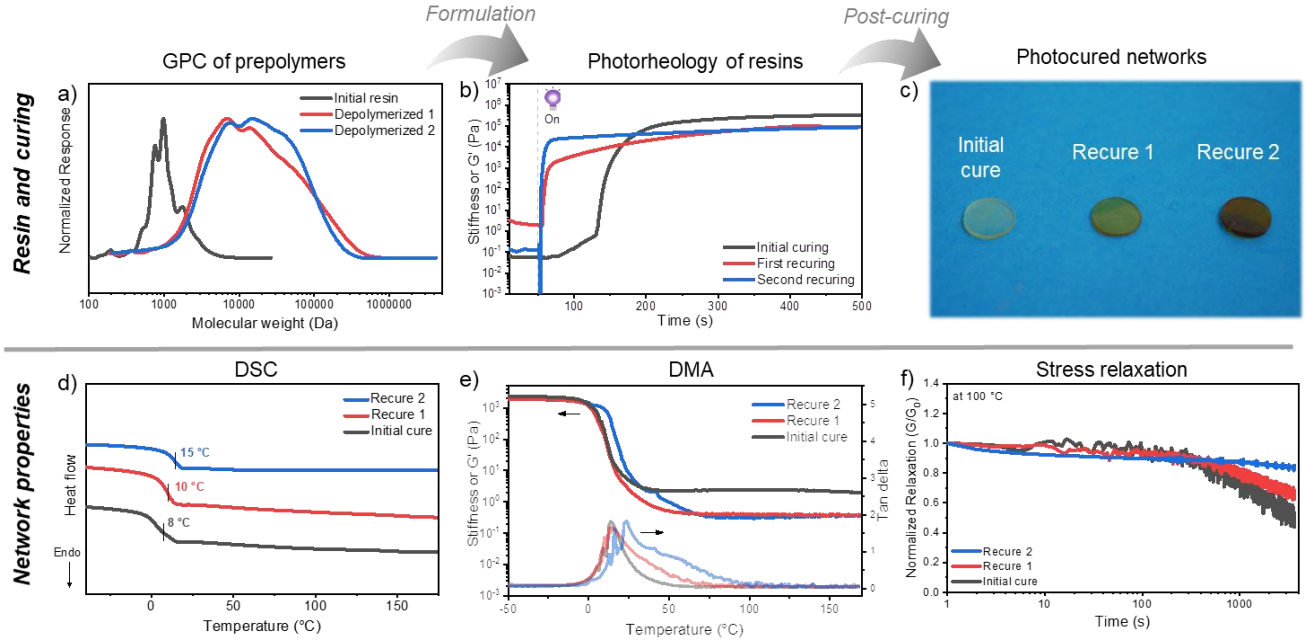


Figure 5 a) GPC elugrams of initial prepolymer, first and second depolymerization cycle ($CHCl_3$,v/v 2% NEt_3) against polystyrene standards b) Photorheology of each resin system taken over 500 s under oscillatory shear at ambient temperature c) Image of initial cure, recure 1 and recure 2 d) Differential scanning calorimetry thermograms of the second heating cycle for the initial and both recures e) Dynamic Mechanical analysis thermograms of storage modulus and tan delta vs temperature for the initial and both recures in the tensile configuration f) Normalized stress relaxation of initial and recured samples at 100 °C and 1% strain taken over 3000 s.

Larger crosslinked films for both the initial and recure 1 were fabricated and post-cured to assess their thermal and mechanical differences. Thermogravimetric analysis found both materials to be thermally stable ($T_{d,\,5\%}$ > 295 °C) with almost identical mass loss profiles (Table S3). The glass transition temperatures (T_g) of the post-cured networks were estimated using Differential Scanning calorimetry (DSC). Surprisingly, the initial cure and recure 1 displayed a comparable T_g value which indicated a good retention of the original thermal characteristics (Figure 5d).

A strategic advantage of using a crosslinked material is the excellent dimensional and mechanical stability at high temperatures. To ensure the initial and recured networks maintained these desirable properties, dynamic mechanical analysis (DMA) was performed in the tensile configuration to assess mechanical performance over a temperature range (Figure 5e). The storage modulus and tan delta were plotted as a function of temperature, with both networks displaying the typical behavior of a crosslinked polymer.[26] The peak observed in the tan delta is a characteristic transition relating to T_g and occurs at a similar temperature in both recure and initial cure, which further supports the observation from the DSC. There is a notable broadening of the tan delta peak in recure 1, which is commonly attributed to heterogeneity in the network, but it is only marginally different from the initial cure.[27] The stiffness, or elasticity, of the network can be better characterized from the storage modulus. Sub T_g, both recure 1 and the initial cure maintain a comparably high storage modulus (Initial - 2292 MPa, Recure 1 – 2202 MPa) before rapidly decreasing until a plateau is reached at ~ 50 °C. The recured sample has a noticeably lower storage modulus at the plateau than the initial cure, reflecting similar observations in the photorheology experiment (Figure 5e). Yet, the crucial property of crosslinked networks is the existence of a sustained plateau at high temperatures, i.e. rubbery plateau, which is observed in both the initial and recured material. Linear plastic materials and some CANs typically undergo a second decrease in storage modulus, where the material begins to flow and lose its original shape. Despite the use of a dissociative dynamic bond, our system maintained a rubbery plateau at high temperatures, providing an attractive property over some previously reported CANs systems.[28]

To further validate the mechanical robustness of the carvone networks, stress relaxation experiments were performed on recure 1 and the initial cure. Relaxation of both the initial cure and recure 1 can be observed to occur around 300 s at 100 °C, but extensive relaxation is not observed at this temperature within this timeframe. However, the slow and minimal relaxation observed at 100 °C for both materials sufficiently satisfies the thermal demands of numerous photocurable resin applications.

Recure 2

The carvone-based network has already demonstrated it can be cured-depolymerized-recured *via* the same photochemical stimulus. But to achieve a truly circular materials economy, a "closed loop" recycling process must be established where consumer products can be reformulated for further use in the same application. Hence, recure 1 must exhibit the same recyclability as the initial carvone network to demonstrate repeat recyclability.

Polymer films of Recure 1 were subjected to the same depolymerization conditions and work-up as the initial carvone network. In a similar fashion, almost total dissolution of the network was observed, with the same trivial quantities of the insoluble particulates (*ca.* 0.1 wt%) observed in the reaction mixture. A similar mass and enone recovery (Mass recover - 57%, enone recovery – 19%) of depolymerized oligomers was achieved with strikingly similar molecular weight (M_n = 6.0 kDa, $Đ$ = 5.2) to the first depolymerization (M_n = 5.8 kDa, $Đ$ = 6.3). These comparable molecular weights allowed the same formulation to be used for the first and second recure (45 wt% DMC, 2 wt% TPO-L). Following this, the curing

profile of both resins was established from photorheology. Both recures possessed a similar gelation time (Recure 1- 9 s, Recure 2 – 4 s) and achieved a storage modulus of a similar magnitude (Recure 1- 0.94 MPa, Recure 2 – 0.73 MPa, Figure 5b). Although this is not surprising given the similar molecular weights of oligomers used in each recure, it was a promising indicator that recure 1 and 2 were mechanically similar. DMA thermograms of recure 2 demonstrated a sustained rubbery plateau up to 170 °C at a similar storage modulus as recure 1. This not only suggests that both recures behave as thermally stable networks, but also feature comparable mechanical performance.

Unusually, there is a significant increase in T_g for recure 2 vs recure 1 and initial cure, despite the lower crosslinking density in recure 1 and 2 (Table S3). A simultaneous broadening of the tan delta peak can also be observed with each recuring cycle, which is driving the tan delta peak to higher temperatures for the recured samples. Together, these observations can be explained through network heterogeneity. It has been noted that some photocured networks are heterogeneous and consist of regions of high crosslink density and regions, or pools, of oligomer and monomer.[27] Broader tan delta peaks are characteristic of an increased heterogeneity in the network and were likely intensified through repeated curing of the same oligomers.[29] However, this is not necessarily a disadvantage, in fact the increased heterogeneity of the sample increased resistance to stress relaxation in recure 1 and 2 *vs* the initial cure.

Conclusion

We have designed a platform utilizing radically-mediated thiol-ene, and the unique structure of carvone, a sustainably-sourced terpenoid to create a recurable resin. Depolymerization and recuring of the carvone-based network was demonstrated through 3 cycles, and the robust mechanical properties, synonymous with crosslinked polymers, were retained in each cycle. Whilst there are several caveats (non-quantitative mass recovery, structural heterogeneity) that limit the 'drop-in' application of materials presented in this study, the simplicity and modularity of the platform could be translated to the ever-growing applications reliant on photocuring technologies. Further investigation and study into dissociative networks should be encouraged so the next generation of photocuring technologies can satisfy the circular materials economy and advance the materials field.

ASSOCIATED CONTENT

Supporting Information

Supporting information contains full synthetic and technical procedures including thermal and mechanical characterization.

The Supporting Information is available free of charge on the ACS Publications website.

Supporting information file

AUTHOR INFORMATION

Corresponding Author

*E-mail:

Present Addresses

School of Chemistry, University of Birmingham, Edgbaston, Birmingham, B15 2TT, U.K.

Author Contributions

C.J.S. and A.P.D. conceived the material synthesis and designed the project idea. C.J.S. performed the synthesis and thermal analysis of the materials. AK characterized model studies. V.C. performed rheological analysis. J.C.W. performed swelling experiments. The paper was written through contributions from all authors and all authors have given approval to the final version of the paper.

Funding Sources

Any funds used to support the research of the manuscript should be placed here (per journal style).

Notes

Any additional relevant notes should be placed here.

ACKNOWLEDGMENT

A.P.D., J.C.W. and C.J.S. acknowledge funding from the European Research Council (ERC) under the European Union's Horizon 2020 research and innovation programme under grant agreement No. 681559. A.K acknowledges funding from the University of Birmingham. V.C. acknowledges funding from Unilever.

ABBREVIATIONS

CAN, Covalent adaptable network; MMP, methyl 3-mercaptopropionate; DMC, dimethyl carbonate; M_n, number-average molar mass; NMR, nuclear magnetic resonance; GPC, Gel Permeation chromatography; DSC, differential scanning calorimetry; DMA, dynamic mechanical analysis; DBU, 1,8-Diazabicyclo(5.4.0)undec-7-ene; DMF, N,N-dimethylformamide; T_g, glass transition temperature; TGA, thermal gravimetric analysis; UV, Ultra-violet

REFERENCES

1. J. C. Worch and A. P. Dove, *ACS Macro Letters*, 2020, **9**, 1494-1506.
2. D. J. Fortman, J. P. Brutman, G. X. De Hoe, R. L. Snyder, W. R. Dichtel and M. A. Hillmyer, *ACS Sustainable Chemistry & Engineering*, 2018, **6**, 11145-11159.
3. J. V. Crivello and E. Reichmanis, *Chemistry of Materials*, 2014, **26**, 533-548.
4. R. Liska, M. Schuster, R. Inführ, C. Turecek, C. Fritscher, B. Seidl, V. Schmidt, L. Kuna, A. Haase, F. Varga, H. Lichtenegger and J. Stampfl, *Journal of Coatings Technology and Research*, 2007, **4**, 505-510.
5. C. E. Hoyle, in *Radiation Curing of Polymeric Materials*, American Chemical Society, 1990, vol. 417, ch. 1, pp. 1-16.
6. C. J. Kloxin and C. N. Bowman, *Chemical Society Reviews*, 2013, **42**, 7161-7173.
7. M. Podgórski, S. Huang and C. N. Bowman, *ACS Applied Materials & Interfaces*, 2021, **13**, 12789-12796.
8. Y. Xu, K. Odelius and M. Hakkarainen, *ACS Sustainable Chemistry & Engineering*, 2020, **8**, 17272-17279.
9. C. Wang, T. M. Goldman, B. T. Worrell, M. K. McBride, M. D. Alim and C. N. Bowman, *Materials Horizons*, 2018, **5**, 1042-1046.
10. Z. Chen, M. Yang, M. Ji, X. Kuang, H. J. Qi and T. Wang, *Materials & Design*, 2021, **197**, 109189.
11. J. Van Damme, O. van den Berg, J. Brancart, L. Vlaminck, C. Huyck, G. Van Assche, B. Van Mele and F. Du Prez, *Macromolecules*, 2017, **50**, 1930-1938.
12. T. Hughes, G. P. Simon and K. Saito, *Polymer Chemistry*, 2019, **10**, 2134-2142.
13. H. A. Houck, E. Blasco, F. E. Du Prez and C. Barner-Kowollik, *Journal of the American Chemical Society*, 2019, **141**, 12329-12337.
14. P. Chakma and D. Konkolewicz, *Angewandte Chemie International Edition*, 2019, **58**, 9682-9695.
15. B. Zhang, P. Chakma, M. P. Shulman, J. Ke, Z. A. Digby and D. Konkolewicz, *Organic & Biomolecular Chemistry*, 2018, **16**, 2725-2734.
16. C. C. C. R. de Carvalho and M. M. R. da Fonseca, *Food Chemistry*, 2006, **95**, 413-422.

17. C. E. Hoyle, T. Y. Lee and T. Roper, *Journal of Polymer Science Part A: Polymer Chemistry*, 2004, **42**, 5301-5338.
18. B. H. Northrop and R. N. Coffey, *Journal of the American Chemical Society*, 2012, **134**, 13804-13817.
19. W. Denissen, J. M. Winne and F. E. Du Prez, *Chemical Science*, 2016, **7**, 30-38.
20. N. J. Van Zee and R. Nicolaÿ, *Progress in Polymer Science*, 2020, **104**, 101233.
21. B. R. Elling and W. R. Dichtel, *ACS Central Science*, 2020, **6**, 1488-1496.
22. C. Taplan, M. Guerre and F. E. Du Prez, *Journal of the American Chemical Society*, 2021, **143**, 9140-9150.
23. N. Van Herck, D. Maes, K. Unal, M. Guerre, J. M. Winne and F. E. Du Prez, *Angewandte Chemie International Edition*, 2020, **59**, 3609-3617.
24. A. C. Weems, K. R. Delle Chiaie, J. C. Worch, C. J. Stubbs and A. P. Dove, *Polymer Chemistry*, 2019, **10**, 5959-5966.
25. D. P. Nair, M. Podgórski, S. Chatani, T. Gong, W. Xi, C. R. Fenoli and C. N. Bowman, *Chemistry of Materials*, 2014, **26**, 724-744.
26. L. Zhang and S. J. Rowan, *Macromolecules*, 2017, **50**, 5051-5060.
27. A. R. Kannurpatti, J. W. Anseth and C. N. Bowman, *Polymer*, 1998, **39**, 2507-2513.
28. M. K. McBride, B. T. Worrell, T. Brown, L. M. Cox, N. Sowan, C. Wang, M. Podgorski, A. M. Martinez and C. N. Bowman, *Annual Review of Chemical and Biomolecular Engineering*, 2019, **10**, 175-198.
29. C. R. Szczepanski, C. S. Pfeifer and J. W. Stansbury, *Polymer*, 2012, **53**, 4694-4701.

5.2 Supporting Information

Chemical Recycling of photocurable resins containing reversible thiol-Michael bonds

Connor J. Stubbs[a], Anissa Khalfa[a], Viviane Chiaradia[a], Josh C. Worch[a], Andrew P. Dove*[a]

[a] *School of Chemistry, University of Birmingham, Edgbaston B15 2TT, United Kingdom*

Corresponding Authors: [redacted]

General Materials and Methods. All compounds, unless otherwise indicated, were purchased from commercial sources, and used as received. Methyl 3-mercaptopropionate was distilled and stored under a nitrogen atmosphere in an ampoule.

NMR Spectroscopic Analysis. All NMR spectroscopy experiments were performed at 300 K on a Bruker DPX-400 NMR instrument equipped operating at 400 MHz for ^{1}H (100.57 MHz for ^{13}C). ^{1}H NMR spectra are referenced to residual protio solvent (δ = 7.26 for $CDCl_3$, δ = 2.91 for DMF-d_7) and ^{13}C NMR spectra are referenced to the solvent signal (δ = 77.16 for $CDCl_3$, δ = 162.7 for DMF-d_7). The resonance multiplicities are described as s (singlet), d (doublet), t (triplet), q (quartet) or m (multiplet).

Mass Spectrometry. High Resolution Electrospray Ionization Mass Spectrometry was performed in the School of Chemistry at University of Birmingham on a Waters Xevo G2-XS QTof Quadrupole Time-of-Flight mass spectrometer.

Gel permeation Chromatography (GPC). GPC measurements were performed in $CHCl_3$ on an Agilent 1260 Infinity II Multi-Detector GPC System fitted with RI, ultraviolet (UV, λ = 309 nm), and viscometer detectors. The polymers were eluted through an Agilent guard column (PLGel 5 μM, 50 × 7.5 mm) and two Agilent mixed-C columns (PLGel 5 μM, 300 × 7.5 mm) using $CHCl_3$ (buffered with 0.5% NEt_3) as the mobile phase (flow rate = 1 mL·min^{-1}, 40 °C). Number average molecular weights (M_n), weight average molecular weights (M_w) and dispersities ($Đ_M = M_w/M_n$) were determined using Agilent GPC software (vA.02.01) against a 15-point calibration curve (M_p = 162–3,187,000 g·mol^{-1}) based on poly(styrene) standards (Easivial PS-M/H, Agilent).

Differential Scanning Calorimetry (DSC). The thermal characteristics of the polymers were determined using differential scanning calorimetry (STARe system DSC3, Mettler Toledo) from −50 to 180 °C at a heating rate of 10 °C·min^{-1} for two heating/cooling cycles unless otherwise specified. The glass transition temperature (T_g) was determined from the inflection point in the second heating cycle of DSC.

Thermogravimetric Analysis (TGA). TGA thermograms were obtained using a TGA/DSC 1 - Thermogravimetric Analyzer (Mettler Toledo). Thermograms were recorded under an N_2 atmosphere at a heating rate of 10 °C·min^{-1}, from 10 − 600 °C, with an average sample weight of *ca*. 5 mg. Aluminium pans were used for all samples. Decomposition temperatures were reported as the 5% weight loss temperature ($T_{d\ 5\%}$).

Fourier-transform infrared (FTIR) spectroscopy. FTIR spectra were collected out using an Agilent Technologies Cary 630 FTIR spectrometer. 16 Scans from 600 to 4000 cm^{-1} were taken at a resolution of 2 cm^{-1}, and the spectra were corrected for background absorbance.

Stress-Relaxation was performed on an Anton Paar MCR 302 using Anton Paar PP8 parallel-plate, a diameter of 8 mm. Temperature was controlled with a P-PTD 200/AIR Peltier and a P-PTD 200 hood. Strain sweeps were performed to ensure stress relaxation experiments were performed in the linear region. Stress relaxation tests were performed at 1% strain at 50 °C, 100 °C, and 140 °C.

Photorheology. The crosslinking kinetic of the resins was examined as a function of gelation time by photorheology using an Anton Paar MCR-302 rheometer fitted with a detachable photoillumination system (Exfo OmniCure S1500 UV light source, broadband Hg-lamp, glass plate). Resin samples were sheared between two parallel plates at 0.2 Hz with an amplitude of 25% for 50 sec without irradiation. After this time, the light source was switched on and measurements were taken every 0.2 sec over the course of 2 min. The intersection point of the storage moduli and loss moduli plots was used to determine the time of gelation of the resin.

Dynamic Mechanical Analysis (DMA). Dynamic mechanical thermal analysis (DMTA) data were obtained using a Mettler Toledo DMA 1 star system and analyzed using the software package STARe V13.00a Thermal sweeps were conducted using films (L x W x thickness = 15 mm x 6 mm x 0.5 mm) cooled to −50 °C and held isothermally for *ca*. 5 minutes. Storage and loss moduli, as well as the loss factor (ratio of *E"* and *E'*, tan δ) were probed as the temperature was swept from −50 to 180 °C, 5 °C min^{-1}. Thermomechanical behavior was determined from three samples in this way.

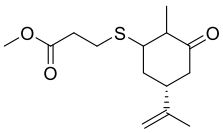
Swell testing and gel fraction. Networks were taken and cut into disks (6.7 × 0.5 mm) and weighed before being submerged in THF and allowed to swell until equilibrium swelling was reached after 24 hours. The initial mass (W_i) and swelling mass (W_s) was used to calculate the swelling ratio (%) as shown in equation S1. The swollen networks were resubmerged in new THF and finally dried to get the dry mass (W_d). This was used to calculate the gel fraction (%) as shown in equation S2.

Equation S1 $$\boldsymbol{Swelling\ ratio}\ (\%) = \frac{\boldsymbol{W_s}}{\boldsymbol{W_i}} \times \mathbf{100}$$

Equation S2 $$\boldsymbol{Gel\ fraction}\ (\%) = \frac{\boldsymbol{W_d}}{\boldsymbol{W_i}} \times \mathbf{100}$$

Experimental Procedures

Synthesis of CarMMP



L-carvone (2.00 g, 1 equiv, 13.3 mmol) and methyl 3-mercaptopropionate (1.76 g, 1.1 equiv, 14.7 mmol) were mixed in bulk at 0 °C until homogenous. DBU (19.5 µL, 1 mol%) was then added in one-portion and the reaction was left to stir at 0 °C for 30 mins before warming to ambient temperature. The mixture was purified using column chromatography with EtOAc/Hexanes and concentrated yielding a colorless oil (1.9 g, 50%). ^{1}H-NMR (400 MHz, Chloroform-*d*) δ 4.85 – 4.65 (m, 2H), 3.67 (s, 3H), 3.43 (dt, J = 4.7, 3.4 Hz, 1H), 2.94 – 2.82 (m, 1H), 2.82 – 2.70 (m, 3H), 2.64 – 2.50 (m, 2H), 2.46 (ddd, J = 13.7, 4.4, 2.1 Hz, 1H), 2.26 – 2.11 (m, 2H), 1.99 (ddd, J = 13.8, 11.8, 3.2 Hz, 1H), 1.74 (s, 3H), 1.12 (d, J = 6.7 Hz, 3H). ^{13}C NMR (101 MHz, Chloroform-*d*) δ 209.67, 172.25, 147.04, 110.38, 51.93, 50.30, 48.75, 46.10, 40.75, 35.96, 34.68, 27.10, 20.89, 12.71. ^{1}H-NMR (400 MHz, DMF-d_7) δ 4.80 (s broad, 2H), 3.65 (s, 3H), 3.60 (dt, *J* = 4.9, 3.3 Hz, 1H), 3.09 – 2.98 (m, 1H), 2.89 – 2.76 (m, 3H), 2.70 – 2.57 (m, 2H), 2.45 (t, J = 13.2 Hz, 1H), 2.24 (dd, J = 13.4, 4.0 Hz, 1H), 2.20 – 2.06 (m, 2H), 1.77 (s, 3H), 1.04 (d, J = 6.7 Hz, 3H). ^{13}C-NMR (101 MHz, DMF-d_7) δ 209.56, 172.59, 148.39, 110.27, 51.77, 50.82, 48.41, 46.40, 41.53, 36.31, 35.01, 27.19, 20.60, 12.76. MS (TOF) calculated for $C_{14}H_{22}O_3S$ + H 271.1368; found 271.1374.

Prepolymer synthesis

L-carvone (10 g, 1.5 equiv, 66.7 mmol) and trimethylolpropane tris(3-mercaptopropionate) (17.68 g, 1 equiv, 44.4 mmol) were mixed in bulk until visible homogenous in a 100 mL RBF with a magnetic stirrer. The RBF was wrapped in foil then TPO-L (0.277 g, 1 wt%) was added and stirred for ~ 5 min until homogenous. The RBF was partially exposed by ripping the foil and irradiated with UV light using a fiber optic cable fitted to an OmniCure S1500 and stirred for *ca.* 2 h. Progress of the reaction was monitored by ^{1}H-NMR spectroscopy for the disappearance of the propenyl group. The resulting colorless oil was poured off and used as the carvone prepolymer. ^{1}H-NMR (400 MHz, Chloroform-*d*) δ 6.75 (s, broad 1H), 4.08 (s,

overlapping 6H), 2.91 – 2.56 (m, overlapping, 14H), 2.54 – 2.27 (m, overlapping, 5H), 2.27 – 1.99 (m, overlapping, 5H), 1.78 (s, J = 1.4 Hz, 4H), 1.76 – 1.55 (m, overlapping, 3H), 1.59 – 1.33 (m, 2H), 1.01 (d, J = 6.8 Hz, 4.3H), 0.91 (t, J = 6.5 Hz, 3H). ^{13}C NMR (101 MHz, $CDCl_3$) δ 199.96, 171.54, 171.32, 63.96, 42.58, 40.84, 40.63, 39.29, 39.19, 38.45, 37.28, 37.15, 37.07, 34.80, 30.52, 28.41, 27.75, 27.67, 23.04, 19.77, 16.01, 15.78, 7.47. GPC analysis ($CHCl_3$ + 0.5% v/v NEt_3): M_w = 1.2 kDa, M_n = 0.9 kDa, $Đ$ = 1.4. FT-IR: 1726 cm^{-1} (C=O ester) 1659 cm^{-1} (C=O enone).

Radical addition of MMP to carvone model reaction

L-carvone (0.8513 g, 1 equiv, 5.68 mmol) and methyl 3-mercaptopropionate (1.4303 g, 2.1 equiv, 11.9 mmol) were mixed in bulk until visible homogenous in a glass vial. TPO-L (0.022 g, 1 wt%) was then added in one portion and vigorously stirred. The mixture was then irradiated with UV light in a Formlabs Form Cure 405 nm curer and sampled periodically (10 s, 30 s, 60 s, 5 min, 10 min, 30 min, 1 h, 1.5 h, 2 h, 3 h) for ^{1}H-NMR spectroscopy.

Dynamic exchange model reaction ambient temperature

CarMMP (135 mg, 0.5 mmol) was dissolved in DMF-d_7 (2 mL) in a glass vial, then DBU (3.7 µL, 5 mol%) was added and stirred rapidly. An aliquot was taken for an initial ^{1}H NMR spectrum. The remaining solution was left stirring at ambient conditions and sampled periodically (30 min, 1 h, 2 h) for ^{1}H NMR spectroscopy.

Dynamic exchange model reaction variable temperature NMR

CarMMP (67.5 mg, 0.25 mmol) was dissolved in DMF-d_7 (0.5 mL) and added to an NMR tube. A reference ^{1}H NMR spectrum was taken at 298 K. DBU (1.9 µL, 5 mol%) was dissolved in DMF-d_7 (0.5 mL) and added to the NMR tube then briefly stirred. ^{1}H NMR spectrums were taken at various temperatures (50, 60, 70, 80, 90, 100 °C) after a 5-minute equilibration time at each temperature.

Depolymerization of initial cure

Shredded initial cure (10.55 g, 1 equiv, 16.9 mmol), DMF (67 mL) and DBU (126 µL, 5 mol%) were added to an ampoule with a magnetic stirrer and stirred. Nitrogen is bubbled through the mixture for ~ 30 min before the flask is sealed and heated at 140 °C for *ca.* 16 h. The reaction is removed from the heat and

filtered through fiberglass wool to remove the insoluble particulates, the residue is dried and weighed to assess the quantity of particulates (49 mg, 0.5% of the original weight). The filtrate is precipitated into methanol (~800 mL), centrifuged and the supernatant is discarded. The remaining orange tacky solid is washed with additional methanol (~200 mL) then discarded. Residual solvent is removed under vacuum for 2 h to yield a tacky orange solid (5.80 g, 55%). GPC analysis ($CHCl_3$ + 0.5% v/v NEt_3): M_w = 36.1 kDa, M_n = 5.8 kDa, $Đ$ = 6.3. FT-IR: 1727 cm^{-1} (C=O ester) 1697 cm^{-1} (C=O ketone) 1667 cm^{-1} (C=O enone)

Depolymerization of Recure 1

Shredded Recure 1 (3.28 g, 1 equiv, 5.26 mmol), DMF (21 mL) and DBU (39 µL, 5 mol%) were added to an ampoule with a magnetic stirrer and stirred. Nitrogen is bubbled through the mixture for ~ 30 min before the flask is sealed and heated at 140 °C for *ca* 16 h. The reaction is removed from the heat and filtered through fiberglass wool to remove the insoluble particulates, the residue is dried and weighed to assess the quantity of particulates (3.7 mg, 0.1% of the original weight). The filtrate is precipitated into methanol (~350 mL), centrifuged and the supernatant is discarded. The remaining orange tacky solid is washed with additional methanol (~100 mL) then discarded. Residual solvent is removed under vacuum for 2 h to yield a tacky orange solid (1.87 g, 57%) GPC analysis ($CHCl_3$ + 0.5% v/v NEt_3): M_w = 31.1 kDa, M_n = 6.0 kDa, $Đ$ = 5.2. FT-IR: 1724 cm^{-1} (C=O ester) 1697 cm^{-1} (C=O ketone) 1666 cm^{-1} (C=O enone).

Initial carvone resin

Carvone prepolymer (7 g, 70 wt%) was added to a vial and stirred in dimethylcarbonate (3 g, 30 wt%) until the liquid was homogenous. The vial was wrapped in foil and TPO-L (0.14 g, 2 wt%) was added, then the vial was shaken for 1 h until the liquid was homogenous.

Resin for Recure 1

Depolymerized 1 (4.94 g, 55 wt%) was added to a vial and stirred in dimethylcarbonate (4.04 g, 45 wt%) until the liquid was homogenous. The vial was wrapped in foil and TPO-L (0.0988 g, 2 wt%) was added, then the vial was shaken for 1 h until the liquid was homogenous.

Resin for Recure 2

Depolymerized 2 (1.87 g, 55 wt%) was added to a vial and stirred in dimethylcarbonate (1.53 g, 45 wt%) until the liquid was homogenous. The vial was wrapped in foil and TPO-L (0.0374 g, 2 wt%) was added, then the vial was shaken for 1 h until the liquid was homogenous.

General curing procedure

Resins were deposited on a glass slide using a glass pipette to ensure a flat surface and even coverage. The glass slide is positioned above the UV light source (an OmniCure S1500 fitted with a fiber optic cable) and irradiated from beneath the glass slide. *Note: this ensured thick films did not exhibit surface wrinkling and defects over extended curing periods.* The resins were inspected periodically until the surface of the film was solid and non-tacky (typically ~1 hour for 1 mm thickness). The films were removed from the glass slide and post-cured in a vacuum oven at 90 °C under reduced pressure for *ca.* 16 h to remove dimethyl carbonate and ensure the network was sufficiently crosslinked.

Limonene resin formulation

Limonene (2 g, 1.5 equiv), trimethylolpropane tris(3-mercaptopropionate) (3.90 g, 1 equiv, 44.4 mmol) and dimethylcarbonate (1.47 g, 20 wt%) were stirred in a vial until homogenous. TPO-L (0.03 g, 2 wt%) was added to the mixture and rapidly stirred until dissolved. The resulting colorless liquid was cured in the same manner as the carvone resins, as described in the general curing procedure.

Thiol-ene kinetics experiment

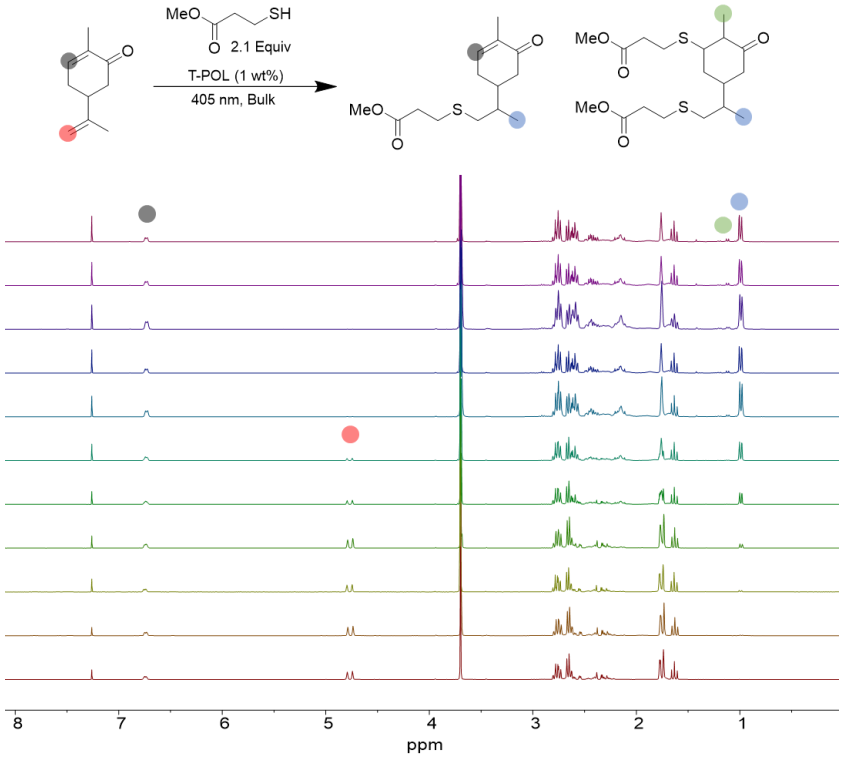


Figure S1 ^{1}H NMR spectra of the addition of MMP to carvone *via* radical mediated thiol-ene at increasing radiation times in $CDCl_3$. Consumption and formation of each functionality was referenced against the methyl ester singlet at 3.69 ppm and summarized in table S1.

Irradiation time (s)	Enone (%)	Propenyl (%)	Thioether (%)	Michael bond (%)
0	100	100	0	0
10	100	98	4	0
30	100	93	10	0
60	100	85	18	0
300	98	44	57	3
600	96	21	78	7
1800	88	0	95	11
3600	85	0	97	13
5400	85	0	97	13
7200	83	0	97	14
10800	83	0	97	17

Table S1 Molar percentage of the monitored functionalities in the radical addition of MMP to carvone against UV irradiation time.

Identifying ^{1}H NMR peaks associated to the Michael product

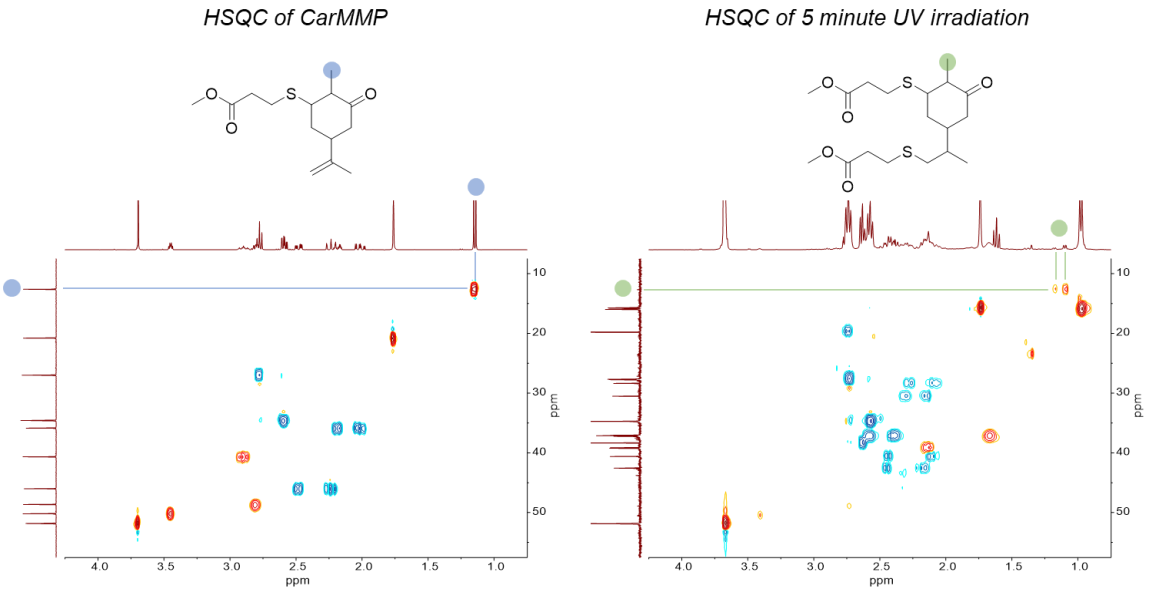


Figure S2 HSQC NMR spectra of CarMMP (left) and crude thiol-ene kinetics experiment 5 minutes of UV irradiation (right) in $CDCl_3$.

Identifying peaks in the ^{1}H NMR that corresponded to the desired Michael product relied on ^{13}C NMR due to the presence of stereoisomers. The HSQC of the assigned CarMMP identified the ^{13}C shift corresponding to the α-methyl ketone of the Michael product. A further HSQC of the thiol-ene kinetics experiment taken after 5 minutes of irradiation highlights the corresponding ^{1}H peaks of the Michael product that can be integrated against the consumption of the enone. Full assignment of CarMMP in $CDCl_3$ can be found below.

Dynamic exchange experiment at ambient temperature

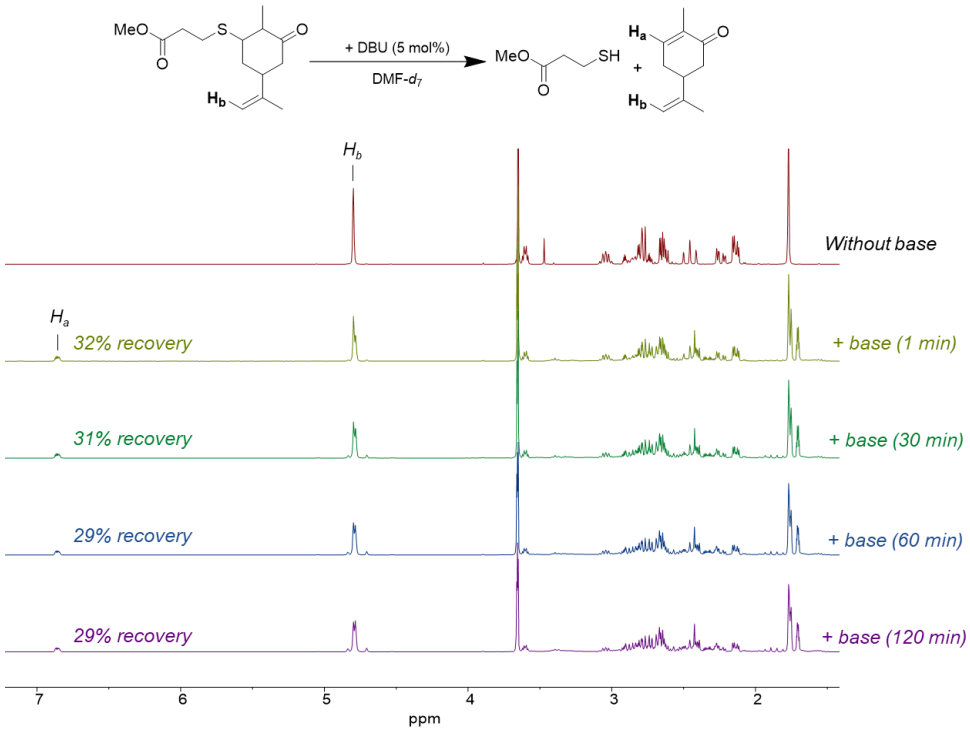


Figure S3 The dynamic exchange of CarMMP at ambient temperature with and without DBU (5 mol%) at different times. Enone at 6.85 ppm quantified from the unconsumed propenyl singlet at 4.80 ppm in DMF-d_7.

Van't Hoff plot

Calculation of the K_{eq} for the dissociation of CarMMP in DMF-d_7 with DBU (5 mol%) was achieved from quantifying the carvone concentration at increasing temperatures. Quantifying the carvone concentration was achieved through the integration of the characteristic enone singlet at 6.85 ppm in DMF-d_7 against the propenyl singlet at 4.80 ppm in DMF-d_7 which was unconsumed in the process. Assuming the absence of side reactions during the experiment, the concentration of Carvone and MMP will be equal. The concentration of CarMMP can also be obtained from the known initial concentration and the concentration of the dissociated species.

$$K_{eq} = \frac{[Carvone][MMP]}{[CarMMP]}$$

Equation S3 Equation for K_{eq} of the dissociation of CarMMP

$$K_{eq} = \frac{[Carvone]^2}{([CarMMP_{int}] - [Carvone])}$$

Equation S4 Equation for K_{eq} using the carvone and initial CarMMP concentration

Temperature (°C)	1000/T (K^{-1})	K_{eq}	ln(K_{eq})
50	3.096	0.471	-0.753
60	3.003	0.672	-0.397
70	2.915	1.281	0.248
80	2.833	2.106	0.745
90	2.755	3.453	1.239
100	2.681	5.283	1.664

Table S2 Data summary used to construct the Van't Hoff plot

Comparison of ^{1}H NMR spectra of the depolymerized networks

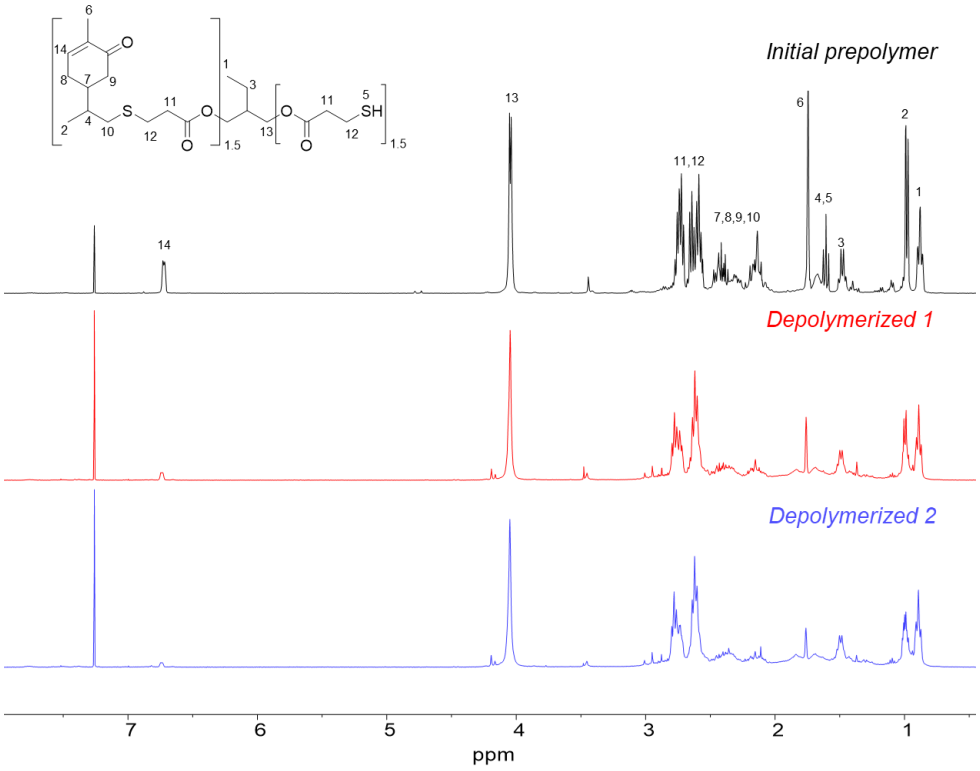


Figure S4 ^{1}H NMR spectra of the initial prepolymer, depolymerized 1 and depolymerized 2 in $CDCl_3$, 400 MHz

NMR Data

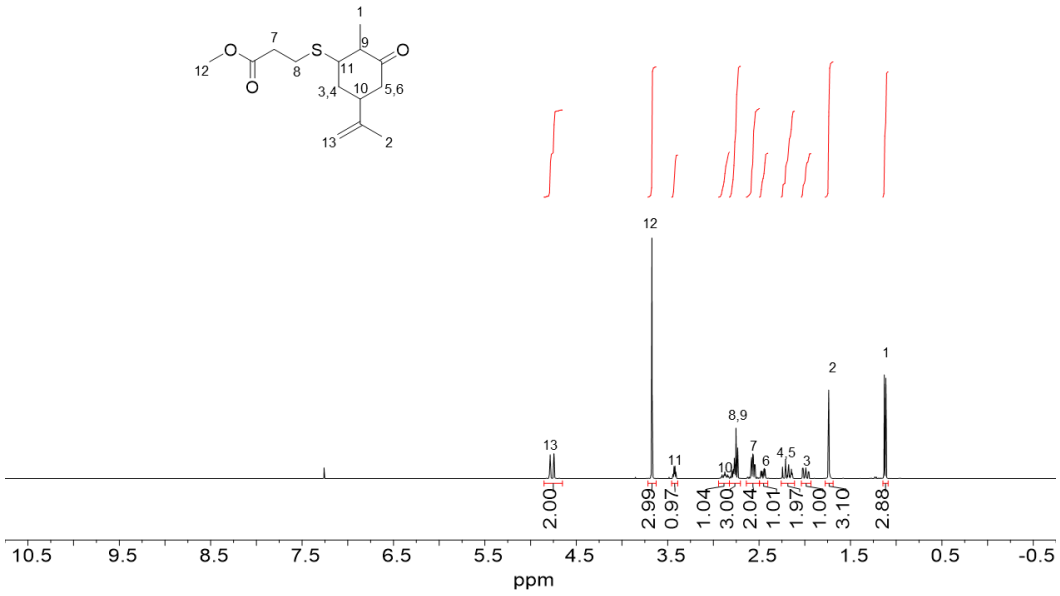


Figure S5. CarMMP ^{1}H NMR Spectrum – 400 MHz, $CDCl_3$.

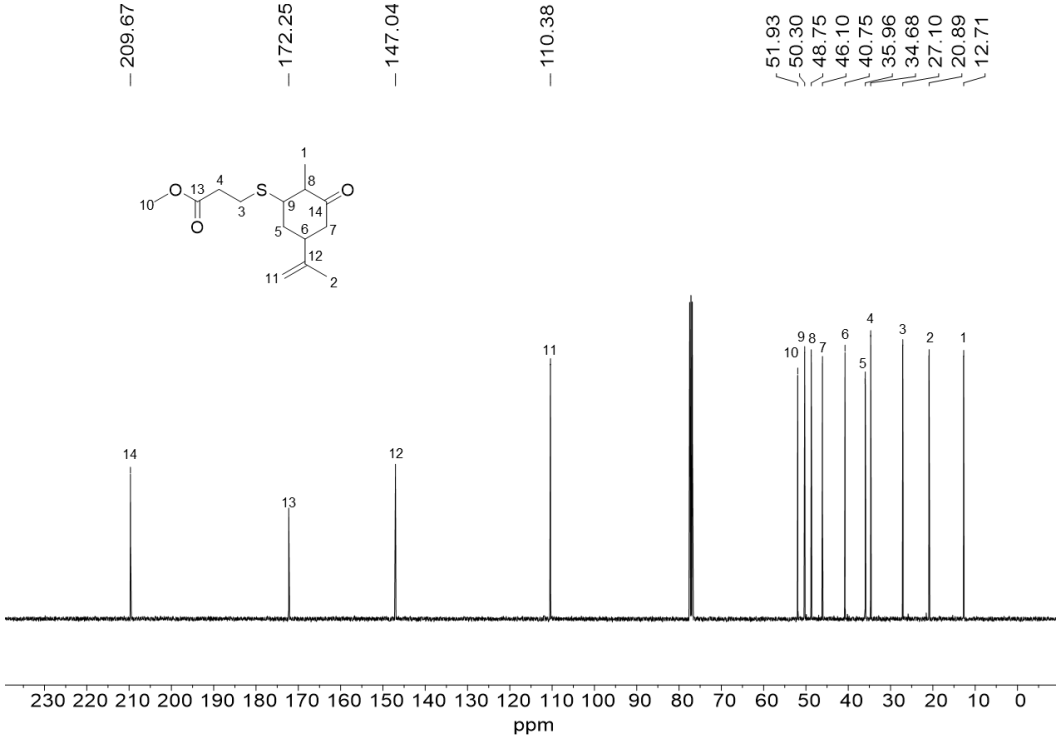


Figure S6. CarMMP ^{13}C NMR Spectrum – 101 MHz, $CDCl_3$.

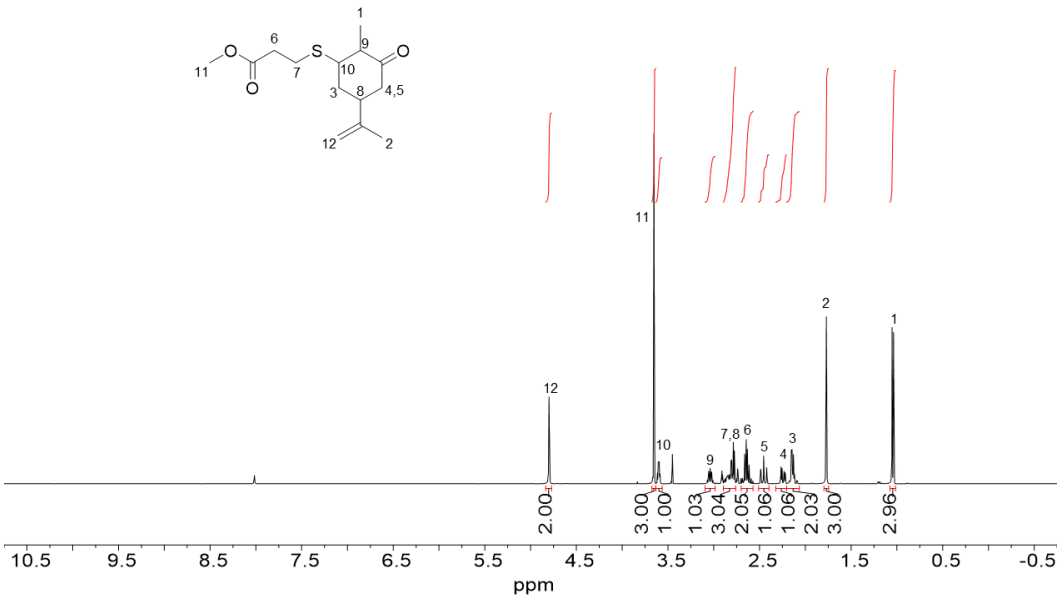


Figure S7. CarMMP ^{1}H NMR Spectrum – 400 MHz, DMF-d_7.

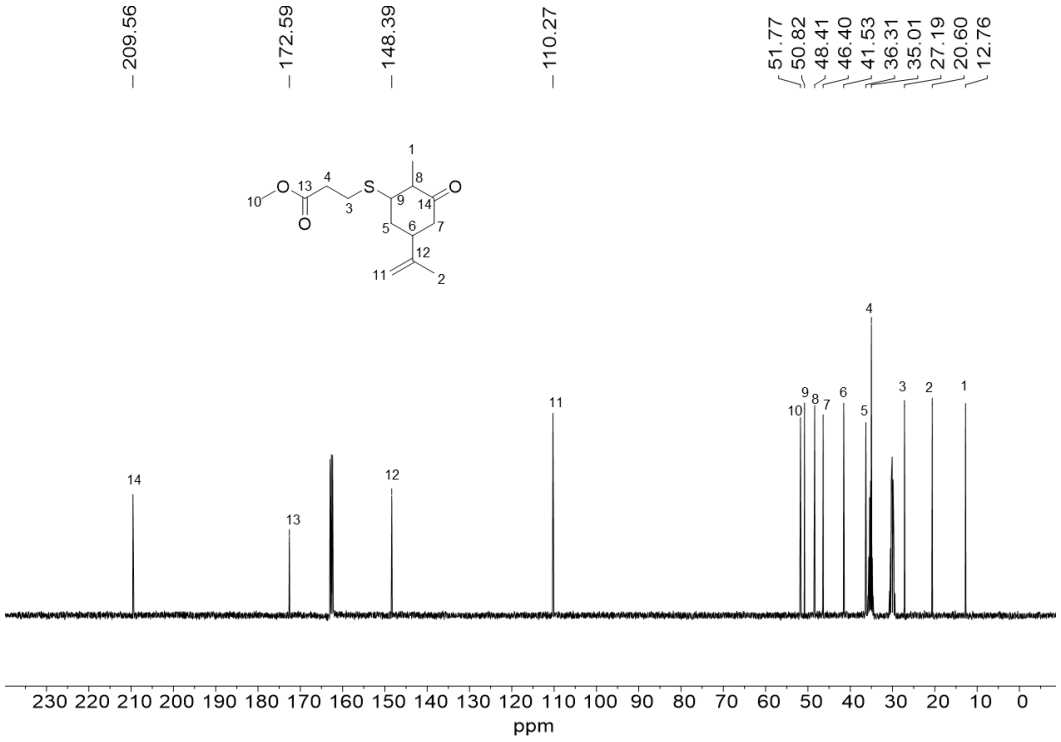


Figure S8. CarMMP ^{13}C NMR Spectrum – 101 MHz, DMF-d_7.

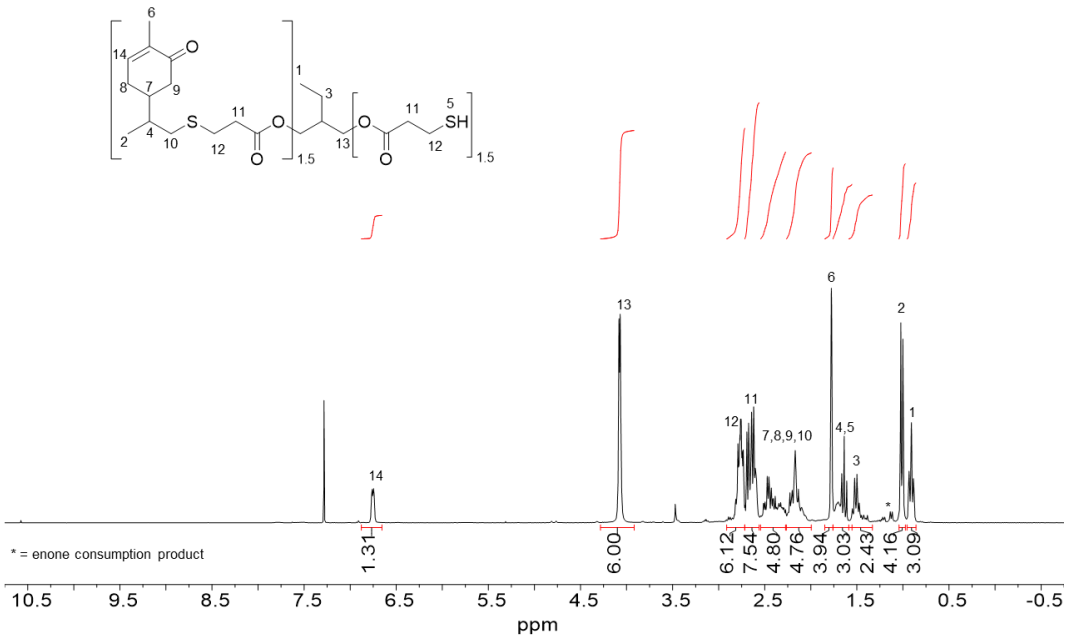


Figure S9. Carvone Prepolymer ^{1}H NMR Spectrum – 400 MHz, $CDCl_3$.

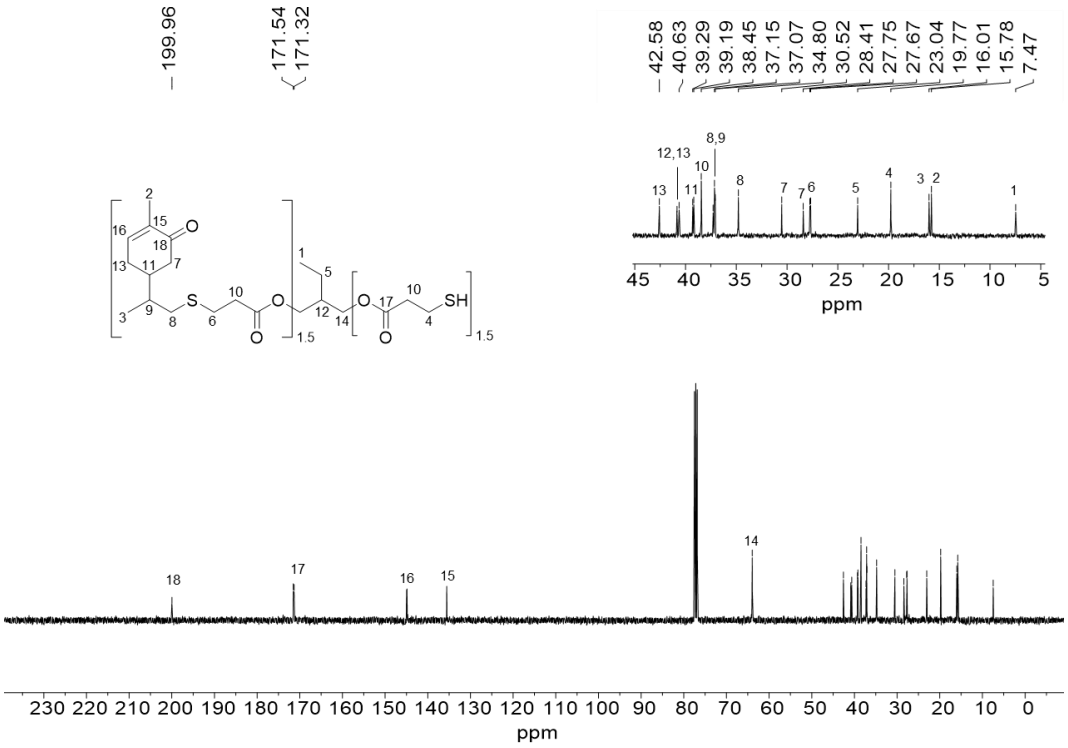


Figure S10. Carvone Prepolymer ^{13}C NMR Spectrum – 101 MHz, $CDCl_3$.

DSC data

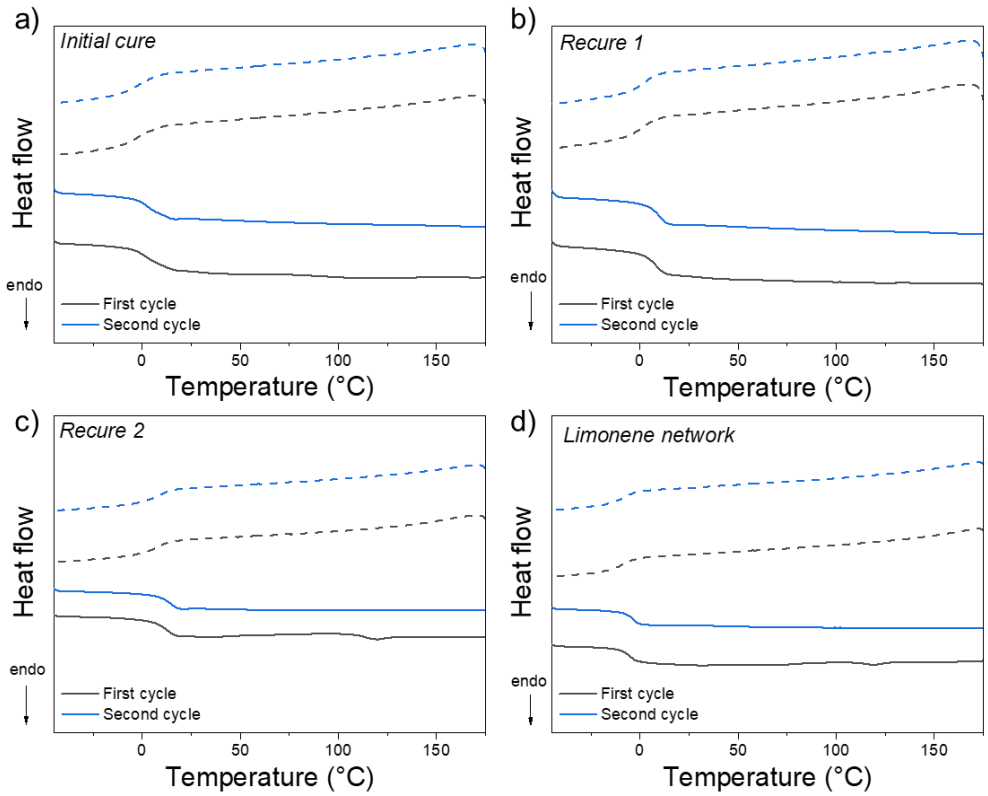


Figure S11. DSC thermograms of a) Initial cure, b) Recure 1, c) Recure 2, d) Limonene network.

TGA Data

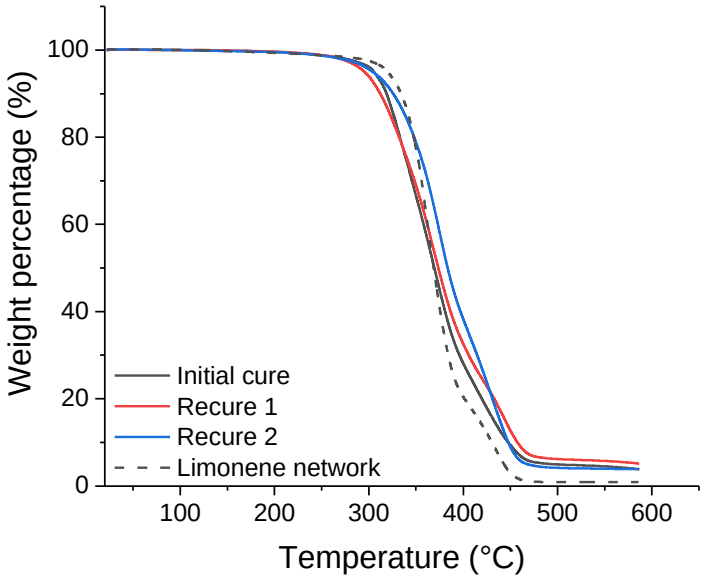


Figure S12. TGA thermograms of carvone and limonene networks

FT-IR data of prepolymers and carvone networks

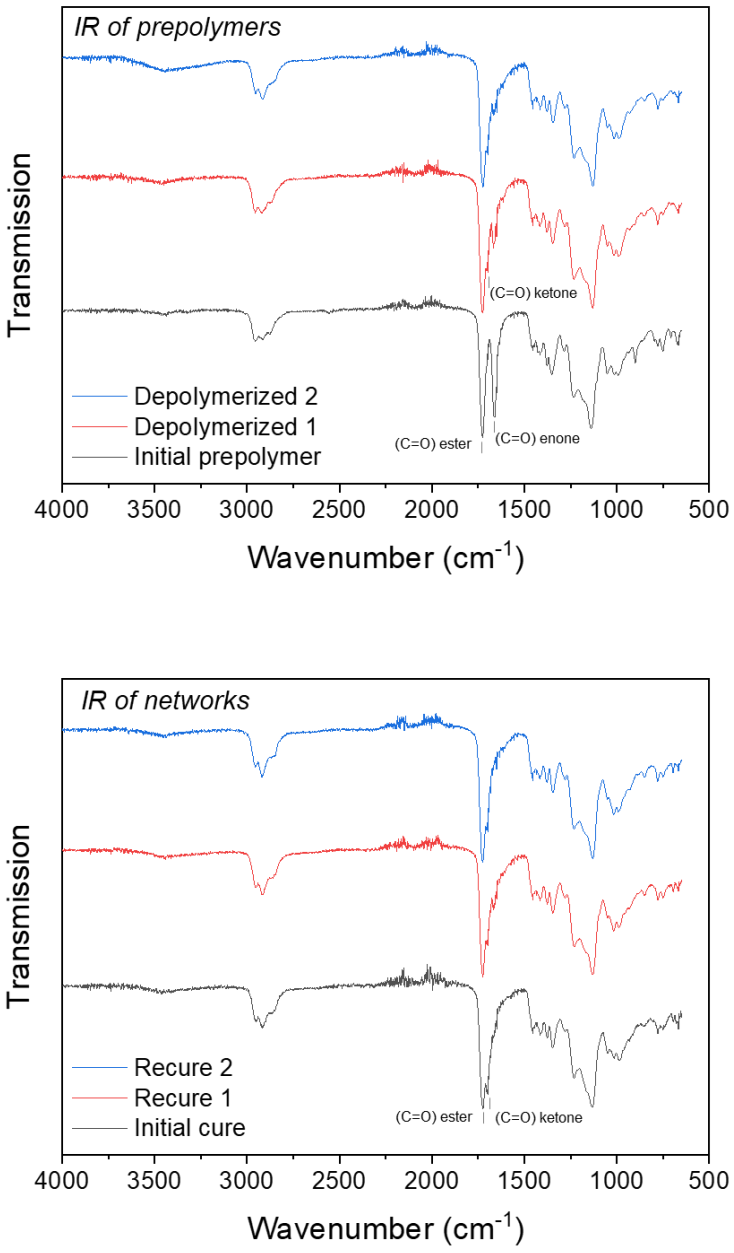


Figure S13. FT-IR spectra of the prepolymers (top) and the post-cured network (bottom)

Photorheology

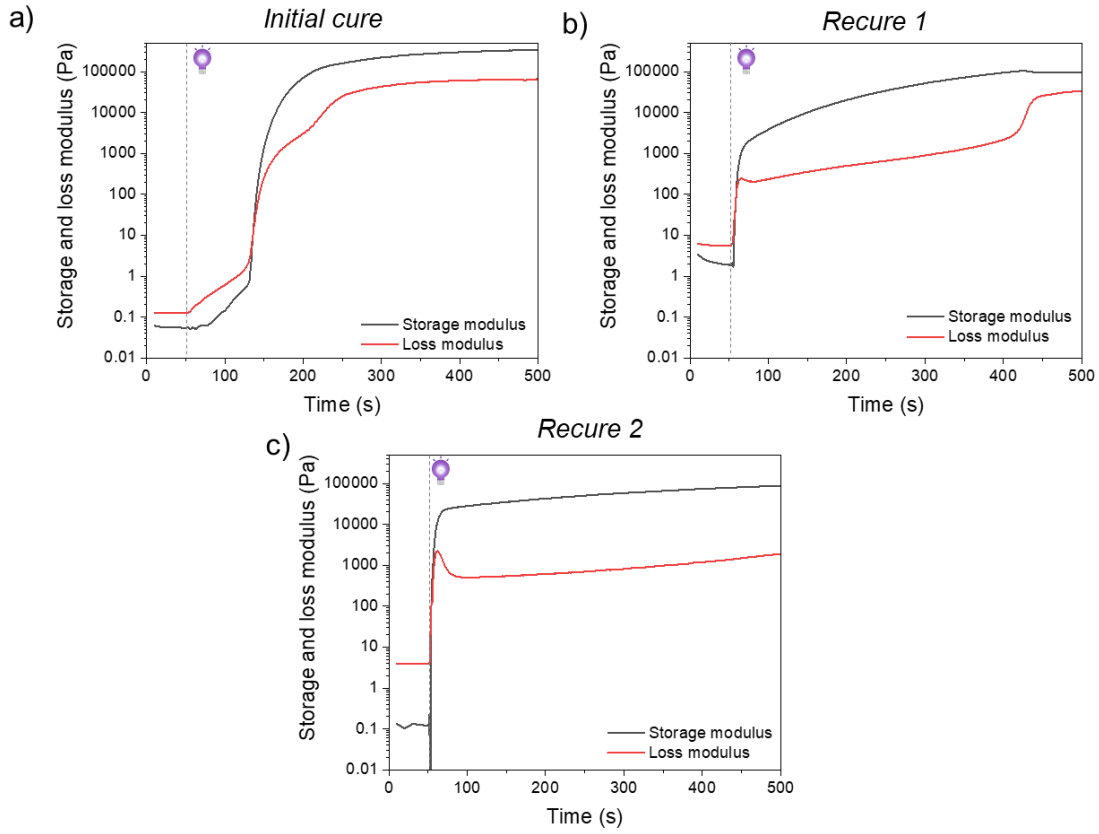


Figure S14. Storage and loss modulus during profiles over 500s obtained from photorheology for a) Initial cure, b) Recure 1, c) Recure 2

DMA

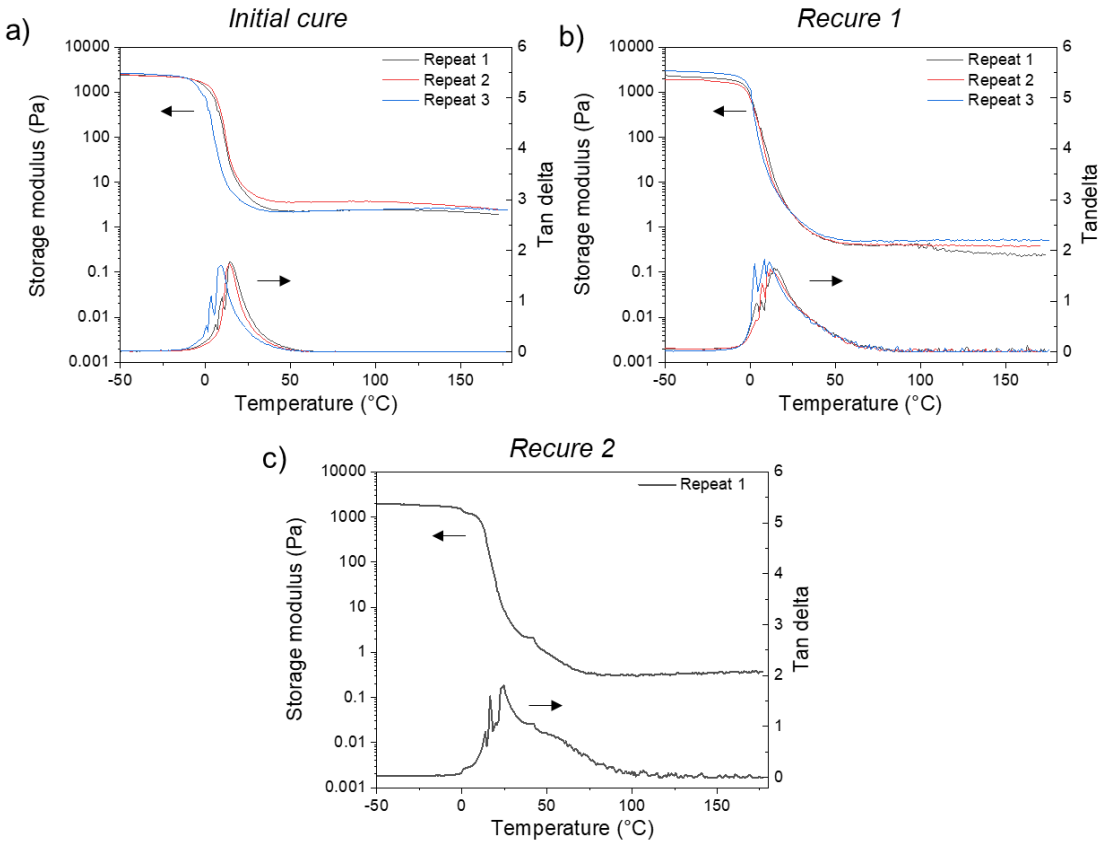


Figure S15. DMTA thermograms of a) Initial cure, b) Recure 1, c) Recure 2

Stress relaxation

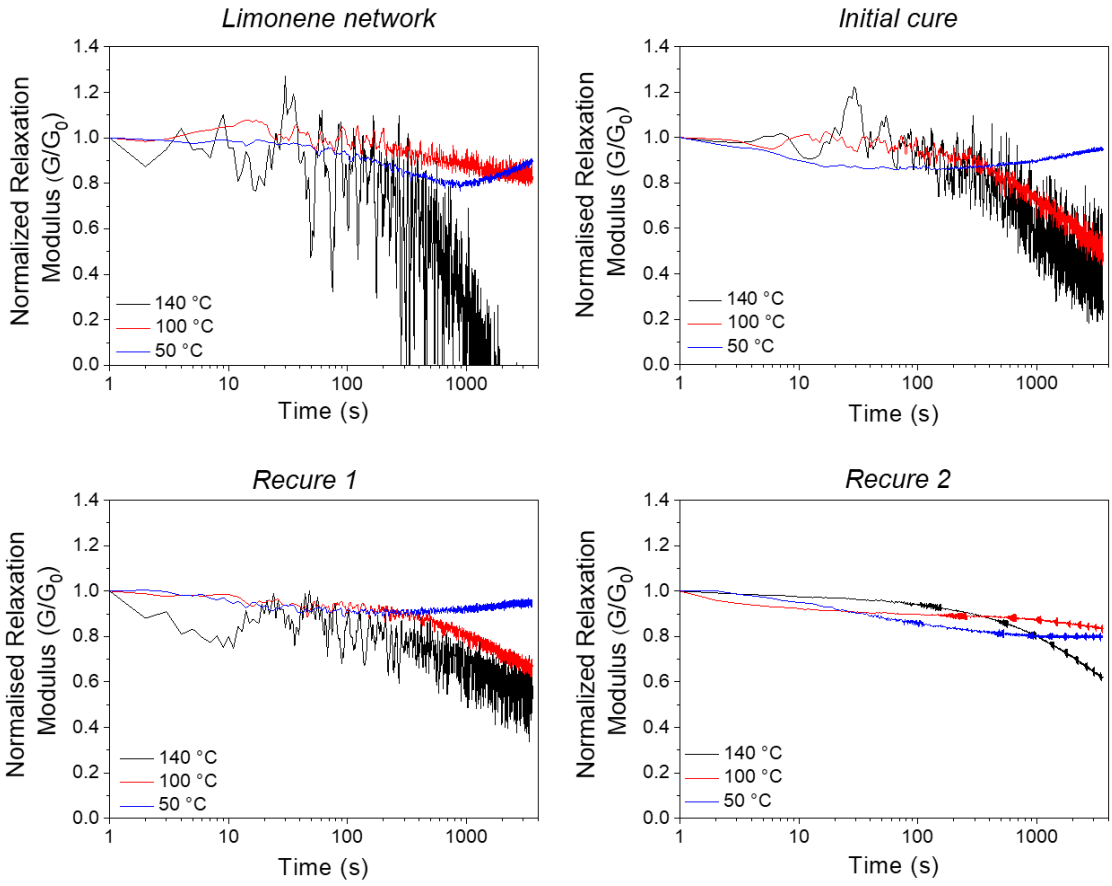


Figure S16. Stress relaxation experiments conducted at 140, 100 and 50 °C for the limonene network, initial carvone network, recure 1 and recure 2.

Network	T_g 1st cycle (°C)[a]	T_g 2nd cycle (°C)[a]	Tan delta peak (°C)[b]	Gel fraction (%)	Degree of swelling (%)	$T_{d,5\%}$ (°C)[c]	Storage modulus @ -25 °C (Pa)[d]	Storage modulus @ 100 °C (Pa)[d]
Initial cure	1	8	12 ± 3	89.4 ± 0.3	239.2 ± 2.9	305	2292 ± 104	2.87 ± 0.74
Recure 1	8	10	12 ± 3	80.6 ± 2.1	315 ± 38.7	295	2202 ± 483	0.43 ± 0.07
Recure 2	13	15	24	85.4 ± 2.7	357.4 ± 2.3	304	1823	0.3
Limonene Film	-5	-3	-	99.5 ± 0.3	261.1 ± 8.3	319	-	-

Table S3 Summary of thermal and mechanical properties for the cured carvone and limonene network

[a] T_g calculated from DSC thermograms
[b] Obtained from DMA thermograms
[c] Temperature at 5% weight loss obtained from TGA thermograms
[d] Storage modulus obtained from DMA at specified temperature

Prepolymer	M_n (kDa)[a]	$Đ$[a]	Enone content (%)[b]	Gelation time (s)[c]	Storage modulus @ 400s (kPa)[d]
Initial	0.9	1.4	100	85	297
Depolymerized 1	5.8	6.3	31	9	94
Depolymerized 2	6.0	5.2	19	4	73

Table S4 Summary of the carvone prepolymers

[a] Obtained from GPC against polystyrene standards in chloroform.
[b] Calculated from ^{1}H-NMR spectroscopy
[c] Obtained from the intersection of storage and loss modulus in photorheology
[d] Storage modulus from photorheology after 400s of irradiation.

Chapter 6 – Conclusion and outlook

The aim of this thesis was to further our understanding of the influences of stereochemistry upon bulk properties of linear polymers. In chapters 2 – 4, we explored stereochemistry around alkenes, rigid 3-membered rings and isohexide derivatives. Chapter 5 diverged from the general theme to investigate and apply features of the thia-Michael addition used in preceding chapters, to create a recyclable photosetting material. This section will be used to summarise the key findings of chapters 2 - 5 and identify trends across the chapters where appropriate. Additionally, this section will provide and outlook upon the field and discuss future developments to further the area.

The initial challenge was to develop a technique to incorporate stereochemistry into a linear polymer without isomerisation or other side reactions. In chapter 2, a procedure using the thia-Michael “Click” reaction between di-thiols and di-acrylate functionalities could be used to synthesise an alternating polymer containing either a *cis* or *trans* alkene bond. Furthermore, the high reactivity enabled compositional control of the stereochemistry content within the polymer backbone and was adapted for other stereocenters in chapters 3 and 4. The high reactivity and mild reaction conditions are just two of the many “Click” features of the thia-Michael addition which were exploited to create polymers containing stereochemistry in this work. Leveraging other “Click” features such as chemoselectivity and modularity would enable a greater control of microstructure and composition in polymer chains. In turn providing us with more complex structure to understand and exploit to tailor bulk properties for specific application.

Altering the stereochemistry within the polymer backbones generally displayed a modest difference in the T_g of all investigated systems. Unfortunately, the lack of crystallinity within the cyclopropane polyesters prevented mechanical characterisation, but led to a better understanding of how the cyclopropane structure itself can inhibit polymer crystallisation. On the other hand, the urethane-based polymers could form freestanding films which possessed stereochemistry dependent mechanical properties. Profoundly, the

stereochemistry of the isohexide unit dictated the material class with one stereoisomer produced a plastic material whilst the other stereoisomer produced an elastomeric material. This unexpected property difference enabled control over the degradation and mechanical behaviour by blending and copolymerising the stereoisomers in different ratios. The bulk property control offered from simple bio-derived isohexides highlight the importance of stereochemistry in materials. A greater understanding into the properties produced from the stereochemistry of bio-derived sources will be crucial in designing future plastic materials.

Polymer crystallinity is a key driving force in the resulting bulk properties of polymeric materials. However, predicting the bulk properties of polymers with different stereoisomers is significantly challenging with some stereoisomers displaying different property trends depending on polymer architecture and functionality. In chapter 4, the isohexides displayed an unexpected range of mechanical properties, unlike previously reported isohexides systems. Molecular dynamic simulations suggested the hydrogen bonding of the polymers was heavily influenced by the isohexide geometry and how hydrogen bonding changed under stress. Further simulations also aided explanation for the property differences between the blended and copolymerised analogues. Whilst computer simulations offered a potential explanation in this example, predicting and explaining the bulk properties of polymer materials remains a key challenge within the area. Advancements in processing power will undoubtedly increase the ease at which polymers can be simulated and predicting structure-property relationships will become common place in the polymer materials community.

The project relating to chapter 5 was a tangential study that arose from the observed reversibility of the thia-Michael addition used in preceding chapters. The designed photocurable resin was found to be re-curable in multiple cycles and maintained typical mechanical behaviour for a networked material. The pursuit of recyclable materials has

begun leveraging reversible covalent bonds that can maintain robustness at operating conditions but reverses under a given stimulus. This is a rapidly growing area in materials chemistry and holds the potential to create a new generation of recyclable materials that mechanically compete with previous non-recyclable systems.

Both stereochemistry and the thia-Michael addition reaction have demonstrated important features that can be leveraged in polymer chemistry. Whilst both of these have seen significant growth in the past decade, there is still an expanse of untapped potential that could significantly improve current commercial materials and further our understanding of structure-property relationships.